In Vitro Studies of Amyotrophic Lateral Sclerosis Using Human Pluripotent Stem Cell-Derived Motor Neurons

A dissertation presented

by

Luis Alberto Williams Gonzalez

to

The Division of Medical Sciences

in partial fulfillment of the requirements

for the degree of Doctor of Philosophy in the subject of

Cell Biology

Harvard University

Cambridge, Massachusetts

April 2015

Dissertation Advisor: Professor Kevin Eggan Luis Alberto Williams Gonzalez

In Vitro Studies of Amyotrophic Lateral Sclerosis Using Human Pluripotent Stem Cell-Derived Motor Neurons

Abstract

Among the disciplines of medicine, the study of neurological disorders such as amyotrophic lateral sclerosis (ALS) is particularly challenging. In ALS, both cortical and spinal motor neurons progressively degenerate, leading to paralysis and death. The fundamental inaccessibility and the postmitotic state of these cells prevent their isolation and culture for studies of degenerative mechanisms or for drug screening efforts. The studies presented here support the premise that human motor neurons (MNs) generated by directed differentiation of induced pluripotent (iPS) or embryonic stem cells (ES) represent a great research tool to address this challenge. We show that MNs derived from patient-specific iPS cells with known ALS-linked mutations can recapitulate molecular and functional phenotypes associated with the disease. The phenotypes observed included transcriptional and morphological changes in mitochondria, protein solubility, membrane hyperexcitability, and defects in cell survival and axonal transport. By utilizing gene-targeting technology we further validated the requirement, and in some cases the sufficiency, of the *SOD1A4V* mutant allele to drive some of these phenotypes. Additionally, by means of a human ES cell line with a stable MN-specific green fluorescence protein (GFP) reporter, we carried out transcriptome profiling of cultured GFP^+

cells following dysregulation of the ALS-associated RNA-binding protein TDP-43. We uncovered novel molecular targets downstream of the activity of TDP-43, one of which is the gene encoding for the tubulin-binding protein STMN2, with functional roles in cytoskeletal dynamics and axonal regeneration. Furthermore, we confirmed STMN2 response to TDP-43 downregulation at the protein level and provide evidence supporting its altered expression in spinal cord tissues from ALS cases. We propose that depletion of this neuronal growth factor following TDP-43 dysregulation could be a molecular mechanism by which the loss of normal nuclear TDP-43, seen in most ALS cases, contributes to MN degeneration. Finally, we discuss how future experiments, by integrating our findings with recent technological breakthroughs in genome-editing, stem cell differentiation and single-cell analysis, will further our understanding of disease mechanisms and facilitate the identification of novel therapeutic interventions.

Table of Contents

Table of Contents (continued)

Table of Contents (continued)

Table of Contents (continued)

List of Figures and Tables

Acknowledgments

The work represented herein would not have been possible without the insight and guidance of my mentor, Dr. Kevin Eggan. I thank Kevin for pushing me to develop independence and confidence as a research scientist, but mostly for his enthusiasm and positive energy which gave me hope at times when stem cells and motor neurons were not 'cooperating'.

Thank you to my dissertation advisory and defense committee members: Dr. Jeff Macklis, Dr. Amy Wagers, Dr. Lee Rubin, Dr. Konrad Hochedlinger, Dr. Tracy Young-Pearse, and Dr. Robert Brown, for providing the necessary combination of expertise, support, and skepticism to help bring this dissertation to fruition.

Deep gratitude goes to my peers—past and present members of the Eggan group, whose knowledge, friendship, and good humor kept me motivated and moving forward throughout these years. I would especially like to mention Brandi Davis-Dusenbery, Gabriella Boulting, Joseph Klim, Dan Mordes, Jack Sandoe, Evangelos Kiskinis, Florian Merkle, Shila Mekhoubad, Sophie de Boer, Rob Moccia, Seth Cassel, Ole Wiskow, Katie Koszka, Megan McCord, Justin Ichida, Nick Atwater, Maura Charlton, Oleg Gelmont and Diane Santos.

I also want to thank my family, for their sacrifice and love, and for giving me the foundation upon which to successfully pursue my studies.

Finally and most importantly I would like to thank my partner David Tabenken. He deserves a Harvard PhD in patience for all he has endured in the past 6 years. His love and unconditional support were instrumental throughout this journey.

CHAPTER 1

Making Spinal Motor Neurons from Pluripotent Stem Cells for the Study of ALS

Portions of this chapter have been published as:

• Davis-Dusenbery BN, **Williams LA**, Klim JR, Eggan K. How to make spinal motor neurons. *Development* 141, 491-501 (2014).

• **Williams LA**, Davis-Dusenbery BN, Eggan K. SnapShot: directed differentiation of pluripotent stem cells. *Cell* 149, 1174-1174 (2012).

• Han SS, **Williams LA**, Eggan K. Constructing and deconstructing stem cell models of neurological disease. *Neuron* 70, 626-644 (2011).

Author contributions to the work presented in this Chapter: B.N.D wrote the 'MN development' and 'Evaluation of MNs produced *in vitro*' sections; S.S.H and L.A.W co-wrote the 'Challenges in the study of ALS and other neurological disorders' section; L.A.W wrote all other sections; K.E. supervised all aspects of this work.

1.1 Abstract

Amyotrophic lateral sclerosis (ALS) is a fatal neurological disorder characterized by the selective and progressive deterioration of cortical and spinal motor neurons. The inability to access these cells from living patients as well as their postmitotic nature prevent their isolation and culture for studies of human neurodegeneration. Significant progress toward overcoming this challenge has been achieved through the synthesis of developmental biology paradigms and advances in stem cell and reprogramming technology. In this chapter we describe how the opportunity to reprogram readily accessible tissue from patients into pluripotent stem cells, combined with methods to direct their differentiation, have now made possible the *in vitro* production of human motor neurons bearing ALS-relevant genotypes. This unprecedented resource has in turn facilitated the development of novel human cellular models of ALS, which offer exciting opportunities for mechanistic studies and therapeutic discovery.

1.2 Introduction

In his memoir *The Diving Bell and the Butterfly*, French journalist Jean-Dominique Bauby lamented 'Other than my eye, two things are not paralyzed, my imagination and my memory'[1]. Such is the plight of those experiencing 'locked-in' syndrome - a condition in which the brain remains relatively intact, but the terminal neurons that connect to all muscles except those servicing the eye are rendered non-functional. As a result, 'locked-in' individuals are left with only their ability to take in visual stimuli and to have thoughts upon which they cannot act.

Two broadly defined neuronal types provide the connection between the brain and our musculature: the upper, or cortical spinal motor neurons (CSMNs) and the lower spinal motor neurons. As their name implies, the cell bodies of CSMNs reside in the cortex and transmit motor information down long axons into the spinal cord[2]. Spinal motor neurons receive this information and through axons that project out of the spinal cord to the musculature, actuate muscle contraction through a specialized synapse, the neuromuscular junction (NMJ)[2]. Significant injury to the descending spinal cord axons after physical trauma or stroke can result in complete paralysis. Although localized peripheral nerve injury to spinal motor neurons may only result in partial paralysis, neurological disorders such as spinal muscular atrophy (SMA) and amyotrophic lateral sclerosis (ALS) can cause a more global deterioration of motor neurons and, in turn, a 'locked-in' condition. A desire to protect and eventually regenerate the motor circuitry in the contexts of spinal cord injury and motor neuron disorders has motivated a myriad of studies into the mechanisms underlying motor neuron development and neurodegeneration.

In this Chapter, we will first review some of the proposed disease mechanisms in ALS, focusing on pathways pertaining to the ALS-associated proteins SOD1 and TDP-43, as they

relate to the research studies presented in Chapters 2, 3 and 4. We will then discuss how some of the challenges inherent to the study of neurological disorders have prompted the application of advances in reprogramming technology to allow the generation of patient-specific pluripotent stem cells. Since developmental biology principles have traditionally informed stem cell differentiation strategies, we will review the molecular events that control motor neuron development during embryogenesis before describing the methods for their *in vitro* production from pluripotent stem cells. Finally we will discuss the potential of human differentiated motor neurons for the development of novel disease models of ALS. It is important to mention that throughout this thesis we focus exclusively on spinal motor neurons (referred to hereafter simply as MNs), and direct readers interested in CSMN development and reprogramming to recent publications of note[3-6]

1.3 Amyotrophic Lateral Sclerosis: Lessons from *SOD1* and *TDP-43* studies

Amyotrophic Lateral Sclerosis (ALS), first described in 1869 by French neurologist Jean-Martin Charcot[7], is the most common adult-onset motor neuron disorder, characterized by the selective and progressive degeneration of both CSMNs and spinal motor neurons[8-10]. In the United States, where it is also known as Lou Gehrig's disease, ALS affects about 2 people per 100,000 per year[10, 11]. Disease onset is typically late, with symptoms such as muscle weakness and twitching (fasciculation) beginning in patients with a median age of 55 years, and progressing to paralysis and death due to respiratory failure within 1-5 years after diagnosis[9, 12]. There are no primary therapies for ALS, and the only approved drug, Riluzole, prolongs median survival in patients by only about two to three months[13]. Approximately 10% of ALS patients present a clear family history, leaving the majority of ALS cases to be considered sporadic, with no known genetic or environmental link[9, 12, 14]. Recent genetic studies have

found that a significant number of familial ALS subjects can carry risk variants in more than one gene, suggesting an oligogenic basis for ALS, which could help explain the phenotypic variability seen even in patients of the same family[15-18].

1.3.1 *SOD1*-linked ALS

Among familial ALS cases, 20% (2% of total cases) are caused by dominant missense mutations in the *SUPEROXIDE DISMUTASE 1* (*SOD1*) gene[8, 10, 19], first linked to ALS more than 20 years ago[20, 21]. The *SOD1* gene product, which is ubiquitously expressed and highly conserved across species, functions as a cytoplasmic antioxidant enzyme, converting toxic superoxide radicals to molecular oxygen and hydrogen peroxide[22]. Until recently, ALS studies had primarily focused on understanding the role of mutant SOD1 in MN degeneration. The retention of enzymatic activity by some of the SOD1 variants associated with ALS[23], the lack of correlation between SOD1 catalytic activity and clinical phenotypes[24], and the demonstration that *Sod1*$^{-/-}$ knockout mice do not develop a MN disease[25], all support the model that mutations in *SOD1* cause ALS through gain-of-function mechanisms[19].

Studies of mutant SOD1 pathways using various cellular and animal models have led to the proposal of several cell autonomous and non-cell autonomous disease-associated mechanisms[10, 12, 19, 26-35]. MN intrinsic mechanisms include aberrant SOD1 chemistry and oxidative stress, protein toxicity through the accumulation of intracellular SOD1 aggregates, mitochondrial dysfunction, aberrant accumulation of neurofilaments and peripherin, and altered axonal transport[10, 12, 19, 36]. Evidence for non-cell autonomous pathways in ALS linked to *SOD1* was first presented by a study using chimeric mice made of mixtures of wildtype cells and cells expressing mutant SOD1[31]. This study indicated that MN death required mutant SOD1 activity in the surrounding non-neuronal cells, and that wild-type nonneuronal cells promoted the

survival of neighboring mutant SOD1 MNs[31]. Subsequent reports utilizing *in vitro* co-cultures of MNs and glial cells have also described a non-cell autonomous neurotoxic activity, mediated by expression of mutant SOD1 in astrocytes and microglia[26-28, 32, 33, 35, 37]. Notably, studies of conditional transgenic mice, in which the mutant *SOD1* transgene was depleted in either astrocytes or microglia but not in MNs, have demonstrated that damage within MNs expressing mutant SOD1 drives disease initiation, whereas neighboring glial cells influence disease progression[29, 30]. Proposed mechanisms for the non-cell autonomous contribution of glial cells to ALS include upregulation of neuroinflammatory pathways (prostaglandin signaling, NF-κB), induction of programmed necrosis, secretion of neurotoxic factors (nitric oxide, superoxide, peroxynitrite) and glutamate excitotoxicity following reduced activity of the EAAT2 transporter[10,12,19,27,35,38,39].

In the past decade, additional linkage analyses and next generation DNA sequencing technologies have led to the identification of several other genes whose variants can cause or increase the risk of ALS[14, 40-43]. The total number of genes in the ALS catalog is now close to 30, with mutations in four genes (*C9ORF72*, *SOD1*, *TARDBP* and *FUS/TLS*) accounting for over 50% of familial ALS cases [14, 41, 44]. Although it is not known how alterations in genes with such diverse cellular functions converge in the death of motor neurons, a few common biological processes have emerged that could represent key determinants of disease onset and progression[41]. Some of the candidate processes in ALS pathogenesis include alterations in RNA processing and protein homeostasis[44, 45], mitochondrial dysfunction[46, 47], and disruptions in cytoskeleton architecture and dynamics[41, 42, 48].

1.3.2 The ALS-FTD continuum

The diversity of genes implicated in ALS, combined with clinical and postmortem

observations, have demonstrated considerable heterogeneity in the origin and presentation of this disorder[8, 9, 41, 49]. Interestingly, genetic, clinical, and biochemical studies have also established a connection between ALS and frontotemporal dementia[44, 50]. FTD, also known as frontotemporal lobar degeneration (FTLD), is the second most common form of dementia after Alzheimer's disease and is characterized by progressive loss of subpopulations of cortical neurons in the frontal and temporal regions[44, 50]. A large proportion of ALS patients manifest a range of behavioral and cognitive changes that lie on the spectrum of FTD, and motor neuron disease is commonly observed in a subset of FTD patients, suggesting the possibility of common mechanisms underlying both disorders[51]. This notion has been strengthened by the discovery that mutations in the same gene, *C9ORF72* for instance, can manifest as ALS, FTD or ALS/FTD, and that neuropathological inclusions containing the same proteins such as TDP-43, are commonly detected in both ALS and FTD cases[44, 52]. Together, these findings support the model of ALS, not as a 'many-genes-single-neurodegenerative disease', but rather as one of the ends in an ALS-FTD continuum of a neurological spectrum disorder[8, 41, 44].

1.3.3 TDP-43 pathology, ALS-linked mutations, and potential disease mechanisms

The association between TDP-43 and ALS/FTD was first reported in 2006, when this protein was identified by mass spectrometry as the major component of ubiquitin-positive inclusions in brain and spinal cord tissues from ALS and FTLD cases[52, 53]. TDP-43 pathology, commonly detected in affected neurons and glial cells, is characterized by the loss of its normal nuclear staining pattern and the presence of round or 'skein-like' cytoplasmic aggregates that are TDP-43 immunoreactive[52-55]. Additional pathological signatures observed by immunoblot assays include the accumulation of phosphorylated and ubiquitinated TDP-43 C-terminal fragments of about ~25 KDa[52], which are generated by proteolytic cleavage by caspases[56].

Together, several immunohistochemical studies have now estimated the frequency of TDP-43 neuropathology to be 97% for ALS, and 45% for FTD cases[44, 55, 57]. Following the first biochemical reports linking TDP-43 to ALS/FTD, several studies provided strong genetic evidence for a causative role of TDP-43 in motor neuron degeneration by demonstrating association of missense mutations in *TARDBP,* the gene encoding TDP-43, with familial and sporadic ALS cases[58-63].

TDP-43 is a ubiquitously expressed DNA/RNA binding protein[64-66], first identified as a 43kDa cellular factor recognizing the *TAR* regulatory element in the long terminal repeat of the HIV virus genome[67]. The major structural features of TDP-43 include two highly conserved RNA Recognition Motifs (RRM1 and RRM2) and a C-terminal glycine-rich region that is often found to mediate protein-protein interactions[65]. More than 40 different TDP-43 mutations have been reported in sporadic and familial ALS cases, with most mutations mapping to the C-terminus region of the protein[68].

Although predominantly nuclear, a small fraction of TDP-43 can also be detected in the cytosol, and it has been shown to shuttle between the two compartments[69, 70]. TDP-43 has functional roles in multiple steps of RNA metabolism, including transcription[67], pre-mRNA splicing[45, 66, 71], pre-miRNA processing[72], stress granule formation[73, 74], and mRNA transport and stability[75, 76]. Immunoprecipitation studies coupled with next generation sequencing have demonstrated that TDP-43 binds to thousands of RNAs in the mammalian CNS[45, 77] and can regulate the RNA levels of genes with functions in brain development and synaptic activity[45].

The issue of whether TDP-43 pathophysiology represents a *gain-of-function*, driven by the accumulation of the toxic cytoplasmic inclusions, a *loss-of-function*, due to loss of nuclear function, or a combination of both mechanisms, remains unsettled[78]. Several cellular and

animal studies have provided evidence for potential gain-of-function toxic mechanisms mediated by TDP-43. Ectopic expression of the ~25 kDa C-terminal TDP-43 fragment in HEK293 cells leads to the formation of toxic, insoluble and ubiquitin-positive and phospho-positive cytoplasmic inclusions within cells[79]. Interestingly, this C-terminal fragment does not sequester full-length nuclear TDP-43, suggesting a toxic gain-of-function mechanism in its induction of cell death[79]. Overexpression of TDP-43 in yeast cells causes formation of highly toxic cytoplasmic inclusions (Johnson et al., 2008). Similar results are observed in cultures of mouse primary motor neurons, where intranuclear microinjection of plasmids encoding wild-type or mutant TDP-43 led to neurotoxicity and aggregation[80]. Transgenic overexpression of wild-type TDP-43 in the CNS of mice is sufficient to drive neuronal loss, motor phenotypes and lethality[81-83], suggesting that disruption of TDP-43 homeostasis in the mammalian CNS can activate molecular pathways associated with motor neuron vulnerability and cell death[78]. The model of dysregulation of TDP-43 levels as a mechanism contributing to disease is strengthened by findings demonstrating that this protein downregulates its own synthesis by promoting the nuclear retention and degradation of the *TDP-43* transcript[45, 84, 85].

In vitro and *in vivo* approaches have also supported the hypothesis of potential disease mechanisms mediated by loss of TDP-43. TDP-43 downregulation in human (HeLa) cells by RNA interference causes cell death in a mechanism mediated by deregulation of retinoblastoma protein[86]. In zebrafish embryos, knockdown of *tardbp* by microinjection of an antisense morpholino causes shorter motor axons and swimming deficits[80]. Since TDP-43 function is essential for early mammalian development[87, 88], recent studies have used conditional genetic deletion[89, 90] or RNAi[91] approaches to interrogate the loss of TDP-43 function in the adult mammalian CNS. Both kinds of approaches have led to the generation of mice with phenotypic

features of ALS, indicating that complete loss of TDP-43 in spinal motor neurons, or even partial depletion of TDP-43 levels in the adult CNS, primarily astrocytes, could play a significant role in neurodegeneration and ALS pathogenesis[87, 88, 91].

While studies modulating TDP-43 expression in various experimental systems have been informative, discerning the contribution of ALS-associated TDP-43 variants to the phenotypes observed, particularly in mouse models, has proved challenging[82, 92]. This issue has been primarily driven by their susceptibility to increased expression of wild-type TDP-43 in CNS tissues[81-83]. A more recent study, using transgenic lines expressing levels of wild-type or mutant human TDP-43 that were comparable to the endogenous TDP-43, demonstrated the generation of transgenic mice exhibiting age-dependent and TDP43-mutant-dependent motor neuron loss, axonal degeneration and hindlimb weakness[71]. Whether these TDP-43 transgenic lines will become as widely accepted as a model of ALS as the *SOD1*^{TgG93A} transgenic mouse remains to be determined.

1.4 Challenges in the study of ALS and other neurological disorders.

While the continued importance of animals in translational research is indisputable, genetic and anatomical variation between rodents and man can lead to imperfect phenotypic correlations between genetic models and the human diseases they attempt to recapitulate. Furthermore, just like with most neurodegenerative diseases, most ALS cases are sporadic in etiology, arising from what appear to be the complex interactions of genetic and environmental risk factors[9, 93, 94]. As a result, it may be difficult or impossible to fully model these conditions in animals. But perhaps most notably, pre-clinical successes in the treatment of existing animal models of ALS and other disorders have not translated into clinical benefits for patients[95,96].

Thus there must be aspects of neurological disease that we do not yet understand well enough to recapitulate or that cannot be recapitulated in animals.

It is possible that an improved understanding of ALS and other neurological diseases could be developed if there were accurate human cellular models of these conditions that relied only on actual patient genotypes and that resulted in degeneration of the disease-affected neural cell types. To date, however, attempts to develop *in vitro* models for nervous system degeneration have been stymied by the fundamental inaccessibility of many specific human neural sub-types. While elements of the peripheral nervous system, such as peripheral nerves or muscle, are sometimes clinically accessed for pathological studies, routine sampling of tissue from the brain and spinal cord of living patients are usually only performed in rare conditions where a tissue diagnosis is necessary for subsequent clinical management. Thus most neural cell-types cannot be accessed in any quantity from living patients. Although post-mortem samples from the nervous system can be obtained, such tissue is ravaged by end-stage manifestations of disease. Moreover, while post mortem samples can be helpful at times in making a specific diagnosis, they have not always proven useful for revealing how the neurological disease process unfolds over time. Even if the routine sampling of neurons directly from patients were possible, an inability to expand and study these post-mitotic cells *in vitro* for prolonged periods would further diminish their utility. However, recent advances in the areas of stem cell and reprogramming biology now seem to provide a novel route to the production of a wide variety of neural types for neurological research. In the next section we will review how these advances have made possible the generation of human pluripotent stem cells bearing relevant genotypes for the study of neurological disorders.

1.5 Generation of human pluripotent stem cells for neurological research

Human pluripotent stem (hPS) cells are characterized by the ability to divide indefinitely in culture (*self-renewal*), while retaining the capacity to differentiate into any cell type from the three germ layers (*pluripotency*)[97], including otherwise inaccessible neural types of nervous system. Based on their origin, the two main categories of hPS cells that have been extensively studied to date are embryonic stem (ES) cells and induced pluripotent stem cells. Human ES cells are derived from the inner cell mass of the blastocyst-stage embryo, which generally exist in excess of clinical need at *in vitro* fertilization (IVF) clinics and are donated to research by individuals under informed consent[98-100]. Of particular interest for the study of neurological disease are stem cell lines produced from embryos discarded after preimplantation genetic diagnosis (PGD) because they were identified to carry disease-initiating mutations. Such ES cell lines in turn carry the disease genes responsible for the condition of interest and could prove useful for mechanistic studies. To date, a very small number of human ES cell lines harboring known mutations for a few monogenic neurological disorders has been established[101-104]. This scarcity of PGD stem cell lines is partly due to the small number of embryos discarded after PGD and because this procedure is only routinely carried out for a select number of monogenic neurological disorders. Another approach for using human ES cell lines for neurological disease modeling is to genetically modify them or their cell derivatives by introduction of the disease-causing mutation[105,106]. However, this approach can only be applied for modeling monogenic diseases, and not for modeling disorders for which all the genetic determinants are unknown or not well understood. In addition, approaches with hES cells do not allow for the modeling of sporadic disease or for correlations to be made between *in vitro* cellular phenotypes and clinical observations made over the lifetime of the patient.

In contrast, the 'reprogramming' of somatic cells by defined pluripotency-associated transcription factors allows the production of induced pluripotent stem (iPS) cells, which possess all of the salient characteristics of ES cells[107]. iPS cells can be generated using readily accessible tissue from patients with any condition, overcoming some of the limitations associated with the derivation and manipulation of human ES cells. The obvious advantage of the induced pluripotency approach is that patient-specific iPS cells carry the precise genetic variants, both known and unknown, which contribute to disease, residing in the context of the patient's own genetic background. Thus, cellular phenotypes observed could potentially be correlated with clinical benchmarks such as rate of disease progression (Figure 1.1).

Somatic cell reprogramming with defined factors was first demonstrated in mouse fibroblasts following ectopic expression of the pluripotency-associated genes *Oct4*, *Sox2* and *Klf4* and the oncogene *c-Myc*[108-111]. Shortly after, a similar approach was recapitulated using human fibroblasts, resulting in the generation of the first human iPS cell lines[112-115]. Subsequent studies have shown that iPS cells can be generated, albeit with lower efficiency, using only three factors (*OCT4, SOX2* and *KLF4*)[116]. Human iPS and ES cells share very similar properties, which include colony morphology, proliferation rate, gene expression profiles, and capacity to differentiate into various cell types of all three germ layers[107]. This pluripotent potential can be assessed through a variety of methods, including the *in vitro* differentiation in cell aggregates called embryoid bodies (EBs), and the *in vivo* formation of teratomas*,* which are benign tumors formed after injection of the stem cells into immunodeficient mice[112-115, 117]. More recently, the generation of large-scale transcriptional and methylation profiles for a vast collection of human ES and iPS cell lines has facilitated the development of reliable and more

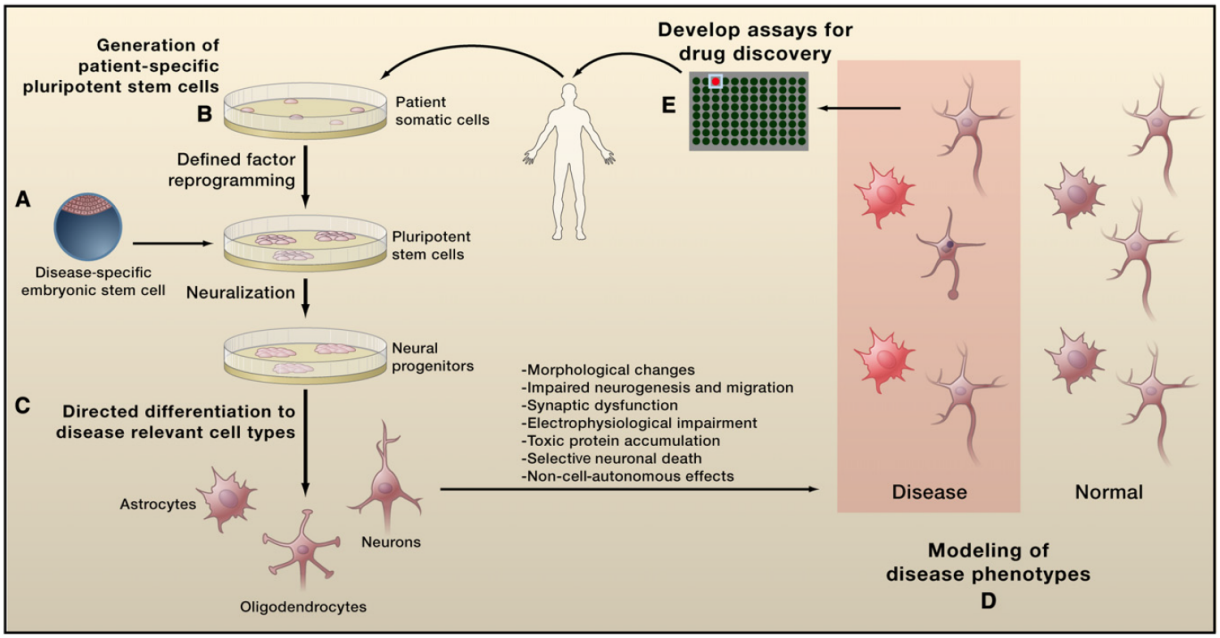

Figure 1.1. Using Human Pluripotent Stem Cells for Disease Modeling and Drug Discovery
Disease and patient-specific pluripotent stem cells can be derived from several sources. **A.** Embryonic stem (ES) cells can be derived from donated embryos identified to carry a disease-causing genetic mutation discovered through preimplantation genetic diagnosis (PGD). However, ES cells from diseased PGD embryos are a scarce resource and lack correlative information of disease onset and progression. **B.** Pluripotent stem cells can also be derived through defined factor reprogramming of readily obtainable somatic cells from patients with a neurological disease, with or without known genetic mutations. Typically, skin fibroblasts obtained from patients are the donor somatic cell type used for reprogramming, though virtually any cell type can be used. **C.** Pluripotent stem cells are expanded in culture and directed to differentiate into cell types important for a particular disease. **D.** Neurons and other neural cell types are studied over time in vitro and, depending on the disease process of interest, can be evaluated for defects in neurogenesis, migration, morphology, synaptic connectivity, survival, and electrophysiological function. Aberrant protein aggregation and non-cell-autonomous factors can also be tested. **E** Once disease-relevant cellular phenotypes are identified, rescue experiments can be performed to help validate the disease model and developed robust assays for drug discovery.

straightforward gene-expression-based assays, which can test differentiation potential by using a large reference set of germ layer-specific and pluripotency-associated genes[118].

Thus far, the majority of human iPS cell lines have been generated using viral transduction of vectors that force the expression of the reprogramming transcription factors. This approach results in multiple genomic integrations of the viral transgenes. While the potential for mutagenesis and tumorigenicity that result from these insertions may preclude the use of these iPS cell lines for transplantation medicine[111], numerous studies have demonstrated that they are adequate for disease modeling purposes[76, 119-127]. Several more recent reprogramming strategies that allow the derivation of genetically unmodified human iPS cells have also been reported[128]. These approaches include the use of non-integrating RNA viruses[129] or episomal vectors[130], excisable lentiviral or transposon vectors[131, 132], or reprogramming proteins modified for cellular uptake[133], and the direct delivery of synthetic mRNAs modified to escape the endogenous antiviral cell response[134]. In addition, small molecules can be used to increase the reprogramming efficiency or to replace the activity of one or more of the reprogramming factors[135-138]. However, the generation of human iPS cells by using *only* small molecules has not been demonstrated. The ultimate method in deriving a disease-specific iPS line will depend on their downstream use.

Although some reports have suggested differential gene expression, mutational load, and DNA methylation patterns between human ES cells and iPS cells[139-142], it is not yet clear what the consequences (if any) of these differences are upon stem cell differentiation on the functionality of the resulting cell type(s)[143, 144]. From a neurological disease modeling point of view, it might be more relevant to determine whether human ES cells and iPS cells differ in their ability to reliable generate the differentiated neural cell type(s) of interest. One study from

our group compared human ES and iPS cells in terms of their capacity to generate functional MNs, and found that, although there was a genetic contribution to the efficiency of MN production by the individual iPS cell lines, overall there was a similar range of differentiation efficiencies between a large number of human ES and iPS cell lines[145]. Our experience suggests that each human pluripotent stem cell line, regardless of whether it is an iPS or ES cell line, has its own discrete properties that must be taken into consideration when using it for directed differentiation in disease modeling studies. Together, these findings also underscore the importance of characterizing, if feasible, more than one pluripotent stem cell line per genotype, as well as multiple patient and control genotypes. This approach would minimize the possibility that phenotypic differences resulting from genetic or epigenetic instability in the cell lines are incorrectly presumed to be relevant to the disease model[146].

As initially anticipated by the implicit promise of reprogramming technology, induced pluripotency by defined factors has made possible the unprecedented generation of a large number of patient-specific iPS cell lines. Because of the relative ease with which iPS cells can be generated from accessible human tissue, such as fibroblasts from a skin biopsy, the derivation of iPS cell lines from patients representing a wide variety of diseases has become almost routine. Many iPS cell lines have now been produced for several neurological disorders, including ALS[76, 119-123, 145, 147-149], SMA[124, 125], Huntington's disease[150], Parkinson's disease[132, 150-152], Familial dysautonomia[126], Rett's syndrome [127, 153], Friedreich ataxia[154, 155], Down syndrome[150], Schizophrenia[156, 157], Angelman syndrome[158], Prader-Willi syndrome[158] , Fragile-X syndrome[159], and Alzheimer's disease[160]. Because of their defining pluripotency property, these patient-specific iPS cells can be differentiated into any desired cell type, including those associated with the clinical phenotype of the cognate neurological disease. In the case of MNs,

significant knowledge of the developmental pathways that operate during neural induction and specification of MN fate has facilitated the design of reliable and efficient protocols for the production of these neurons starting from ES and iPS cells[27, 119, 145, 148, 161-170]. Before describing some of these *in vitro* differentiation strategies, we will review the relevant inductive signals that control MN development *in vivo*.

1.6 MN development

Decades of embryological studies and genetic analyses in model organisms have illuminated the molecular basis of neural induction and further differentiation and specification of MNs during development. In the early 20th century, Spemann and Mangold's work with amphibian embryos revealed that signals emanating from the dorsal lip of the blastopore, now termed the Spemann-Mangold 'organizer', were required for the induction of neural fate during gastrulation[171]. Further studies demonstrated that rather than providing positive signals to induce neural cell fate, the organizer was the source of factors that inhibit Bone morphogenetic protein (BMP) signaling, including Chordin, Follistatin and Noggin[172]. Although the requirement to inhibit BMP signaling is conserved in higher organisms, additional inductive signals, including Fibroblast growth factors (FGFs), Epidermal growth factors (EGFs) and Wnts have been identified[173] (Figure 1.2A).

Following their initial generation, the cells of the neural tube are specified along both the rostral-caudal and the dorso-ventral axes. Gradients of signaling molecules along each axis provide a roadmap to guide the differentiation of the emerging neuronal types of each region. Progenitor domains are first specified and then refined through the cooperative action of external signals and downstream transcription factors[174, 175]. Along the rostral-caudal axis, the neural tube is specified into the major components of the CNS, including the brain, midbrain,

hindbrain and spinal cord. Although multiple signals have been proposed to contribute to the caudalization of the neurons in the spinal cord, chief among them is retinoic acid (RA). Early in development, RA, produced through the activity of Retinaldehyde dehydrogenase 2 (RALDH-2; also known as ALDH1A2), emanates from the caudal paraxial mesoderm and is crucial for the initial distinction of neurons of the hindbrain and spinal cord from those in the forebrain and midbrain[176] (Figure 1.2A).

1.6.1 Specification of MN fate

Within the dorso-ventral axis of the neural tube, progenitor cells are divided into five ventral progenitor domains termed p0, p1, p2, pMN and p3, which in turn give rise to interneuron subtypes V0-3 and motor neurons. A gradient of Sonic hedgehog (Shh), secreted from the notochord and cells of the floor plate provides ventral topographic information by regulating the expression of homeodomain (HD) and basic helix-loop-helix (bHLH) transcription factors[174]. Transcription factors downstream of Shh can be roughly divided into two classes based on their regulation in response to Shh signaling. Class II proteins, including Nkx6.1, Olig2 and Nkx2.2, are activated by Shh and in turn repress the expression of class I proteins, including Pax6, Irx3, Dbx1 and Dbx2[174, 175, 177] (Figure 1.2B). The cross-repressive activity between class II and class I proteins allows the consolidation of progenitor identity as well as the generation of sharp boundaries between adjacent domains[177]. MN progenitors express the HD transcription factors Nkx6.1 and Nkx6.2, which act to repress the other progenitor domains[177] (Figure 1.2B).

Expression of Olig2 within the pMN domain promotes expression of Ngn2, which is important for cell cycle exit as well as for induction of terminal MN transcription factors including Hb9 (Mnx1), Isl1, Isl2 and Lhx3[178]. More recently, additional molecular

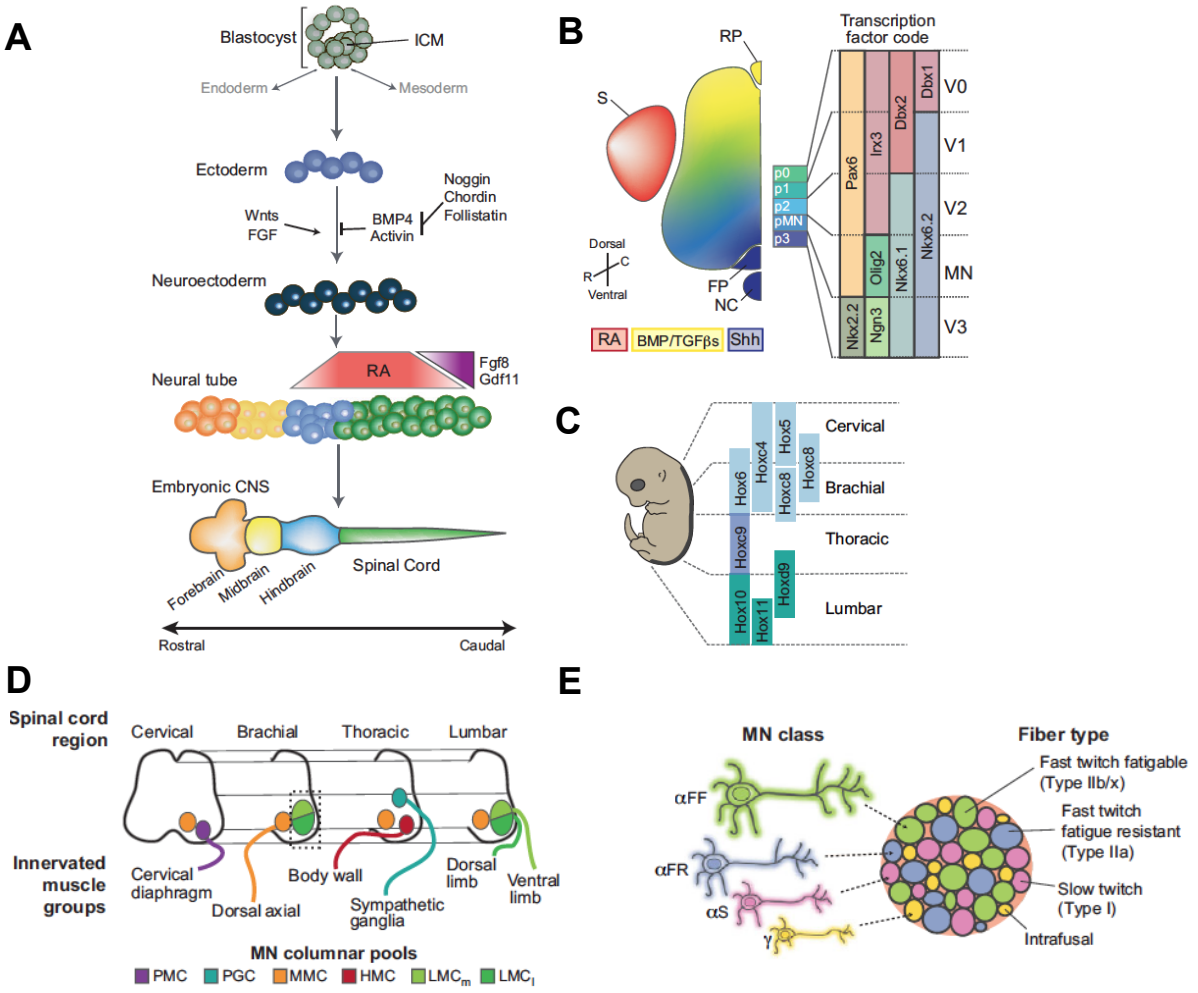

Figure 1.2 Spinal cord development and motor neuron specification.
A. In early development, gastrulation results in the specification of the cells of the inner cell mass (ICM) into the three germ layers: ectoderm, endoderm and mesoderm. The dorsal region of the ectoderm is further specified into the neuroectoderm through the inhibition of BMP and activin signaling, and, in higher organisms, enhanced FGF and Wnt signaling. Neuralization proceeds through the formation of a neural plate and subsequent generation of neural folds, which in turn fuse to give rise to the neural tube. The neural tube is then patterned along the rostro-caudal axis (anterior-posterior) by a gradient of retinoic acid (RA) generated primarily by the action of Raldh2. In particular, a high level of RA allows the initial boundary of the spinal cord and hindbrain versus forebrain and hindbrain to be delineated. Fgfs and Gdf11 oppose the activity of RA and allow specification of more caudal spinal cord cell types. **B.** Once the spinal cord is specified, continued release of RA (shaded red) from the somites (S) acts to refine the positional character of neurons along the rostral caudal axis. The spinal cord is also patterned along the dorso-ventral axis through the combined action of sonic hedgehog (Shh; shaded blue) emanating from the notochord (NC) and floor plate (FP) and BMP/TGFβ signaling (shaded yellow) from the roof plate (RP). The ventral spinal cord can be divided into five progenitor domains (p0-p3 and pMN), which give rise to V0-V3 interneurons and motor neurons. The borders of progenitor domains are established through the cross-repressive action of pairs of transcription factors that are either induced (Class II, in green and blue) or repressed (Class I, in yellow and red) by Shh signaling. The combinatorial action of transcription factors allows the specification of each cell type. For example, pMNs (MN progenitors) express Pax6, Olig2, Nkx6.1 and Nkx6.2. **C.** The Hox genes play a crucial role in the specification of MNs along the rostral-caudal axis. Similar to patterning along the ventral-dorsal axis, the coordinated interactions between Hox family members allow regional boundaries to be delineated. Specific expression of Hox accessory factors, such as FoxP1, can further specify MN subtypes. **D-E.** Further sub-classification of spinal MNs based on anatomical (**D**) and functional (**E**) properties (further discussed in text)

mechanisms, including microRNA pathways, have also been shown to regulate the boundary between some progenitor domains[179].

1.6.2 MN subtype specification

Although all MNs derive from a single ventral progenitor domain, further specification of MNs allows the coordinated movement of hundreds of distinct muscle groups. MNs can be further classified based on their anatomical and functional properties. Anatomically, MNs are divided into five major MN columnar identities: the phrenic motor column (PMC), lateral motor column (LMC), preganglionic column (PGC), hypaxial motor column (HMC) and median motor column (MMC)[180-182]. MNs of each column reside in stereotypical regions along both the rostro-caudal and dorso-ventral axes. The MNs of the LMC can be further subdivided into MNs projecting either ventrally or dorsally within the limb, designated as medial (LMC_m) or lateral (LMC_l) groups, respectively (Figure 1.2D). MN columnar pools can be further organized according to their innervation of particular muscle group targets. The MNs of each pool can be further classified based on functional properties. These are defined by the type of muscle fiber innervated, and are associated with morphological differences between MN classes. Individual muscles are composed of a mixture of fiber types, which can be grouped into two major categories: extrafusal and intrafusal. Whereas intrafusal fibers modulate the sensitivity of muscle to stretch, extrafusal fibers are primarily responsible for skeletal movement. Extrafusal muscle fibers can be further classified into fast twitch fatigable (FF, Type IIb/x), fast twitch fatigue resistant (FR, Type IIa) and slow twitch (S, Type I). α-MNs innervate these three extrafusal fiber types, whereas γ-MNs innervate intrafusal fibers. Both types of fibers can also be innervated by β-MNs (not shown). In addition to differences in the type of muscle fiber innervated, MN classes exhibit morphological differences with α-FF MNs

typically representing the largest neurons, and γ- and β-MNs being smaller[182] (Figure 1.2E).

The positional identity of MNs along the rostro-caudal axis is determined by the coordinated action of multiple signaling molecules. High levels of RA promote rostral (e.g. cervical and brachial) identity whereas FGFs and Gdf11 activity give rise to more caudal (e.g. thoracic and lumbar) MNs[183]. The combined signals from RA, FGFs, Wnts and TGF-β family members are integrated primarily by the Hox transcription factors to specify MN rostro-caudal subtype identity[180]. Mouse and Human *Hox* genes are arrayed in four chromosomal clusters (*HoxA, HoxB, HoxC* and *HoxD*), each of which harbors a subset of 13 paralogous *Hox* genes (*Hox1-Hox13*). Within each cluster, the expression pattern of the *Hox* genes is spatially and temporally collinear with their chromosomal organization, such that *Hox1* genes are expressed in the rostral region of the organism and *Hox13* genes are expressed caudally[184]. Consistent with their conserved role in body patterning, *Hox* gene expression within the spinal cord determines MN columnar identity and selective muscle innervation, with *Hox4-8* genes expressed at brachial levels, *Hox8* and *Hox9* at the thoracic level and *Hox10* and *Hox11* in the lumbar region[180, 185] (Figure 1.2C). Further specification of individual MN subtypes is provided by fine-tuning the Hox protein expression pattern both spatially and temporally[181, 186, 187]. The ability of different *Hox* genes to play an important role in determination of MN identity is perhaps surprising given that the homeodomains of Hox proteins are largely conserved between paralogs. However, there is accumulating evidence that further specificity of Hox function can be provided by accessory factors, including downstream effectors such as the Forkhead box (Fox) protein P1 and the HD protein Nkx6.1[181]. FoxP1 is expressed at high levels in LMC MNs and *FoxP1*$^{-/-}$ mouse embryos exhibit disrupted columnar MN identities and alterations in MN cell body position and axonal wiring[188, 189].

As discussed in the next section, the body of work describing the molecular underpinnings of MN specification during development has enabled recapitulation of these signals *in vitro* for the generation of MNs in 'a dish'. An exciting consequence of this progress is that it allows sufficient quantities of MNs to be derived in a controlled environment to interrogate further detailed mechanisms of MN development and specification. For example, a recent study used a series of chromatin immunoprecipitation assays during MN differentiation *in vitro* to investigate molecular details regulating *Hox* gene expression[190]. The authors found that addition of RA during MN differentiation led to recruitment of RA receptors to the *Hox1-5* chromatin domain that was followed by a rapid domain-wide removal of H3K27me3 and acquisition of cervical MN identity. Moreover, Cdx2, a transcription factor induced by Wnt and FGF, regulated the clearance of H3K27me3 from the *Hox1-9* chromatin domains, resulting in brachial or thoracic MN specification[190]. Thus, the early modification of chromatin by patterning factors contributes to the specification of the rostro-caudal identity of MNs. This type of mechanistic, genome-wide study would surely be impossible with the limited quantities and mixed populations of cells that can be purified from the early embryo. Continued integration of findings from developmental studies in model organisms and *in vitro*-derived MNs will allow a greater understanding of MN specification, and as a consequence further improve strategies to recapitulate MN development *in vitro*.

1.7 Making MNs by directed differentiation of pluripotent stem (PS) cells

Early in embryonic development, one of the first cellular differentiation events occurs during gastrulation, which results in the formation of the three germ layers: ectoderm, mesoderm, and endoderm. Similarly, many of the directed differentiation methods rely on the initial specification of ES and iPS cells into one of these multipotent lineages, followed by the

generation of the particular cell type of interest, through activation or inhibition of relevant extracellular inductive signals, including TGF-β/BMP, NOTCH, SHH, WNT, FGF, VEGF, EGF and retinoic acid[191] (Figure 1.3). In the case of spinal motor neurons, just as their *in vivo* embryonic development can be broken down into distinct stages, so too can their *in vitro* differentiation from PS cells. Specifically, the steps of neural induction followed by caudal and ventral patterning must all be appropriately executed for MNs to be produced.

1.7.1 Neural induction

In the absence of factors that promote pluripotency, such as leukemia inhibitory factor (LIF) and FGF, PS cells spontaneously differentiate into diverse lineages and lose the ability to self-renew[192]. Although spontaneous differentiation represents a hurdle for the maintenance of pluripotency, it can be exploited to give rise to differentiated cell types. Spontaneous differentiation into multiple lineages, including neurons, can be enhanced by inducing PS cells under non-adherent culture conditions to form multicellular aggregates, termed embryoid bodies (EBs)[193]. However, the efficiency of neural induction using these spontaneous approaches is low, and significant cellular heterogeneity within EBs hinders further mechanistic studies[194]. Multiple strategies have been proposed to improve the production of neural precursors and cells with neuronal phenotypes from differentiating populations of PS cells. These approaches include treatment of EB cultures with RA[194], adherent co-culture of PS cells with PA6 or MS-5 stromal feeder cell lines[195, 196], continued propagation of nestin$^+$ proliferating cells in defined media containing mitogens such as FGF2 and EGF[197-199], lineage selection using genetic reporters[200], and selective enzymatic digestion or manual selection of neural tube-like rosette structures[169, 201] (Figure 1.3).

More recent studies have shown that simultaneous inhibition of the TGFβ/Activin/Nodal

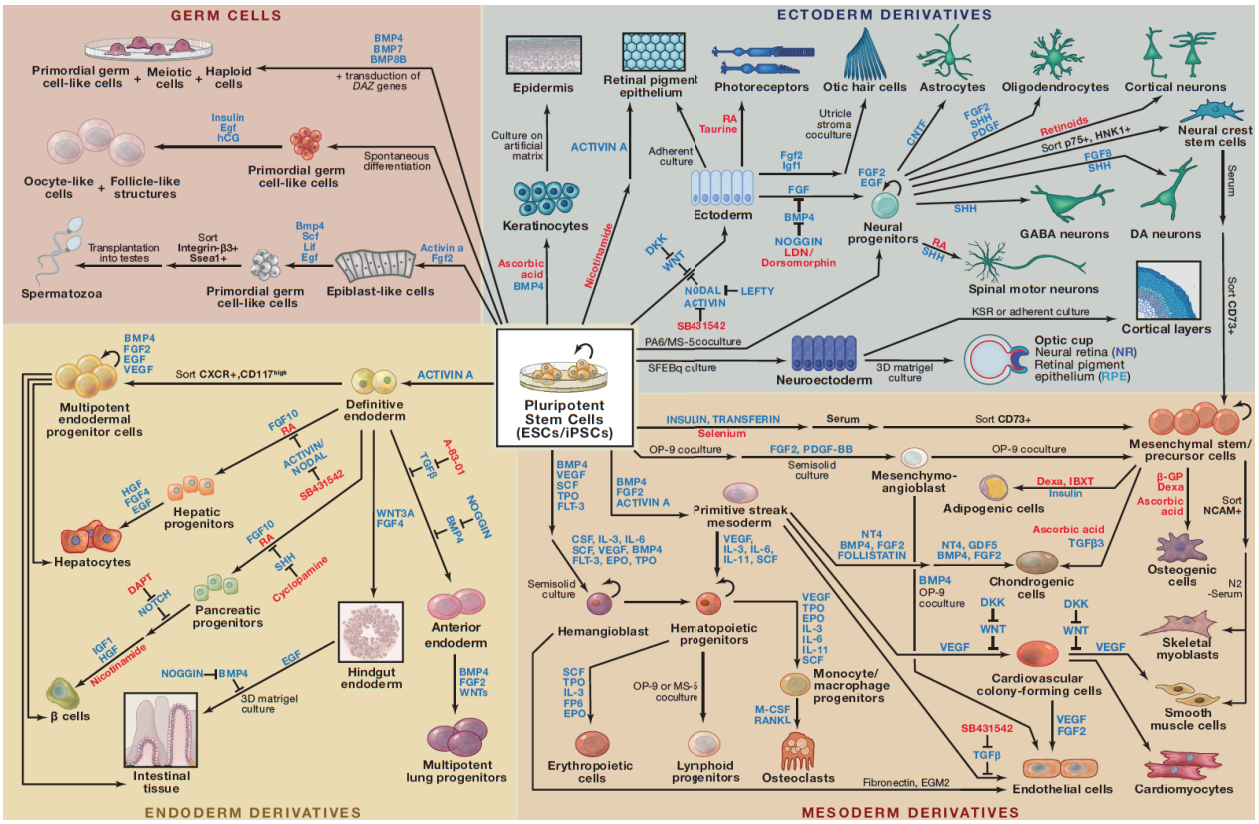

Figure 1.3 Directed differentiation of pluripotent stem cells

Embryonic stem (ES) cells and induced pluripotent stem (iPS) cells posses great potential for applications in regenerative medicine, disease modeling, and developmental biology studies. This potential relies on the ability of these cells to differentiate into the hundreds of cell types within the body. Here, we highlight some of strategies for directing the differentiation of ES iPS cells into defined cell types. Most cell types and pathways depicted correspond to published work on human cells, except for the production of spermatozoa, oocyte-like cells, otic hair cells, cortical layers, and optic cup, which were generated with mouse pluripotent stem cells. In order to uncover these differentiation strategies, stem cell biologists have relied heavily on previous research in model organisms, including *Drosophila*, *Xenopus*, chick, and mouse. Early in embryonic development, one of the first cellular differentiation events occurs during gastrulation, which results in the formation of the three germ layers: ectoderm, mesoderm, and endoderm. Similarly, many of the directed differentiation methods rely on the initial specification of ES/iPS cells into one of these multipotent lineages, followed by the generation of the particular cell type of interest. The relevant signaling pathways to manipulate *in vitro* can be gleaned from developmental studies; however, directing the differentiation to defined cell types requires considerable optimization of the precise concentrations, timing, and combinations of factors and small molecules. In this figure, we have indicated key growth and differentiation factors for each pathway in blue and small molecules in red; specific culturing conditions such as coculture with stromal cells are also indicated. Successful differentiation toward a particular cell type is typically determined by the expression of specific markers identified through *in vivo* studies, but in many cases, additional phenotypic analyses of cells derived from pluripotent stem cells are performed. Although the field of directed differentiation has made rapid progress, many issues remain, including the validation of the maturity and functionality of many of the human cell types derived in and the generation of more complex structures with tissue- or organ-like organization and function. Nevertheless, these challenges represent exciting opportunities for future studies and discoveries.

and BMP signaling pathways, through the use of either small molecule antagonists or recombinant inhibitors, can induce a rapid and very efficient (>80%) neural conversion of human PS cells[164, 202-204]. Similar to the processes that occur during early development, inhibition of the TGFβ and BMP pathways is thought to promote differentiation of PS cells along the neuronal lineage primarily through inhibition of self-renewal, as well as blocking differentiation towards alternative lineages[164] (Figure 1.4A). Several other pathways, involving EGFs, FGFs and Wnts, have been described to regulate neuronal differentiation of human and mouse PS cells. In particular, FGF2 has been shown to promote induction and survival of neural progenitors[198, 205, 206]. Therefore, enhancing FGF2 signaling during the neural induction phase of differentiation can increase the number of neural progenitors[198], whereas inhibiting it at subsequent stages promotes their transition into differentiated neurons[202].

1.7.2 Caudal and ventral patterning

Following neural induction of PS cells, neural progenitor cells can be patterned according to developmental principles. Treatment with retinoic acid promotes caudal (spinal cord) identity, while the addition of either recombinant Shh or small molecule agonists of the Shh signaling pathway, such as SAG (Smoothend agonist) or Purmorphamine, promotes ventralization[161, 166] (Figure 1.4A). Time course studies have revealed that differentiation *in vitro* proceeds with the same temporal regulation of transcription factors as is observed *in vivo*, with $Sox1^+$ neural progenitors giving rise to $Olig2^+$ MN progenitors, which then in turn begin to express Hb9 and Isl1[166] (Figure 1.4B). In the mouse, $Hb9^+$ MNs begin to appear within 3-5 days after addition of patterning factors[28, 166]. The timing of MN differentiation from human PS cells is more protracted and it can, depending on the specific protocol utilized, require an

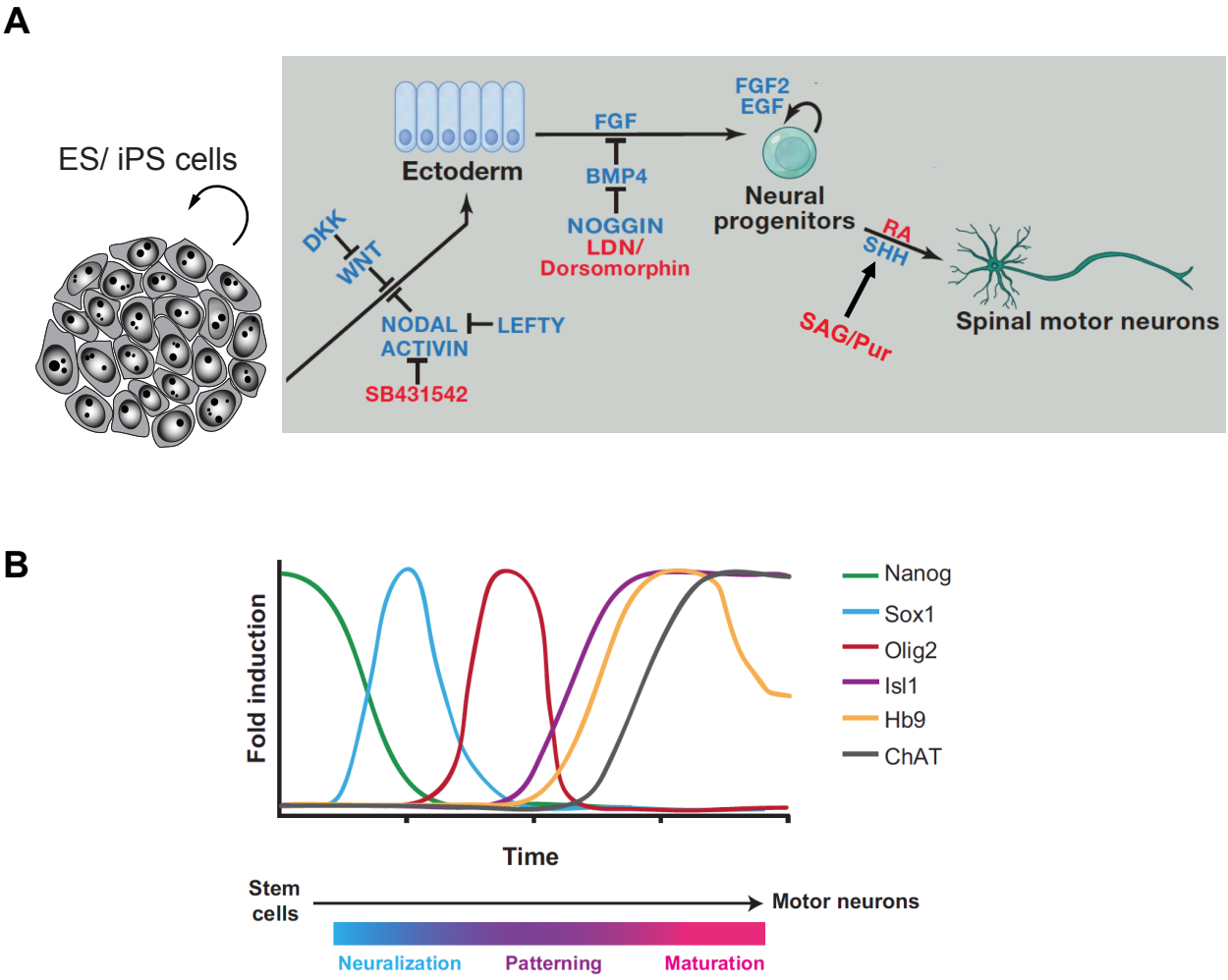

Figure 1.4 Directed differentiation of pluripotent stem cells into spinal motor neurons
A. Pluripotent stem cells (either ES or iPS cells) can be efficiently directed to differentiate into neuronal progenitors through inhibition of BMP (BMP4) and TGF-β (NODAL/ACTIVIN) signaling cascades (dual SMAD inhibition). This can be accomplished with recombinant protein inhibitors (NOGGIN) or with small molecules (SB431542 and LDN/Dorsomorphin). Additional signals, such as retinoids, Wnts and FGFs, also promote neuronal induction (not shown). Neural progenitors can be expanded in culture in response to FGF and EGF signaling. Neural progenitors are then patterned into spinal motor neurons using retinoic acid (RA) to promote caudalization, and either recombinant SONIC HEDGEHOG (SHH) or small molecule agonists of SHH signaling [such as Smoothend Agonist (SAG) and Purmorphamine (Pur)] to promote ventralization. **B.** Expression of transcriptional markers of motor neuron differentiation during development is recapitulated during directed differentiation of ES/iPS cells. The precise timing of each event varies between mouse and human cells and can be influenced by timing of small molecules and culture conditions. Neural induction involves repression of pluripotent marker genes, including NANOG, and induction of SOX1. Expression of the MN progenitor marker OLIG2 precedes the induction of terminal MN markers, including ISLET1, HB9 and ChAT.

additional 2-4 weeks after neural induction before electrophysiologically active, HB9^{+}/ISLET1^{+} neurons are present[145, 161, 164, 169].

In contrast to the well-understood developmental mechanisms that allow the specification of generic MNs, how individual MN subtypes are generated *in vivo* is relatively less well understood. Despite this, several groups have made progress in manipulating MN subtypes generated by directed differentiation. While early in development RA signaling promotes spinal cord identity, continued exposure to RA establishes a rostral MN identity. In context of murine ES cell differentiation, protocols that include treatment of cells with RA typically result in MNs with a cervical character, as judged by expression of Hoxc4 and Hoxa5 and lack of expression of Foxp1 or Hox8-11[207]. Although MN differentiation is typically less efficient in the absence of RA, mouse and human studies have both shown that either endogenous Wnt and FGF signaling or inhibition of BMP/Activin/Nodal signaling cascades allow generation of MNs with a more caudal positional identity[163, 170, 207, 208]. Moreover, in the context of human MN differentiation, a recent study reported a shift in the proportion of MNs expressing the MMC marker LHX3 or the LMC marker FOXP1 when SHH signaling was activated via a combination of SAG and Purmorphamine instead of recombinant SHH[161]. This exquisite sensitivity of differentiating MNs to alterations in experimental protocol emphasizes the need to continually evaluate MN differentiation strategies and also presents a new avenue for the optimization of further MN subtype specification.

Although the basic principles of MN specification are well established, many groups have reported differences in the timing and efficiency of differentiation, as well as the identity of the resulting MNs. This variability may arise from overt differences in protocols, such as the combination, concentration, and timing of addition of specific growth factors, as well as less

transparent differences such as the cellular density or precise media composition used to culture cells following specification. Concern about the extent to which minor modifications in protocols alter the identity of the resulting MNs is amplified because most groups rely on expression of transgenic reporters or a small handful of canonical marker genes, which may not be able to report on subtle MN subtype specific differences. Given the potential impact of these modifications on downstream studies such as *in vitro* disease modeling of MN disorders, continued effort to both carefully interrogate the effects of altering differentiation protocols and to standardize methods and analyses across multiple labs is crucial.

1.8 Evaluation of MNs produced *in vitro*

MNs can be assessed according to four primary characteristics which provide insights into the equivalency of *in vitro* derived MNs to *bona fide* cells; i) neuronal morphology and expression of characteristic MN marker genes, ii) characteristic electrophysiological activity and response to stimuli, iii) formation of functional neuromuscular junctions, iv) engraftment into the spinal cord *in vivo*.

1.8.1 Morphology and marker analyses

When cultured in isolation, MNs exhibit unipolar morphology with a single axon extending from the soma, which is elaborated with dendrites. Although in dense cultures distinguishing the axon from surrounding dendrites can be difficult, this is aided by immunostaining of the Microtubule associated protein 2 (MAP2), which marks proximal dendrites. Additional immunostaining of neuronal cytoskeletal proteins, such as β-III Tubulin (recognized with Tuj1 antibody), as well as evaluation of the phosphorylation status of neurofilaments using SMI antibodies allow full appreciation of the complicated neuronal morphology typically present in MNs (Figure 1.5A).

A critical step towards the development of methods to generate specific cell types *in vitro* is the selection of appropriate cell type specific markers that can allow the identification of differentiated cell types without the anatomical information provided *in vivo*. Like all other neurons, MNs are postmitotic, a property which can be determined by lack of BrdU incorporation into cellular DNA or by the lack of cell proliferation antigens such as Ki67. MNs can be further distinguished from other neurons based on the expression of canonical MN identity transcription factors, including Islet1 and Hb9, as well as markers of a more mature and cholinergic MN phenotype, such as the biosynthetic enzyme Choline acetyltransferance (ChAT), and the Vesicular acetylcholine transporter (VAChT)[145, 161, 165, 166, 209] (Figure 1.5A). Expression of Islet1 and Hb9 transcription factors is thought to be common to the majority of MNs, however as development proceeds, it is clear that some MNs express different subsets of the aforementioned proteins[161, 210]. The use of a single marker of MNs is further complicated by the observation that some 'canonical' MN genes, such as Islet1, are also expressed in other neuronal cell types[211].

A basic appreciation of MN subtype can be gained by determining the expression profile of Hox genes and accessory factors such as FoxP1[161]. In addition to immunocytochemistry, other methods like *in situ* hybridization or single-cell qRT-PCR, can be used to determine the expression of MN genes in single cells. It should be emphasized that although expression of canonical MNs markers has been shown to be a reliable indicator of other MN characteristics, expression of a small number of markers alone is an insufficient metric to evaluate the success of differentiation strategies. For this reason, genome-wide analysis of transcriptional profiles of purified MNs by RNA sequencing or microArrays represents a more effective strategy for

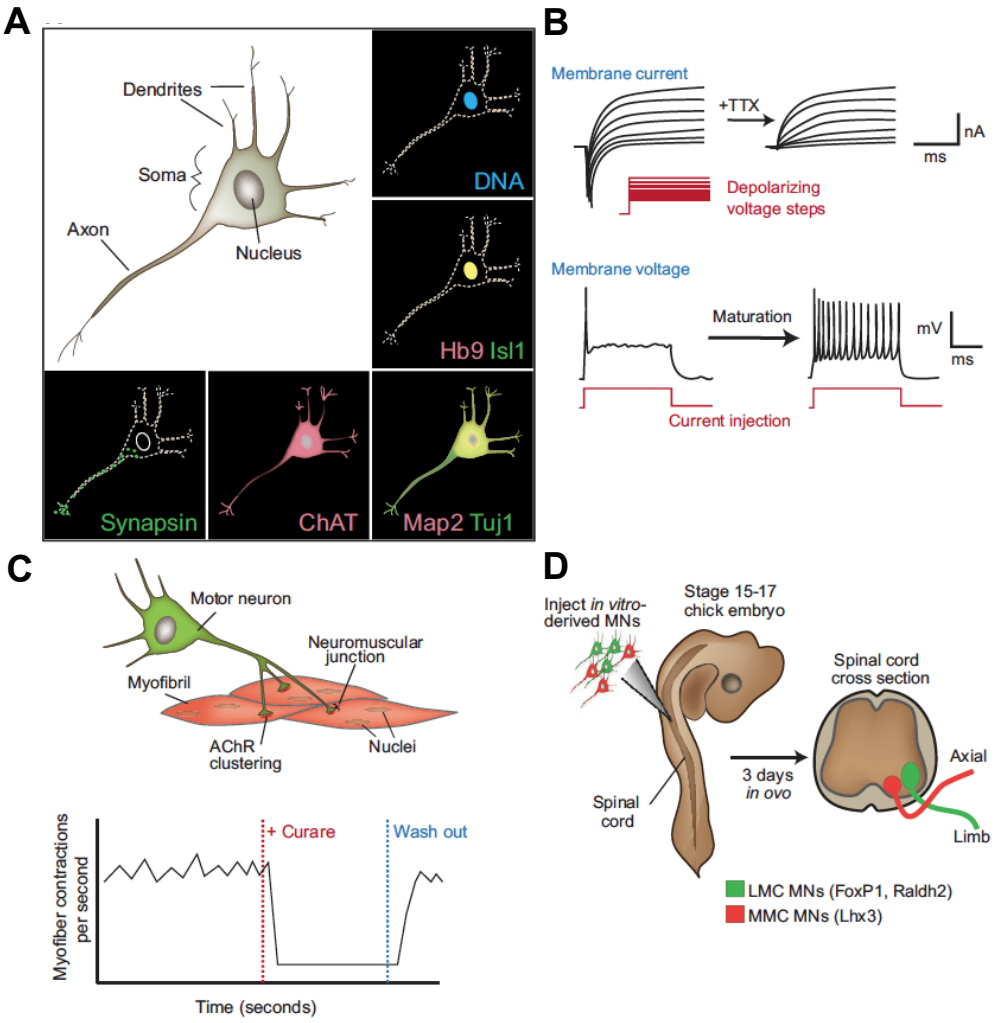

Figure 1.5 Strategies to evaluate motor neurons (MNs) generated *in vitro*.
A. Unipolar neuronal morphology as well as expression of at least a subset of MN markers represents a minimal suggested requirement towards classification of *in vitro*-derived cells as MNs. Neuronal morphology can be additionally assessed by immunostaining for cytoskeletal proteins, such as β-III TUBULIN (recognized with TUJ1 antibody) and MAP2. Whereas β-III TUBULIN is present in both axons and dendrites, MAP2 expression is limited to proximal dendrites. MN identity can be evaluated based on the expression of transcription factors, such as HB9 and ISLET1, which are frequently co-expressed. However, subsets of MNs may express only one of these markers. Although typically not present immediately following differentiation, further maturation in culture of differentiated MNs results in the expression of synaptic markers, such as SYNAPSIN, and biosynthetic enzymes required for the cholinergic activity of MNs, such as ChAT. Additional staining for column-specific markers, such as FOXP1 (not shown), can further illuminate the specific subtypes of MNs generated. **B.** Electrophysiological activity of MNs. Top: voltage clamp recordings of membrane current in response to depolarizing voltage steps show fast inactivating outward currents that are eliminated following addition of tetrodotoxin (TTX). Bottom: relatively immature MNs exhibit single action potentials in response to current injection, whereas repetitive action potential firing is characteristic of functional maturation. **C.** Co-culture of MNs with multi-nucleated myofibrils allows interrogation of neuromuscular junction (NMJ) formation. Functional NMJs elicit myofiber contraction, which can be blocked with curare, a reversible inhibitor of acetylcholine receptors (AchRs). Following removal of curare (washout) myofibers innervated by functional NMJs will resume contraction. **D.** Engraftment of *in vitro*-derived MNs into the developing spinal cord represents a particularly stringent method for evaluating MN phenotype. Both the cell body position and axon projection pattern can be influenced by intrinsic MN subtype properties. The extent to which appropriate engraftment in the chick embryo mimics human or mouse motor neuron physiology remains an open question.

evaluating MNs obtained through different methods in order to assess their equivalency to *bona fide* cells.

1.8.2 Electrophysiological activity

The primary function of all neurons is transmission of electrochemical signals, a property that requires the maintenance of voltage gradients across the cell membrane. The precise combination of ion pumps, ion channels and receptors embedded within the membrane allow different types of neurons to interpret and respond uniquely to stimuli. Electrophysiological recordings have demonstrated that PS cell-derived MNs exhibit many of the electrical characteristics relevant to motor neuron function and circuitry, including a response to applications of GABA, glutamate, and glycine with increased inward currents, indicating expression of proper functional receptors for these neurotransmitters[145, 161] (Figure 1.5B). These cells can also display spontaneous activity, express a range of voltage-activated channels, and can fire action potentials in response to short current injections, as well as generate calcium transients in response to kainate[145, 161]. Time-in-culture-dependent electrophysiological phenotypes that have also been observed in PS cell-derived MNs include decrease in input resistance, spike frequency adaptation and rebound action potential firing[162, 212].

As in the case of molecular markers of MNs, stereotypical electrophysiological response alone is insufficient to categorize cells as MNs. It is also important to note that different types of MNs exhibit differences in excitability and firing patterns, and that these responses evolve as MNs mature[182]. For example, rat embryonic and postnatal MNs exhibit marked differences in amplitude and rate of action potentials as well as differing responses to neurotransmitters[213]. Because patch clamping individual cells represents a technically challenging and low throughput method, it is frequently difficult to determine the extent to which

electrophysiological characteristics vary between cells, even among cells of the same culture. New technological advances such as multi-electrode arrays and 'all optical' electrophysiology recordings[214] will facilitate the interrogation of global and single-cell electrical properties, respectively, which in turn will offer the exciting opportunity to screen multiple genetic backgrounds or drug treatments for altered electrophysiological activity.

1.8.3 Formation of neuromuscular junctions *in vitro* and *in vivo* engraftment

The principle function of MNs in vivo is to innervate target muscles and integrate signals from the CNS to allow coordinated muscle contraction and body movement. Thus, the ultimate evidence that *in vitro*-derived MNs recapitulate their *in vivo* counterparts is the ability to reproducibly engraft into the adult spinal cord, project to appropriate targets, and to restore connectivity of a damaged CNS through formation of neuromuscular junctions (NMJs).

At the most basic level, it is clear that both mouse and human MNs differentiated from PS cells can form functional NMJs *in vitro* when co-cultured with muscle fibers[166, 167, 169, 212] (Figure 1.5C). Clustering of Acetylcholine Receptors on myotubes adjacent to developing axons is observed within one day of co-culture with MNs differentiated from mouse ES or iPS cells; and as early as two days after initiation of co-culture, small endplate potentials can be detected by patch clamping innervated myotubes[212, 215]. In addition to electrophysiological responses to differentiated MNs, innervated myotubes begin to exhibit coordinated contractions, which can be abrogated with the reversible acetylcholine receptor inhibitor curare[166, 215, 216] (Figure 1.5C). Although clustering of myotube acetylcholine receptors is a hallmark of NMJ formation, it is worth noting that different substrates can promote this clustering, even in the absence of MNs[217, 218]. Thus, it is critical to also evaluate the functionality of NMJs. Recent advances in the optogenetics field have presented the possibility

of engineering MNs which express light-activated channelrhodopsins such that neuronal activity, and as a consequence, myotube contraction, can be induced simply by shining light of a specific wavelength onto the co-cultures[219]. The ability to tightly control MN activation should allow more in depth studies of the synaptic junction formed *in vitro* and could provide a method to control MN activity when implanted *in vivo*. Moreover, as neuromuscular junctions have been shown to undergo age-related degeneration in both normal mice[220] and in models of ALS[221], it will be particularly interesting to determine if these events can be recapitulated and manipulated *in vitro*.

In addition to forming functional neuromuscular junctions with co-cultured myotubes, transplantation experiments have shown that *in vitro*-derived MNs are capable of integrating into the developing spinal cord. Perhaps due to the ease of manipulation, most studies have been performed using chick embryos[119, 161, 166, 209, 215, 216]. For instance, transplantation of differentiated MNs and interneurons from an *Hb9::*GFP reporter ES cell line into the chick neural tube demonstrated survival of many GFP^+ MNs after transplantation. Importantly, although the dorso-ventral position of the graft was not controlled, GFP^+ MNs settled in the ventral-lateral domain, while interneurons (marked by a rodent specific antibody to Lim2) were observed in the dorsoventral domain[166]. In addition, grafted *Hb9::*GFP^+ MNs differentiated from both mouse and human ES cell lines have been shown to project axons into the periphery where they reached muscle targets and displayed elaborated terminals expressing multiple synaptic markers[119, 161, 166, 209].

Evidence that *in vitro*-derived MNs can correctly engraft into the developing spinal cord is further supported by an elegant study using different small molecules to direct the differentiation of mouse ES cells into two specific MN subtypes: cervical MMC MNs and

brachial LMC MNs. When GFP labeled LMC MNs were mixed with RFP labeled MMC MNs and injected into the chick neural tube, the cell bodies of these neurons settled in the appropriate domains within the spinal cord and their axons projected to targets predicted by their transcription factor expression[207] (Figure 1.5D). A more recent study demonstrated that MNs differentiated from genetically-corrected SMA iPS cells, could survive transplantation and correctly engraft in the spinal cord of a one day old mouse model of SMA[124]. Furthermore, these cells could ameliorate disease phenotypes and extend the life span of *SMN* mutant mice, at least in part by providing neurotrophic support[124].

In general, transplantation studies provide strong evidence that PS cell-derived MNs bear strong resemblance to their *in vivo* counterparts. However, these studies are technically challenging, largely qualitative and provide limited opportunities for mechanistic study. As the ability to generate MNs *in vitro* through diverse methods continues to progress it is critical to reach a consensus of best practices for evaluating MNs. Taken in isolation, gene expression, electrophysiological response, and NMJ formation *in vitro* are, in our view, insufficient indicators of the success of MN differentiation strategies. Instead, we propose a multi-tiered approach that combines each of these metrics to allow diverse aspects of MN biology to be evaluated in the differentiated cells. Incorporation of a stringent 'quality control' step in the production of differentiated MNs will increase the downstream utility of these cells, particularly in studies attempting to model and elucidate MN disease processes.

1.9 Using human differentiated MNs for the study of ALS

The ability to produce large quantities of human differentiated cells exhibiting MN properties *in vitro*, combined with the opportunity granted by iPS cell technology to generate cell lines of multiple ALS-relevant genotypes, has dramatically changed the landscape of ALS

research. Since the first report, less than a decade ago, of iPS cells and differentiated MNs generated from a familial ALS patient with a mutation in the *SOD1* gene[147], several studies, including some of the work presented in this thesis, have now documented the utility of human MNs differentiated from ES and iPS cells for the study of ALS (Table 1.1). Remarkably, these studies have demonstrated, not only that MNs differentiated from patient-specific iPS cells can recapitulate *in vitro* some of the features associated with disease, but also that they can provide insights into novel potential disease mechanisms and therapeutic strategies (Table 1.1). The success of stem cell-based approaches for the study of neurodegeneration is not limited to ALS research[146, 222]. Molecular, cellular and functional phenotypes in human differentiated neurons associated with several other neurological disorders such as Parkinson's disease[151, 152, 223, 224], Lesch-Nyhan syndrome[225], Huntington's disease[226], SMA[124, 125], Alzheimer's disease[160, 227], Schizophrenia[156], and Rett syndrome[127], have also been documented in the past few years.

In the case of ALS, various disease-related phenotypes have been described in iPS cell lines established from sporadic cases and from patients with mutations in the ALS-linked genes *SOD1*, *VAPB/ALS8, TDP43, C9ORF72,* and *FUS* (Table 1.1). The reported *in vitro* phenotypes, which are summarized in Table 1.1, include cell death, cytoskeletal abnormalities, protein aggregation, ER and mitochondrial dysfunction, alterations in RNA metabolism, and changes in the electrical activity of the cells, with both hyper- and hypo-excitability observed (Table 1.1). Of significance, the establishment of human stem cell-based experimental systems has also facilitated the exploration of different strategies to mitigate some of these pathological phenotypes, like the use of *C9ORF72* antisense oligonucleotides to target RNA toxicity[149], or the chemical activation of voltage-gated potassium channels to block membrane hyperexcitability and improve cell survival[119, 120] (Table 1.1).

Table 1.1: Published *in vitro* studies of ALS using human pluripotent stem cell-derived MNs

Year Published [Ref.]	ES cells/ iPS cells/ both	ALS-associated variant	Reported Disease-Related *in vitro* Phenotype	Additional Comments
2008 [1]	iPS cell	SOD1L144F	-	First report of patient-specific iPS cell lines.
2008 [2]	ES cell line	Co-culture with human primary astrocytes overexpressing SOD1G37R	* Selective motor neuron loss, which correlated with increased inflammatory response in SOD1-mutant astrocytes. * Activation in mutant astrocytes of NOX2 to produce toxic superoxide. * NOX2 inhibitor, apocynin, prevented the loss of motor neurons.	Validation of non-cell autonomous contribution to ALS using human cells.
2008 [3]	ES cell line	Co-culture with murine primary glial cells overexpressing SOD1G93A	* Selective sensitivity of motor neurons, but not interneurons, to toxic effect of mutant SOD1 glial cells. * Toxicity mediated, at least partially by prostaglandin signaling.	* Validation of non-cell autonomous contribution to ALS using human cells. * Describes generation of HUES3 *Hb9::GFP* cell line.
2011 [4]	iPS and ES cell lines	*SOD1L144F *SOD1G85S	-	Characterization of differentiation efficiency into MNs. No differences between ES and iPS cells, or between ALS or control genotypes.
2011 [5]	iPS cell lines	*ALS8-VAPBP56S	* Reduced VAPB protein levels in ALS8-derived motor neurons. * In contrast to over-expression systems, cytoplasmic aggregates could not be identified.	
2012 [6]	iPS cell lines	*TDP43M337V	* Elevated levels of soluble and detergent-resistant TDP-43 protein * Decreased MN survival in longitudinal studies * Increased vulnerability to antagonism of the PI3K pathway.	
2012 [7]	iPS cell lines	*TDP43Q343R *TDP43M337V *TDP43G298S	* Increased mutant TDP-43 protein in detergent-insoluble fractions. * Increased number of TDP-43 immunoreactive cytosolic puncti ('aggregates') * Upregulation of genes involved in RNA metabolism and downregulation of genes encoding cytoskeletal proteins. * No difference in MN survival under basal conditions, but increased susceptibility to arsenite-induced cell death. * A histone acetyltransferase inhibitor (anacardic acid) rescued some of the abnormal motor neuron phenotypes.	

Table 1.1: Published *in vitro* studies of ALS using human pluripotent stem cell-derived MNs (continued)

Year Published [Ref.]	ES cells/ iPS cells/ both	ALS-associated variant	Reported Disease-Related *in vitro* Phenotype	Additional Comments
2013 [8]	ES/iPS cell lines	*SOD1L144F *TDP43M337V	* A small molecule inhibitor (kenpaullone) of GSK-3 and HGK kinases identified in a screen using mouse ES cell-derived MNs, was shown to also promote the survival of HUES3 *Hb9::*GFP^+ MNs, and MNs differentiated from patient iPS cells expressing SOD1 or TDP-43 variants.	* SOD1L144F cell line is the same from Refs [1] and [4]. * TDP43M337V cell line is from same patient as in [6]
2013 [9]	iPS cell lines	**C9ORF72* intronic (GGGGCC) repeat expansions (exp)	* Detection of pathological intranuclear GGGGCCexp RNA foci. * Dysregulated gene expression different from mutant SOD1 transcriptome. * Sequestration of GGGGCCexp RNA binding protein ADARB2. * Increased susceptibility to glutamate induced excitotoxicity. * Cytosolic RAN (Repeat Associated Non-ATG) translation peptides detected. * Phenotypes were rescued with antisense oligonucleotide (ASO) therapeutics to the C9ORF72 transcript or repeat expansion.	* For the first time, a form of ALS is studied with human differentiated MNs before the development of animal models. * Findings suggest possible toxic gain-of-function mechanisms mediated by the GGGGCCexp.
2013 [10]	iPS cell lines	**C9ORF72* intronic (GGGGCC) repeat expansions (exp)	* No significant loss of *C9ORF72* expression observed * *C9ORF72* RNAi was not toxic to cultured human motor neurons. * Increased transcription of the repeat and accumulation into RNA foci. * Repeat-containing RNA foci colocalized with hnRNPA1 and Pur-α, suggesting potential alterations to RNA metabolism. * Dysregulation of genes involved in membrane excitability * Hypoexcitability * ASO targeting the *C9ORF72* transcript suppressed RNA foci formation and reversed gene expression alterations.	
2013 [11]	iPS cell lines	Sporadic ALS (sALS) (16 different patients)	* Small intranuclear TDP-43 aggregates detected in MNs in 3/16 genotypes. * Phenotype could be ameliorated following treatment with cardiac glycosides.	Only study thus far to have characterized a large cohort of sALS-patient iPS cell lines.
2013 [12]	iPS cell lines	*TDP43A90V	* Increased susceptibility to cellular stress induced by 10 nM straurosporine. * Reduced total TDP-43 levels. * Increased percentage of cells with mislocalized (cytoplasmic) TDP-43 * Reduced levels of microRNA-9 (miR-9)	

Table 1.1: Published *in vitro* studies of ALS using human pluripotent stem cell-derived MNs (continued)

Year Published [Ref.]	ES cells/ iPS cells/ both	ALS-associated variant	Reported Disease-Related *in vitro* Phenotype	Additional Comments
2013 [13]	iPS cell line	*TDP43M337V	* Generation of functional astroglia from the iPS cell lines * Mutant astrocytes exhibited increased levels of TDP-43, subcellular mislocalization of TDP-43, and decreased cell survival * Co-culture experiments of mutant TDP-43 astrocytes with human differentiated MNs did not indicate non-cell autonomous toxic pathways mediated by TDP-43, as is the case with mutant SOD1.	* First study to look at the effect of iPS cell-derived astrocytes expressing a TDP-43 variant * TDP43M337V iPS cell line used is the same as in [6]
2014 [14]	iPS cell lines	*SOD1A4V **C9ORF72* (GGGGCCexp)	* Reduced survival of $SOD1^{+/A4V}$ MNs. * Reduced soma size * Dysregulated mitochondrial genes and disturbed mitochondrial morphology. * Induction of ES stress and unfolded protein response (UPR) pathways. * Accumulation of insoluble SOD1 upon proteasome inhibition * Dysregulation of transcripts in *C9ORF72*exp MNs, a subset of which overlapped with the genes responsive to mutant SOD1. * Genetic correction of the mutant *SOD1A4V* allele by gene targeting rescued several of the phenotypes.	* Along with [15, 16], they represent first ALS studies with iPS cells using genome-editing technology to more rigorously demonstrate *in vitro* phenotypes are mediated by expression of the ALS-associated variant. * Part of this study includes work described in Chapter 2.
2014 [15]	iPS cell lines	*SOD1D90A	* Detection of small SOD1 aggregates * Detection of NEUROFILAMENT inclusions in cytoplasm and neurites. * Neurite degeneration (presence of 'bead-like' swellings) * Altered NEUROFILAMENT subunit proportion, with reduction of NF-L * All comparisons included isogenic control and "non-MN" cells.	
2014 [16]	iPS cell lines	*SOD1A4V *SOD1D90A *SOD1G85S *FUSM511X *FUSH517Q **C9ORF72* (GGGGCCexp)	* Increased membrane excitability for MNs expressing different ALS-variants * Genetic correction of the mutant *SOD1A4V* allele by gene targeting rescued the hyperexcitability phenotype. * Retigabine, a Kv7 channel activator, both blocked the hyperexcitability phenotype and improved MN survival for cells expressing mutant SOD1.	* SOD1A4V iPS cell lines are the same as in [14] * Part of this study includes work described in Chapter 2.

Table 1.1: Published *in vitro* studies of ALS using human pluripotent stem cell-derived MNs (continued)

Year Published [Ref.]	ES cells/ iPS cells/ both	ALS-associated variant	Reported Disease-Related *in vitro* Phenotype	Additional Comments
2014 [17]	ES cell line	Co-culture of ES cell-derived MNs with human primary astrocytes obtained from sporadic ALS cases	* Non-cell autonomous neurotoxic activity mediated by the induction of necroptotic pathways	
2014 [18]	iPS cell lines	*TDP43G298S *TDP43A315T *TDP43M337V	* Deficits in the axonal transport of mRNA granules containing the TDP-43 bound *NEUROFILAMENT* mRNA	* TDP43M337V is the same iPS cell line used in [6] * Part of this study includes work described in Chapter 4.
2014 [19]	iPS cell lines	*TDP43M337V	* Induction of autophagy by a family of small molecules improved the survival of iPS cell-differentiated MNs and astrocytes expressing TDP43M337V.	TDP43M337V is the same iPS cell line used in [6]
2014 [20]	ES cell line	Co-culture with murine glial cells overexpressing SOD1G93A and with pharmacological and genetic modulation of the prostanoid receptor DP1	* Non-cell autonomous toxicity to human differentiated MNs mediated by DP1 signaling in microglial cells. * Chemical inhibition or genetic ablation of DP1 in glial cells ameliorated their neurotoxic activity. * Genetic ablation of DP1 in SOD1G93A mice extended their life span, decreased microglia activation reduced motor neuron loss.	One of the first studies to validate in an animal model of ALS a therapeutic target first identified in assays utilizing human differentiated MNs.
2015 [21]	iPS cell lines	*TDP43M337V **C9ORF72* (GGGGCCexp)	* Dynamic electrical activity of MNs expressing either ALS-variant, with initial hyperexcitability (at 2 weeks), which eventually progressed to reduced excitation (7-10 weeks). * Loss of both fast inactivating Na^+ currents and persistent voltage-activated K^+ currents after 7-10 weeks in culture.	This study demonstrates the importance of characterizing the same phenotype at multiple time-points, and helps explains conflicting findings by [10] and [16], regarding the membrane excitability of *C9ORF72* (GGGGCCexp) MNs.

Table 1.1: Published *in vitro* studies of ALS using human pluripotent stem cell-derived MNs (continued)

References in Table

1. Dimos, J.T. et al. Induced pluripotent stem cells generated from patients with ALS can be differentiated into motor neurons. *Science* **321**, 1218-21 (2008).
2. Marchetto, M.C. et al. Non-cell-autonomous effect of human SOD1 G37R astrocytes on motor neurons derived from human embryonic stem cells. *Cell Stem Cell* **3**, 649-57 (2008).
3. Di Giorgio, F.P., Boulting, G.L., Bobrowicz, S. & Eggan, K.C. Human embryonic stem cell-derived motor neurons are sensitive to the toxic effect of glial cells carrying an ALS-causing mutation. *Cell Stem Cell* **3**, 637-48 (2008).
4. Boulting, G.L. et al. A functionally characterized test set of human induced pluripotent stem cells. *Nature biotechnology* (2011).
5. Mitne-Neto, M. et al. Downregulation of VAPB expression in motor neurons derived from induced pluripotent stem cells of ALS8 patients. *Hum Mol Genet* **20**, 3642-52 (2011).
6. Bilican, B. et al. Mutant induced pluripotent stem cell lines recapitulate aspects of TDP-43 proteinopathies and reveal cell-specific vulnerability. *Proc Natl Acad Sci U S A* **109**, 5803-8 (2012).
7. Egawa, N. et al. Drug screening for ALS using patient-specific induced pluripotent stem cells. *Sci Transl Med* **4**, 145ra104 (2012).
8. Yang, Y.M. et al. A small molecule screen in stem-cell-derived motor neurons identifies a kinase inhibitor as a candidate therapeutic for ALS. *Cell Stem Cell* **12**, 713-26 (2013).
9. Donnelly, C.J. et al. RNA toxicity from the ALS/FTD C9ORF72 expansion is mitigated by antisense intervention. *Neuron* **80**, 415-28 (2013).
10. Sareen, D. et al. Targeting RNA foci in iPSC-derived motor neurons from ALS patients with a C9ORF72 repeat expansion. *Sci Transl Med* **5**, 208ra149 (2013).
11. Burkhardt, M.F. et al. A cellular model for sporadic ALS using patient-derived induced pluripotent stem cells. *Mol Cell Neurosci* **56**, 355-64 (2013).
12. Zhang, Z. et al. Downregulation of microRNA-9 in iPSC-derived neurons of FTD/ALS patients with TDP-43 mutations. *PLoS One* **8**, e76055 (2013).
13. Serio, A. et al. Astrocyte pathology and the absence of non-cell autonomy in an induced pluripotent stem cell model of TDP-43 proteinopathy. *Proc Natl Acad Sci U S A* **110**, 4697-702 (2013).
14. Kiskinis, E. et al. Pathways disrupted in human ALS motor neurons identified through genetic correction of mutant SOD1. *Cell Stem Cell* **14**, 781-95 (2014).
15. Chen, H. et al. Modeling ALS with iPSCs reveals that mutant SOD1 misregulates neurofilament balance in motor neurons. *Cell Stem Cell* **14**, 796-809 (2014).
16. Wainger, B. et al. Intrinsic Membrane Hyperexcitability of ALS Patient-Derived Motor Neurons. *Cell Reports* (2014).
17. Re, D.B. et al. Necroptosis drives motor neuron death in models of both sporadic and familial ALS. *Neuron* **81**, 1001-8 (2014).
18. Alami, N.H. et al. Axonal transport of TDP-43 mRNA granules is impaired by ALS-causing mutations. *Neuron* **81**, 536-43 (2014).
19. Barmada, S.J. et al. Autophagy induction enhances TDP43 turnover and survival in neuronal ALS models. *Nat Chem Biol* **10**, 677-85 (2014).
20. de Boer, A.S. et al. Genetic validation of a therapeutic target in a mouse model of ALS. *Sci Transl Med* **6**, 248ra104 (2014).
21. Devlin, A.C. et al. Human iPSC-derived motoneurons harbouring TARDBP or C9ORF72 ALS mutations are dysfunctional despite maintaining viability. *Nat Commun* **6**, 5999 (2015).

Additionally, it is worth noting that human differentiated MNs obtained from 'wild-type' ES cells have also proved valuable in the study of ALS, particularly in the understanding of non-cell autonomous contributions to pathogenesis mediated by astrocytes and microglia[27, 32, 35] (Table 1.1). Lastly, considering the long and rapidly increasing list of ALS-associated genes of diverse cellular functions[40, 41, 43], and the amount of time required to create transgenic mouse models, the ability to more immediately study these ALS variants using human stem cell-based models, will no doubt help uncover common disease mechanisms and candidate targets for therapeutic interventions. However, it is critical to keep in mind that human differentiated MNs will be most powerfully leveraged as tools for biomedical research when these new mechanistic insights and potential therapeutics are further validated in animal models, neuropathological samples, and ultimately, ALS patients.

1.10 Concluding remarks and perspectives

Decades of research into CNS development, stem cell biology and nuclear reprogramming have been synthesized to allow the *in vitro* generation of human differentiated cells bearing motor neuron phenotypes and ALS-relevant genotypes. The desire to establish novel and clinically informative *in vitro* models of ALS using human differentiated MNs inspired the work presented in the next chapters of this thesis. These studies, along with other reports, have demonstrated the utility of human stem cell-based approaches for neurological research.

While progress in the past few years has been remarkable, substantial challenges still remain. The molecular diversity of MN subtypes *in vivo* is only partially understood. Perhaps as a consequence of this, only a small number of markers are currently used to evaluate MN subtypes generated *in vitro*, and the extent to which altering methods of MN production may influence the identity and phenotype of the resulting cells is largely unknown. The ability to

differentiate and enrich for specific MN subtypes is significant in the context of ALS studies, given selective susceptibility in patients of different subclasses of MNs to disease processes. For instance, MNs of the oculomotor complex in the midbrain controlling eye movements, and MNs of sacral spinal cord controlling bowel and bladder function are preferentially spared.

Regardless of the specific MN production strategy, downstream disease-related phenotypic assays warrant careful consideration of the experimental conditions used for plating and culturing these cells. These include variations in the methods of dissociation, cell density, substrate, media composition, cellular heterogeneity, and time in culture. Without controlling for and understanding these variables, we run into the risk of comparing the MN 'apples' generated and cultured by one protocol or in one laboratory to the MN 'oranges' generated by another.

Finally, the use of recent advances in genome-editing technologies to create isogenic cell lines will impart more rigorous methods to compare disease and control neurons in phenotypic assays related to pathogenic processes. Needless to say, human cellular models alone will not be able to produce clinically important read-outs of ALS, like reduced forced vital capacity, swallowing dysfunction, dysarthria, or limb motor impairment. However, recapitulation of key molecular and cellular events involved in disease could prove of great significance to the understanding and treatment of this fatal disorder.

1.11 References

1. Bauby, J.-D. The diving bell and the butterfly (A.A. Knopf : Distributed by Random House, New York, 1997).

2. Purves, D. Neuroscience (Sinauer, Sunderland, Mass., 2008).

3. Shoemaker, L.D. & Arlotta, P. Untangling the cortex: Advances in understanding specification and differentiation of corticospinal motor neurons. *Bioessays* **32**, 197-206 (2010).

4. Woodworth, M.B., Custo Greig, L., Kriegstein, A.R. & Macklis, J.D. SnapShot: cortical development. *Cell* **151**, 918-918 e1 (2012).

5. Greig, L.C., Woodworth, M.B., Galazo, M.J., Padmanabhan, H. & Macklis, J.D. Molecular logic of neocortical projection neuron specification, development and diversity. *Nat Rev Neurosci* (2013).

6. Arlotta, P. & Berninger, B. Brains in metamorphosis: reprogramming cell identity within the central nervous system. *Curr Opin Neurobiol* **27**, 208-14 (2014).

7. Rowland, L.P. How amyotrophic lateral sclerosis got its name: the clinical-pathologic genius of Jean-Martin Charcot. *Arch Neurol* **58**, 512-5 (2001).

8. Andersen, P.M. & Al-Chalabi, A. Clinical genetics of amyotrophic lateral sclerosis: what do we really know? *Nat Rev Neurol* **7**, 603-15 (2011).

9. Ravits, J. et al. Deciphering amyotrophic lateral sclerosis: what phenotype, neuropathology and genetics are telling us about pathogenesis. *Amyotroph Lateral Scler Frontotemporal Degener* **14 Suppl 1**, 5-18 (2013).

10. Dion, P.A., Daoud, H. & Rouleau, G.A. Genetics of motor neuron disorders: new insights into pathogenic mechanisms. *Nat Rev Genet* **10**, 769-82 (2009).

11. Kiernan, M.C. et al. Amyotrophic lateral sclerosis. *Lancet* **377**, 942-55 (2011).

12. Pasinelli, P. & Brown, R.H. Molecular biology of amyotrophic lateral sclerosis: insights from genetics. *Nat Rev Neurosci* **7**, 710-23 (2006).

13. Miller, R.G., Mitchell, J.D. & Moore, D.H. Riluzole for amyotrophic lateral sclerosis (ALS)/motor neuron disease (MND). *Cochrane Database Syst Rev* **3**, CD001447 (2012).

14. Al-Chalabi, A. et al. Genetic and epigenetic studies of amyotrophic lateral sclerosis. *Amyotroph Lateral Scler Frontotemporal Degener* **14 Suppl 1**, 44-52 (2013).

15. Cady, J. et al. Amyotrophic lateral sclerosis onset is influenced by the burden of rare variants in known amyotrophic lateral sclerosis genes. *Ann Neurol* **77**, 100-13 (2015).

16. van Blitterswijk, M. et al. Evidence for an oligogenic basis of amyotrophic lateral sclerosis. *Hum Mol Genet* **21**, 3776-84 (2012).

17. Renton, A.E., Chio, A. & Traynor, B.J. State of play in amyotrophic lateral sclerosis genetics. *Nat Neurosci* **17**, 17-23 (2014).

18. van Blitterswijk, M. et al. VAPB and C9orf72 mutations in 1 familial amyotrophic lateral sclerosis patient. *Neurobiol Aging* **33**, 2950 e1-4 (2012).

19. Bruijn, L.I., Miller, T.M. & Cleveland, D.W. Unraveling the mechanisms involved in motor neuron degeneration in ALS. *Annu Rev Neurosci* **27**, 723-49 (2004).

20. Rosen, D.R. Mutations in Cu/Zn superoxide dismutase gene are associated with familial amyotrophic lateral sclerosis. *Nature* **364**, 362 (1993).

21. Deng, H.X. et al. Amyotrophic lateral sclerosis and structural defects in Cu,Zn superoxide dismutase. *Science* **261**, 1047-51 (1993).

22. Fridovich, I. Superoxide radical and superoxide dismutases. *Annu Rev Biochem* **64**, 97-112 (1995).

23. Borchelt, D.R. et al. Superoxide dismutase 1 with mutations linked to familial amyotrophic lateral sclerosis possesses significant activity. *Proc Natl Acad Sci U S A* **91**, 8292-6 (1994).

24. Ratovitski, T. et al. Variation in the biochemical/biophysical properties of mutant superoxide dismutase 1 enzymes and the rate of disease progression in familial amyotrophic lateral sclerosis kindreds. *Hum Mol Genet* **8**, 1451-60 (1999).

25. Reaume, A.G. et al. Motor neurons in Cu/Zn superoxide dismutase-deficient mice develop normally but exhibit enhanced cell death after axonal injury. *Nat Genet* **13**, 43-7 (1996).

26. Xiao, Q. et al. Mutant SOD1(G93A) microglia are more neurotoxic relative to wild-type microglia. *J Neurochem* **102**, 2008-19 (2007).

27. Di Giorgio, F.P., Boulting, G.L., Bobrowicz, S. & Eggan, K.C. Human embryonic stem cell-derived motor neurons are sensitive to the toxic effect of glial cells carrying an ALS-causing mutation. *Cell Stem Cell* **3**, 637-48 (2008).

28. Di Giorgio, F.P., Carrasco, M.A., Siao, M.C., Maniatis, T. & Eggan, K. Non-cell autonomous effect of glia on motor neurons in an embryonic stem cell-based ALS model. *Nat Neurosci* **10**, 608-14 (2007).

29. Boillee, S. et al. Onset and progression in inherited ALS determined by motor neurons and microglia. *Science* **312**, 1389-92 (2006).

30. Yamanaka, K. et al. Astrocytes as determinants of disease progression in inherited amyotrophic lateral sclerosis. *Nat Neurosci* **11**, 251-3 (2008).

31. Clement, A.M. et al. Wild-type nonneuronal cells extend survival of SOD1 mutant motor neurons in ALS mice. *Science* **302**, 113-7 (2003).

32. Marchetto, M.C. et al. Non-cell-autonomous effect of human SOD1 G37R astrocytes on motor neurons derived from human embryonic stem cells. *Cell Stem Cell* **3**, 649-57 (2008).

33. Nagai, M. et al. Astrocytes expressing ALS-linked mutated SOD1 release factors selectively toxic to motor neurons. *Nat Neurosci* **10**, 615-22 (2007).

34. Beers, D.R. et al. Wild-type microglia extend survival in PU.1 knockout mice with familial amyotrophic lateral sclerosis. *Proc Natl Acad Sci U S A* **103**, 16021-6 (2006).

35. de Boer, A.S. et al. Genetic validation of a therapeutic target in a mouse model of ALS. *Sci Transl Med* **6**, 248ra104 (2014).

36. Sreedharan, J. & Brown, R.H., Jr. Amyotrophic lateral sclerosis: Problems and prospects. *Ann Neurol* **74**, 309-16 (2013).

37. Haidet-Phillips, A.M. et al. Astrocytes from familial and sporadic ALS patients are toxic to motor neurons. *Nat Biotechnol* **29**, 824-8 (2011).

38. Frakes, A.E. et al. Microglia induce motor neuron death via the classical NF-kappaB pathway in amyotrophic lateral sclerosis. *Neuron* **81**, 1009-23 (2014).

39. Re, D.B. et al. Necroptosis drives motor neuron death in models of both sporadic and familial ALS. *Neuron* **81**, 1001-8 (2014).

40. Steinberg, K.M., Yu, B., Koboldt, D.C., Mardis, E.R. & Pamphlett, R. Exome sequencing of case-unaffected-parents trios reveals recessive and de novo genetic variants in sporadic ALS. *Sci Rep* **5**, 9124 (2015).

41. Guerreiro, R., Bras, J. & Hardy, J. SnapShot: Genetics of ALS and FTD. *Cell* **160**, 798-798 e1 (2015).

42. Smith, B.N. et al. Exome-wide rare variant analysis identifies TUBA4A mutations associated with familial ALS. *Neuron* **84**, 324-31 (2014).

43. Cirulli, E.T. et al. Exome sequencing in amyotrophic lateral sclerosis identifies risk genes and pathways. *Science* (2015).

44. Ling, S.C., Polymenidou, M. & Cleveland, D.W. Converging mechanisms in ALS and FTD: disrupted RNA and protein homeostasis. *Neuron* **79**, 416-38 (2013).

45. Polymenidou, M. et al. Long pre-mRNA depletion and RNA missplicing contribute to neuronal vulnerability from loss of TDP-43. *Nat Neurosci* **14**, 459-68 (2011).

46. Li, Q. et al. ALS-linked mutant superoxide dismutase 1 (SOD1) alters mitochondrial protein composition and decreases protein import. *Proc Natl Acad Sci U S A* **107**, 21146-51 (2010).

47. Pasinelli, P. et al. Amyotrophic lateral sclerosis-associated SOD1 mutant proteins bind and aggregate with Bcl-2 in spinal cord mitochondria. *Neuron* **43**, 19-30 (2004).

48. Wu, C.H. et al. Mutations in the profilin 1 gene cause familial amyotrophic lateral sclerosis. *Nature* **488**, 499-503 (2012).

49. Swinnen, B. & Robberecht, W. The phenotypic variability of amyotrophic lateral sclerosis. *Nat Rev Neurol* **10**, 661-70 (2014).

50. Van Langenhove, T., van der Zee, J. & Van Broeckhoven, C. The molecular basis of the frontotemporal lobar degeneration-amyotrophic lateral sclerosis spectrum. *Ann Med* **44**, 817-28 (2012).

51. Forman, M.S., Trojanowski, J.Q. & Lee, V.M. TDP-43: a novel neurodegenerative proteinopathy. *Curr Opin Neurobiol* **17**, 548-55 (2007).

52. Neumann, M. et al. Ubiquitinated TDP-43 in frontotemporal lobar degeneration and amyotrophic lateral sclerosis. *Science* **314**, 130-3 (2006).

53. Arai, T. et al. TDP-43 is a component of ubiquitin-positive tau-negative inclusions in frontotemporal lobar degeneration and amyotrophic lateral sclerosis. *Biochem Biophys Res Commun* **351**, 602-11 (2006).

54. Tan, C.F. et al. TDP-43 immunoreactivity in neuronal inclusions in familial amyotrophic lateral sclerosis with or without SOD1 gene mutation. *Acta Neuropathol* **113**, 535-42 (2007).

55. Mackenzie, I.R. et al. Pathological TDP-43 distinguishes sporadic amyotrophic lateral sclerosis from amyotrophic lateral sclerosis with SOD1 mutations. *Ann Neurol* **61**, 427-34 (2007).

56. Buratti, E. & Baralle, F.E. The molecular links between TDP-43 dysfunction and neurodegeneration. *Adv Genet* **66**, 1-34 (2009).

57. Mackenzie, I.R. et al. Nomenclature and nosology for neuropathologic subtypes of frontotemporal lobar degeneration: an update. *Acta Neuropathol* **119**, 1-4 (2010).

58. Kabashi, E. et al. TARDBP mutations in individuals with sporadic and familial amyotrophic lateral sclerosis. *Nat Genet* **40**, 572-4 (2008).

59. Sreedharan, J. et al. TDP-43 mutations in familial and sporadic amyotrophic lateral sclerosis. *Science* **319**, 1668-72 (2008).

60. Van Deerlin, V.M. et al. TARDBP mutations in amyotrophic lateral sclerosis with TDP-43 neuropathology: a genetic and histopathological analysis. *Lancet Neurol* **7**, 409-16 (2008).

61. Yokoseki, A. et al. TDP-43 mutation in familial amyotrophic lateral sclerosis. *Ann Neurol* **63**, 538-42 (2008).

62. Rutherford, N.J. et al. Novel mutations in TARDBP (TDP-43) in patients with familial amyotrophic lateral sclerosis. *PLoS Genet* **4**, e1000193 (2008).

63. Gitcho, M.A. et al. TDP-43 A315T mutation in familial motor neuron disease. *Ann Neurol* **63**, 535-8 (2008).

64. Ayala, Y.M. et al. Structural determinants of the cellular localization and shuttling of TDP-43. *J Cell Sci* **121**, 3778-85 (2008).

65. Buratti, E. & Baralle, F.E. Multiple roles of TDP-43 in gene expression, splicing regulation, and human disease. *Front Biosci* **13**, 867-78 (2008).

66. Buratti, E. et al. Nuclear factor TDP-43 and SR proteins promote in vitro and in vivo CFTR exon 9 skipping. *EMBO J* **20**, 1774-84 (2001).

67. Ou, S.H., Wu, F., Harrich, D., Garcia-Martinez, L.F. & Gaynor, R.B. Cloning and characterization of a novel cellular protein, TDP-43, that binds to human immunodeficiency virus type 1 TAR DNA sequence motifs. *J Virol* **69**, 3584-96 (1995).

68. Lattante, S., Rouleau, G.A. & Kabashi, E. TARDBP and FUS mutations associated with amyotrophic lateral sclerosis: summary and update. *Hum Mutat* **34**, 812-26 (2013).

69. Lagier-Tourenne, C., Polymenidou, M. & Cleveland, D.W. TDP-43 and FUS/TLS: emerging roles in RNA processing and neurodegeneration. *Hum Mol Genet* **19**, R46-64 (2010).

70. Chen-Plotkin, A.S., Lee, V.M. & Trojanowski, J.Q. TAR DNA-binding protein 43 in neurodegenerative disease. *Nat Rev Neurol* **6**, 211-20 (2010).

71. Arnold, E.S. et al. ALS-linked TDP-43 mutations produce aberrant RNA splicing and adult-onset motor neuron disease without aggregation or loss of nuclear TDP-43. *Proc Natl Acad Sci U S A* **110**, E736-45 (2013).

72. Kawahara, Y. & Mieda-Sato, A. TDP-43 promotes microRNA biogenesis as a component of the Drosha and Dicer complexes. *Proc Natl Acad Sci U S A* **109**, 3347-52 (2012).

73. Liu-Yesucevitz, L. et al. Tar DNA binding protein-43 (TDP-43) associates with stress granules: analysis of cultured cells and pathological brain tissue. *PLoS One* **5**, e13250 (2010).

74. Parker, S.J. et al. Endogenous TDP-43 localized to stress granules can subsequently form protein aggregates. *Neurochem Int* **60**, 415-24 (2012).

75. Volkening, K., Leystra-Lantz, C., Yang, W., Jaffee, H. & Strong, M.J. Tar DNA binding protein of 43 kDa (TDP-43), 14-3-3 proteins and copper/zinc superoxide dismutase (SOD1) interact to modulate NFL mRNA stability. Implications for altered RNA processing in amyotrophic lateral sclerosis (ALS). *Brain Res* **1305**, 168-82 (2009).

76. Alami, N.H. et al. Axonal transport of TDP-43 mRNA granules is impaired by ALS-causing mutations. *Neuron* **81**, 536-43 (2014).

77. Tollervey, J.R. et al. Characterizing the RNA targets and position-dependent splicing regulation by TDP-43. *Nat Neurosci* **14**, 452-8 (2011).

78. Lee, E.B., Lee, V.M. & Trojanowski, J.Q. Gains or losses: molecular mechanisms of TDP43-mediated neurodegeneration. *Nat Rev Neurosci* **13**, 38-50 (2012).

79. Zhang, Y.J. et al. Aberrant cleavage of TDP-43 enhances aggregation and cellular toxicity. *Proc Natl Acad Sci U S A* **106**, 7607-12 (2009).

80. Kabashi, E. et al. Gain and loss of function of ALS-related mutations of TARDBP (TDP-43) cause motor deficits in vivo. *Hum Mol Genet* **19**, 671-83 (2010).

81. Xu, Y.F. et al. Wild-type human TDP-43 expression causes TDP-43 phosphorylation, mitochondrial aggregation, motor deficits, and early mortality in transgenic mice. *J Neurosci* **30**, 10851-9 (2010).

82. Tsao, W. et al. Rodent models of TDP-43: recent advances. *Brain Res* **1462**, 26-39 (2012).

83. Igaz, L.M. et al. Dysregulation of the ALS-associated gene TDP-43 leads to neuronal death and degeneration in mice. *J Clin Invest* **121**, 726-38 (2011).

84. Avendano-Vazquez, S.E. et al. Autoregulation of TDP-43 mRNA levels involves interplay between transcription, splicing, and alternative polyA site selection. *Genes Dev* **26**, 1679-84 (2012).

85. Ayala, Y.M. et al. TDP-43 regulates its mRNA levels through a negative feedback loop. *EMBO J* **30**, 277-88 (2010).

86. Ayala, Y.M., Misteli, T. & Baralle, F.E. TDP-43 regulates retinoblastoma protein phosphorylation through the repression of cyclin-dependent kinase 6 expression. *Proc Natl Acad Sci U S A* **105**, 3785-9 (2008).

87. Sephton, C.F. et al. TDP-43 is a developmentally regulated protein essential for early embryonic development. *J Biol Chem* **285**, 6826-34 (2010).

88. Wu, L.S. et al. TDP-43, a neuro-pathosignature factor, is essential for early mouse embryogenesis. *Genesis* **48**, 56-62 (2010).

89. Wu, L.S., Cheng, W.C. & Shen, C.K. Targeted depletion of TDP-43 expression in the spinal cord motor neurons leads to the development of amyotrophic lateral sclerosis-like phenotypes in mice. *J Biol Chem* **287**, 27335-44 (2012).

90. Iguchi, Y. et al. Loss of TDP-43 causes age-dependent progressive motor neuron degeneration. *Brain* **136**, 1371-82 (2013).

91. Yang, C. et al. Partial loss of TDP-43 function causes phenotypes of amyotrophic lateral sclerosis. *Proc Natl Acad Sci U S A* **111**, E1121-9 (2014).

92. Da Cruz, S. & Cleveland, D.W. Understanding the role of TDP-43 and FUS/TLS in ALS and beyond. *Curr Opin Neurobiol* **21**, 904-19 (2011).

93. Schymick, J.C., Talbot, K. & Traynor, B.J. Genetics of sporadic amyotrophic lateral sclerosis. *Hum Mol Genet* **16 Spec No. 2**, R233-42 (2007).

94. Moloney, E.B., de Winter, F. & Verhaagen, J. ALS as a distal axonopathy: molecular mechanisms affecting neuromuscular junction stability in the presymptomatic stages of the disease. *Front Neurosci* **8**, 252 (2014).

95. Perrin, S. Preclinical research: Make mouse studies work. *Nature* **507**, 423-5 (2014).

96. Gladman, M., Cudkowicz, M. & Zinman, L. Enhancing clinical trials in neurodegenerative disorders: lessons from amyotrophic lateral sclerosis. *Curr Opin Neurol* **25**, 735-42 (2012).

97. Yu, J. & Thomson, J.A. Pluripotent stem cell lines. *Genes Dev* **22**, 1987-97 (2008).

98. Thomson, J.A. et al. Embryonic stem cell lines derived from human blastocysts. *Science* **282**, 1145-7 (1998).

99. Cowan, C.A. et al. Derivation of embryonic stem-cell lines from human blastocysts. *N Engl J Med* **350**, 1353-6 (2004).

100. Chen, A.E. et al. Optimal timing of inner cell mass isolation increases the efficiency of human embryonic stem cell derivation and allows generation of sibling cell lines. *Cell Stem Cell* **4**, 103-6 (2009).

101. Mateizel, I. et al. Derivation of human embryonic stem cell lines from embryos obtained after IVF and after PGD for monogenic disorders. *Hum Reprod* **21**, 503-11 (2006).

102. Mateizel, I., Spits, C., De Rycke, M., Liebaers, I. & Sermon, K. Derivation, culture, and characterization of VUB hESC lines. *In Vitro Cell Dev Biol Anim* **46**, 300-8 (2010).

103. Verlinsky, Y. et al. Human embryonic stem cell lines with genetic disorders. *Reprod Biomed Online* **10**, 105-10 (2005).

104. Eiges, R. et al. Developmental study of fragile X syndrome using human embryonic stem cells derived from preimplantation genetically diagnosed embryos. *Cell Stem Cell* **1**, 568-77 (2007).

105. Karumbayaram, S. et al. Human embryonic stem cell-derived motor neurons expressing SOD1 mutants exhibit typical signs of motor neuron degeneration linked to ALS. *Dis Model Mech* **2**, 189-95 (2009).

106. Urbach, A., Schuldiner, M. & Benvenisty, N. Modeling for Lesch-Nyhan disease by gene targeting in human embryonic stem cells. *Stem Cells* **22**, 635-41 (2004).

107. Narsinh, K.H., Plews, J. & Wu, J.C. Comparison of human induced pluripotent and embryonic stem cells: fraternal or identical twins? *Mol Ther* **19**, 635-8 (2011).

108. Takahashi, K. & Yamanaka, S. Induction of pluripotent stem cells from mouse embryonic and adult fibroblast cultures by defined factors. *Cell* **126**, 663-76 (2006).

109. Maherali, N. et al. Directly reprogrammed fibroblasts show global epigenetic remodeling and widespread tissue contribution. *Cell Stem Cell* **1**, 55-70 (2007).

110. Wernig, M. et al. In vitro reprogramming of fibroblasts into a pluripotent ES-cell-like state. *Nature* **448**, 318-24 (2007).

111. Okita, K., Ichisaka, T. & Yamanaka, S. Generation of germline-competent induced pluripotent stem cells. *Nature* **448**, 313-7 (2007).

112. Takahashi, K. et al. Induction of pluripotent stem cells from adult human fibroblasts by defined factors. *Cell* **131**, 861-72 (2007).

113. Park, I.H. et al. Reprogramming of human somatic cells to pluripotency with defined factors. *Nature* **451**, 141-6 (2008).

114. Yu, J. et al. Induced pluripotent stem cell lines derived from human somatic cells. *Science* **318**, 1917-20 (2007).

115. Lowry, W.E. et al. Generation of human induced pluripotent stem cells from dermal fibroblasts. *Proc Natl Acad Sci U S A* **105**, 2883-8 (2008).

116. Nakagawa, M. et al. Generation of induced pluripotent stem cells without Myc from mouse and human fibroblasts. *Nat Biotechnol* **26**, 101-6 (2008).

117. Maherali, N. & Hochedlinger, K. Guidelines and techniques for the generation of induced pluripotent stem cells. *Cell Stem Cell* **3**, 595-605 (2008).

118. Bock, C. et al. Reference maps of human ES and iPS cell variation enable high-throughput characterization of pluripotent cell lines. *Cell* **144**, 439-452 (2011).

119. Kiskinis, E. et al. Pathways disrupted in human ALS motor neurons identified through genetic correction of mutant SOD1. *Cell Stem Cell* **14**, 781-95 (2014).

120. Wainger, B. et al. Intrinsic Membrane Hyperexcitability of ALS Patient-Derived Motor Neurons. *Cell Reports* (2014).

121. Bilican, B. et al. Mutant induced pluripotent stem cell lines recapitulate aspects of TDP-43 proteinopathies and reveal cell-specific vulnerability. *Proc Natl Acad Sci U S A* **109**, 5803-8 (2012).

122. Sareen, D. et al. Targeting RNA foci in iPSC-derived motor neurons from ALS patients with a C9ORF72 repeat expansion. *Sci Transl Med* **5**, 208ra149 (2013).

123. Egawa, N. et al. Drug screening for ALS using patient-specific induced pluripotent stem cells. *Sci Transl Med* **4**, 145ra104 (2012).

124. Corti, S. et al. Genetic correction of human induced pluripotent stem cells from patients with spinal muscular atrophy. *Sci Transl Med* **4**, 165ra162 (2012).

125. Ebert, A.D. et al. Induced pluripotent stem cells from a spinal muscular atrophy patient. *Nature* **457**, 277-80 (2009).

126. Lee, G. et al. Modelling pathogenesis and treatment of familial dysautonomia using patient-specific iPSCs. *Nature* **461**, 402-6 (2009).

127. Marchetto, M.C.N. et al. A model for neural development and treatment of rett syndrome using human induced pluripotent stem cells. *Cell* **143**, 527-39 (2010).

128. Gonzalez, F., Boue, S. & Belmonte, J.C. Methods for making induced pluripotent stem cells: reprogramming a la carte. *Nat Rev Genet* (2011).

129. Fusaki, N., Ban, H., Nishiyama, A., Saeki, K. & Hasegawa, M. Efficient induction of transgene-free human pluripotent stem cells using a vector based on Sendai virus, an RNA virus that does not integrate into the host genome. *Proc Jpn Acad Ser B Phys Biol Sci* **85**, 348-62 (2009).

130. Yu, J. et al. Human induced pluripotent stem cells free of vector and transgene sequences. *Science* **324**, 797-801 (2009).

131. Kaji, K. et al. Virus-free induction of pluripotency and subsequent excision of reprogramming factors. *Nature* **458**, 771-5 (2009).

132. Soldner, F. et al. Parkinson's disease patient-derived induced pluripotent stem cells free of viral reprogramming factors. *Cell* **136**, 964-77 (2009).

133. Kim, D. et al. Generation of human induced pluripotent stem cells by direct delivery of reprogramming proteins. *Cell Stem Cell* **4**, 472-6 (2009).

134. Warren, L. et al. Highly efficient reprogramming to pluripotency and directed differentiation of human cells with synthetic modified mRNA. *Cell Stem Cell* **7**, 618-30 (2010).

135. Huangfu, D. et al. Induction of pluripotent stem cells by defined factors is greatly improved by small-molecule compounds. *Nat Biotechnol* **26**, 795-7 (2008).

136. Li, W. et al. Generation of human-induced pluripotent stem cells in the absence of exogenous Sox2. *Stem Cells* **27**, 2992-3000 (2009).

137. Lin, T. et al. A chemical platform for improved induction of human iPSCs. *Nat Methods* **6**, 805-8 (2009).

138. Zhu, S. et al. Reprogramming of human primary somatic cells by OCT4 and chemical compounds. *Cell Stem Cell* **7**, 651-5 (2010).

139. Chin, M.H. et al. Induced pluripotent stem cells and embryonic stem cells are distinguished by gene expression signatures. *Cell Stem Cell* **5**, 111-23 (2009).

140. Doi, A. et al. Differential methylation of tissue- and cancer-specific CpG island shores distinguishes human induced pluripotent stem cells, embryonic stem cells and fibroblasts. *Nat Genet* **41**, 1350-3 (2009).

141. Lister, R. et al. Hotspots of aberrant epigenomic reprogramming in human induced pluripotent stem cells. *Nature* **471**, 68-73 (2011).

142. Gore, A. et al. Somatic coding mutations in human induced pluripotent stem cells. *Nature* **471**, 63-7 (2011).

143. Bilic, J. & Izpisua Belmonte, J.C. Concise review: Induced pluripotent stem cells versus embryonic stem cells: close enough or yet too far apart? *Stem Cells* **30**, 33-41 (2012).

144. Puri, M.C. & Nagy, A. Concise review: Embryonic stem cells versus induced pluripotent stem cells: the game is on. *Stem Cells* **30**, 10-4 (2012).

145. Boulting, G.L. et al. A functionally characterized test set of human induced pluripotent stem cells. *Nature biotechnology* (2011).

146. Sandoe, J. & Eggan, K. Opportunities and challenges of pluripotent stem cell neurodegenerative disease models. *Nat Neurosci* **16**, 780-9 (2013).

147. Dimos, J.T. et al. Induced pluripotent stem cells generated from patients with ALS can be differentiated into motor neurons. *Science* **321**, 1218-21 (2008).

148. Chen, H. et al. Modeling ALS with iPSCs reveals that mutant SOD1 misregulates neurofilament balance in motor neurons. *Cell Stem Cell* **14**, 796-809 (2014).

149. Donnelly, C.J. et al. RNA toxicity from the ALS/FTD C9ORF72 expansion is mitigated by antisense intervention. *Neuron* **80**, 415-28 (2013).

150. Park, I.-H. et al. Disease-specific induced pluripotent stem cells. *Cell* **134**, 877-86 (2008).

151. Reinhardt, P. et al. Genetic correction of a LRRK2 mutation in human iPSCs links parkinsonian neurodegeneration to ERK-dependent changes in gene expression. *Cell Stem Cell* **12**, 354-67 (2013).

152. Nguyen, H.N. et al. LRRK2 Mutant iPSC-Derived DA Neurons Demonstrate Increased Susceptibility to Oxidative Stress. *Cell Stem Cell* **8**, 267-80 (2011).

153. Cheung, A.Y. et al. Isolation of MECP2-null Rett Syndrome patient hiPS cells and isogenic controls through X-chromosome inactivation. *Hum Mol Genet* (2011).

154. Ku, S. et al. Friedreich's ataxia induced pluripotent stem cells model intergenerational GAA·TTC triplet repeat instability. *Cell Stem Cell* **7**, 631-7 (2010).

155. Liu, J. et al. Generation of induced pluripotent stem cell lines from Friedreich ataxia patients. *Stem Cell Rev* **7**, 703-13 (2010).

156. Brennand, K.J. et al. Modelling schizophrenia using human induced pluripotent stem cells. *Nature* **473**, 221-5 (2011).

157. Chiang, C.H. et al. Integration-free induced pluripotent stem cells derived from schizophrenia patients with a DISC1 mutation. *Mol Psychiatry* **16**, 358-60 (2011).

158. Chamberlain, S.J. et al. Induced pluripotent stem cell models of the genomic imprinting disorders Angelman and Prader-Willi syndromes. *Proc Natl Acad Sci U S A* **107**, 17668-73 (2010).

159. Urbach, A., Bar-Nur, O., Daley, G.Q. & Benvenisty, N. Differential modeling of fragile X syndrome by human embryonic stem cells and induced pluripotent stem cells. *Cell Stem Cell* **6**, 407-11 (2010).

160. Kondo, T. et al. Modeling Alzheimer's disease with iPSCs reveals stress phenotypes associated with intracellular Abeta and differential drug responsiveness. *Cell Stem Cell* **12**, 487-96 (2013).

161. Amoroso, M.W. et al. Accelerated high-yield generation of limb-innervating motor neurons from human stem cells. *J Neurosci* **33**, 574-86 (2013).

162. Takazawa, T. et al. Maturation of spinal motor neurons derived from human embryonic stem cells. *PLoS One* **7**, e40154 (2012).

163. Patani, R. et al. Retinoid-independent motor neurogenesis from human embryonic stem cells reveals a medial columnar ground state. *Nat Commun* **2**, 214 (2011).

164. Chambers, S.M. et al. Highly efficient neural conversion of human ES and iPS cells by dual inhibition of SMAD signaling. *Nat Biotechnol* **27**, 275-80 (2009).

165. Karumbayaram, S. et al. Directed differentiation of human-induced pluripotent stem cells generates active motor neurons. *Stem Cells* **27**, 806-11 (2009).

166. Wichterle, H., Lieberam, I., Porter, J.A. & Jessell, T.M. Directed differentiation of embryonic stem cells into motor neurons. *Cell* **110**, 385-97 (2002).

167. Li, X.J. et al. Specification of motoneurons from human embryonic stem cells. *Nat Biotechnol* **23**, 215-21 (2005).

168. Li, X.J. et al. Directed differentiation of ventral spinal progenitors and motor neurons from human embryonic stem cells by small molecules. *Stem Cells* **26**, 886-93 (2008).

169. Hu, B.Y. & Zhang, S.C. Differentiation of spinal motor neurons from pluripotent human stem cells. *Nat Protoc* **4**, 1295-304 (2009).

170. Maury, Y. et al. Combinatorial analysis of developmental cues efficiently converts human pluripotent stem cells into multiple neuronal subtypes. *Nat Biotechnol* **33**, 89-96 (2015).

171. Hamburger, V. The heritage of experimental embryology : Hans Spemann and the organizer (Oxford University Press, New York, 1988).

172. De Robertis, E.M. Spemann's organizer and self-regulation in amphibian embryos. *Nat Rev Mol Cell Biol* **7**, 296-302 (2006).

173. Stern, C.D. Neural induction: old problem, new findings, yet more questions. *Development* **132**, 2007-21 (2005).

174. Alaynick, W.A., Jessell, T.M. & Pfaff, S.L. SnapShot: spinal cord development. *Cell* **146**, 178-178 e1 (2011).

175. Jessell, T.M. Neuronal specification in the spinal cord: inductive signals and transcriptional codes. *Nat Rev Genet* **1**, 20-9 (2000).

176. Maden, M. Retinoic acid in the development, regeneration and maintenance of the nervous system. *Nat Rev Neurosci* **8**, 755-65 (2007).

177. Briscoe, J., Pierani, A., Jessell, T.M. & Ericson, J. A homeodomain protein code specifies progenitor cell identity and neuronal fate in the ventral neural tube. *Cell* **101**, 435-45 (2000).

178. Novitch, B.G., Chen, A.I. & Jessell, T.M. Coordinate regulation of motor neuron subtype identity and pan-neuronal properties by the bHLH repressor Olig2. *Neuron* **31**, 773-89 (2001).

179. Chen, J.A. et al. Mir-17-3p controls spinal neural progenitor patterning by regulating Olig2/Irx3 cross-repressive loop. *Neuron* **69**, 721-35 (2011).

180. Dasen, J.S. & Jessell, T.M. Hox networks and the origins of motor neuron diversity. *Curr Top Dev Biol* **88**, 169-200 (2009).

181. Philippidou, P. & Dasen, J.S. Hox Genes: Choreographers in Neural Development, Architects of Circuit Organization. *Neuron* **80**, 12-34 (2013).

182. Kanning, K.C., Kaplan, A. & Henderson, C.E. Motor neuron diversity in development and disease. *Annu Rev Neurosci* **33**, 409-40 (2010).

183. Liu, J.P., Laufer, E. & Jessell, T.M. Assigning the positional identity of spinal motor neurons: rostrocaudal patterning of Hox-c expression by FGFs, Gdf11, and retinoids. *Neuron* **32**, 997-1012 (2001).

184. Pearson, J.C., Lemons, D. & McGinnis, W. Modulating Hox gene functions during animal body patterning. *Nat Rev Genet* **6**, 893-904 (2005).

185. Dasen, J.S., Tice, B.C., Brenner-Morton, S. & Jessell, T.M. A Hox regulatory network establishes motor neuron pool identity and target-muscle connectivity. *Cell* **123**, 477-91 (2005).

186. Lacombe, J. et al. Genetic and functional modularity of Hox activities in the specification of limb-innervating motor neurons. *PLoS Genet* **9**, e1003184 (2013).

187. Philippidou, P., Walsh, C.M., Aubin, J., Jeannotte, L. & Dasen, J.S. Sustained Hox5 gene activity is required for respiratory motor neuron development. *Nat Neurosci* **15**, 1636-44 (2012).

188. Dasen, J.S., De Camilli, A., Wang, B., Tucker, P.W. & Jessell, T.M. Hox repertoires for motor neuron diversity and connectivity gated by a single accessory factor, FoxP1. *Cell* **134**, 304-16 (2008).

189. Rousso, D.L., Gaber, Z.B., Wellik, D., Morrisey, E.E. & Novitch, B.G. Coordinated actions of the forkhead protein Foxp1 and Hox proteins in the columnar organization of spinal motor neurons. *Neuron* **59**, 226-40 (2008).

190. Mazzoni, E.O. et al. Saltatory remodeling of Hox chromatin in response to rostrocaudal patterning signals. *Nat Neurosci* **16**, 1191-8 (2013).

191. Williams, L.A., Davis-Dusenbery, B.N. & Eggan, K.C. SnapShot: directed differentiation of pluripotent stem cells. *Cell* **149**, 1174-1174 (2012).

192. Evans, M. Discovering pluripotency: 30 years of mouse embryonic stem cells. *Nat Rev Mol Cell Biol* **12**, 680-6 (2011).

193. Odorico, J.S., Kaufman, D.S. & Thomson, J.A. Multilineage differentiation from human embryonic stem cell lines. *Stem Cells* **19**, 193-204 (2001).

194. Bain, G., Kitchens, D., Yao, M., Huettner, J.E. & Gottlieb, D.I. in Dev Biol 342-57 (1995).

195. Kawasaki, H. et al. Induction of midbrain dopaminergic neurons from ES cells by stromal cell-derived inducing activity. *Neuron* **28**, 31-40 (2000).

196. Lee, H. et al. Directed differentiation and transplantation of human embryonic stem cell-derived motoneurons. *Stem Cells* **25**, 1931-9 (2007).

197. Okabe, S., Forsberg-Nilsson, K., Spiro, A.C., Segal, M. & McKay, R.D. in Mech Dev 89-102 (1996).

198. Joannides, A.J. et al. A scaleable and defined system for generating neural stem cells from human embryonic stem cells. *Stem Cells* **25**, 731-7 (2007).

199. Reubinoff, B.E. et al. Neural progenitors from human embryonic stem cells. *Nat Biotechnol* **19**, 1134-40 (2001).

200. Li, M., Pevny, L., Lovell-Badge, R. & Smith, A. Generation of purified neural precursors from embryonic stem cells by lineage selection. *Curr Biol* **8**, 971-4 (1998).

201. Zhang, S.C., Wernig, M., Duncan, I.D., Brustle, O. & Thomson, J.A. In vitro differentiation of transplantable neural precursors from human embryonic stem cells. *Nat Biotechnol* **19**, 1129-33 (2001).

202. Chambers, S.M. et al. Combined small-molecule inhibition accelerates developmental timing and converts human pluripotent stem cells into nociceptors. *Nat Biotechnol* **30**, 715-20 (2012).

203. Zhou, J. et al. High-efficiency induction of neural conversion in human ESCs and human induced pluripotent stem cells with a single chemical inhibitor of transforming growth factor beta superfamily receptors. *Stem Cells* **28**, 1741-50 (2010).

204. Smith, J.R. et al. Inhibition of Activin/Nodal signaling promotes specification of human embryonic stem cells into neuroectoderm. *Dev Biol* **313**, 107-17 (2008).

205. Streit, A., Berliner, A.J., Papanayotou, C., Sirulnik, A. & Stern, C.D. Initiation of neural induction by FGF signalling before gastrulation. *Nature* **406**, 74-8 (2000).

206. Wilson, S.I., Graziano, E., Harland, R., Jessell, T.M. & Edlund, T. An early requirement for FGF signalling in the acquisition of neural cell fate in the chick embryo. *Curr Biol* **10**, 421-9 (2000).

207. Peljto, M., Dasen, J.S., Mazzoni, E.O., Jessell, T.M. & Wichterle, H. Functional diversity of ESC-derived motor neuron subtypes revealed through intraspinal transplantation. *Cell Stem Cell* **7**, 355-66 (2010).

208. Patani, R. et al. Activin/Nodal inhibition alone accelerates highly efficient neural conversion from human embryonic stem cells and imposes a caudal positional identity. *PLoS One* **4**, e7327 (2009).

209. Soundararajan, P., Miles, G.B., Rubin, L.L., Brownstone, R.M. & Rafuse, V.F. Motoneurons derived from embryonic stem cells express transcription factors and develop phenotypes characteristic of medial motor column neurons. *J Neurosci* **26**, 3256-68 (2006).

210. Vult von Steyern, F. et al. The homeodomain transcription factors Islet 1 and HB9 are expressed in adult alpha and gamma motoneurons identified by selective retrograde tracing. *Eur J Neurosci* **11**, 2093-102 (1999).

211. Sun, Y. et al. A central role for Islet1 in sensory neuron development linking sensory and spinal gene regulatory programs. *Nat Neurosci* **11**, 1283-93 (2008).

212. Miles, G.B. et al. Functional properties of motoneurons derived from mouse embryonic stem cells. *J Neurosci* **24**, 7848-58 (2004).

213. Gao, B.X. & Ziskind-Conhaim, L. Development of ionic currents underlying changes in action potential waveforms in rat spinal motoneurons. *J Neurophysiol* **80**, 3047-61 (1998).

214. Hochbaum, D.R. et al. All-optical electrophysiology in mammalian neurons using engineered microbial rhodopsins. *Nat Methods* **11**, 825-33 (2014).

215. Toma, J.S. et al. Motoneurons derived from induced pluripotent stem cells develop mature phenotypes typical of endogenous spinal motoneurons. *J Neurosci* **35**, 1291-306 (2015).

216. Son, E.Y. et al. Conversion of mouse and human fibroblasts into functional spinal motor neurons. *Cell Stem Cell* **9**, 205-18 (2011).

217. Peng, H.B. & Cheng, P.C. Formation of postsynaptic specializations induced by latex beads in cultured muscle cells. *J Neurosci* **2**, 1760-74 (1982).

218. Gingras, J. et al. Controlling the orientation and synaptic differentiation of myotubes with micropatterned substrates. *Biophys J* **97**, 2771-9 (2009).

219. Tye, K.M. & Deisseroth, K. Optogenetic investigation of neural circuits underlying brain disease in animal models. *Nat Rev Neurosci* **13**, 251-66 (2012).

220. Valdez, G. et al. Attenuation of age-related changes in mouse neuromuscular synapses by caloric restriction and exercise. *Proc Natl Acad Sci U S A* **107**, 14863-8 (2010).

221. Valdez, G., Tapia, J.C., Lichtman, J.W., Fox, M.A. & Sanes, J.R. Shared resistance to aging and ALS in neuromuscular junctions of specific muscles. *PLoS One* **7**, e34640 (2012).

222. Han, S.S., Williams, L.A. & Eggan, K.C. Constructing and deconstructing stem cell models of neurological disease. *Neuron* **70**, 626-44 (2011).

223. Chung, C.Y. et al. Identification and rescue of alpha-synuclein toxicity in Parkinson patient-derived neurons. *Science* **342**, 983-7 (2013).

224. Sanchez-Danes, A. et al. Disease-specific phenotypes in dopamine neurons from human iPS-based models of genetic and sporadic Parkinson's disease. *EMBO Mol Med* **4**, 380-95 (2012).

225. Mekhoubad, S. et al. Erosion of dosage compensation impacts human iPSC disease modeling. *Cell Stem Cell* **10**, 595-609 (2012).

226. Jeon, I. et al. Neuronal properties, in vivo effects, and pathology of a Huntington's disease patient-derived induced pluripotent stem cells. *Stem Cells* **30**, 2054-62 (2012).

227. Yagi, T. et al. Modeling familial Alzheimer's disease with induced pluripotent stem cells. *Hum Mol Genet* **20**, 4530-9 (2011).

CHAPTER 2

In vitro modeling of *SOD1*-linked ALS with isogenic human pluripotent stem cell-derived motor neurons

Portions of this chapter have been published as:

• Kiskinis E*, Sandoe J*, **Williams LA**, Boulting GL, Moccia R, Wainger BJ, Han S, Peng T, Thams S, Mikkilineni S, Mellin C, Merkle FT, Davis-Dusenbery BN, Ziller M, Oakley D, Ichida J, Di Costanzo S, Atwater N, Maeder ML, Goodwin MJ, Nemesh J, Handsaker RE, Paull D, Noggle S, McCarroll SA, Joung JK, Woolf CJ, Brown RH, Eggan K. Pathways Disrupted in Human ALS Motor Neurons Identified through Genetic Correction of Mutant SOD1. *Cell Stem Cell* **14**, 781-795 (2014).

• Wainger BJ*, Kiskinis E*, Mellin C, Wiskow O, Han SS, Sandoe J, Perez NP, **Williams LA**, Lee S, Boulting G, Berry JD, Brown RH Jr, Cudkowicz ME, Bean BP, Eggan K, Woolf CJ. Intrinsic membrane hyperexcitability of amyotrophic lateral sclerosis patient-derived motor neurons. *Cell Rep* **7**, 1-11 (2014).

Author contributions to the work presented in this Chapter: E.K. and G.L.B. generated 39b and RB9d iPS cell lines; L.A.W. optimized MN differentiation protocol. E.K. and G.L.B. carried out phenotypic assays comparing 39b and Rb9d MNs with 11a and 18a MNs; J.S. and L.A.W. executed all gene targeting experiments to generate 39b-$SOD1^{+/+}$ and HUES3 $SOD1^{+/A4V}$ cell lines; E.K., J.S. and L.A.W. carried out molecular, biochemical and phenotypic assays comparing isogenic MNs; R.M. analyzed RNA-Seq data; B.J.W. and C.M. performed all electrophysiological recordings under the supervision of C.J.W.; T.P and S.M. assisted with experiments characterizing MN soma size and mitochondria; S.A.M. and R.E.H. sequenced and analyzed the genomes of 39b isogenic cell lines; R.H.B. collected and provided Patient RB9 material; E.K., J.S., L.A.W., G.L.B. and K.E. designed the research, E.K. and K.E. wrote the *Cell Stem Cell* manuscript describing some of the work presented in this chapter; L.A.W., G.L.B. and J.S. contributed extensively in the preparation of this manuscript; L.A.W. wrote the sections of the work described here that are not part of the *Cell Stem Cell* and *Cell Rep* manuscripts; K.E. supervised all aspects of this study.

2.1 Introduction

Amyotrophic lateral sclerosis (ALS) is a fatal neurological condition characterized by the selective death of motor neurons (MNs)[1]. While most ALS cases are sporadic, approximately 5-10% of ALS patients have a family history[2]. Classical family-based linkage studies and DNA sequencing approaches have demonstrated that ALS can be caused by a variety of mutations in more than two dozen genes acting on diverse cellular processes[3-7]. Mutations in the *SUPEROXIDE DISMUTASE* 1 (*SOD1*) gene were originally identified through their autosomal-dominant inheritance pattern in some familial ALS pedigrees[8]. The SOD1 gene product functions as a cytoplasmic antioxidant enzyme, converting toxic superoxide radicals to molecular oxygen and hydrogen peroxide[9]. Mutations in SOD1 account for up to 20% of familial ALS cases, and 1-2% of all ALS[2, 10]. Among SOD1-linked ALS cases in the United States, 50% are caused by the SOD1A4V variant (alanine to valine substitution at codon 4), which clinically is associated with a rapidly progressive form of this disorder[11, 12].

The discovery of SOD1 mutations led to widely studied transgenic rodent models of ALS[13,14]. While indisputably valuable, these animals as well as many cell-based models[15, 16], overexpress heterologous human SOD1 at super-physiological levels. Therefore, it is generally accepted that findings from these systems carry the caveat that they could be artifacts of protein overexpression[17]. Furthermore, successful therapeutic interventions from animal studies have failed in ALS clinical trials[17, 18], suggesting imperfect phenotypic correlations between rodents and patients, and underscoring the need for additional models of ALS using cells with a disease-relevant human genetic background and physiology.

Since it is not possible to retrieve and culture viable MNs from ALS post-mortem samples or living patients, our group and others have proposed that induced pluripotent stem (iPS) cells from ALS patients and their differentiation into MNs[19] could complement existing animal

models, allowing hypotheses to be tested in human MNs expressing mutations in a variety of ALS-causing loci, all at physiological levels[20-23]. However, a major technical challenge in disease modeling experiments using human iPS cells is the inherent genetic heterogeneity among cell lines derived from different individuals, which could inadvertently drive or mask disease-associated cellular phenotypes[24]. For single-gene disorders, some of this variation can be overcome by using genome-editing technology to either correct or induce the single disease-causing mutation, thus generating otherwise isogenic disease and control human pluripotent stem cells lines[24, 25]. Here, we have combined reprogramming and stem cell differentiation approaches with genome engineering and disease-pertinent phenotypic assays to study ALS *in vitro* using iPS cell-derived MNs from ALS patients harboring the *SOD1A4V* mutation. We found that $SOD1^{+/A4V}$ MNs exhibited cell survival and soma size deficits, insoluble SOD1 after proteasome inhibition, and transcriptional and morphological disturbances to mitochondria. In addition, we showed that these cells could recapitulate the increased membrane excitability reported in neurophysiological studies of ALS patients[26-29]. Notably, by genetic correction of the *SOD1A4V* mutant allele in a patient iPS cell line, we demonstrated a causal relationship between the ALS-linked mutation and the observed *in vitro* phenotypes. Finally, we described the characterization of an independent set of $SOD1^{+/A4V}$ and $SOD1^{+/+}$ isogenic cell lines, generated after induction of the *SOD1A4V* mutation in a human embryonic stem (ES) cell line that reports for MN fate after differentiation[30].

2.2 Results

2.2.1 Generation of iPS cells and functional MNs from $SOD1^{+/A4V}$ ALS Patients

We derived skin fibroblasts from two female ALS patients (study participants 39 and RB9) carrying the same autosomal dominant *SOD1A4V* mutation ($SOD1^{+/A4V}$) (Figure 2.1A-B). We

then generated iPS cells via retroviral transduction of the reprogramming genes *OCT4*, *SOX2* and *KLF4,* and validated their integrity through standard pluripotency assays (Figure 2.1C-F). *SOD1*$^{+/A4V}$ iPS cell lines stably exhibited typical human pluripotent stem cell morphology with large nuclear-to-cytoplasmic ratios and prominent nucleoli, growing in dense colonies with well-defined borders, and immunoreactive against human pluripotency markers including nuclear NANOG and the cell surface antigen TRA-1-81 (Figure 2.1C). Clones 39b and RB9d exhibited a stable karyotype, and expressed endogenous *OCT4, SOX2* and *KLF4* at levels similar to those of ES cells, while they repressed the reprogramming transgenes (data not shown). The pluripotent profile and the differentiation potential of 39b and RB9 iPS cell lines was also verified using a well established lineage scorecard assay (Figure 2.1E-F), which is based on the comparative expression profile of a panel of both pluripotency genes and germ layer-specific differentiation genes against a large set of human pluripotent stem cell lines used as reference[31].

To obtain MNs from the iPS cell lines, we employed a 24-day spinal MN differentiation protocol (Figure 2.2A), based on neural induction by dual inhibition of SMAD signaling[32], and MN specification through exposure to retinoic acid and a small molecule agonist of SONIC HEDGEHOG signaling[33, 34]. *SOD1*$^{+/A4V}$ iPS cell lines generated MNs that expressed the neuronal-specific cytoskeletal protein β-III TUBULIN (TUJ1^{+}), and the MN-specific transcription factors ISLET1/2 (ISL) and HB9 (Figure 2.2B). In addition, these iPS cell-derived MNs expressed the more mature neuronal markers MICROTUBULE-ASSOCIATED PROTEIN 2 (MAP2) and the biosynthetic enzyme CHOLINE ACETYLTRANSFERASE (ChAT), as well as the lateral motor column identity HOX co-factor FOXP1[33, 35](Figure 2.2B). This differentiation strategy generated populations in which >97% of all cells were TUJ1^{+} neurons, with 21-38% of these neurons

A

Patient	Sex	Diagnosis	Genotype	Age of onset	Age at Biopsy	Reference
39	Female	FALS	*SOD1*$^{+/A4V}$	43	44	This study
RB9	Female	FALS	*SOD1*$^{+/A4V}$	45	50	This study
11	Male	Healthy	*SOD1*$^{+/+}$	N.A.	37	Boulting et al. (2011)
18	Female	Healthy	*SOD1*$^{+/+}$	N.A.	48	Boulting et al. (2011)

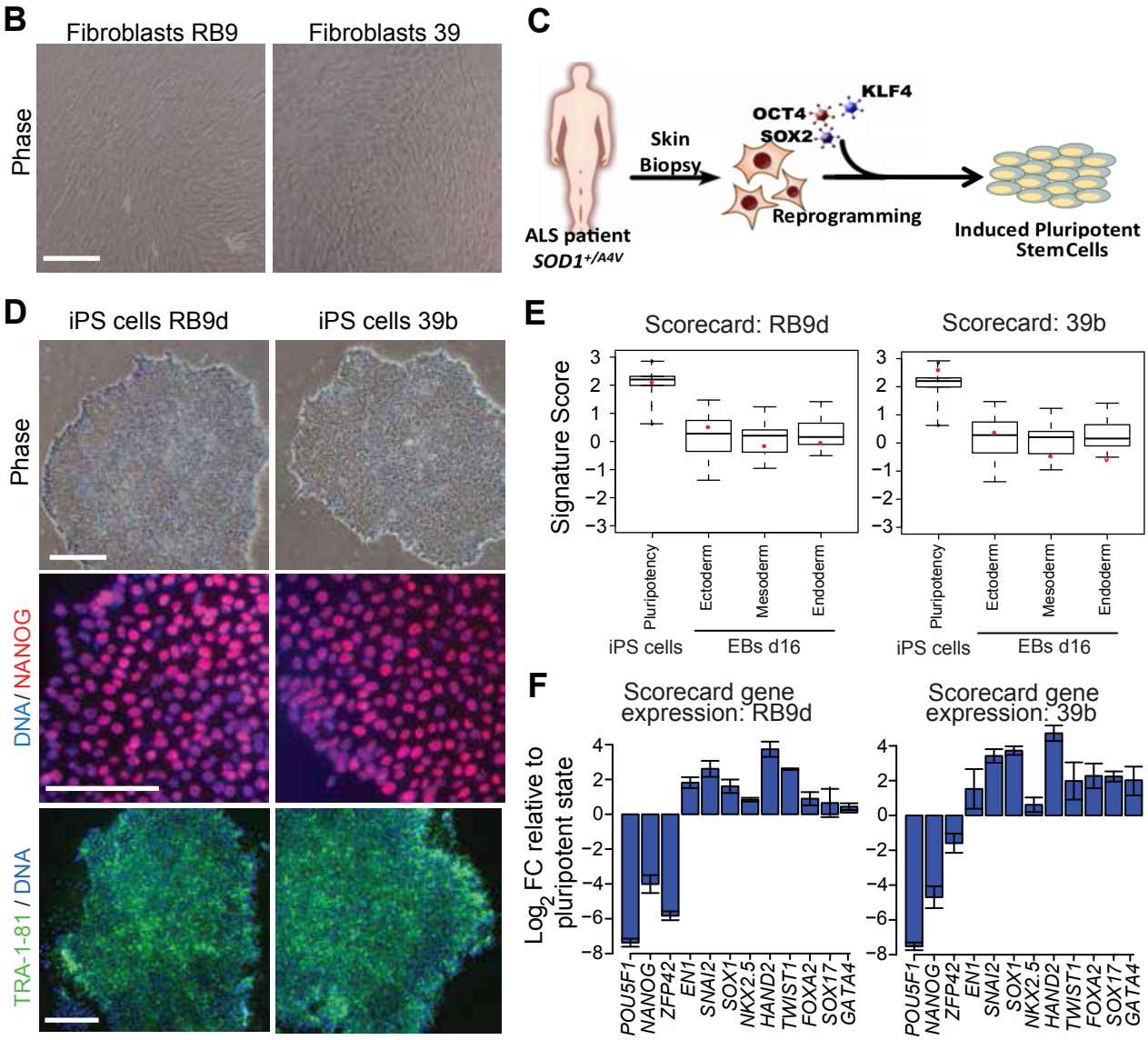

Figure 2.1 Generation of iPS cell lines from *SOD1*$^{+/A4V}$ ALS patients

A. Information summary of famial ALS (FALS) patients and healthy controls used in this study. NA:not applicable. **B.** Skin biopsy-derived fibroblasts from *SOD1*$^{+/A4V}$ patients RB9 and 39. **C.** Patient fibroblasts were converted into iPS cells by retroviral transduction of the reprogamming genes *OCT4*, *SOX2* and *KLF4*. **D.** Patient iPS cell colonies are morphologically similiar to those of human embryonic stem cells, and express the transcription factor NANOG and cell surface antigen TRA-1-81, consistent with a pluripotent state (Scale bar = 100μm). **E.** Scorecard analysis for iPS cell lines RB9 clone 'd' (Rb9d) and 39 clone 'b' (39b), which is based on comparative expression of both pluripotency genes and germ layer-specific differentiation genes, assayed before and after 16 days of undirected differentiation as embryoid bodies (EBs d16). Red dots indicate the values for each of the two iPS cell lines compared to a large reference set of human pluripotent cell lines. **F.** Relative gene expression of pluripotency and differentiation genes in EBs after 16 days of random differentiation. FC: fold change.

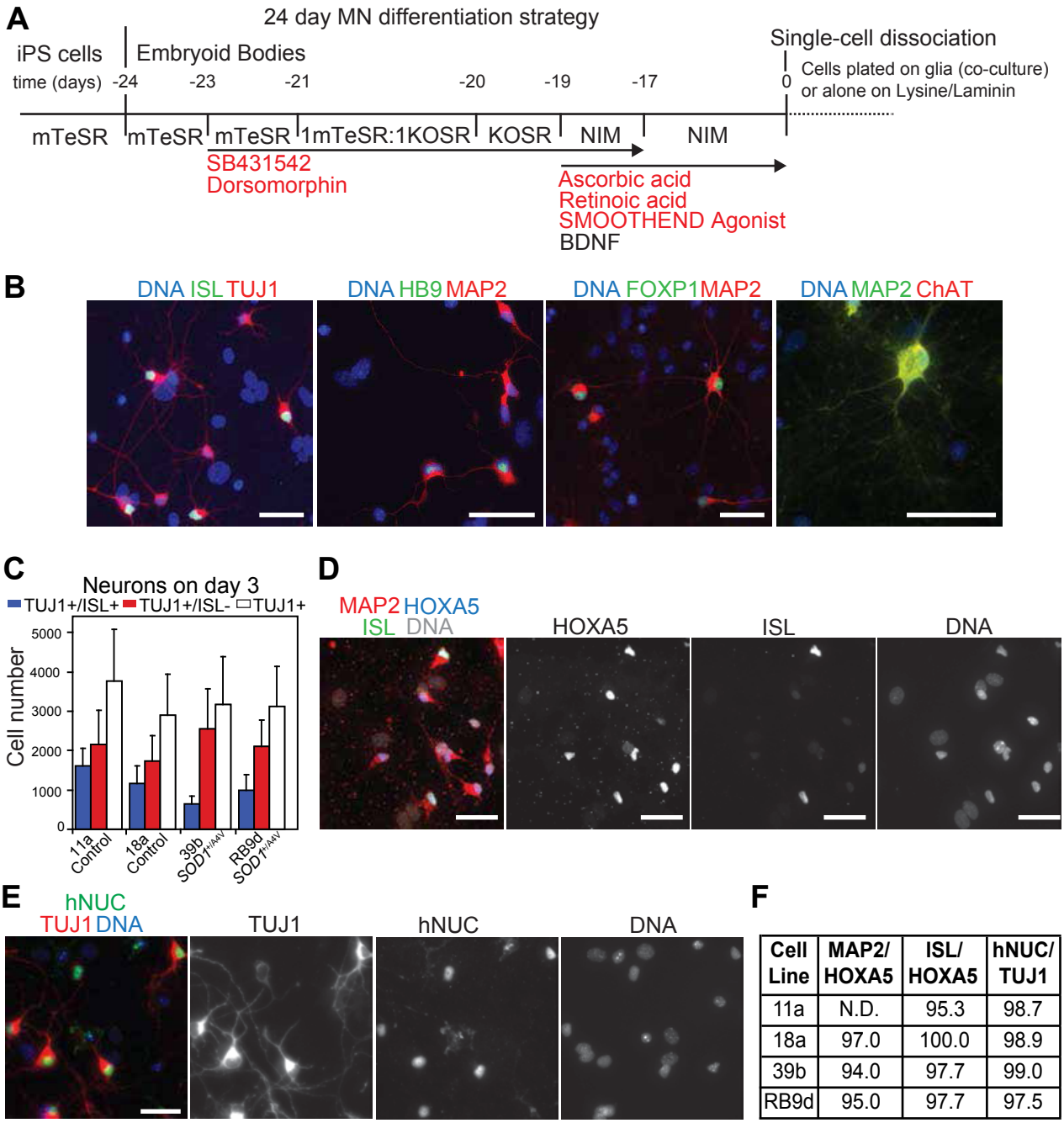

Cell Line	MAP2/ HOXA5	ISL/ HOXA5	hNUC/ TUJ1
11a	N.D.	95.3	98.7
18a	97.0	100.0	98.9
39b	94.0	97.7	99.0
RB9d	95.0	97.7	97.5

Figure 2.2 Differentiation and characterization of iPS cell-derived MNs

A. Schematic of MN differentiation protocol (see methods section for details). **B.** MN differentiations typically yielded neurons that expressed the cytoskeletal proteins β-III TUBULIN (TUJ1+) and MAP2, the MN transcription factors HB9 and ISLET, and the ChAT enzyme. ~40-50% of MNs expressed the lateral motor column identity marker FOXP1. Representative images correspond to the 39b iPS cell-derived neurons. **C.** Quantification of efficiencies of MN (ISL+) differentiation among the different iPS cell lines. **D.** ~95-100% of MNs express the cervical identity factor HOXA5. Representative images correspond to the Rb9 iPS cell-derived neurons. **E.** In co-cultures with mouse glia, iPS cell-differentiated cells can be recognized with a human-specific antibody against a nuclear antigen. > 97% of human cells were TUJ1+. Representative images correspond to cells derived from 11a. **F.** Quantifications for each cell line of the percentages of MAP2+, ISL+, or hNUC+ differentiated cells that were also positive for HOXA5, HOXA5, or TUJ1, respectively. All scales bars = 50μm)

being ISL$^+$ MNs (n=6) (Figures 2.2C and 2.2E-F). All ISL+ and MAP2+ cells were HOXA5$^+$ (Figure 2.2D and 2.2F), suggesting the acquisition of a cervical identity along the anterior-posterior axis[33, 36]. To assess their functionality, we transduced MNs with a lentivirus encoding a RED FLUORESCENCE PROTEIN (RFP) reporter under control of the *Hb9* promoter (*Hb9::RFP*) and performed whole-cell patch clamp recordings at day 15 of culture (Figure 2.3A-B). RFP$^+$ MNs exhibited sodium and potassium currents, fired action potentials, and responded to excitatory and inhibitory neurotransmitters as previously shown for other iPSC-derived MNs[34] (Figure 2.3B-F).

2.2.2 Increased apoptosis and altered morphometry in *SOD1$^{+/A4V}$* MNs

Having demonstrated that we could produce MNs from *SOD1$^{+/A4V}$* patients, we proceeded to ask whether these neurons might manifest a phenotype distinct from *SOD1$^{+/+}$* control MNs under standard culture conditions. To address this, we compared *SOD1$^{+/A4V}$* MNs with MNs produced in parallel from two previously characterized control iPS cell lines (11a, 18a)[34], selected based on their similarity in neuronal differentiation capacity, iPS cell reprogramming method and donor age (Figure 2.1A). Differentiated neuronal preparations were plated on primary glial monolayers and the total number of ISL$^+$/TUJ1$^+$ MNs was assessed after 3 and 30 days in culture (Figure 2.4A). We found that in comparison to the number of MNs present in cultures made from each line at day 3, there were statistically significant fewer *SOD1$^{+/A4V}$* MNs at day 30 (n=3, m>8000, $p<0.05$) (Figure 2.4B). Interestingly, the decline in *SOD1$^{+/A4V}$* cultures seemed to be specific to MNs, rather than reflective of an overall deficit in neurons; with no significant difference in the number of ISL-negative/TUJ1$^+$ cells (presumptive non-MNs) between cases and controls at day 30 (n=3, m>25,000) (Figure 2.4C).

We considered two explanations for the selective decline in MN number in *SOD1$^{+/A4V}$*

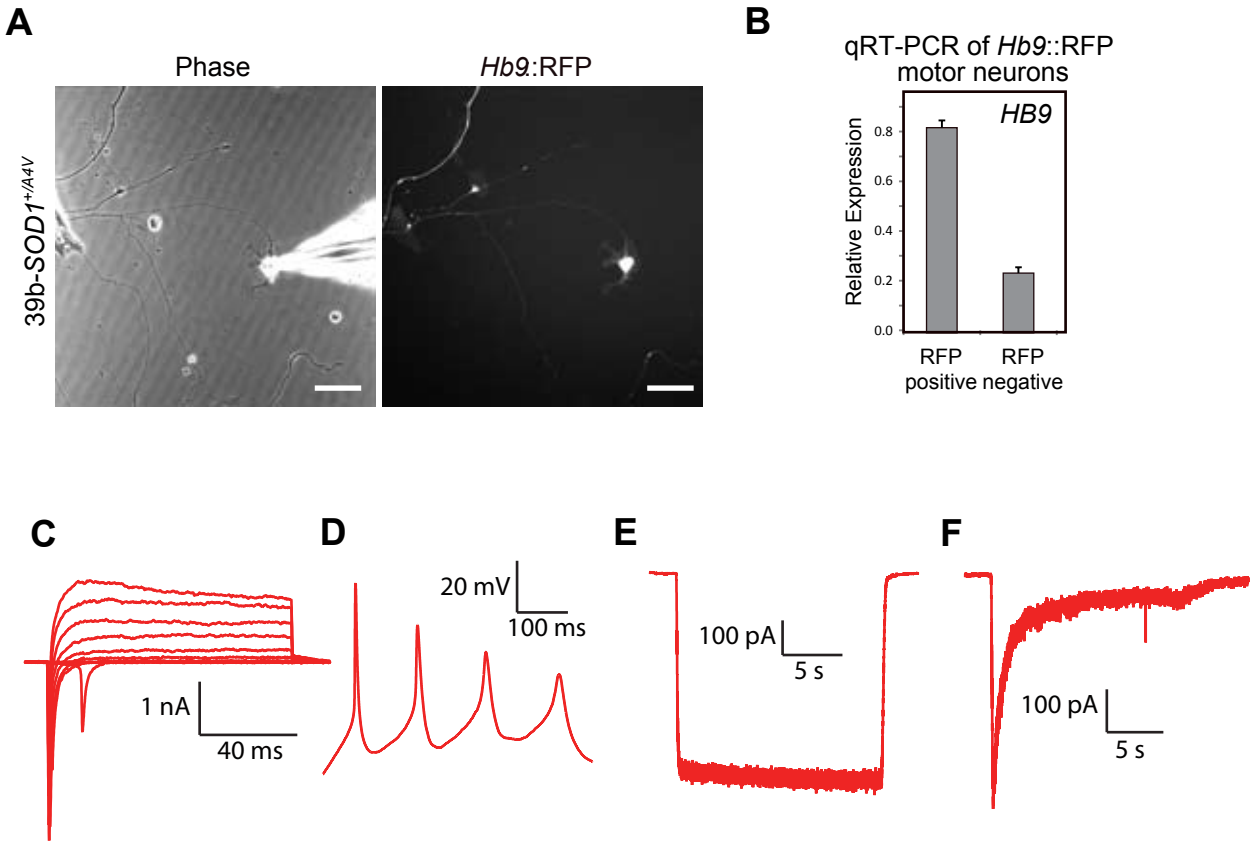

Figure 2.3 *Hb9::*RFP+ MNs are electrophysiologically active
A. Representative image of a 39b iPS cell-derived MN identified by *Hb9::*RFP lentiviral expression (right panel) and during patch-clamp recording (left panel), after 15 days in culture (Scale bar =50μm). **B.** *Hb9::*RFP^{+} cells show a 4-fold enrichment in expression levels of the endogenous *HB9* gene relative to the RFP negative fraction, as determined by qRT-PCR. **C.** In whole-cell patch clamp recordings and upon depolarization, MNs exhibited intial inward currents followed by slow outward currents, indicative of functional sodium and potassium channels, respectively. **D.** Current clamp recording demonstrating repetitive firing of action potentials. **E-F.** Consistent with with the expression of functional receptors for excitatory glutamatergic and inhibitory neurotransmitters, *Hb9::*RFP+ MNs exhibited responses to Kainate(**E**) and GABA(**F**). **C-F.** Representative recordings correspond to cells differentiated from iPS cell line 39b.

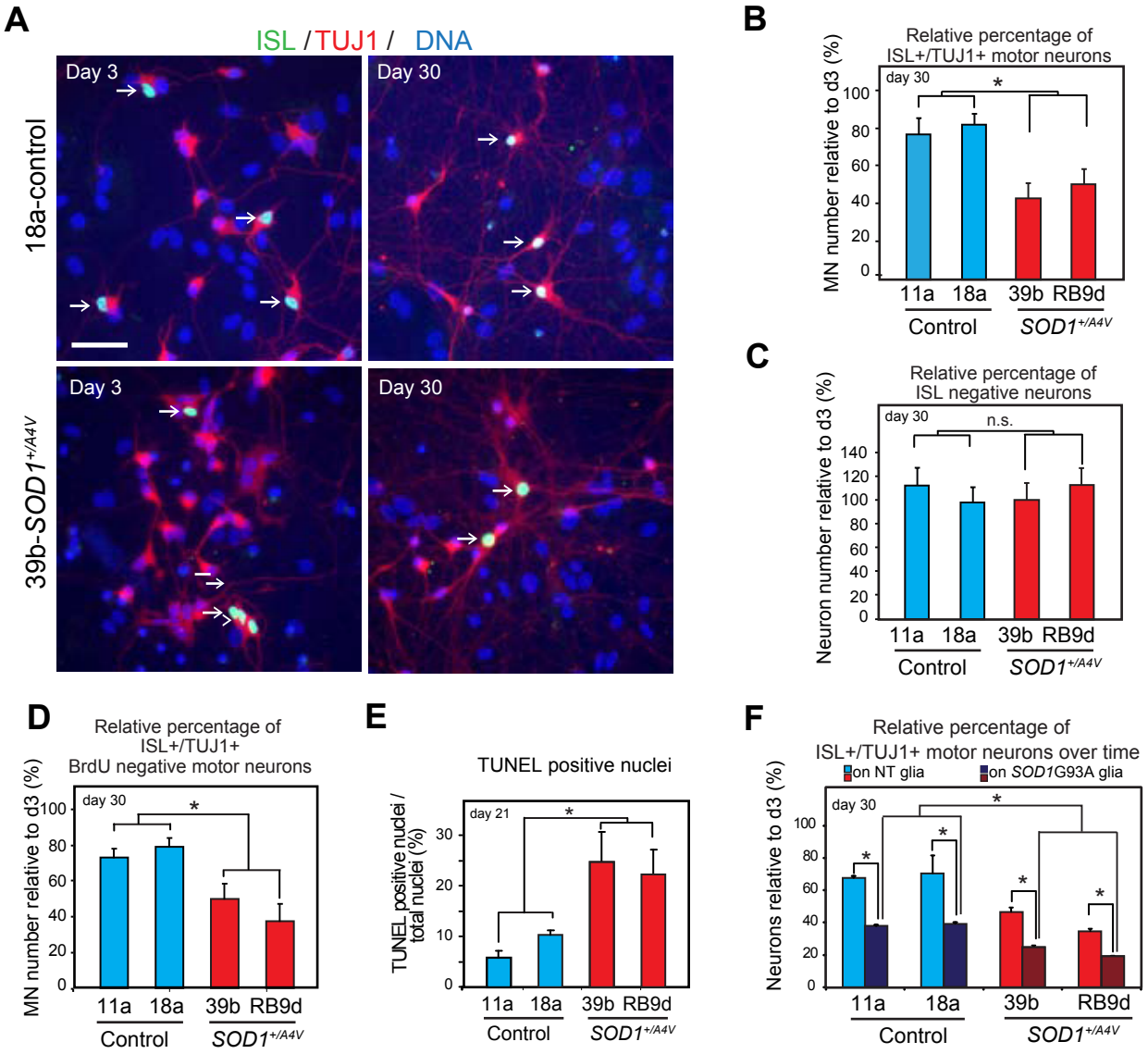

Figure 2.4 *SOD1*$^{+/A4V}$ MNs exhibit a cell survival phenotype

A. Neuronal cultures on glial monolayers 3 and 30 days post-differentiation from control and *SOD1*$^{+/A4V}$ iPS cells. MNs co-stained for ISL and TUJ1 are indicated by white arrows (scale bar = 50 μm). **B-C** Quantification of ISL^{+}/TUJ1^{+} MNs (n = 3, m > 8,000, ±SEM, $p < 0.05$) (in B) and ISL^{-}(negative)/TUJ1^{+} neurons (n = 3, m >25,000, ±SEM, $p < 0.05$) (in C) after 30 days in culture. **D.** Quantification of ISL^{+}/TUJ1^{+} MNs that are BrdU negative after 30 days in culture (n = 1, m > 3,600, ±SD, $p < 0.05$). **E.** Quantification of TUNEL^{+} nuclei of neuronal cultures without glia assayed 21 days after differentiation (n = 2, m > 13,000, ±SD, $p < 0.05$)**. F.** MNs are sensitive to the toxic effects of primary glia from SOD1G93A mice, and expression of the SOD1A4V variant exacerbates the survival deficit.

cultures. We first reasoned that if MN progenitor cells remained in the cultures, and if *SOD1*$^{+/A4V}$ progenitors were less abundant or functional, then the *SOD1*$^{+/A4V}$ MN number might selectively decline over time. To test this, we monitored progenitor activity via long-term BrdU incorporation. When we chronically administered BrdU to cultures from day 0 to day 30, then assessed BrdU incorporation, we observed that only 2-3% of MNs were labeled (BrdU^{+}, ISL+, TUJ1^{+}), and that this modest rate of labeling was similar in control and *SOD1*$^{+/A4V}$ cultures (Figure 2.5A-C). These findings suggest that the vast majority (>97%) of MNs in our cultures were postmitotic prior to "day 0" and that the selective decline of MNs we observed in *SOD1*$^{+/A4V}$ cultures was not due to a decrease in progenitor activity (Figure 2.5A-C).

The second hypothesis was that the selective decline of MN number in *SOD1*$^{+/A4V}$ cultures might result from an increased rate of cell death. We therefore used the BrdU incorporation strategy to specifically quantify only the MNs born before day 0. Using this criterion, we again found that significantly more *SOD1*$^{+/A4V}$ MNs were lost over the 30 days in culture (m=3,686, $p<0.05$) (Figure 2.4D). To determine whether increased apoptosis caused the preferential loss of postmitotic *SOD1*$^{+/A4V}$ MNs, we performed TUNEL staining. At day 21 of culture, we found a significant increase in apoptosis in the two *SOD1*$^{+/A4V}$ cases compared to the two controls ($n=2$, $p<0.05$) (Figure 2.4E).

To determine if the survival difference we observed between *SOD1*$^{+/A4V}$ and control MNs was cell autonomous, we co-cultured MNs with preparations of primary glia from the *SOD1*^{G93A} mouse model. We found that both *SOD1*$^{+/+}$ and *SOD1*$^{+/A4V}$ MNs exhibted a survival phenotype when co-cultured with *SOD1*^{G93A} versus control glia (Figure 2.4F), which is consistent with previous *in vitro* studies of non-cell autonomous toxicity of mutant SOD1[30]. However, even in the *SOD1*^{G93A} culture environment *SOD1*$^{+/A4V}$ MNs exhibited a cell survival

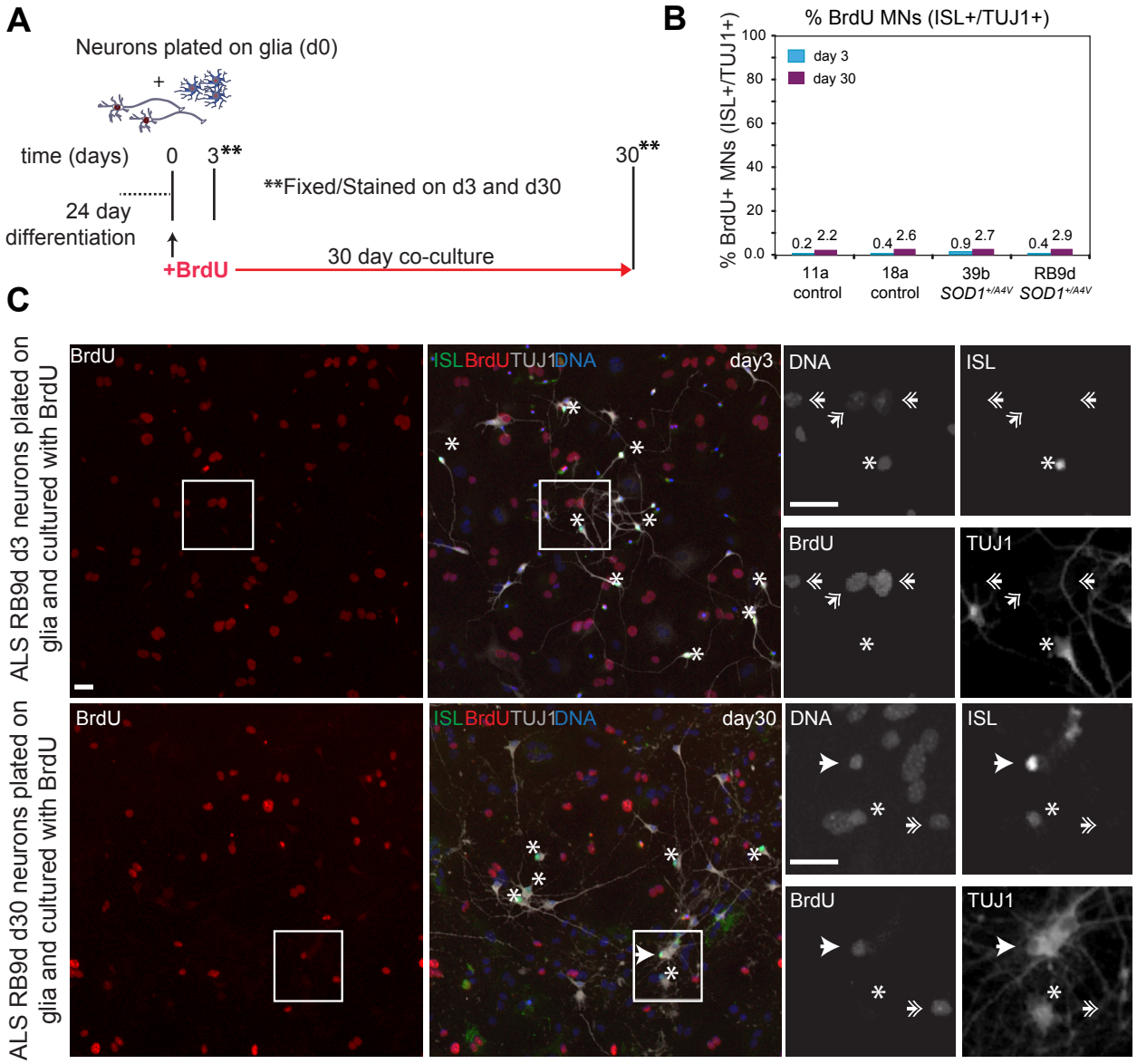

Figure 2.5 Neuronal Proliferation does not contribute to MN survival phenotype
A. Schematic of experimental strategy to evaluate the level of MN proliferation after dissociation; 1μM BrdU was added in plated co-cultures from days 0-30 and percentage of BrdU positive cells was analyzed. Between 0.2-0.8% of all MNs incorporated BrdU between days 0-3 while 2-2.8% between days 0-30 across all the iPS cell lines. Importantly, the mitoticly active supporting glial cells were exposed to BrdU in this experiment and many are BrdU+ (large DAPI+ nuclei). **B.** Quantification of MNs that are BrdU+ after 30 days in culture ($n = 1$, $m > 3{,}600$, ±SD, $p < 0.05$). **C.** A representative image of BrdU incorporation after the addition of 1μM BrdU to dissociated MN cultures after 3 and 30 days. Top right inserts show an ISL+/BrdU negative MN, bottom inserts show two ISL+ MNs, with only one being positive for BrdU. Single arrows indicates BrdU+/ISL+ MNs; Double arrows indicate BrdU+/ISL negative cells; Asterisks indicate BrdU negative/ISL+ MNs, (Scale bar = 30μm).

deficit compared to *SOD1*$^{+/+}$ MNs (Figure 2.4F), suggesting that cell-autonomous components contribute, at least partially, to the effects described above.

Finally, we also found that the pro-apoptotic phenotype we identified in *SOD1*$^{+/A4V}$ human MNs was accompanied by altered morphological characteristics similar to those seen in patients and in the *SOD1*^{G93A} mouse model[37, 38]. In particular, *SOD1*$^{+/A4V}$ MNs at day 30 exhibited a significantly smaller soma size and fewer, as well as shorter processes compared to controls (n=3, m=88, $p<0.01$) (Figure 2.6A-G). Again, these effects were not observed in ISL-negative/TUJ1^{+} non-MNs (n=3, m=90) (Figure 2.6D). Interestingly, further analysis suggested that larger MNs were most vulnerable to loss, as MNs larger than 150μm^2 made up less than 40% of the total MN population in *SOD1*$^{+/A4V}$ cases, compared to ~65% in the case of controls (Figure 2.6E).

2.2.3 Gene targeting and correction of the *SOD1A4V* mutant allele

Distinct iPS cell lines can harbor significant variation in transcription and DNA methylation[31]. This variation, in conjunction with a cell line's particular genetic make-up, give it its own distinctive functional characteristics[34], which may confound disease modeling experiments[39]. Additionally, ALS patients can harbor more than one disease-causing genetic variant[40], raising the possibility that the phenotypes we observed were not solely due to the *SOD1A4V* mutation. To address these issues, we used a two-step, zinc-finger nuclease (ZFN)-mediated gene targeting strategy[41, 42] to correct the *SOD1A4V* mutant allele in the iPS cell line 39b (Figure 2.7A, methods).

Gene targeting and correction of the *SOD1A4V* mutation were confirmed through cloning and sequencing of a single PCR fragment amplified with primers situated outside of the 5' and 3' homology arms (Figure 2.7A-B). To confirm that the gene edit had eliminated expression of

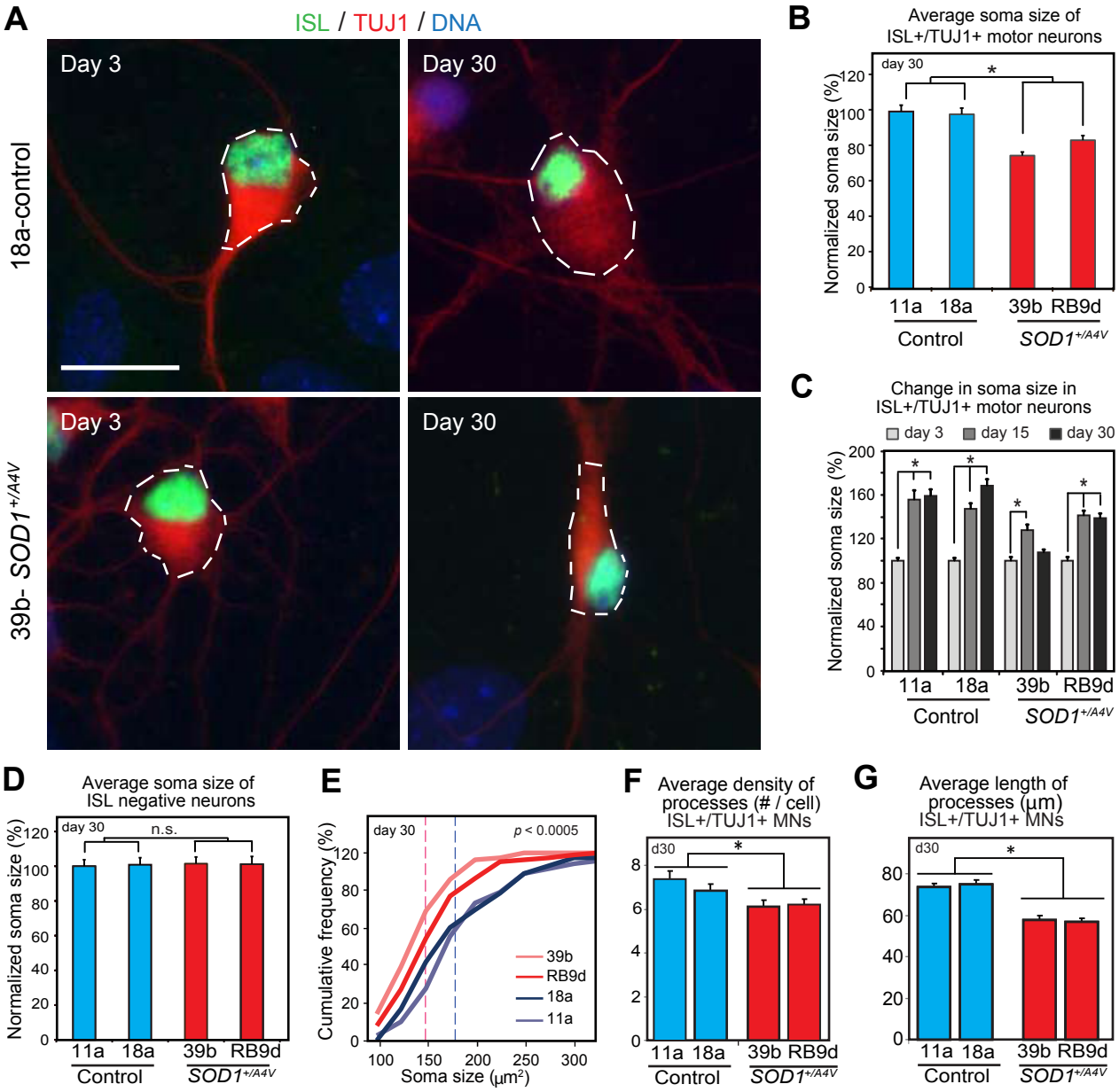

Figure 2.6 *SOD1*$^{+/A4V}$ MNs exhibit morphometric deficits compared to control MNs

A. Representative images of measured soma size (white-dotted circumference) of control and *SOD1*$^{+/A4V}$ MNs (scale bar = 20 μm). **B.** Quantification of ISL^{+} MN soma size with values normalized to those of controls (n = 3, m = 340, ±SEM, p < 0.01). **C.** MN soma size after 3, 15, and 30 days in culture normalized to day 3 for each cell line. Although MNs increase in size over time in all four cell lines, they do so to a lesser degree in *SOD1*$^{+/A4V}$ cases. **D.** Quantification of ISL-negative neuron soma size with values normalized to those of controls (n = 3, m = 446, ±SEM, p = n.s.). **E**. Cumulative frequency graphs of MN soma size after 30 days in culture. Dotted lines indicate averages for control and disease. n.s., not significant; n = experiment; m = cell number. **F.** Quantification of MN processes, evaluated as total number of TUJ1-positive processes per cell showed that *SOD1*$^{+/A4V}$ MNs are less elaborate after 30 days in culture. **G.** *SOD1*$^{+/A4V}$ MNs exhibit shorter processes (n=3, p <0.05, ± s.e.m.).

mutant transcripts, we queried the *SOD1* cDNA from both 39b parental (*SOD1*$^{+/A4V}$) and targeted (*SOD1*$^{+/+}$) iPS cell lines for the presence of a *Psh*A1 Restriction Fragment Length Polymorphism (RFLP) resulting from the non-synonymous substitution encoding the SOD1A4V variant. While this PCR-RFLP, was clearly detected in cDNA from the 39b-*SOD1*$^{+/A4V}$ cell line, it was eliminated after gene-correction (Figure 2.7C). Quantitative PCR demonstrated that the corrected 39b-*SOD1*$^{+/+}$cell line did not harbor multiple insertions of the targeting vector (Figure 2.7D). We also found that *SOD1* transcript levels were similar in both iPS cell lines (Figure 2.7E).

We next used immunoblot assays to examine SOD1 protein levels in cell extracts from the parental 39b-*SOD1*$^{+/A4V}$ iPS cell line, the intermediate 39b-*SOD1*$^{+/-}$ heterozygous knockout line, and the corrected derivative 39b-*SOD1*$^{+/+}$. We found that while the intermediate 39b-*SOD1*$^{+/-}$ cell line, which expresses only one *SOD1* allele, exhibited approximately half of the SOD1 levels of the parental line, correcting the mutation restored SOD1 protein levels (Figure 2.7F). As expected, based on the reported lower protein stability of the SOD1A4V variant[43], correction of the *SOD1A4V* mutation resulted in a modest increase in SOD1 protein levels relative to those detected in the parental cell line (Figure 2.7F).

Given that undesired genetic variations could potentially arise as result of ZFN off-target activity or clonal expansion, we proceeded to carefully evaluate the genomic sequence and integrity of the parental and gene-edited cell lines. We carried out whole genome sequencing for the 39b-*SOD1*$^{+/A4V}$ (33.4x coverage) and 39b-*SOD1*$^{+/+}$ (31.1x coverage) cell lines and determined that sequencing read depth for the two samples closely matched each other throughout the genome, excluding the possibility that large-scale copy-number variations (CNVs) had arisen during passaging, genome editing, or clonal expansion. Furthermore, the top

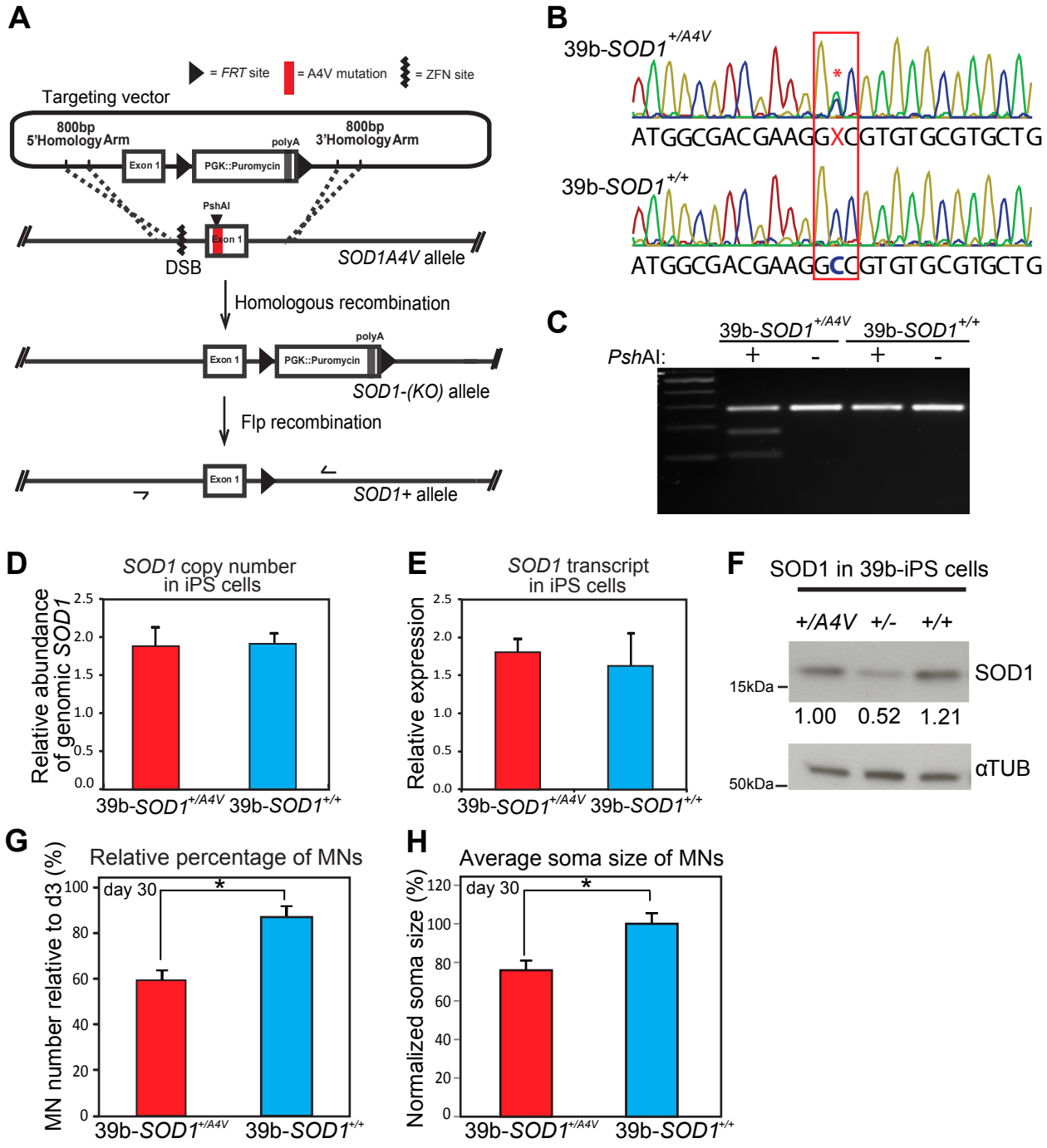

Figure 2.7 Genetic correction of *SOD1A4V* allele rescues MN survival and soma size deficits

A. Gene targeting strategy used to generate the isogenic 39b-*SOD1*$^{+/+}$ iPS cell line. See Methods section for details (ZFN, zinc-finger nuclease; FRT, Flippase Recognition Target). **B** Sequencing chromatograms of *Exon1* of *SOD1* in iPS cell line 39b before and after targeting demonstrate the correction of the A4V mutation. **C**. PshAI restriction digestion of amplified SOD1 cDNA before and after gene targeting. The mutation creates a PshAI restriction site that is absent in the corrected line. **D.** qPCR of genomic *SOD1* shows that there are no extra copies of the gene in the corrected line. **E.** qRT-PCR of cDNA shows that the expression levels of *SOD1* are the same in the corrected line (n = 3, ±SEM)**. G-H** Genetic Correction of the *SOD1A4V* Mutant Allele Rescues MN Survival and Soma Size Deficits. Isogenic 39b-*SOD1*$^{+/+}$ MNs exhibit increased cell survival (n=6,m>13,000,±SEM,p <0.05) (in G) and restored soma size (n = 3, m = 280, ±SEM, p < 0.01) (in H)

12,000 genomic loci with sequence similarity to the binding site of the ZFN pair described in this study did not deviate between the parental or gene edited cell lines, indicating highly specific nuclease activity.

In order to detect other potential genome sequence changes in the corrected cell line, we also compared the fine-scale (SNP and indel) sequence calls between the two iPS cell lines across their genomes. Overall, we found the corrected cell line to be surprisingly free of such events. However, these analyses were sufficiently sensitive to identify a likely mitotic recombination event on the q arm of chr12 (from 108Mb to the end of the chromosome). Deeper analysis of this region demonstrated that the event had not induced novel or rare protein-coding variants. Neither had it induced coding variants associated with any known disease state, suggesting this event was likely to be phenotypically neutral. Analysis of the protein-coding sequences of 26 candidate genes implicated in ALS[4, 6] identified a single protein-altering sequence difference between the two cell lines, which corresponded to the genome edit of the A4V variant in *SOD1*.

Following validation of the genetic correction of the ALS-linked allele, we used 39b-*SOD1*$^{+/A4V}$ and 39b-*SOD1*$^{+/+}$ isogenic cell lines to ask whether the SOD1A4V-encoding variant was necessary for the MN survival and soma size phenotypes observed in the patient versus control comparisons. Importantly, correction of the mutation resulted in a significant rescue of both MN survival ($n=6, m>13000, p<0.05$) and relative soma size deficits ($n=3, m=140, p<0.01$) (Figure 2.7G-H).

2.2.4 Solubility of mutant SOD1 in iPS cell-derived MN cultures

SOD1 protein variants that cause ALS are prone to unfolding, misfolding and ultimately aggregation[44, 45]. Aggregation of SOD1 protein and the formation of SOD1-rich inclusions is a

pathological finding in animals models of this disease[46], as well as at autopsy in the spinal cords of *SOD1*-linked cases[47, 48] and some sporadic cases[49]. SOD1 aggregation can be detected in spinal cord extracts using detergent solubility assays[50]. However, the relevance of SOD1 insoluble aggregates to disease processes is poorly understood and it remains unresolved whether SOD1 aggregation lies on the critical pathway to neuronal degeneration, and whether these structures are toxic or protective in nature[51].

The pair of isogenic iPS cell lines we developed allowed us to address the state of SOD1 protein in differentiated human MNs expressing physiological levels of this protein. Using immunoblot assays on detergent-soluble (RIPA) and detergent-insoluble (UREA) fractions obtained from cultures of differentiated $SOD1^{+/+}$ and $SOD1^{+/A4V}$ MNs, we found no evidence of insoluble SOD1 protein under basal culture conditions (Figure 2.8A). In order to sensitize our culture system and validate the ability of our assay to detect insoluble SOD1 protein, we treated MN cultures with the proteasome inhibitor MG132, which increased SOD1 protein levels 2-4 fold (Figure 2.8A-D), and resulted in the accumulation of detergent-insoluble (urea-soluble) SOD1 in $SOD1^{+/A4V}$ neurons, but not in isogenic control cells (Figure 2.8A).

These studies suggest that while it is possible to induce accumulation of insoluble mutant SOD1 protein in human MNs, insoluble protein did not accumulate to appreciable levels under normal culture conditions. Although we cannot rule out the possibility that undetectable levels of aggregated SOD1 protein were the cause of the cell survival deficits of $SOD1^{+/A4V}$ MNs (Figure 2.4), our findings are consistent with recent claims that soluble mutant SOD1 can have substantial phenotypic effects[44].

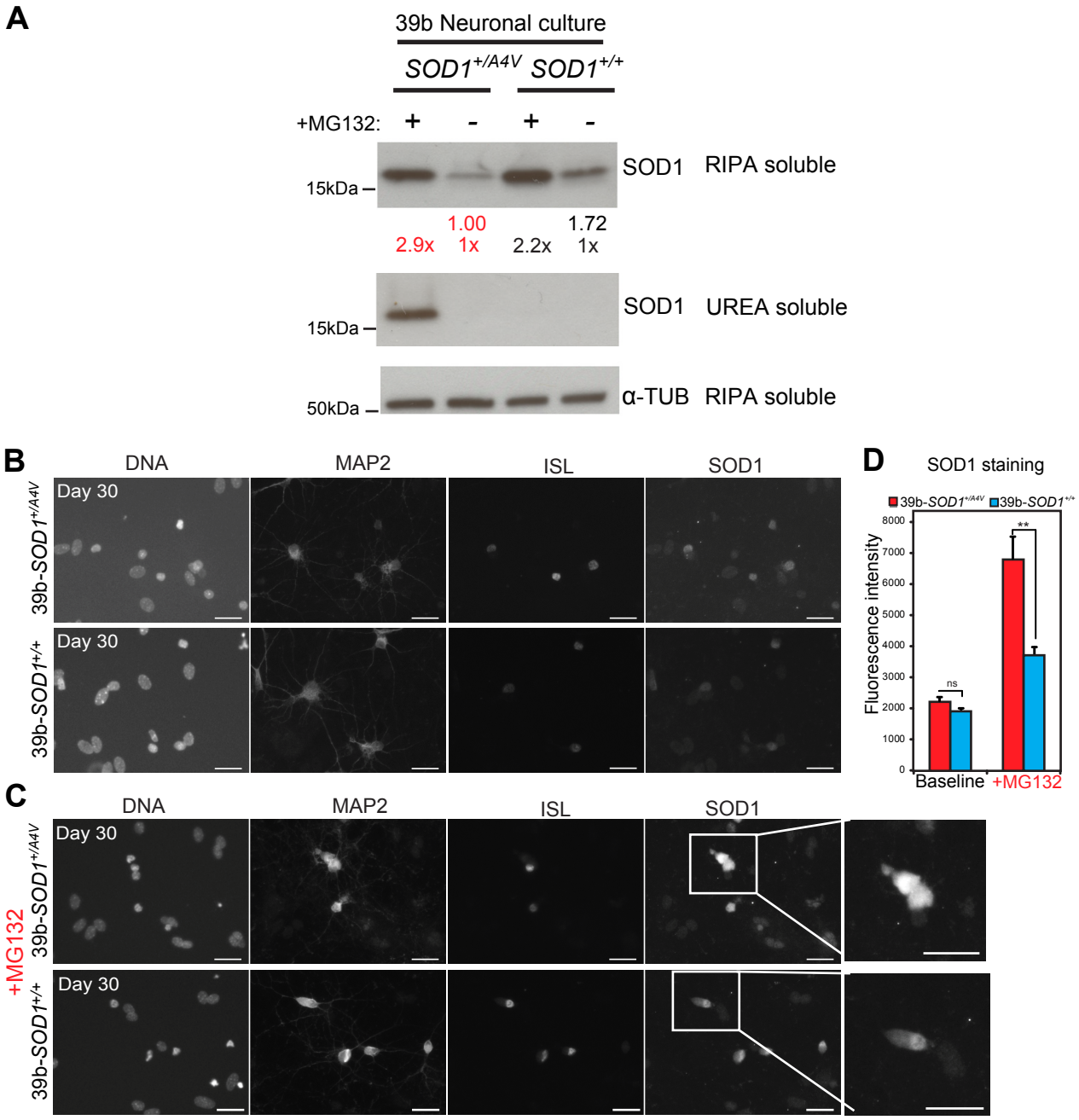

Figure 2.8 Proteasome inhibition causes SOD1 protein aggregation in *SOD1*$^{+/A4V}$ neurons.
A. Immunoblot analysis of SOD1 protein in detergent-soluble (RIPA) and detergent-insoluble (UREA) fractions obtained from differentiated neuronal cultures 12 days after differentiation. Insoluble SOD1 is not detected under basal culture conditions. After proteasome inhibition following treatment with MG132, insoluble SOD1selectively accumulates only in *SOD1*$^{+/A4V}$ neurons and not in the corrected cells. **B-D.** Immunocytochemistry analyses of SOD1 expression in differentiated MNs following treatment with MG132 detected increased immunoreactivity to SOD1 in *SOD1*$^{+/A4V}$ MNs, supporting the findings from immunoblot assays.

2.2.5 RNA-Seq of purified *SOD1*$^{+/A4V}$ and isogenic control MNs

Although the changes in gene expression induced in the mouse nervous system by mutant SOD1 have been extensively studied[52-55], it is unknown how mutant SOD1 impacts transcript levels in human MNs. In order to gain insight into molecular pathways affected by the *SOD1*A4V mutation, we performed RNA sequencing (RNA-Seq). As in earlier experiments, we differentiated 39b-*SOD1*$^{+/A4V}$ and isogenic control iPS cells into MNs, and plated these cells onto a murine glial monolayer. We next transduced these cultures with an *Hb9::RFP* lentiviral reporter[56], and at day 15 of co-culture we purified RFP^{+} MNs for transcriptional studies (Figure 2.9A). We chose day 15 for analysis as at this time point MNs were physiologically active (Figure 2.3), but there was only a trend towards reduced MN survival in *SOD1*$^{+/A4V}$ cultures (data not shown). Therefore, we reasoned that on day 15 we might identify the transcriptional changes that predisposed mature MNs to apoptosis.

RNA and sequencing libraries were prepared from *SOD1*$^{+/A4V}$ and *SOD1*$^{+/+}$ RFP+ cells and then subjected to sequencing. The quality of all libraries was validated using FastQC and reads were quantified after alignment and mapping to the reference genome hg19. We first asked whether the effects of the *SOD1*$^{+/A4V}$ genotype on transcriptional patterns in differentiated MNs were greater than the variability present between biological replicates of our experimental system. Indeed, unsupervised hierarchical clustering segregated samples based on their *SOD1* genotype, suggesting that effects of the mutant allele were driving measurable transcriptional differences between *SOD1*$^{+/A4V}$ and *SOD1*$^{+/+}$ MNs (Figure 2.9B). We determined, as a measure of the transcripts most affected by the ALS-linked mutation, the identity of the 30 transcripts most increased and decreased in abundance in mutant MNs relative to controls, at a false discovery rate (FDR) of 5% (Figure 2.9C). Validating the importance of this unbiased

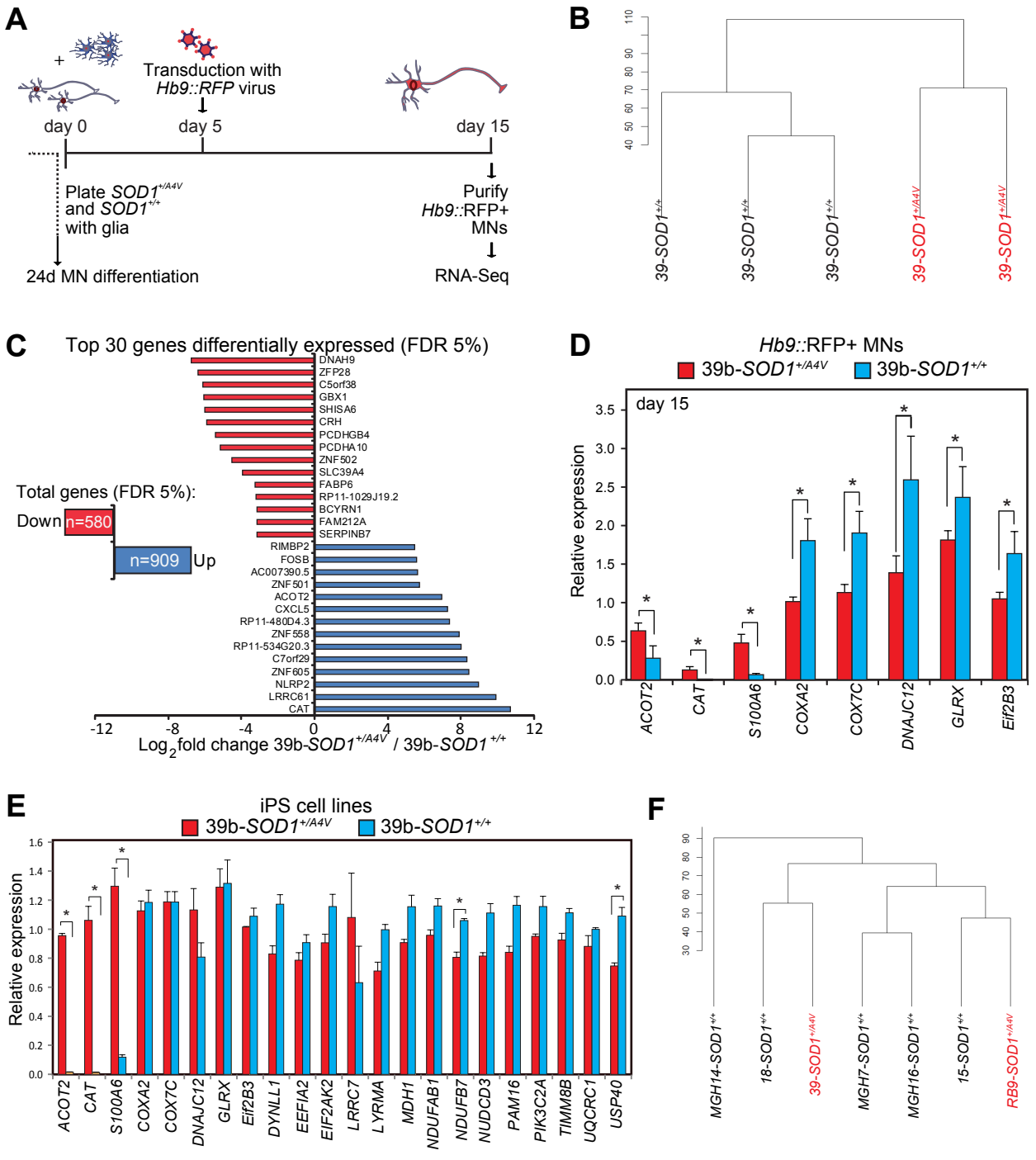

Figure 2.9 RNA-Seq revealed transcriptional changes induced by mutant SOD1 in *SOD1*$^{+/A4V}$ MNs

A. Experimental outline: Isogenic *SOD1*$^{+/A4V}$ and *SOD1*$^{+/+}$ MNs were co-cultured with primary glial cells, transduced with an *Hb9::RFP* lentivirus, and FACS-purified on day 15 for RNA isolation and sequencing. **B.** Dendogram demonstrating clear genotypic clustering, based on transcriptional changes measured by RNA-Seq. **C.** Total number of genes and top 30 genes (based on fold change) misregulated in *SOD1*$^{+/A4V}$ MNs (FDR of 5%). **D.** qRT-PCR validation of misregulated genes in independent samples. **E.** qRT-PCR analysis in 39b-*SOD1*$^{+/A4V}$ and isogenic 39b-*SOD1*$^{+/+}$ iPS cell lines. Genes identified as being differentially regulated as a result mutant SOD1 in *Hb9::*RFP^{+} MNs were evaluated in the parental iPC cells, with 19% of these genes detected as also being significantly different. **F.** Cluster dendogram of RNA sequencing of fibroblast samples obtained from *SOD1*$^{+/A4V}$ ALS patients and *SOD1*$^{+/+}$ sex-matched healthy controls, showing that ALS fibroblasts (highlighted in red) did not segregate from controls.

approach, we found that a considerable number of genes identified to be misregulated in *SOD1*$^{+/A4V}$ MNs have not, to our knowledge, previously been implicated as modulated by mutant SOD1. These included *ACOT2*, an enzyme that hydrolyzes Coenzyme A esters[57]; the transcription factor *FOSB* which regulates BDNF expression[58], and *NLRP2,* a NOD-like receptor and pro-apoptotic component of the inflammasome[59] (Figure 2.9C). Consistent with the model of mutant SOD1 protein as a driver of oxidative stress and neuroinflammation[46, 60], the genes encoding for the antioxidant enzyme CATALASE (*CAT*) and the inflammatory chemokine CXCL5 were among most highly deregulated in *SOD1*$^{+/A4V}$ MNs (Figure 2.9C). qRT-PCR analyses of a representative subset of genes in independent experiments validated our RNA-Seq findings (Figure 2.9D).

To understand whether a subset of the gene expression changes found by RNA-seq were likely to be specific to MNs and not present in other cell types less affected in ALS, we determined the expression of a subset of differentially expressed transcripts in the pair of isogenic 39b iPS cell lines. Of 22 genes analyzed, only 19% were detected as differentially expressed both in iPS cells and in MNs (Figure 2.9E). Furthermore, we performed RNA-seq on fibroblast samples obtained from 5 healthy control individuals and the two ALS *SOD1*$^{+/A4V}$ patients (39 and RB9). Contrary to what we observed when MN samples were analyzed (Figure 2.9B), unsupervised hierarchical clustering failed to segregate fibroblast transcriptomes based on the *SOD1* genotype (Figure 2.9F).

In order to probe the RNA-seq data for biological meaning we utilized two bioinformatic tools that query for enriched gene ontology terms. We first performed gene-annotation enrichment analysis with DAVID[61], using all the genes that were significantly altered (909 upregulated and 580 downregulated) in *SOD1*$^{+/A4V}$ MNs at a FDR of 5%. A total of 27 and 65

gene terms were enriched when increased and reduced transcripts, respectively, were considered. Transcripts implicated in cytoskeleton organization, where amongst the most significantly induced (rank of significance 5, FDR=5.84x10^{-7}) in *SOD1*$^{+/A4V}$ MNs, consistent with the morphological alterations that we observed in these cells relative to isogenic controls (Figure 2.6). Among the transcripts most significantly decreased by mutant SOD1, there was a very strong enrichment for genes implicated in mitochondrial function and structure. In particular, 60% of all downregulated ontology terms were related to mitochondria. A total of 93 genes curated in the term 'mitochondrion' (rank of significance 1, FDR=6.3x10^{-26}), including various cytochrome C components, ATP transportin and ribosomal protein subunits were strongly repressed in the presence of the mutation.

As an alternative approach for querying our RNA-seq data for over-represented gene properties, we performed Gene Set Enrichment Analysis (GSEA)[62]. GSEA identified 100 gene sets to be significantly repressed in *SOD1*$^{+/A4V}$ MNs (NES<1.5); and notably, gene sets associated with mitochondrial function were again amongst the most significantly suppressed.

2.2.6 *SOD1*$^{+/A4V}$ neurons exhibit disturbances in mitochondrial morphology and motility

To determine whether the changes in mitochondrial genes that we identified by RNA-Seq in *SOD1*$^{+/A4V}$ MNs were indicative of actual disturbances to mitochondria, we performed electron microscopy (EM) studies (Figure 2.10A-B). Whereas mitochondrial morphology was normal in neurons differentiated from a control iPS cell line (18a), mitochondria in *SOD1*$^{+/A4V}$ neurons (39b and RB9d) often were structurally deranged and more vacuolar in appearance, and accumulated in large numbers in neuronal processes (Figure 2.10B). We concluded that distortion in mitochondrial morphology was mediated by expression of mutant SOD1, because correction of the *SOD1A4V* allele eliminated this phenotype (Figure 2.10B). To further validate

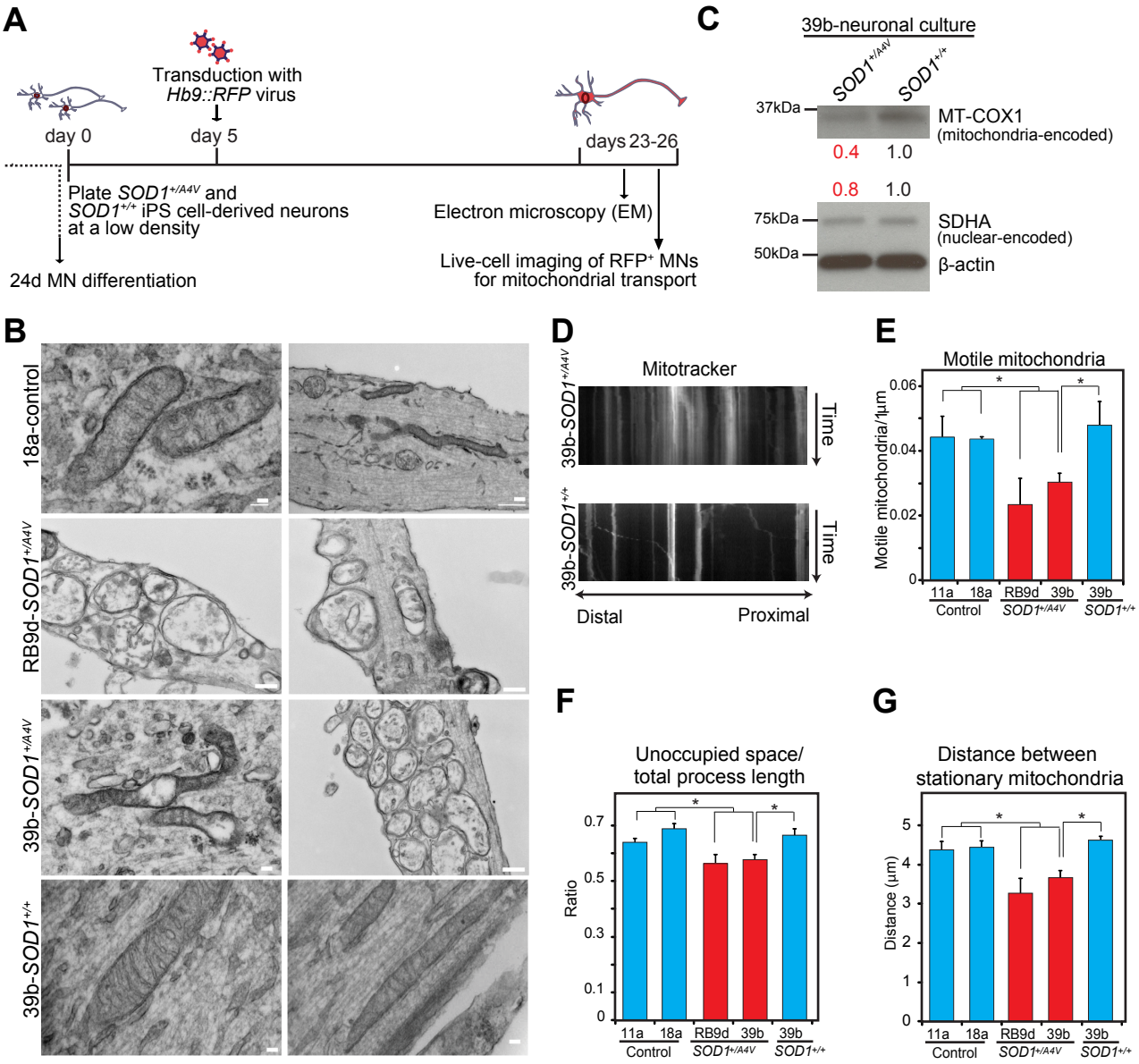

Figure 2.10 Mitochondrial defects in *SOD1*$^{+/A4V}$ neurons are rescued by correction of the *SOD1* mutant allele
A. Experimental outline: *SOD1*$^{+/A4V}$ and isogenic control MN cultures were plated at low densities, transduced with an *Hb9::RFP* construct, and analyzed on days 23–26. **B.** EM analysis demonstrating that in contrast to control neurons (top panel) and *SOD1*$^{+/+}$-corrected cells (bottom panel), *SOD1*$^{+/A4V}$ neurons (middle panels) often exhibited swelling, morphological disorganization, and clustering of mitochondria in neurites. Representative images from three independent experiments are shown (Thick scale bar =100nm). **C.** Immunoblot assays showing reduced levels of mitochondrial proteins in *SOD1*$^{+/A4V}$ neurons compared to isogenic control cells. **D.** Representative kymographs of MitoTracker-stained mitochondria in RFP^{+} MNs after live-cell imaging. Distal and proximal orientation relative to the cell body is indicated. **E-G.** *SOD1*$^{+/A4V}$ MNs exhibit mitochondria transport deficiencies relative to controls with fewer motile mitochondria (**E**), less space unoccupied by these organelles relative to axon length (**F**), and shorter distances between stationary mitochondria (**G**).

mitochondrial damage in differentiated *SOD1*$^{+/A4V}$ MNs, we used immunoblot assays to quantify the levels of two mitochondrial proteins, SDHA (SUCCINATE DEHYDROGENASE COMPLEX SUBUNIT A), which is encoded in the nucleus, and MT-COX1 (CYTOCHROME C OXIDASE I), encoded by the mitochondrial genome. We found that *SOD1*$^{+/+}$ gene-edited neurons exhibited increased levels of both SDHA and MT-COX1 proteins relative to the parental *SOD1*$^{+/A4V}$ cells, which is consistent with mitochondrial defects being mediated by mutant SOD (Figure 2.10C).

As changes in mitochondrial dynamics have been previously reported in cellular and animal models of ALS[63, 64], we next sought to examine the movements of mitochondria within the neuronal processes of *Hb9*::RFP+ MNs differentiated from control and *SOD1*$^{+/A4V}$ iPS cells, using MitoTracker-Green, which selectively stained mitochondria. We then carried out live-cell imaging to register mitochondrial movement along MN processes over the course of 5 minutes, and we generated time/distance kymographs for further analyses (Figure 2.10A and 2.10D). We found that expression of mutant SOD1 resulted in a significant decrease in the number of motile mitochondria (Figure 2.10E). This deficit was coupled to an increase in mitochondrial density in processes, as measured by the shorter distance between stationary mitochondria and the significantly smaller amount of space unoccupied by these organelles (Figures 10F-G).

2.2.7 Hyperexcitability of iPS cell-derived *SOD1*$^{+/A4V}$ MNs

Previous nerve conduction studies evaluating axonal threshold (strength-duration time constant and recovery cycle times) in ALS patients have demonstrated increased axonal membrane excitability[27, 28], and the degree of hyperexcitability correlated with ALS patient survival[29]. These data indicate that increased membrane excitability may be relevant as a contributor to the disease, and modeling suggests that either increased persistent sodium or reduced delayed-rectifier potassium currents could be responsible for the axonal

hyperexcitability[28, 65]. However, whether hyperexcitability results from changes in the autonomous properties of MNs cannot be determined by this technique[66].

In order to examine the electrophysiological phenotype of isogenic *SOD1*$^{+/A4V}$ and *SOD1*$^{+/+}$ differentiated MNs, we first used extracellular multielectrode arrays (MEA) to record spontaneous firing in these cells. Because substantial cell death begins in the patient iPS cell-derived MNs after 15 days of neuronal maturation in our culture conditions, we compared MEA recordings of *SOD1*$^{+/+}$ and *SOD1*$^{+/A4V}$ MNs neurons at 14 days, to avoid the possibility that increased firing might reflect either neuronal death or the selective survival of hyperexcitable neurons. Analysis of MEA data revealed that *SOD1*$^{+/A4V}$ differentiated neurons had a far higher spontaneous firing rate than the genetically corrected *SOD1*$^{+/+}$ control neurons (Figure 2.11A). We also used whole-cell patch recordings to characterize individual *SOD1*$^{+/A4V}$ and *SOD1*$^{+/+}$ MNs labeled with the *Hb9::RFP* lentiviral reporter[56] (Figure 2.11B), and detected a marked difference in the number of action potentials elicited during ramp depolarization (Figure 2.11C-D), confirming the findings from MEA experiments. Taken together, these results indicate that in our *in vitro* model the hyperexcitability phenotype precedes cell death, and that it requires the ALS-linked *SOD1* mutation.

2.2.8 Validation of *SOD1*-associated phenotypes using a distinct set of isogenic cell lines

In order to further validate some of the cellular phenotypes we described above, we decided to generate an independent set of *SOD1*$^{+/A4V}$ and *SOD1*$^{+/+}$isogenic cell lines by introducing the *SOD1A4V* mutation into the wild-type *SOD1* locus of the human embryonic stem cell line HUES3 *Hb9::GFP*[30]. This experimental approach on this particular cell line allowed us to address two relevant questions. First, by inducing the *SOD1A4V* mutation in a human cell line

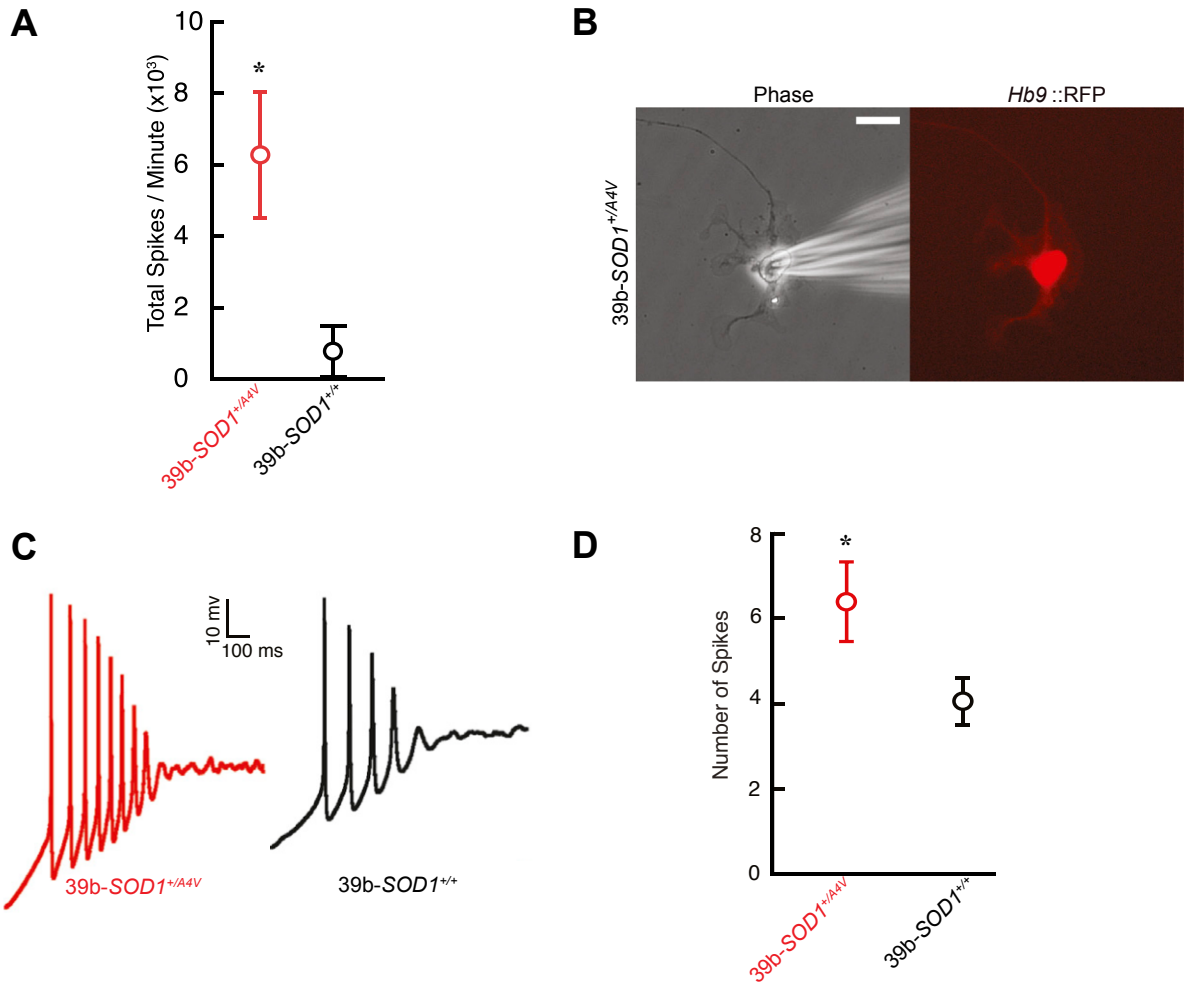

Figure 2.11 Physiological recordings reveal increased excitability in *SOD1$^{A4V/+}$* MNs.
A. Total action potential firing rate during 1 min of recording using multielectrode arrays (MEAs) on differentiated MNs cocultured with glial cells for 14 days on the arrays (39b-*SOD1$^{+/A4V}$* n=4, mean 6,278 ± 1,758 spikes/min; 39b-*SOD1$^{+/+}$*, n = 4, mean 775 ± 712 spikes/min; Error bars represent SEM; *p = 0.01, t test). **B**. An iPS cell-derived MN during patch-clamp recording (left panel) after 28 days of culture (Scale bar = 20µm). MNs in the culture were identified by expression of an *Hb9::RFP* lentiviral reporter (right panel). **C.** Representative current clamp recordings during ramp depolarization from ALS patient-derived *SOD1$^{+/A4V}$* MNs and isogenic controls. **D.** Average number of action potentials during ramp depolarization for *SOD1$^{+/A4V}$* (n=19; mean 6.4±0.9) and *SOD1$^{+/+}$* (n=17; mean 4.1±0.5) MNs from three independent experiments (*p<0.05, Mann-Whitney U test).

that was not derived from a patient with a clinical history of ALS, we can assess the sufficiency of the SOD1A4V protein variant to drive *in vitro* disease-related phenotypes. This is important to account for the possibility that the genetic background of the 39b patient iPS cell-derived MNs included additional mutations in other ALS-linked genes or risk factors that exacerbated their *in vitro* phenotypes. In addition, the *Hb9::GFP* construct in the HUES3 cell line can be used to purify by FACS the differentiated spinal MNs away from the heterogeneous mixture of cell types obtained after differentiation[33, 67-70]. Several *in vitro*[30, 56, 68, 71] and *in vivo*[72-74] studies have demonstrated that expression of mutant SOD1 in other neural cell types can be toxic to MNs and influence disease progression. Therefore, by isolating GFP^+ MNs from other neural cell types, we could further elucidate the contribution to ALS of cell-autonomous versus non-cell autonomous pathways.

Using again a two-step nuclease-mediated gene targeting strategy[42], we introduced the *SOD1A4V* mutation into the HUES3 *Hb9::GFP* genetic background (Figure 2.12A). After corroborating the desired *SOD1* gene edit (Figure 2.12B-D), we directed the differentiation of $SOD1^{+/+}$ and $SOD1^{+/A4V}$ HUES3 *Hb9::GFP* cells into MNs using dual SMAD inhibition for neural induction, and retinoic acid and SHH signaling for MN patterning[32, 33] (Figure 2.13). GFP^+ MNs of both genotypes could be isolated using FACS (Figure 2.13A), and *SOD1* transcript and protein expression in these cells was confirmed (Figure 2.13B-C). GFP^+ expressed the MN transcription factor ISL (Figure 2.13D), and even in the absence of a glial monolayer they could be cultured with good viability for 10 or more days (Figure 2.13E).

We next used the isogenic $SOD1^{+/+}$ and $SOD1^{+/A4V}$ HUES3-differentiated MNs to assay three *in vitro* phenotypes. First, we used immunoblot assays to probe the solubility state of SOD1 protein in cultures of differentiated MNs. We determined that proteasome inhibition in

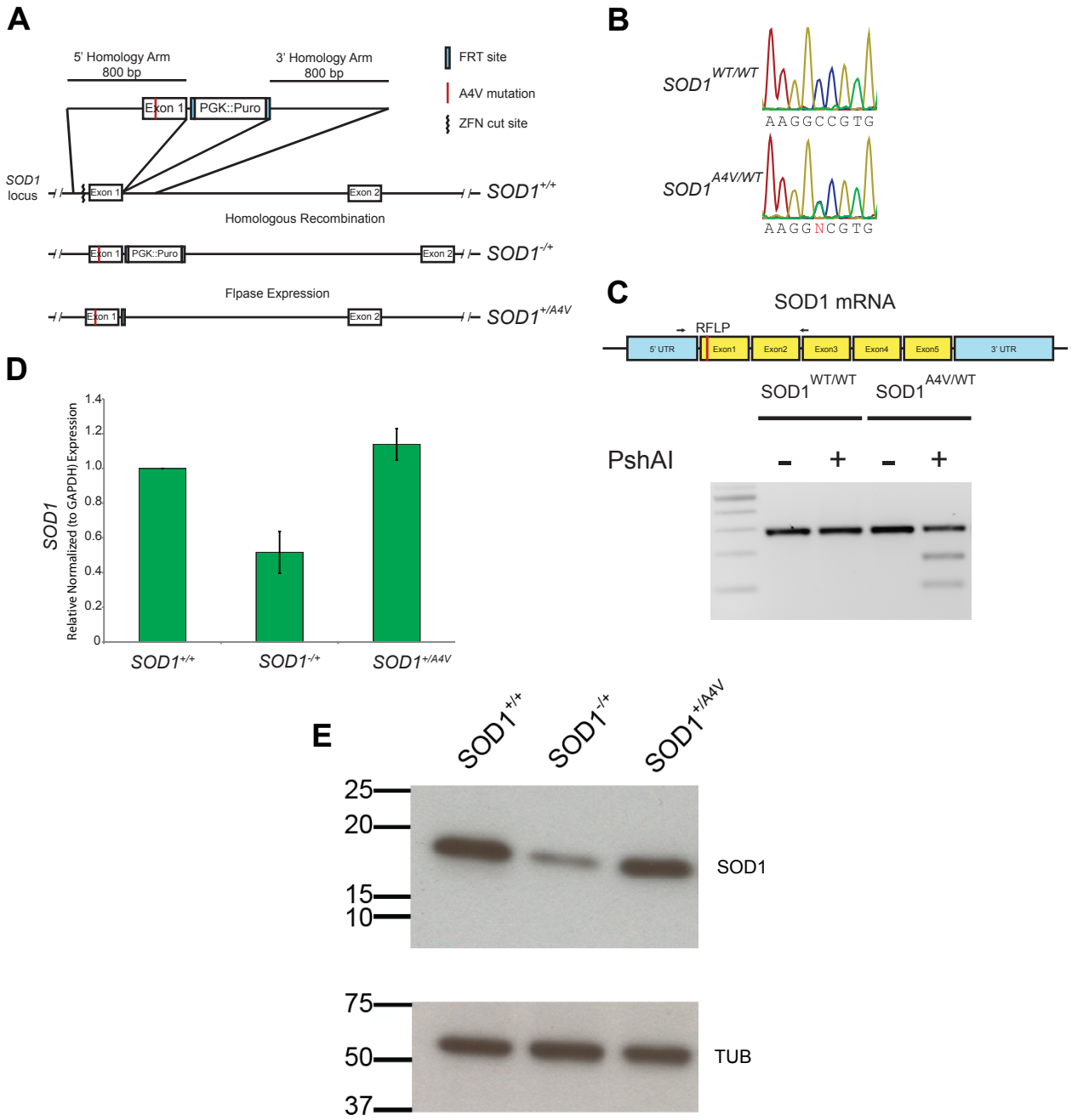

Figure 2.12 Introduction of the *SOD1A4V* mutant allele into the *SOD1* locus of HUES3 *Hb9::GFP*
A. Diagram of gene targeting strategy (see Methods section for details). **B.** Sequencing of the *SOD1* locus and PCR-RFLP analysis for a unique PshAI restriction site confirmed correct targeting. **D-E.** qRT-PCR and immunoblot assays for SOD1 expression in targeted stem cell lines demonstrated reduced levels of the *SOD1* transcript (in D) and protein (in E) in the intermediate HUES3 $SOD1^{-/+}$ cell line, which are restored in the HUES $SOD1^{+/A4V}$ targeted cell line.

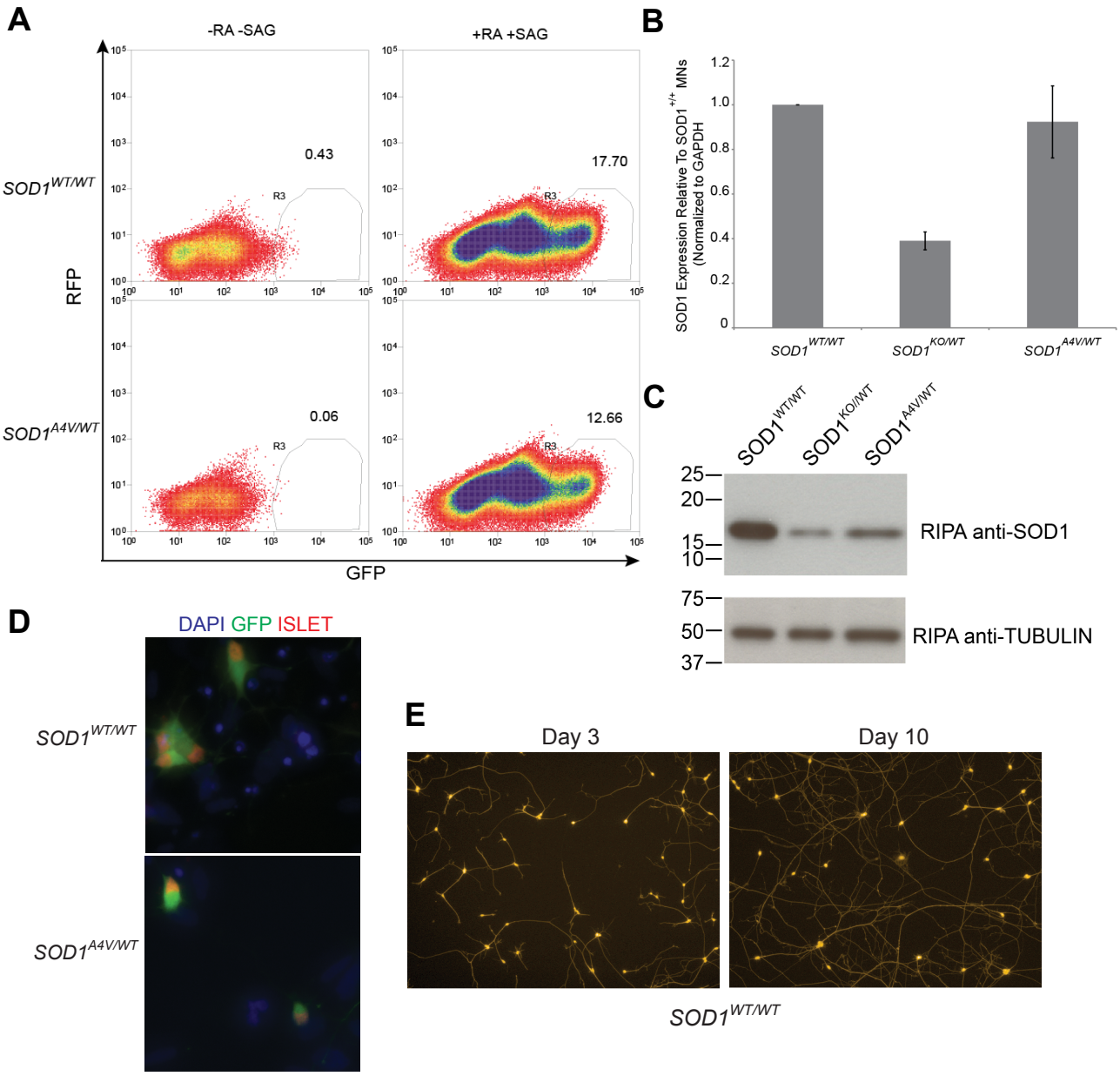

Figure 2.13 GFP⁺ MNs from *SOD1*$^{+/+}$ and *SOD1*$^{+/A4V}$ isogenic HUES3 cells

A. FACS plots depicting a distinct population of differentiated cells which express the GFP reporter. Differentiated neural cells not exposed to the MN patterning molecules RA and SAG were used as negative control to gate for green fluorescence. **B-C.** qRT-PCR and immunoblot assays demonstrated that *Hb9::*GFP⁺ MNs of both genotypes express the *SOD1* transcript (in B) and SOD1 protein (in C). **D.** *Hb9::*GFP⁺ express the transcription factor ISLET1 indicating spinal MN identity. **E**. *Hb9::*GFP⁺ cells can be plated after FACS isolation and maintained as purified MN cultures, as determined by live-cell imaging of MN cultures stained with a live-cell dye, at sequential time points (day 3 and day 10)

cultured neurons differentiated from HUES3 *SOD1*$^{+/A4V}$ but not HUES3 *SOD1*$^{+/+}$ resulted in accumulation of SOD1 protein in the detergent-insoluble fraction (Figure 2.14A). These results demonstrate the sufficiency of the *SOD1A4V* mutation to alter the processing of the SOD1 protein, and validate our previous observations with the 39b-derived neurons (Figure 2.8A).

Second, using multielectrode array (MEA) recordings we assessed the electrophysiological activity of purified *SOD1*$^{+/+}$ and *SOD1*$^{+/A4V}$ GFP^{+} MNs co-cultured with murine glia. By collecting MEA data every 3 days over a 40-day period, we found that cultures with HUES3 *SOD1*$^{+/A4V}$ MNs exhibited heightened spike rates after 3 weeks in culture (Figure 2.14B), similar to our previous findings with unsorted 39b-derived MNs (Figure 2.11). These observations suggest that expression of mutant SOD1 in MNs is sufficient to induce their increased membrane excitability phenotype, and that this can occur through cell-autonomous pathways.

Lastly, we interrogated the cell autonomous impact of the induced *SOD1A4V* mutant allele on the cell survival of MNs. To this end, FACS-purified GFP^{+} MNs of both *SOD1* genotypes were seeded on a monolayer of murine glial cells on 8-well tissue culture slides, and at day 3 and day 30 after plating, these co-cultures were fixed and stained using antibodies recognizing a human-specific nuclear antigen (HumNuc^{+}) and the neuronal cytoskeletal protein β-III TUBULIN (TUJ1^{+}) (Figure 2.14C). Using whole-well imaging and automated counting of HumNuc+ cells, we detected a trend for reduced cell survival for HUES3 *SOD1*$^{+/A4V}$ MNs compared to their *SOD1*$^{+/+}$ isogenic control (Figure 2.14D). Currently, we have three non-exclusive hypotheses that could explain why the more prominent cell survival deficit we observed with the *SOD1*$^{+/A4V}$ iPS cell-derived MNs (Figure 2.4) was not recapitulated here. One model is the non-cell autonomous contribution to the survival phenotype from other

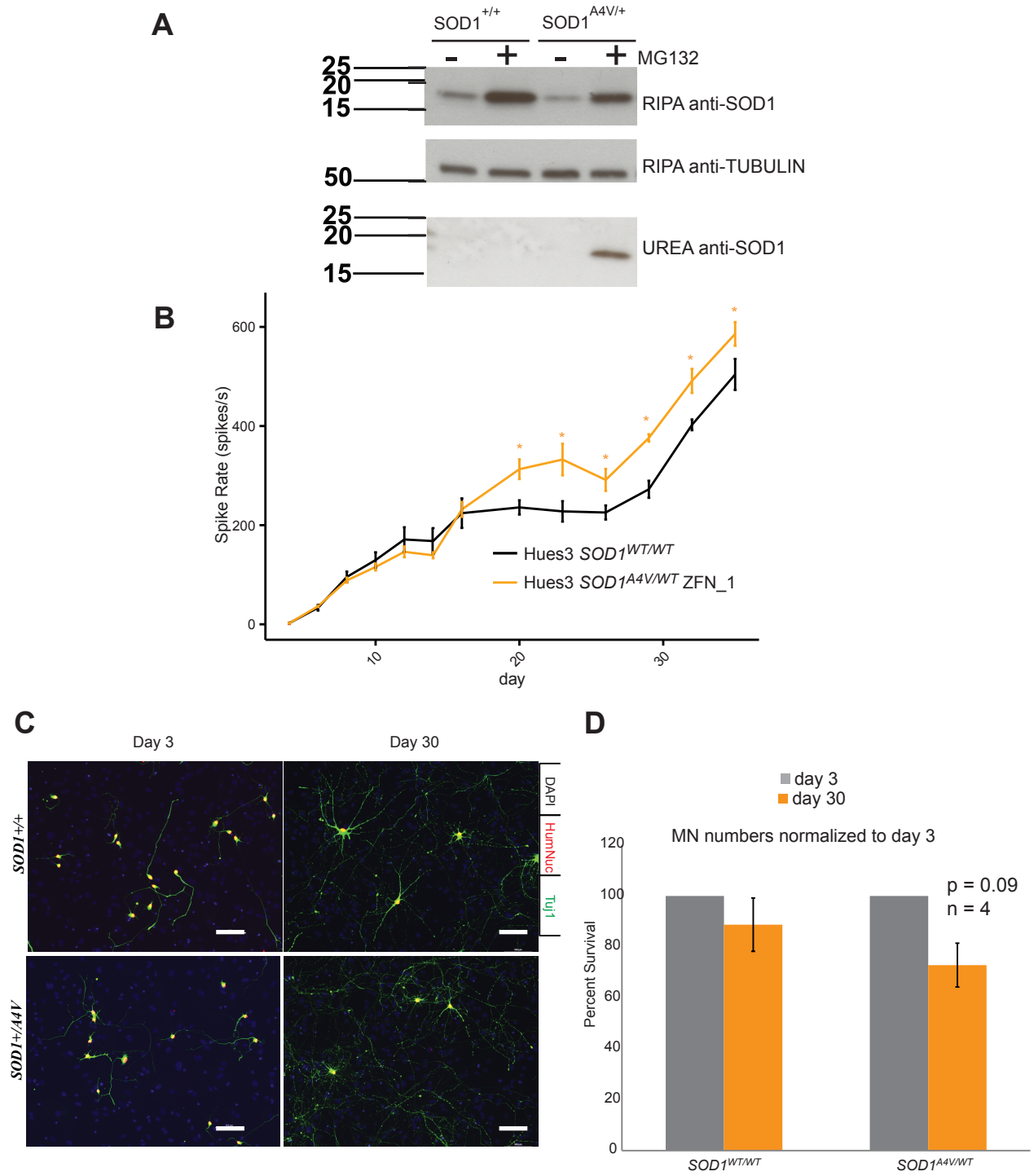

Figure 2.14 Characterization of GFP⁺ MNs from *SOD1*$^{+/+}$ and *SOD1*$^{+/A4V}$ isogenic HUES3 cells.
A. Solubility status of SOD1 proteint in *SOD1*$^{+/+}$ and *SOD1*$^{+/A4V}$ cultures of differentiated MNs. SOD1 accumulates in the insolube (UREA) protein fraction when cultures expressing the SOD1A4V variant are treated with the proteosome inhibitor MG132. **B.** *SOD1*$^{+/A4V}$ MNs derived from HUES3 show increased membrane excitability as determined by longitudinal MEA recordings ($p<0.05$). **C-D.** Cell survival assays indicate a trend for reduced survival in MNs expressing the SOD1A4V variant relative to the isogenic control. Representative images of Human Nuclei and TUJ1 staining at days 3 and 30 are shown in (C). A modest but not statistically-significant reduction in MN survival was found in the HUES3-*SOD1*$^{+/A4V}$ MNs when compared to *SOD1*$^{+/+}$($p = 0.09$, $n= 4$).

differentiated non-MN cell types expressing mutant SOD1, which is eliminated in the co-culture experiments with purified GFP^+ MNs. A second explanation is that the genetic background of the HUES3 cell line includes mutations that decrease the pro-apoptotic phenotype induced by mutant SOD1[75]. Additionally, subjecting the HUES3 differentiated cells to the shear stress of FACS could select early on for a subgroup of particularly hardy MNs that perform better in culture. Further work with experimental conditions more similar to the ones used with the iPS cell-derived neurons (unsorted cells and $ISL^+/TUJ1^+$ counts; Figure 2.4) is in progress, and will help us address some of these hypotheses.

2.3 Discussion

Transgenic rodent models of ALS have been indispensable for developing hypotheses concerning how mutant SOD1 proteins induce MN degeneration. However, studies in these animals have yet to yield an effective treatment[17, 18]. We reasoned that the gulf between successful animal studies and more positive clinical outcomes might be bridged with model systems that would enable hypotheses originating from animals to be validated and extended in the context of human MNs bearing only patient mutations. Utilizing iPS cell technology and directed differentiation, we set up a well-controlled cell culture system and interrogated the differential properties of MNs derived from ALS patient iPS cells and healthy controls. Advances in genome editing tools, which we have employed here, allowed our studies of the SOD1A4V variant to be elevated beyond correlative distinctions between ALS cases and controls, to the establishment of causal connections between this mutation and the resulting phenotypes.

Our studies demonstrate that the *SOD1A4V* missense mutation was necessary to cause a pro-apoptotic phenotype in cultured human differentiated MNs, restricting their long-term

survival. By employing RNA sequencing, we defined the transcriptional differences between human *SOD1*$^{+/A4V}$ and isogenic *SOD1*$^{+/+}$ control MNs, and determined that mutant SOD1 induced the downregulation of mitochondrial pathways. Additionally, we identified novel candidate genes, previously unstudied, which are substantially modulated by this mutation. These new genes will require further investigation as they may potentially represent therapeutic targets. The data set could serve as an invaluable resource for many future studies of ALS. It is important to note that the expression profiles that we present reflect the pathway disturbances and expression changes of *SOD1*$^{+/A4V}$ MNs at a single time-point. Future work involving an appropriate time-course analysis should unveil the progressive nature and sequence of events that lead to MN degeneration.

We also show that *SOD1*$^{+/A4V}$ MNs manifest additional *in vitro* phenotypes that recapitulate some of the hallmarks of disease found in both patients and in animal models. These phenotypes included deficits in mitochondrial transport and morphology, and increased membrane excitability, which were dependent on the presence of the *SOD1A4V* mutation. Notably, further work by other members of our group and collaborators at Harvard Medical School has demonstrated that the FDA-approved drug retigabine, a Kv7 potassium channel activator, blocks the hyperexcitability phenotype and improves the *in vitro* survival of *SOD1*$^{+/A4V}$ MNs[76, 77], suggesting that increased membrane excitability may contribute to MN degeneration in ALS.

Taken together, our results validate the utility of human pluripotent stem cell-derived MNs in the development of novel *in vitro* models of ALS. In the future, a combination of similar iPS/ES cell and gene-editing technologies could be used to investigate whether mutations in the long list of ALS-associated genes of diverse functions[3, 6, 7] coalesce in the same, similar or

distinct molecular pathways to degeneration. The answer to this question will allow the design and implementation of more effective therapies, perhaps targeted to specific sub-types of ALS.

2.4 Material and Methods

2.4.1 Cell culture

Cell cultures were maintained at 37ºC, 5% CO2. Human fibroblasts were cultured in KO-DMEM (Life Tecnologies), supplemented with 20% Earl's salts 199 (Gibco), 10% Hyclone (Gibco), 1x GlutaMax (Invitrogen), and 100μM 2-mercaptoethanol, and passaged by trypsinization (0.25% trypsin EDTA, Invitrogen). ES and iPS cells were maintained on Matrigel (BD Biosciences) with mTeSR1 media (Stem Cell Technologies). Media was changed every 24 hours and cell lines were passaged by dispase (Gibco, 1mg/mL for 30min at 37ºC).

2.4.2 Derivation of human fibroblasts and iPS cell generation

Human fibroblasts were generated from 3 mm forearm dermal biopsies following informed consent as described previously[19]. Generation of iPS cells was carried out by retroviral transduction of *OCT4*, *SOX2* and *KLF4*, as previously reported[34]. Retroviruses were prepared by the Harvard Gene Therapy Initiative group at Harvard Medical School (Boston, MA). For iPS cell derivation, 30,000 human fibroblasts were transduced at an MOI of 3-5 per gene.

2.4.3 'Scorecard' assay

RNA samples for analysis of pluripotency with 'Scorecard' assay were produced and analyzed as described previously[31], with minor modifications. Whole iPS and ES cell colonies were isolated by dispase treatment and plated in suspension in the presence of mTeSR1 media, cell aggregates or 'embryoid bodies' (EBs) were allowed to form and 48hrs later EBs were switched to KOSR media without FGF (DMEM/F12, 10% KOSR, Non-essential aminoacids (NEAA),

GlutaMax, and 100μM 2-mercaptoethanol). EBs were grown for a total of 16 days, at the end of which, cells were lysed and total RNA was extracted using Trizol (Invitrogen). Subsequently, RNA was analyzed on the NanoString nCounter using a custom codeset. The calculation of the lineage scores for the different iPS cell lines was performed according to our previous reports[31, 34], and using our published dataset for 20 human ES cell lines reference.

2.4.4 Motor neuron differentiation

MN differentiation was carried out after modifying our previously reported protocol[34] to incorporate a more efficient step of neural induction[32]. Briefly, pluripotent stem cell colonies were dissociated with accutase (Stem Cell Technologies) and single cells were plated in suspension for 24 hours in mTeSR1 media using low-adherence dishes, at a density of 400,000 cells/mL and in the presence of 10 μM of ROCK inhibitor (Sigma, Y-27632). Embryoid bodies (EBs) were formed and media was gradually diluted (50% on day 3, and 100% on day 4) to KOSR medium (DMEM/F12, 10% KOSR) between days 1-4, and then switched to a neural induction medium (NIM: DMEM/F12, NEAA, Heparin (2mg/ml), N2 supplement (Gibco) on day 5. EBs were kept on NIM from days 5-24. Additional treatments of cells with small molecules and recombinant proteins were as followed: days 1-6 SB431542 (10μM, Sigma Aldrich) and Dorsmorphin (100nM, Stemgent); days 5-24 BRAIN DERIVED NEUROTROPHIC FACTOR (BDNF, 10ng/mL, R&D), ascorbic acid (AA, 0.4μg/mL, Sigma), retinoic acid (RA, 1μM, Sigma) and Smoothened Agonist 1.3 (SAG1.3, 1μM, Calbiochem). At day 24, EBs were dissociated to single cells with Papain/DNase (Worthington Bio) and plated onto poly-D-lysine/laminin-coated tissue culture surfaces (8 well chamber slides (BD biosciences) / plates /coverslips).

2.4.5 Fluorescent Activated Cell Sorting (FACS) of HUES3 *Hb9::*GFP$^+$ MNs

For experiments with the HUES3 *Hb9::GFP* cell line, day 24 differentiated EBs were dissociated to single cells with a Papain/DNase (Worthington Bio) solution. Dissociated cells were spun down and resuspended in motor neuron (MN) medium (Neurobasal (Life Technologies, N2 supplement (Gibco), B-27 supplement (Gibco), GlutaMax and NEAA) with 10μM of ROCK inhibitor (Sigma, Y-27632) and 10ng/mL of neurotrophic factors GDNF, BDNF and CNTF (R&D). Cells were then passed through a 45 μm filter before FACS at the Harvard University FAS Bauer Core Facility. The Beckman Coulter Moflo XDP cell sorter was routinely used to purify *Hb9::*GFP$^+$ cells into collection tubes containing MN medium. Differentiated cells not exposed to MN patterning molecules (RA and SAG) were used to gate for green fluorescence.

2.4.6 Survival assays for iPS cell-differentiated MNs

After 24 days of differentiation, neuronal EBs were dissociated and 20,000 cells were plated onto poly-D-lysine/Laminin coated 8-well chamber slides (BD biosciences) containing a confluent monolayer of primary cortical mouse glia. Primary glial preparations from P0-P2 mouse pups were generated as previously described[30, 34]. Fresh glial preparations (<1 month, <2 passages) were routinely used. Co-cultures were maintained in MN medium (Neurobasal (Life Technologies, N2 supplement (Gibco), B-27 supplement (Gibco), GlutaMax and NEAA) supplemented with 10ng/mL of GDNF, BDNF and CNTF (R&D) and ascorbic acid (AA, 0.4μg/ml, Sigma) and fed every 2-3 days. Slides were fixed at various time points (3, 15, 20, 30 days), cultures were immunostained using ISL and TUJ1 antibodies, nuclei were stained with DAPI. For assessment of cell numbers at various time points after plating, whole-well images were quantified in a manner blinded to the genotype and condition of the experiment. Neuronal

numbers on day 3 were set as 100% and numbers on subsequent time points were expressed as a percentage of day 3. To evaluate cell death, neuronal cultures were plated without glia on coverslips and live cells were assayed using the In Situ Cell Death Kit (Roche Diagnostics) according to manufacturer's instructions.

2.4.7 Survival assays for HUES3 *Hb9::*GFP$^+$ MNs

After FACS purification 24-day differentiated *Hb9::*GFP$^+$ MNs, 20,000 cells were plated on poly-D-lysine/Laminin coated 8-well chamber slides (BD biosciences) containing a confluent monolayer of primary cortical mouse glia[30, 34]. Co-cultures were maintained using the same above-mentioned conditions as for the iPS cell-derived MNs. The 8-well slides (BD biosciences) were fixed on days 3 and 30, and cells were immunostained using TUJ1 and an antibody recognizing a human-specific nuclear (HumNuc) antigen. All cell nuclei were stained with DAPI. Number of HumNuc+ cells was determined using whole-well imaging and the ImageJ software package for automated quantification. MN numbers on day 3 were set as 100%, and day 30 MN numbers were expressed as a percentage relative to day 3.

2.4.8 Immunocytochemistry

Cell cultures were fixed in 4% PFA for 15 minutes at 4°C, permeabilized with 0.2% Triton-X in 1x PBS for 45 minutes and blocked with 10% donkey serum in 1x PBS-T (Triton 0.1%) for 1 hour. Cells were then incubated overnight at 4°C with primary antibody (diluted in blocking solution). At least 4 washes (5 min incubation each) with 1xPBS-T were carried out, before incubating the cells with secondary antibodies for 1 hour at room temperature (diluted in blocking solution). DNA was visualized by DAPI stain. The following antibodies were used in this study: Primary TRA1-81 (1:500, Chemicon, MAB4381), Nanog (1:500, R&D, AF 1997),

Islet1/2 (1:200, DSHB, 40.2D6), Hb9 (1:100, DSHB, MNR2 81.5C10-c), ChAT (1:100, Chemicon, AB144P), TUJ1 (1:1000, Sigma, T2200), MAP2 (1:10000, Abcam ab5392), BrdU (3H579, Santa Cruz Biotechnology, sc-70441), Ki67 (1:400, Abcam, ab833), GFP (1:500, Life Technologies, A10262), SOD1 (1:2000, Agrisera#AS09 540), Human Nuclear (Millipore MAB1281), Hoxa5 and FoxP1 (courtesy of Susan Morton, Jessell lab). Secondary antibodies used (488, 555, 594, and 647) were Alexa Alexa®Fluor (1:1000, Life Technologies) and DyLight (1:500, Jackson ImmunoResearch Laboratories).

2.4.9 Immunoblot Assays

For analysis of SOD1 protein expression, cells were lysed in RIPA buffer (150mM Sodium Chloride; 1% Triton X-100; 0.5% sodium deoxycholate; 0.1% SDS; 50 mM Tris pH 8.0) containing protease and phosphatase inhibitors (Roche) for 20 min on ice, and centrifuged at high speed. Supernatant was transferred to a different tube (detergent-soluble), and the remaining cell pellet was washed 2x with RIPA buffer, after which detergent insoluble fraction were obtained with using UREA buffer (8M UREA; 4% CHAPS; 40 mM Tris; 0.2% Bio-Lyte® 3/10 ampholyte). 5µg of detergent-soluble and equivalent volumes of detergent-insoluble protein samples were separated by SDS-PAGE (Bio Rad Laboratories), transferred to PDVF membranes and probed with antibodies against SOD1 antibody (Agrisera #AS09 540) or α-TUBULIN (Sigma Aldrich # T6199). For mitochondrial biogenesis analysis, 6µg of detergent soluble protein samples were analyzed using the MitoBiogenesisTM Western Blot Cocktail (ab123545).

2.4.10 Gene targeting with ZFNs

Zinc finger nucleases (ZFNs) were constructed using previously reported methods[41, 42].

Briefly, pools of ZF pre-selected zinc finger (ZF) domains were ligated together to create a combinatorial library of three-finger proteins. A bacterial two-hybrid-based selection system was used to interrogate the ZF library for proteins that could bind the appropriate target sequences of interest. ZF proteins that bound the target sequence were cloned into a mammalian expression vector and fused to heterodimeric FokI nuclease protein domains to construct ZFNs. Active ZFNs capable of inducing a double strand break at the desired locus were selected by screening pairs of nucleases for the capability to induce characteristic insertion/deletion (indel) mutations at the *SOD1* target site in HEK293 cells. Once an efficient targeting ZFN pair was identified, it was used in the experiments with the iPS and ES cells. For editing of the *SOD1* locus in the pluripotent stem cells (39b and HUES3), 2.5 million dissociated (accutase) cells were nucleofected using the Lonza Human Stem Cell Kit II and Nucleofector program A-023. A total of 1 mg of ZFN plasmid and 5mg of targeting plasmid ($SOD1^{+}$ for 39b and $SOD1^{A4V}$ for HUES3) per 2.5 million cells were used. After nucleofection the cells were plated on matrigel-coated tissue culture dishes with mTeSR1 medium (Stem Cell Technologies) and 10 μM of ROCK inhibitor (Sigma, Y-27632). Puromycin selection (0.5μg/mL) was applied for 1 week, 48 hours after which surviving stem cell colonies picked and expanded as independent clones. gDNA was extracted and PCR was used to confirm proper targeting of the cassette into the *SOD1* locus. To remove the puromycin cassette from the intermediate targeted cell lines (39b-$SOD1^{+/-}$ and HUES3-$SOD1^{+/-}$), 2.5 million cells were nucleofected with 1mg of a mammalian expression plasmid containing a hygromycin cassette and 5mg of a mammalian expression plasmid containing the Flp recombinase (Lonza Human Stem Cell Kit II and Nucleofector program A-023). Transfected cells were immediately plated on matrigel with mTeSR1 medium and 10 μM of ROCK inhibitor. 24 hours after nucleofection,

hygromycin selection was applied for 48 hours. Resistant colonies were allowed to expand for 1 week, and they were picked and cultured as independent clones. gDNA was extracted for confirmation of puromycin-cassette removal by PCR and DNA-sequencing. *SOD1* expression was verified by qRT-PCR after RNA extraction and cDNA synthesis. PCR-RFLP using *Psh*AI digestion demonstrated proper targeting. Sequencing of PCR products was also used to demonstrate correction (39b) or induction of the $SOD1^{A4V}$ allele. Copy number qPCR, to rule out random integration events, was performed as described previously[78].

2.4.11 Nanostring karyotyping

Karyotyping was undertaken using the Nanostring nCounter Human Karyotype Panel (Nanostring Technologies, USA) and performed as per the manufacturers instructions. In brief, the protocol is as follows: 600ng of genomic DNA was *Alu*1 digested at 37 °C for 2 hours, before being denatured at 95°C for 5 minutes. To prevent re-naturing, samples were kept on ice. A total of 300ng of *Alu*1-digested DNA per sample was mixed with hybridization buffer, capture and reporter codes. Following a 16 hour incubation at 65°C, samples were transferred to a Nanostring Prep station where hybridized DNA was bound to an imaging cartridge before imaging. Using reference samples, a copy number was calculated for each chromosome following normalization of the data using nSolver (Nanostring Technologies, USA) and Microsoft Excel.

2.4.12 Genome sequencing and analysis.

DNA samples were derived from the parental 39b cell line and the gene corrected clone using phenol chloroform extraction. The sequencing libraries were made with 50ng genomic DNA using the Illumina Nexterra DNA kit. Deep (30Å~) WGS was performed using the

Illumina HiSeq 2500 Platform (500 bp library, 101 bp reads). All subsequent alignments and analysis were performed with hg19 as a reference. To investigate whether there were changes in copy number due to the cell line transformation, we used Genome STRiP[79] to extract and process the read depth signal from the aligned sequencing data. To look for regions of copy number change, we evaluated the ratio of normalized read depth in the derived cell line compared to the parental cell line in each window. To find rare coding SNPs in ALS genes, we annotated coding variants called by Haplotype caller with SNPeff[80]. SNPs classified as missense, silent, or nonsense were retained. We then integrated allele frequencies for the European population from the thousand genomes project[81]. Variants were selected that overlapped target genes for ALS. To find variants that differed between cell lines, we compared the genotypes of both lines in a stringent manner similar to the methodologies used to discover *de novo* mutations. For a variant to be confidently different between cell lines, we required a read depth of at least 2 and a likelihood score (PL) of at least 30 across both lines. Homozygous variants were required to have no more than 5% of the reads observed from the alternate allele, while heterozygous variants were required to have at least 30% of reads observed from the less frequent allele and at most 70% of the reads from the more frequent allele. To examine the off-target effects of the designed nuclease, variants within the top 12,000 potential off-target nuclease cut sites were selected from this filtered set of confident variants.

2.4.13 RNA preparation, qRT-PCR and RNA sequencing

Total RNA was isolated from relevant cell types using Trizol LS (Invitrogen) according to manufacturer's instructions. MNs were differentiated as described above, MN cultures were plated on glial monolayers, transduced on days 5-7 with a lentivirus encoding the *Hb9::RFP* reporter construct[56], and FACS was used for purification of RFP^+ MNs on day 15. A total of

300-1000ng of total RNA was used to synthesize cDNA by reverse transcription according to the iSCRIPT kit (Bio-rad). Quantitative RT-PCR (qRT-PCR) was then performed using SYBR green (Bio-Rad) and the iCycler system (Bio-rad). Quantitative levels for all genes were normalized to the average levels of 3 housekeeping genes: *GAPDH*/β-*ACTIN/YWHAZ*, and expressed relative to the relevant control samples or the lowest expressing sample in the experiment. qRT-PCR for retroviral and endogenous reprogramming genes was carried out as previously reported[34]. All primer sequences are available upon request. For next-generation RNA sequencing (RNA-Seq), RNA integrity numbers (RIN) above 7.5, determined by a bioAnalyzer, were used for library preparation. In brief, RNA sequencing libraries were generated from ~250ng of total RNA using the illumina TruSeq RNA kit v2, according to the manufacturer's directions. Libraries were sequenced at the Harvard Bauer Core Sequencing facility on a HiSeq 2000 platform. All FASTQ files were analyzed using FastQC software (v0.10.1) to confirm that Phred scores were acceptable at all read positions (median Phred score>25 and lower quartile>20). The FASTQ files were aligned to the GRCh37/hg19 reference genome using Tophat (v 2.0.7)[82, 83]. Differential expression testing was performed independently using two separate analysis packages: Cufflinks (v 2.1.1) and DESeq. The Cufflinks output was visualized with the cummeRbund R package using a false discovery rate of 0.05. For DESeq analysis, gene level annotation count files were first generated using the HTseq count Python script (v 0.5.4). DESeq analysis was performed using the methods recommended by the package authors. Gene Ontology term enrichment was determined for significantly differentially expressed genes at a false discovery rate cutoff of 0.05 using the Database for Annotation, Visualization and Integrated Discovery (DAVID) v6.7. Gene Set Enrichment Analysis (GSEA, Broad Institute) was performed by first creating a pre-ranked

gene list of all genes included in differential expression testing ordered by $\log_2$ fold change. Analysis was performed using the GSEA pre-ranked tool with the REACTOME and KEGG Pathway MSigDB collections.

2.4.14 Mitochondrial transport assays and EM analysis

After 24 days of differentiation, neuronal EBs were dissociated and 20,000 cells were plated on poly-D-lysine/laminin-coated 35 mm glass-bottom culture dishes (MatTek Corporation) or coverslips (BD-Biosciences). Cultures were infected with *Hb9::RFP* lentivirus[56] 5 days after dissociation, and MNs were selected based on expression of RFP. On days 23-26, MNs were stained with MitoTracker® Green FM (50nM, Invitrogen) and transferred to a custom observation chamber mounted on the stage of the microscope. Live microscopy of mitochondrial transport was performed with a Nikon Eclipse Ti equipped with an automated stage and In Vivo Scientific incubator. Mitochondrial movements were recorded for 5 minutes with 4-second time-lapse intervals using NIS-Elements (Nikon) using a 63x lens. Kymographs were generated from each video using NIS-Elements Analyzing Software (Nikon). Mitochondria were considered motile if they traveled faster than 0.017 μm/second. The average distance between mitochondria was calculated excluding motile mitochondria, and the total unoccupied space was divided by total process length analyzed to yield the proportion of processes unoccupied by mitochondria. Average distance was measured using the top portion of each kymograph using NIS-Elements Analyzing Software (Nikon). For Electron Microscopy analysis, MN cultures were fixed with 2.5% glutaraldehyde-2% paraformaldehyde in 0.1M sodium cacodylate buffer (pH 7.4) and maintained at 4°C overnight. Cultures were then post-fixed in 1% OsO4-1.5% KFeCN6 for 30 min, washed in water 3x and incubated in 1% aqueous uranyl acetate for 30mn followed by 2x washes in water and subsequent

dehydration in grades of alcohol (5min each; 50%, 70%, 95%, 2x100%). Cells were then embedded in plastic and ~60nm thick sections were cut, picked up onto copper grids, stained with lead citrate and analyzed in a JEOL 1200EX Transmission Electron Microscope. At least 3 independent differentiation experiments were analyzed in each case and a technician blinded for sample IDs took all the pictures.

2.4.15 Electrophysiology recordings

For patch electrophysiology of iPS cell-differentiated MNs, cells were plated at a density of 20,000 cells/cm^2 on poly-D-lysine/laminin-coated coverslips, in the presence of primary mouse glial monolayers and allowed to mature for 2-4 weeks. MNs were identified by RFP fluorescence, after transduction with the *Hb9::RFP* lentivirus[56]. Whole-cell voltage-clamp or current-clamp recordings were made using a Multiclamp 700B (Molecular Devices) at room temperature (21-23C). Data were digitized with a Digidata 1440A A/D interface and recorded using pCLAMP 10_software (Molecular Devices). Data were sampled at 20 kHz and low-pass filtered at 2 kHz. Patch pipettes were pulled from borosilicate glass capillaries on a Sutter Instruments P-97 puller and had resistances of 2-4 MW. The pipette capacitance was reduced by wrapping the shank with Parafilm and compensated for using the amplifier circuitry. Series resistance was typically 5-10 MW, always less than 15 MW, and compensated by at least 80%. Linear leakage currents were digitally subtracted using a P/4 protocol. Voltages were elicited from a holding potential of -80 mV to test potentials ranging from -80 mV to 30 mV in 10 mV increments. The intracellular solution was a potassium-based solution and contained K gluconate, 135; MgCl2, 2; KCl, 6; HEPES, 10; Mg ATP, 5; 0.5 (pH 7.4 with KOH). The extracellular was sodium-based and contained NaCl, 135; KCl, 5; CaCl2, 2; MgCl2, 1; glucose, 10; HEPES, 10, pH 7.4 with NaOH). Kainate and GABA were purchased from Sigma. For

MEA recordings of iPS cell-differentiated MNs, cells were plated on poly-D-lysine/laminin coated M768-GLx 12-well plates (Axion BioSystems) at typical densities of 40,000-80,000 per well, and recorded after approximately 14 days using an Axion Maestro (Axion BioSystems) MEA device and analyzed using Axion Integrated Studio. Total spike counts were determined by summing total spikes recorded over one minute from the 64 electrodes in each well. For MEA recordings of HUES3 *Hb9::GFP* derived-MNs, differentiated cells were dissociated and 50,000 GFP^+ sorted were combined with 50,000 murine primary glial cells. The MN and glia cells were spotted onto wells of 12 well-MEA plates, and allowed to attach for 30 minutes. After 30 minutes, MN media was added to all wells of the MEA plate. For MEA recording, the Axion system was heated to 37 degrees. Subsequently, MEA plate to be recorded was taken from the tissue culture incubator and placed in the Axion device for 1 minute, after which recordings were taken for 2 minutes.

2.4.16 Statistical analysis

Statistical significance was assessed using the Student's *t*-test (1 tail & 2 tail); *$p<0.05$ was considered significant. Two-tailed, unpaired tests were used except to confirm specific hypotheses, in which case one-tailed, unpaired tests were used. Error bars represent ±s.e.m, unless otherwise stated.

2.5 References

1. Hardiman, O., van den Berg, L.H. & Kiernan, M.C. Clinical diagnosis and management of amyotrophic lateral sclerosis. *Nat Rev Neurol* **7**, 639-49 (2011).

2. Dion, P.A., Daoud, H. & Rouleau, G.A. Genetics of motor neuron disorders: new insights into pathogenic mechanisms. *Nature Reviews Genetics* **10**, 769-782 (2009).

3. Cirulli, E.T. et al. Exome sequencing in amyotrophic lateral sclerosis identifies risk genes and pathways. *Science* (2015).

4. Sreedharan, J. & Brown, R.H., Jr. Amyotrophic lateral sclerosis: Problems and prospects. *Ann Neurol* (2013).

5. Al-Chalabi, A. & Hardiman, O. The epidemiology of ALS: a conspiracy of genes, environment and time. *Nat Rev Neurol* **9**, 617-28 (2013).

6. Guerreiro, R., Bras, J. & Hardy, J. SnapShot: Genetics of ALS and FTD. *Cell* **160**, 798-798 e1 (2015).

7. Steinberg, K.M., Yu, B., Koboldt, D.C., Mardis, E.R. & Pamphlett, R. Exome sequencing of case-unaffected-parents trios reveals recessive and de novo genetic variants in sporadic ALS. *Sci Rep* **5**, 9124 (2015).

8. Rosen, D.R. et al. Mutations in Cu/Zn superoxide dismutase gene are associated with familial amyotrophic lateral sclerosis. *Nature* **362**, 59-62 (1993).

9. Fridovich, I. Superoxide radical and superoxide dismutases. *Annu Rev Biochem* **64**, 97-112 (1995).

10. Siddique, T. & Deng, H.X. Genetics of amyotrophic lateral sclerosis. *Hum Mol Genet* **5 Spec No**, 1465-70 (1996).

11. Rosen, D., Bowling, A. & Patterson…, D. A frequent ala 4 to val superoxide dismutase-1 mutation is associated with a rapidly progressive familial amyotrophic lateral sclerosis. *Human molecular ...* (1994).

12. Juneja, T., Pericak-Vance, M.A., Laing, N.G., Dave, S. & Siddique, T. Prognosis in familial amyotrophic lateral sclerosis: progression and survival in patients with glu100gly and ala4val mutations in Cu,Zn superoxide dismutase. *Neurology* **48**, 55-7 (1997).

13. Gurney, M.E. et al. Motor neuron degeneration in mice that express a human Cu,Zn superoxide dismutase mutation. *Science* **264**, 1772-5 (1994).

14. Howland, D.S. et al. Focal loss of the glutamate transporter EAAT2 in a transgenic rat model of SOD1 mutant-mediated amyotrophic lateral sclerosis (ALS). *Proc Natl Acad Sci U S A* **99**, 1604-9 (2002).

15. Oh, Y.K., Shin, K.S., Yuan, J. & Kang, S.J. Superoxide dismutase 1 mutants related to amyotrophic lateral sclerosis induce endoplasmic stress in neuro2a cells. *J Neurochem* **104**, 993-1005 (2008).

16. Wada, T. et al. Amyotrophic lateral sclerosis model derived from human embryonic stem cells overexpressing mutant superoxide dismutase 1. *Stem Cells Transl Med* **1**, 396-402 (2012).

17. Gladman, M., Cudkowicz, M. & Zinman, L. Enhancing clinical trials in neurodegenerative disorders: lessons from amyotrophic lateral sclerosis. *Curr Opin Neurol* **25**, 735-42 (2012).

18. Perrin, S. Preclinical research: Make mouse studies work. *Nature* **507**, 423-5 (2014).

19. Dimos, J.T. et al. Induced pluripotent stem cells generated from patients with ALS can be differentiated into motor neurons. *Science* **321**, 1218-21 (2008).

20. Bilican, B. et al. Mutant induced pluripotent stem cell lines recapitulate aspects of TDP-43 proteinopathies and reveal cell-specific vulnerability. *Proc Natl Acad Sci U S A* **109**, 5803-8 (2012).

21. Donnelly, C.J. et al. RNA toxicity from the ALS/FTD C9ORF72 expansion is mitigated by antisense intervention. *Neuron* **80**, 415-28 (2013).

22. Egawa, N. et al. Drug screening for ALS using patient-specific induced pluripotent stem cells. *Sci Transl Med* **4**, 145ra104 (2012).

23. Sareen, D. et al. Targeting RNA foci in iPSC-derived motor neurons from ALS patients with a C9ORF72 repeat expansion. *Sci Transl Med* **5**, 208ra149 (2013).

24. Sandoe, J. & Eggan, K. Opportunities and challenges of pluripotent stem cell neurodegenerative disease models. *Nat Neurosci* **16**, 780-9 (2013).

25. Soldner, F. et al. Generation of isogenic pluripotent stem cells differing exclusively at two early onset Parkinson point mutations. *Cell* **146**, 318-331 (2011).

26. Vucic, S. & Kiernan, M.C. Axonal excitability properties in amyotrophic lateral sclerosis. *Clin Neurophysiol* **117**, 1458-66 (2006).

27. Bostock, H., Sharief, M.K., Reid, G. & Murray, N.M. Axonal ion channel dysfunction in amyotrophic lateral sclerosis. *Brain* **118 (Pt 1)**, 217-25 (1995).

28. Kanai, K. et al. Altered axonal excitability properties in amyotrophic lateral sclerosis: impaired potassium channel function related to disease stage. *Brain* **129**, 953-62 (2006).

29. Kanai, K. et al. Motor axonal excitability properties are strong predictors for survival in amyotrophic lateral sclerosis. *J Neurol Neurosurg Psychiatry* **83**, 734-8 (2012).

30. Di Giorgio, F., Boulting, G., Bobrowicz, S. & Eggan, K. Human embryonic stem cell-derived motor neurons are sensitive to the toxic effect of glial cells carrying an ALS-causing mutation. *Cell Stem Cell* **3**, 637-648 (2008).

31. Bock, C. et al. Reference Maps of human ES and iPS cell variation enable high-throughput characterization of pluripotent cell lines. *Cell* **144**, 439-52 (2011).

32. Chambers, S. et al. Highly efficient neural conversion of human ES and iPS cells by dual inhibition of SMAD signaling. *Nature biotechnology* **27**, 275-280 (2009).

33. Amoroso, M.W. et al. Accelerated High-Yield Generation of Limb-Innervating Motor Neurons from Human Stem Cells. *J Neurosci* **33**, 574-586 (2013).

34. Boulting, G.L. et al. A functionally characterized test set of human induced pluripotent stem cells. *Nature biotechnology* **29**, 279-286 (2011).

35. Dasen, J.S., De Camilli, A., Wang, B., Tucker, P.W. & Jessell, T.M. Hox repertoires for motor neuron diversity and connectivity gated by a single accessory factor, FoxP1. *Cell* **134**, 304-16 (2008).

36. Dasen, J.S. & Jessell, T.M. Hox networks and the origins of motor neuron diversity. *Curr Top Dev Biol* **88**, 169-200 (2009).

37. Kiernan, J.A. & Hudson, A.J. Changes in sizes of cortical and lower motor neurons in amyotrophic lateral sclerosis. *Brain* **114 (Pt 2)**, 843-53 (1991).

38. McIlwain, D.L. Nuclear and cell body size in spinal motor neurons. *Adv Neurol* **56**, 67-74 (1991).

39. Mekhoubad, S. et al. Erosion of dosage compensation impacts human iPSC disease modeling. *Cell Stem Cell* **10**, 595-609 (2012).

40. Lattante, S. et al. Contribution of major amyotrophic lateral sclerosis genes to the etiology of sporadic disease. *Neurology* **79**, 66-72 (2012).

41. Sander, J.D. et al. Selection-free zinc-finger-nuclease engineering by context-dependent assembly (CoDA). *Nat Methods* **8**, 67-9 (2011).

42. Maeder, M.L. et al. Rapid "open-source" engineering of customized zinc-finger nucleases for highly efficient gene modification. *Mol Cell* **31**, 294-301 (2008).

43. Cardoso, R.M. et al. Insights into Lou Gehrig's disease from the structure and instability of the A4V mutant of human Cu,Zn superoxide dismutase. *J Mol Biol* **324**, 247-56 (2002).

44. Brotherton, T.E. et al. Localization of a toxic form of superoxide dismutase 1 protein to pathologically affected tissues in familial ALS. *Proc Natl Acad Sci U S A* **109**, 5505-10 (2012).

45. Bruijn, L.I. et al. Aggregation and motor neuron toxicity of an ALS-linked SOD1 mutant independent from wild-type SOD1. *Science* **281**, 1851-4 (1998).

46. Bruijn, L.I., Miller, T.M. & Cleveland, D.W. Unraveling the mechanisms involved in motor neuron degeneration in ALS. *Annu Rev Neurosci* **27**, 723-49 (2004).

47. Kerman, A. et al. Amyotrophic lateral sclerosis is a non-amyloid disease in which extensive misfolding of SOD1 is unique to the familial form. *Acta Neuropathol* **119**, 335-44 (2010).

48. Shibata, N. et al. Intense superoxide dismutase-1 immunoreactivity in intracytoplasmic hyaline inclusions of familial amyotrophic lateral sclerosis with posterior column involvement. *J Neuropathol Exp Neurol* **55**, 481-90 (1996).

49. Bosco, D. et al. Wild-type and mutant SOD1 share an aberrant conformation and a common pathogenic pathway in ALS. *Nature neuroscience* **13**, 1396-1403 (2010).

50. Deng, H.-X. et al. Conversion to the amyotrophic lateral sclerosis phenotype is associated with intermolecular linked insoluble aggregates of SOD1 in mitochondria. *Proceedings of the National Academy of Sciences of the United States of America* **103**, 7142-7147 (2006).

51. Pasinelli, P. & Brown, R. Molecular biology of amyotrophic lateral sclerosis: insights from genetics. *Nature reviews. Neuroscience* **7**, 710-723 (2006).

52. Saxena, S., Cabuy, E. & Caroni, P. A role for motoneuron subtype-selective ER stress in disease manifestations of FALS mice. *Nat Neurosci* **12**, 627-36 (2009).

53. Yoshihara, T. et al. Differential expression of inflammation- and apoptosis-related genes in spinal cords of a mutant SOD1 transgenic mouse model of familial amyotrophic lateral sclerosis. *J Neurochem* **80**, 158-67 (2002).

54. Ferraiuolo, L. et al. Microarray analysis of the cellular pathways involved in the adaptation to and progression of motor neuron injury in the SOD1 G93A mouse model of familial ALS. *J Neurosci* **27**, 9201-19 (2007).

55. Olsen, M.K. et al. Disease mechanisms revealed by transcription profiling in SOD1-G93A transgenic mouse spinal cord. *Ann Neurol* **50**, 730-40 (2001).

56. Marchetto, M.C. et al. Non-cell-autonomous effect of human SOD1 G37R astrocytes on motor neurons derived from human embryonic stem cells. *Cell Stem Cell* **3**, 649-57 (2008).

57. Hunt, M.C., Solaas, K., Kase, B.F. & Alexson, S.E. Characterization of an acyl-coA thioesterase that functions as a major regulator of peroxisomal lipid metabolism. *J Biol Chem* **277**, 1128-38 (2002).

58. Krasnova, I.N. et al. CREB phosphorylation regulates striatal transcriptional responses in the self-administration model of methamphetamine addiction in the rat. *Neurobiol Dis* **58**, 132-43 (2013).

59. Minkiewicz, J., de Rivero Vaccari, J.P. & Keane, R.W. Human astrocytes express a novel NLRP2 inflammasome. *Glia* **61**, 1113-21 (2013).

60. Mizwicki, M.T. et al. Tocilizumab attenuates inflammation in ALS patients through inhibition of IL6 receptor signaling. *Am J Neurodegener Dis* **1**, 305-15 (2012).

61. Huang da, W., Sherman, B.T. & Lempicki, R.A. Systematic and integrative analysis of large gene lists using DAVID bioinformatics resources. *Nat Protoc* **4**, 44-57 (2009).

62. Subramanian, A. et al. Gene set enrichment analysis: a knowledge-based approach for interpreting genome-wide expression profiles. *Proc Natl Acad Sci U S A* **102**, 15545-50 (2005).

63. Magrane, J. et al. Mutant SOD1 in neuronal mitochondria causes toxicity and mitochondrial dynamics abnormalities. *Hum Mol Genet* **18**, 4552-64 (2009).

64. Magrane, J., Cortez, C., Gan, W.B. & Manfredi, G. Abnormal mitochondrial transport and morphology are common pathological denominators in SOD1 and TDP43 ALS mouse models. *Hum Mol Genet* **23**, 1413-24 (2013).

65. Tamura, N. et al. Increased nodal persistent Na+ currents in human neuropathy and motor neuron disease estimated by latent addition. *Clin Neurophysiol* **117**, 2451-8 (2006).

66. Fritz, E. et al. Mutant SOD1-expressing astrocytes release toxic factors that trigger motoneuron death by inducing hyperexcitability. *J Neurophysiol* **109**, 2803-14 (2013).

67. Lamas, N.J. et al. Neurotrophic requirements of human motor neurons defined using amplified and purified stem cell-derived cultures. *PLoS One* **9**, e110324 (2014).

68. de Boer, A.S. et al. Genetic validation of a therapeutic target in a mouse model of ALS. *Sci Transl Med* **6**, 248ra104 (2014).

69. Takazawa, T. et al. Maturation of spinal motor neurons derived from human embryonic stem cells. *PLoS One* **7**, e40154 (2012).

70. Yang, Y.M. et al. A small molecule screen in stem-cell-derived motor neurons identifies a kinase inhibitor as a candidate therapeutic for ALS. *Cell Stem Cell* **12**, 713-26 (2013).

71. Di Giorgio, F., Carrasco, M., Siao, M., Maniatis, T. & Eggan, K. Non-cell autonomous effect of glia on motor neurons in an embryonic stem cell-based ALS model. *Nature neuroscience* **10**, 608-614 (2007).

72. Boillee, S. et al. Onset and progression in inherited ALS determined by motor neurons and microglia. *Science* **312**, 1389-92 (2006).

73. Clement, A.M. et al. Wild-type nonneuronal cells extend survival of SOD1 mutant motor neurons in ALS mice. *Science* **302**, 113-7 (2003).

74. Yamanaka, K. et al. Astrocytes as determinants of disease progression in inherited amyotrophic lateral sclerosis. *Nat Neurosci* **11**, 251-3 (2008).

75. Andersen, P.M. & Al-Chalabi, A. Clinical genetics of amyotrophic lateral sclerosis: what do we really know? *Nat Rev Neurol* **7**, 603-15 (2011).

76. Kiskinis, E. et al. Pathways disrupted in human ALS motor neurons identified through genetic correction of mutant SOD1. *Cell Stem Cell* **14**, 781-95 (2014).

77. Wainger, B. et al. Intrinsic Membrane Hyperexcitability of ALS Patient-Derived Motor Neurons. *Cell Reports* (2014).

78. D'Haene, B., Vandesompele, J. & Hellemans, J. Accurate and objective copy number profiling using real-time quantitative PCR. *Methods* **50**, 262-70 (2010).

79. Handsaker, R.E., Korn, J.M., Nemesh, J. & McCarroll, S.A. Discovery and genotyping of genome structural polymorphism by sequencing on a population scale. *Nat Genet* **43**, 269-76 (2011).

80. Abecasis, G.R. et al. An integrated map of genetic variation from 1,092 human genomes. *Nature* **491**, 56-65 (2012).

81. Cingolani, P. et al. A program for annotating and predicting the effects of single nucleotide polymorphisms, SnpEff: SNPs in the genome of Drosophila melanogaster strain w1118; iso-2; iso-3. *Fly (Austin)* **6**, 80-92 (2012).

82. Trapnell, C. et al. Differential analysis of gene regulation at transcript resolution with RNA-seq. *Nat Biotechnol* **31**, 46-53 (2013).

83. Trapnell, C. et al. Differential gene and transcript expression analysis of RNA-seq experiments with TopHat and Cufflinks. *Nature protocols* **7**, 562-578 (2012).

CHAPTER 3

Novel molecular targets of TDP-43 dysregulation in human motor neurons

identified by transcriptional profiling

The following researchers contributed to the work presented in this Chapter: Luis A. Williams, Brandi N. Davis-Dusenbery, Dan Mordes, Seth Cassel, Brian Wainger and Kevin Eggan.

Author contributions: L.A.W., B.N.D. and K.E. designed the research; L.A.W. and B.N.D. contributed equally to all the experiments; B.N.D. analyzed RNA-Seq data; D.M. collected post-mortem samples carried out immunohistochemical assays; S.C. assisted with confocal microscopy; B.W. performed electrophysiological recordings; L.A.W. wrote the chapter; K.E. supervised all aspects of this work.

3.1 Introduction

TDP-43 (*TAR* DNA-binding protein of 43 kDa) is a primarily nuclear DNA/RNA binding protein[1] with functional roles in transcriptional regulation[2], splicing[3, 4], pre-miRNA processing[5], stress granule formation[6, 7], and mRNA transport and stability[8, 9]. Dominant mutations in *TARDBP*, the gene encoding TDP-43, can cause the late onset neurological disorder amyotrophic lateral sclerosis (ALS)[10-13], characterized by the progressive loss of motor neurons, which leads to paralysis and death[14]. Whether motor neuron degeneration linked to TDP-43 is the result of loss-of-function mechanisms, gain-of-function mechanisms, or a combination of both, remains unclear[15]. However, neuropathological findings in post-mortem tissues from most ALS cases, in which TDP-43 is absent from the nucleus and sequestered into large cytoplasmic inclusions[16, 17], suggest that loss of normal nuclear TDP-43 function can contribute to neurodegeneration[15]. Consistent with this hypothesis, recent reports have described the generation of mice with phenotypic features of ALS using either conditional genetic inactivation of the *Tardbp* gene with motor neuron specific promoters[18, 19], or RNAi-mediated knockdown of TDP-43 in brain and spinal cord tissues[20]. These targeted depletion and knockdown strategies became necessary as earlier knockout studies established TDP-43 function to be required for mammalian embryonic development[21, 22].

Similar to other RNA binding factors, TDP-43 downregulates its protein synthesis by direct binding to a highly conserved *3'UTR* region on its own transcripts[23]. This interaction promotes alternative splicing, nuclear retention and ultimately degradation of *TDP-43* RNAs[4, 23, 24]. This auto-regulatory mechanism can occur within the mammalian central nervous system (CNS)[4], as evident by the significant downregulation of endogenous TDP-43 protein observed in transgenic mice overexpressing a *TDP-43* construct lacking the cognate 3'-*UTR*[25, 26]. Notably,

these animal studies have also demonstrated that overexpression of wild-type TDP-43 in the CNS is sufficient to drive neuronal loss, motor deficits, and lethality[25-27], suggesting that upregulation of TDP-43 can also lead to molecular pathways associated with motor neuron vulnerability and cell death[15].

Although large-scale transcriptional profiling after TDP-43 depletion in the mouse brain has been reported[4], we reasoned that interrogation of *human* genes differentially expressed after TDP-43 dysregulation in a well-defined and homogenous population of cells affected in ALS could provide insights into novel molecular disease mechanisms. Since the vulnerable cortical and spinal motor neurons in living ALS patients are fundamentally inaccessible for isolation and culture, we and others have proposed the directed differentiation of pluripotent stem cells as an alternative source of human cells with motor neuron properties, that can be used for the study of ALS and other neurological disorders[28-31].

By inserting the spinal motor neuron identity reporter construct *Hb9::GFP* into the human embryonic stem (ES) cell line HUES3[32], our group has generated a useful tool for the development of novel motor neuron *in vitro* production and culture strategies[30, 33-36], and the study of cell survival pathways in response to ALS-related toxic stimuli[32, 37]. Here, we have used this reporter ES cell line in combination with RNA sequencing technology to investigate global changes in gene expression levels in differentiated human motor neurons after dysregulation of TDP-43 levels. We have identified several genes downstream of TDP-43 activity, including genes encoding components of the BMP branch of TGF-β signaling, cell cycle regulators, and the neuronal-growth associated factor STMN2. We show that *STMN2* downregulation is specific to loss of *TDP-43,* and not immediately sustained by the levels of two other ALS-linked genes, *FUS* and *C9ORF72*. We also demonstrate the regulation of the

STMN2 gene by TDP-43 at the protein level, and provide evidence suggesting that STMN2 is altered in *bona fide* adult motor neurons from ALS patients, supporting our premise that discoveries from human stem cell-based models could be of relevance to the underlying biology of ALS.

3.2 Results

3.2.1 Differentiation and purification of human spinal motor neurons (MNs)

In order to produce and purify MNs for our transcriptional studies, we directed the differentiation of the hES cell line HUES3 *Hb9::GFP*[32-34] into GFP$^+$ MNs using a slightly modified 14-day strategy under adherent culture conditions[38, 39]. This differentiation approach relies first on highly efficient neural induction achieved with dual small molecule inhibition (SB431542 and LDN193189) of SMAD signaling, followed by accelerated neurogenesis and MN patterning through inhibition of FGF (SU5402) and NOTCH (DAPT) signaling, and activation of Retinoic acid (RA) and SONIC HEDGEHOG (SAG) signaling pathways (Figure 3.1A). After 14 days, *Hb9::*GFP$^+$ differentiated cells were purified via fluorescence activated cell sorting (FACS)[32, 34] and plated on Matrigel^{TM}-coated tissue culture dishes (Figure 3.1A). We routinely obtained ~18-20% of GFP$^+$ cells (Figure 3.1B-C), which expressed the endogenous HOMEOBOX HB9 and the MN transcription factor ISLET 1, as well as the panneuronal cytoskeletal proteins β-III TUBULIN and MICROTUBULE ASSOCIATED PROTEIN 2 (MAP2) (Figure 3.2A-D). In accordance with their predicted post-mitotic phenotype, cultured *Hb9::*GFP$^+$ cells did not express the cell proliferation antigen KI67 (Figure 3.2E-F). Using whole-cell patch-clamp recordings, we determined that by 10 days after sorting (d10), which is the time when downstream assays were carried out, purified MNs were electrophysiologically active (Figure 3.3). Upon depolarization, these cells exhibited initial fast inward currents

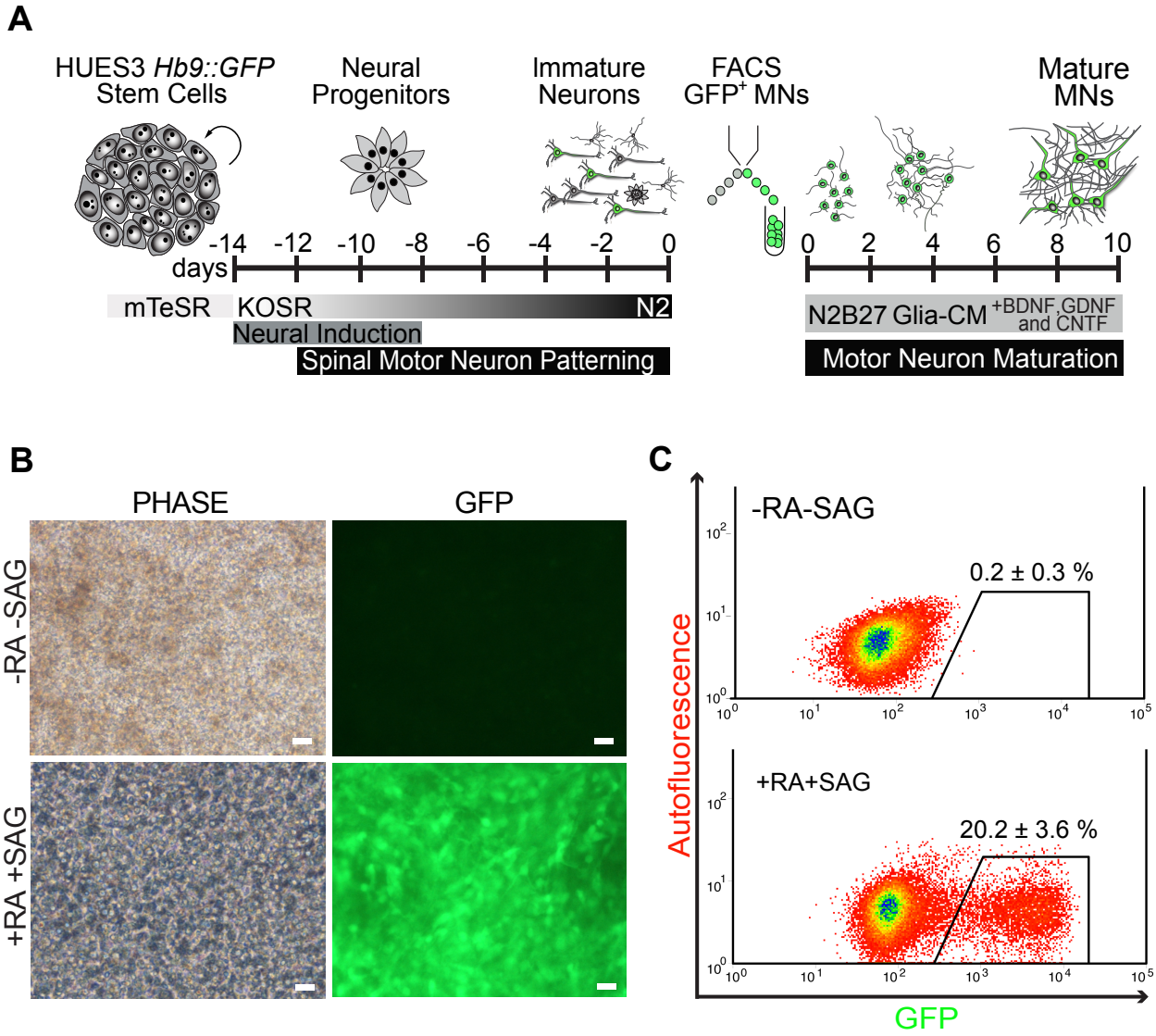

Figure 3.1 Directed differentiation of HUES3 *Hb9::GFP* cells into GFP⁺ MNs.
A. MN differentiation, purification and culture strategy. HUES3 *Hb9::GFP* stem cells were maintained under pluripotent conditions using mTeSR1 medium. For MN differentiation, cells were exposed, under adherent culture conditions, to a gradient of KOSR and N2 medium. Neural fate was induced during the first six by dual SMAD inhibition (LDN193189 and SB431542) and accelerated neurogenesis and MN patterning was achieved through inhibition of FGF (SU5402) and NOTCH (DAPT) signaling and activation of Retinoic acid (RA) and SONIC HEDGEHOG signaling pathways. After 14 days of differentiation (d0), *Hb9::GFP*⁺ cells were purified using fluorescence activated cell sorting (FACS). GFP⁺ cells were plated on matrigel-coated tissue culture dishes and fed with N2B27 neurobasal medium conditioned by mouse primary glial cells (glia-CM), and supplemented with neurotrophic factors BDNF, GDNF and CNTF to allow their maturation. **B.** Differentiated HUES3 *Hb9::GFP* cells express the GFP reporter for spinal MN identity at d0, only when exposed to the MN patterning molecules RA and the small molecule agonist (SAG) of the SHH signaling pathway (Scale bar = 20 μm). **C.** FACS plots depicting the gates for GFP expression used for the purification of MNs. Routinely, ~20% of differentiated cells were GFP+. Neural induced cells not treated with RA and SAG were used as negative control for the gating of GFP.

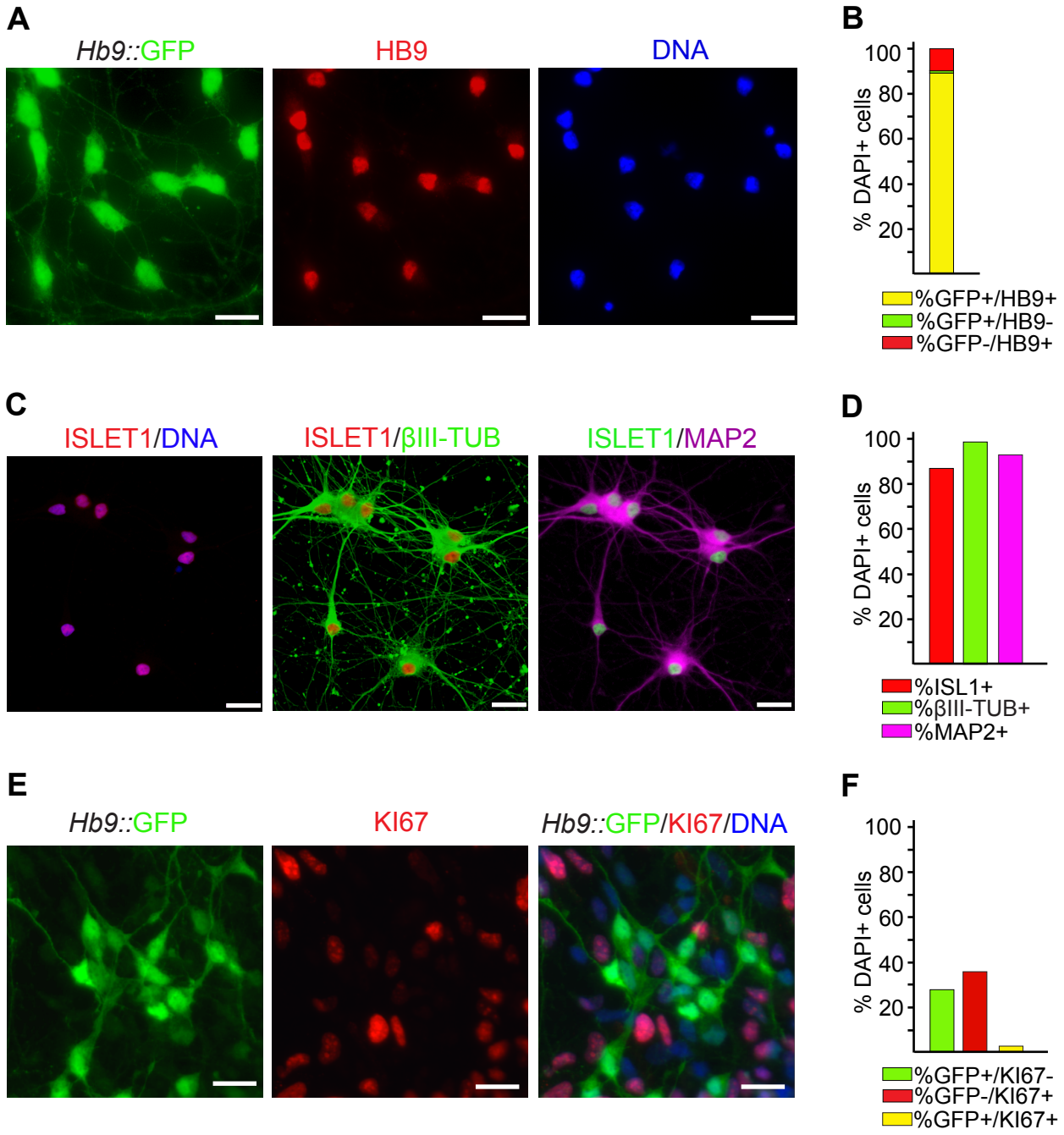

Figure 3.2 *Hb9::*GFP⁺ cells express MN markers and are post-mitotic
A. Purified *Hb9::*GFP⁺ cells cultured for 2 days after FACS express GFP and the endogenous spinal MN transcription factor HB9, as determined by immunocytochemistry. Nuclei (DNA) were stained using DAPI (Scale bar = 10 μm). **B.** The significant percentage (90%) of DAPI⁺ cells that were immunoreactive to both GFP and HB9 antibodies validated the *Hb9::*GFP reporter system. **C.** *Hb9::*GFP⁺ cells cultured for 10 days after FACS express the spinal MN transcription factor ISLET1(ISL1), and elaborate complex processes detected with the panneuronal cytoskeletal markers βIII-TUBULIN(βIII-TUB) and MICROTUBULE ASSOCIATED PROTEIN 2(MAP2) (Scale bar = 20 μm). **D.** Percentage of DAPI⁺ cells that were immunoreactive to ISL1 (88%), βIII-TUB (99%) and MAP2 (93%). **E-F.** *Hb9::*GFP⁺ cells in a culture of differentiated but not FACS-purified MNs do not express the cell proliferation antigen KI67, consistent with a post-mitotic state (Scale bar = 10 μm).

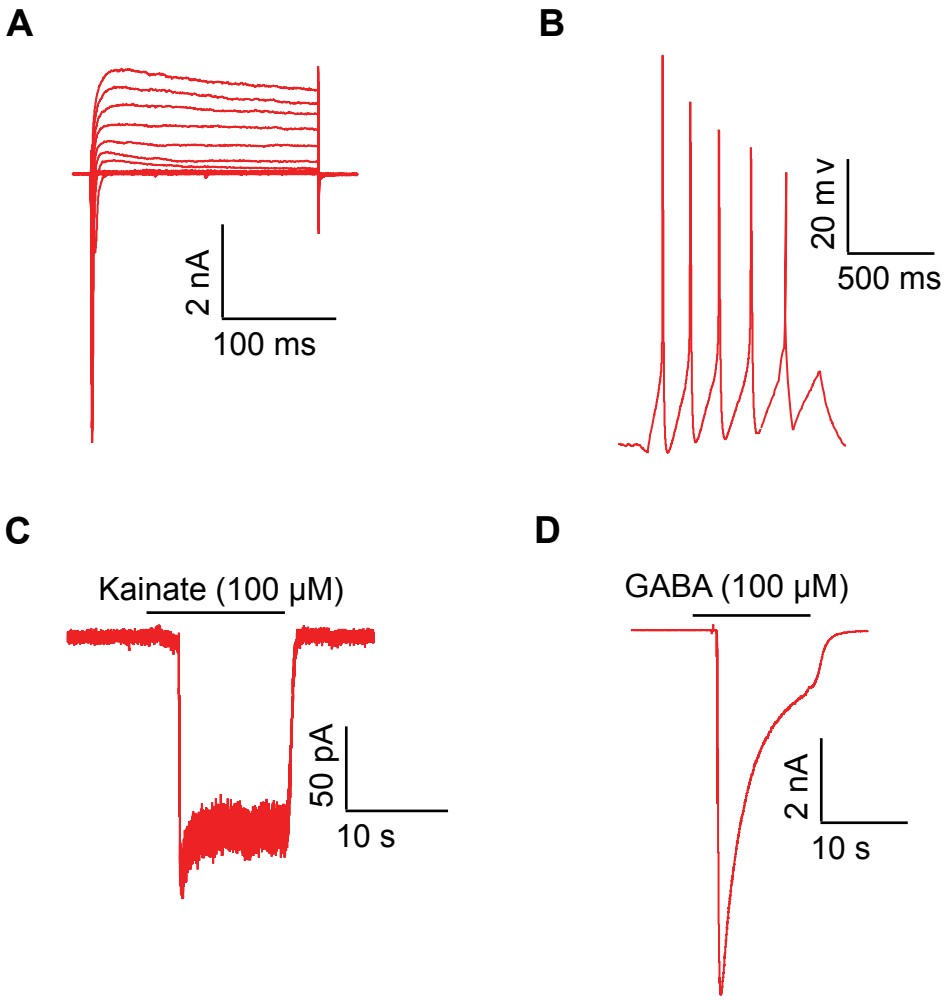

Figure 3.3 Purified *Hb9::*GFP^{+} cells are electrophysiologically active
FACS-purified human differentiated MNs were plated on matrigel-coated dishes, and whole-cell patch-clamp recordings were used after 10 days in culture to determine their electrophysiological properties. **A.** Upon depolarization in voltage-clamp mode, cells exhibited fast inward currents followed slow outward currents, indicating the expression and opening of voltage-activated sodium and potassium channels, respectively. **B.** In current-clamp mode, depolarization elicited repetive action potential firing. **C-D.** Response to Kainate and GABA is consistent with the expression of functional receptors for excitatory glutamatergic and inhibitory transmitters, respectively.

followed by slow outward currents, consistent with the expression of functional voltage-activated sodium and potassium channels, respectively (Figure 3.3A). In addition, differentiated human MNs demonstrated repetitive action potential firing (Figure 3.3B), and responses to both excitatory and inhibitory neurotransmitters (Figure 3.3C-D).

3.2.2 TDP-43 downregulation in human differentiated MNs using RNAi

Having demonstrated we could generate and culture pure populations of human differentiated cells with MN properties, we decided to use unbiased transcriptome profiling to investigate potential molecular mechanisms associated with the pathological reduction of nuclear TPP-43 observed ALS tissues[16, 17]. To this end, we first carried out RNA interference (RNAi)-mediated knockdown of *TDP-43* levels in the purified stem cell-derived MNs. Using a short interfering RNA (siRNA) that targets the *TDP-43* transcript (siTDP43), two different control siRNAs with scrambled sequences that do not target any specific gene (siRED and siSCR), and three distinct time points after siRNA delivery (2, 4 and 6 days), we determined that 4 days after siRNA transfection was the optimal time point when downregulation of *TDP-43* first reached significant levels (Figure 3.4A-B). By means of the siRED scrambled control, which is conjugated to a 555-Alexa® fluorophore, we demonstrated high-level of siRNA delivery (~94.6%) into the cells (Figure 3.4C-D). Four days after siRNA transfection, cells were collected and total RNA and protein were isolated. qRT-PCR assays validated the significant downregulation of *TDP-43* mRNA levels at this time point, in MNs treated with siTDP43 but not the scrambled controls (Figure 3.5A). Moreover, depletion of TDP-43 was also confirmed by immunoblot assays, with siTDP43-treated MNs showing a 65% reduction in levels of TDP-43 protein (Figure 3.5B).

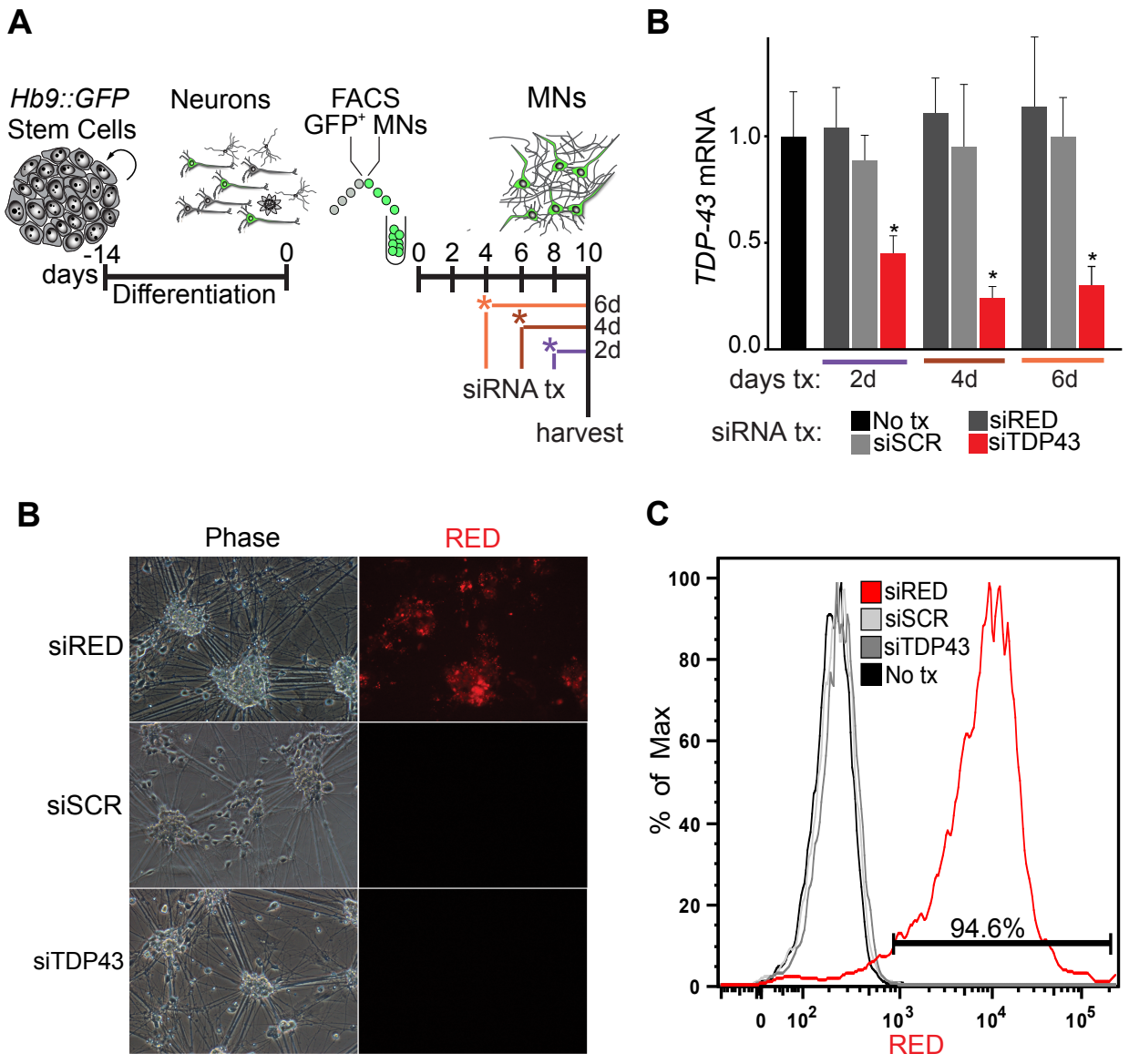

Figure 3.4 siRNA delivery into MNs for the downregulation of TDP-43

A. RNAi strategy for TDP-43 knockdown: *Hb9::*GFP^{+} MNs were purified by FACS after 14 days of directed differentiation, and plated for additional culture and siRNA treatment. Cells were transfected with control siRNAs (siSCR and siRED) or an siRNA targeting the *TDP-43* transcript at different time points (d4, d6 and d8 after plating), and harvested for RNA extraction on d10. **B.** Relative levels of *TDP-43* mRNA in MNs exposed to different siRNAs for 2, 4 or 6 days. qRT-PCR results were normalized using *GAPDH* levels, and are expressed relative to the 'No tx' (No siRNA treatment) sample. **C.** Phase and red fluorescence images of cultured MNs 4 days after treatment with different siRNAs. siRED is a scramble control conjugated to Alexa Fluor® 555. **D.** Flow cytometry analysis of MNs expressing red fluorescence 4 days after transfection indicates highly-effcient delivery of siRNAs.

3.2.3 RNA-Seq of human differentiated MNs with reduced levels of TDP-43

In order to interrogate the global changes in gene expression in response to partial loss of TDP-43 in human MNs, we prepared RNA sequencing (RNA-Seq) libraries from the cells treated with the different siRNAs and obtained, after next generation sequencing, gene expression was annotated in 'FPKM's, or number of fragments per kilobase of exon per million fragments mapped. Unsupervised hierarchical clustering segregated RNA-Seq samples treated with siTDP-43 from control groups, indicating that reduction of TDP-43 levels in these cells resulted in measurable transcriptional differences (Figure 3.5C). Examination of the FPKM values for the *TDP-43* gene in the different RNA-Seq samples confirmed the significant reduction in the abundance of *TDP-43* transcripts only in MNs treated with siTDP43 (Figure 3.5D). Differential analysis of gene expression was carried out using the 'Tuxedo' suite of bioinformatics tools[40, 41], which at a false discovery rate (FDR) of 5% identified a total of 493 statistically significant differentially expressed genes in human MNs after TDP-43 knockdown (Figure 3.5E). In these cells, FPKM values were significantly higher for 202 genes ('upregulated'), and significantly lower for 291 genes ('downregulated') compared to those values in MNs treated with the scrambled sequence siRNA controls (Figure 3.5E).

In addition to altering the total transcriptional levels of hundreds of genes in the mammalian CNS[4], reduced levels of TDP-43 can also influence alternative splicing[4, 20, 42-44]. Although global analysis of splicing variants traditionally involves splicing-sensitive exon arrays[4, 44], the development of computational approaches for isoform deconvolution of RNA-Seq reads is rapidly evolving[41, 45, 46]. Examination of our data with the recently introduced bioinformatics algorithm 'Cuffdiff 2'[41] estimated 240 isoforms that significantly changed (FDR>0.05) in the differentiated MNs after TDP-43 downregulation, and detected the *POLDIP3* (*POLYMERASE*

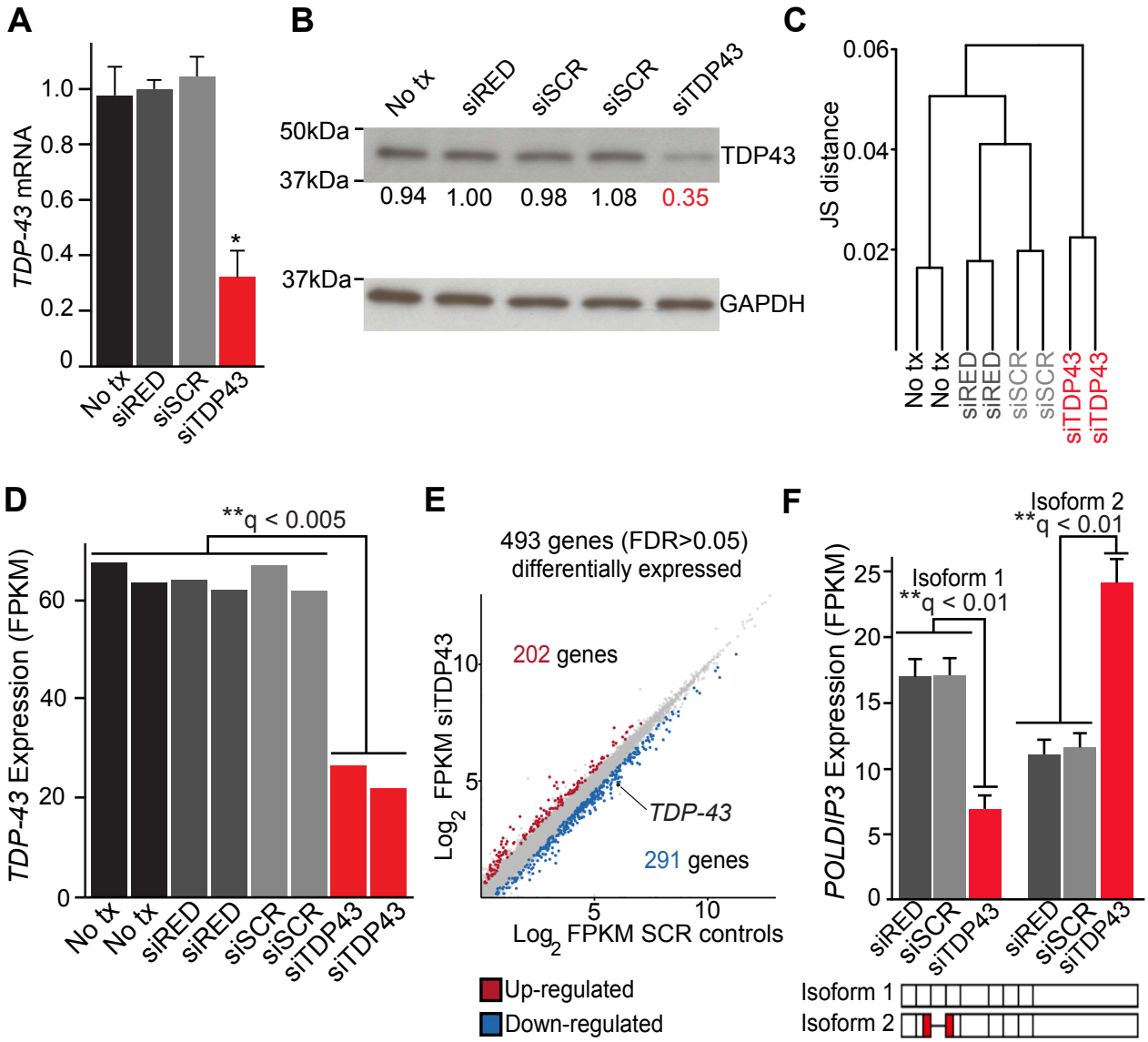

Figure 3.5 RNA-Seq of human differentiated MNs with reduced levels of TDP-43 mRNA and protein
A. qRT-PCR of *RNA* samples obtained from human differentiated MNs and used for RNA-Seq confirmed the significant downregulation of *TDP-43* transcripts in cells treated with siTDP43, 4 days after treatment ('tx'). Levels for each sample were normalized to *GAPDH* and expressed relative to the siRED-treated sample. **B.** Immunoblot assays demonstrated ~65% reduction in the levels of TDP-43 protein in human MNs after RNAi. Image J software was used for quantification. Each sample was normalized using GAPDH, and TDP-43 protein levels were calculated relative to the siRED-treated control sample. **C.** Dendogram generated after unsupervised hierarchical clustering of the RNA-Seq data demonstrated grouping of biological replicas and separation of siTDP43-treated samples. **D.** Analysis of *TDP-43* expression after RNA-Seq validated the knockdown. FPKM: number of fragments per kilobase of exon per million fragments mapped. **E.** A scatter plot comparing the FPKM values (gene expression) in human MNs after *TDP-43* knockdown (siTDP43) versus controls (cells treated with scrambled siRNAs). Genes identified as significant (false discovery rate 'FDR'>0.05) after differential expression analysis are highlighted (red and blue), including *TDP-43* (black dot). **F.** Alteration in the splicing pattern of the *POLDIP3* gene was detected as result of *TDP-43* knockdown, with siTDP43-treated cells showing significant reduction of isoform 1, and increased levels of spliced variant 2 (which lacks *Exon3*).

DELTA-INTERACTING PROTEIN 3) gene as the top candidate for differential splicing, with two significant isoform-switching events (Figure 3.5F), which have been previously associated with deficits in TDP-43 function both *in vitro*[43, 47] and *in vivo*[20, 47].

3.2.4 Overlap of results with RNA-Seq data from MNs overexpressing TDP-43

To further probe the TDP-43 knockdown RNA-seq data set for genes most likely downstream of TDP-43 activity, we overlapped the differential expression analysis results with those obtained following an additional RNA-Seq experiment, in which we interrogated the identity of deregulated transcripts in MNs in response to upregulation of TDP-43. To generate this second set of RNA-Seq data, we first used gene editing technology to target a *CAGs::TDP43::TDP43-3'UTR* expression cassette into the "safe harbor" *AAVS1* genomic region[48] of the HUES3 *Hb9::*GFP cell line (Figure 3.6A). We confirmed by PCR and quantitative PCR the correct single-copy integration of the expression construct into the targeted locus (Figure 3.6B-C). After MN directed differentiation, the efficiency of production of *Hb9::*GFP$^+$ cells for the targeted cell line was similar to that of the parental HUES3 (data not shown). qRT-PCR and immunoblot assays showed that upon MN differentiation, TDP-43 transcript and protein levels were increased around 3 fold in *AAVS1-TDP43* cells compared to MNs derived from HUES3 (Figure 3.6D-G). In addition, this TDP-43 upregulation was supported by immunocytochemistry (Figure 3.7).

We cultured differentiated *Hb9::*GFP$^+$ cells of both genotypes for 10 days, under similar conditions to those used in the *TDP-43* knockdown experiment (Figures 3.8A), and we next obtained RNA from these cells for global transcriptional profiling via RNA-Seq. Analyses of this second set of data segregated the different transcriptomes based on TDP-43 levels (Figure 3.8B), which were confirmed by examining *TDP-43* FPKM values for both *AAVS1-TDP43* and

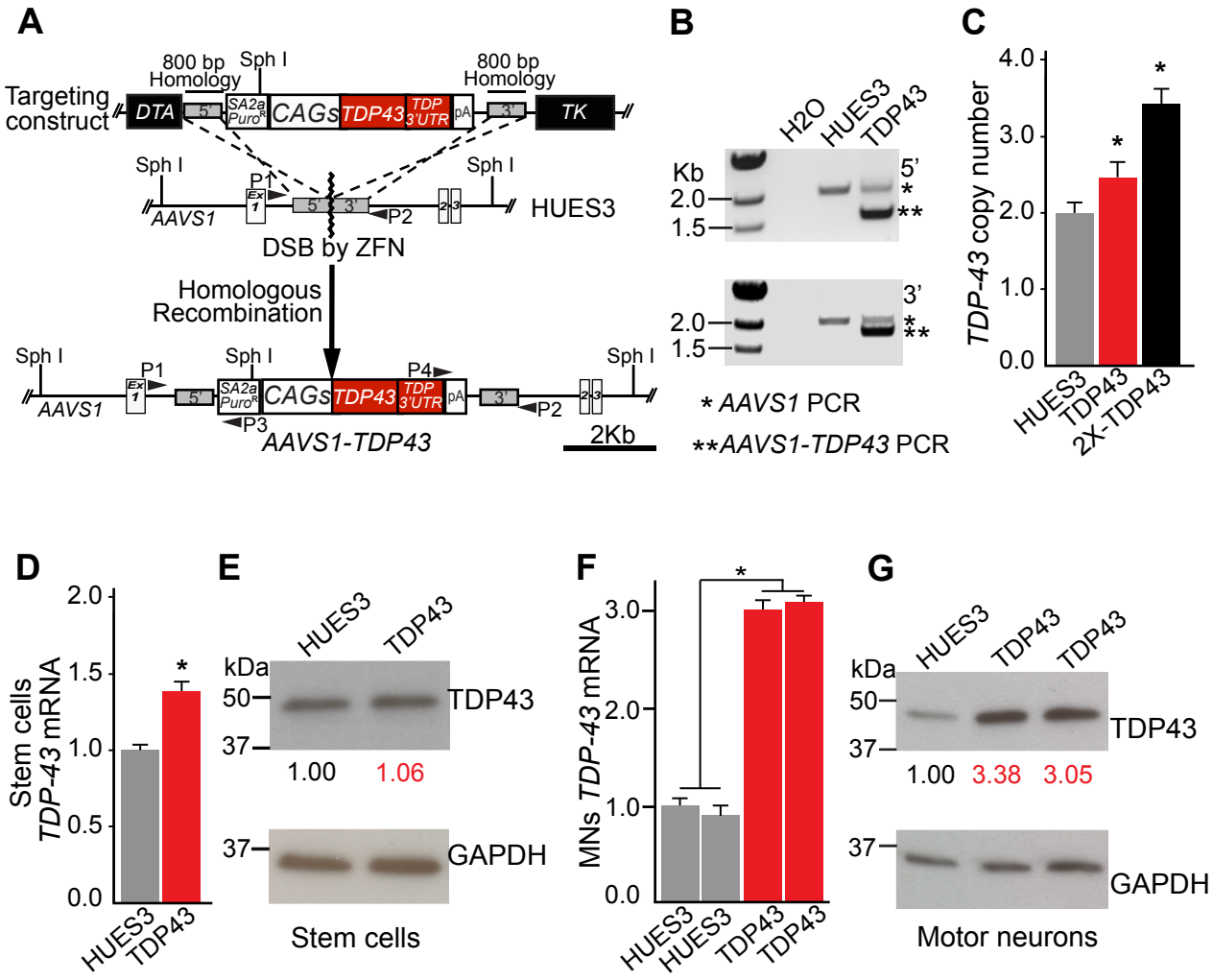

Figure 3.6 Generation of human differentiated MNs with increased levels of TDP-43

A. Gene targeting strategy used to introduce a TDP-43 expression cassette into the *AAVS1* 'safe harbor' locus of the HUES3 *Hb9::GFP* cell line. A double-strand break (DSB) in the in the *AAVS1* locus was induced using previously published zinc-finger nucleases (ZFN) [ref. 48]. The endogenous *3'UTR* of the *TDP-43* mRNA was incorporated into the expression construct to reduce the levels of exogenous TDP-43. **B.** Confirmation of correct targeting by PCR amplification of 5' and 3' regions of homology; genomic DNA from parental HUES3 cell line was used as control. **C.** Confirmation of single-copy integration using qPCR; genomic DNA from a targeted cell line in which the PCR assay presented in (B) indicated homozygous targeting (2X-TDP43) was used as a control to calibrate copy number. **D-E.** TDP-43 levels in *AAVS1*-TDP-43 stem cells (TDP43) as determined by qRT-PCR and immunoblot assays. In stem cells there is a modest upregulation of TDP-43 transcript levels but not of total TDP-43 protein relative to HUES3. **F-G.** Both TDP-43 RNA and protein levels increased in *AAVS1*-TDP43 following differentiation into MNs to about 3-fold the levels in HUES3-derived MNs. This is consistent with previous unpublished observations of induction *CAGs*-driven expression in differentiated cells.

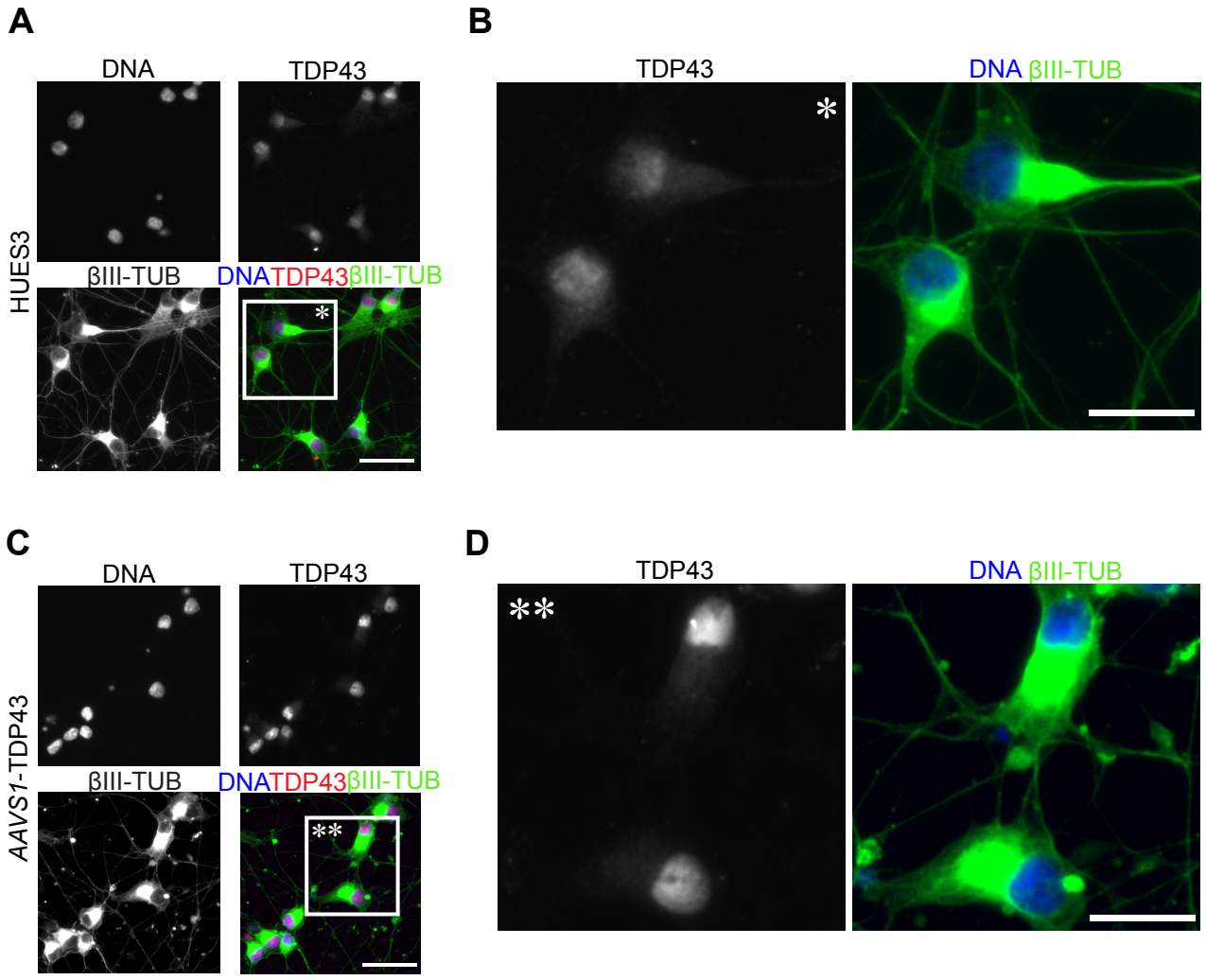

Figure 3.7 Immunocytochemistry confirms upregulation of TDP-43 in *AAVS1*-TDP43 MNs
*Hb9::*GFP+ MNs were obtained from HUES3 and *AAVS1*-TDP43 ES cell lines and cultured for 10 days after FACS purification in different wells of the same 8-well chamber slide. Cells were then fixed and stained using antibodies against TDP-43 and the panneuronal cytoskeletal protein β-III TUBULIN. **A-B** MNs derived from HUES3.**C-D** MNs differentiated from the targeted AAVS1-TDP43 cell line. Images were taken using the same exposure. Immunoreactivity to TDP-43 stronger in *AAVS1*-TDP43 MNs, consistent with overexpression of TDP-43 in these cells (Scale bar = 25 μm)

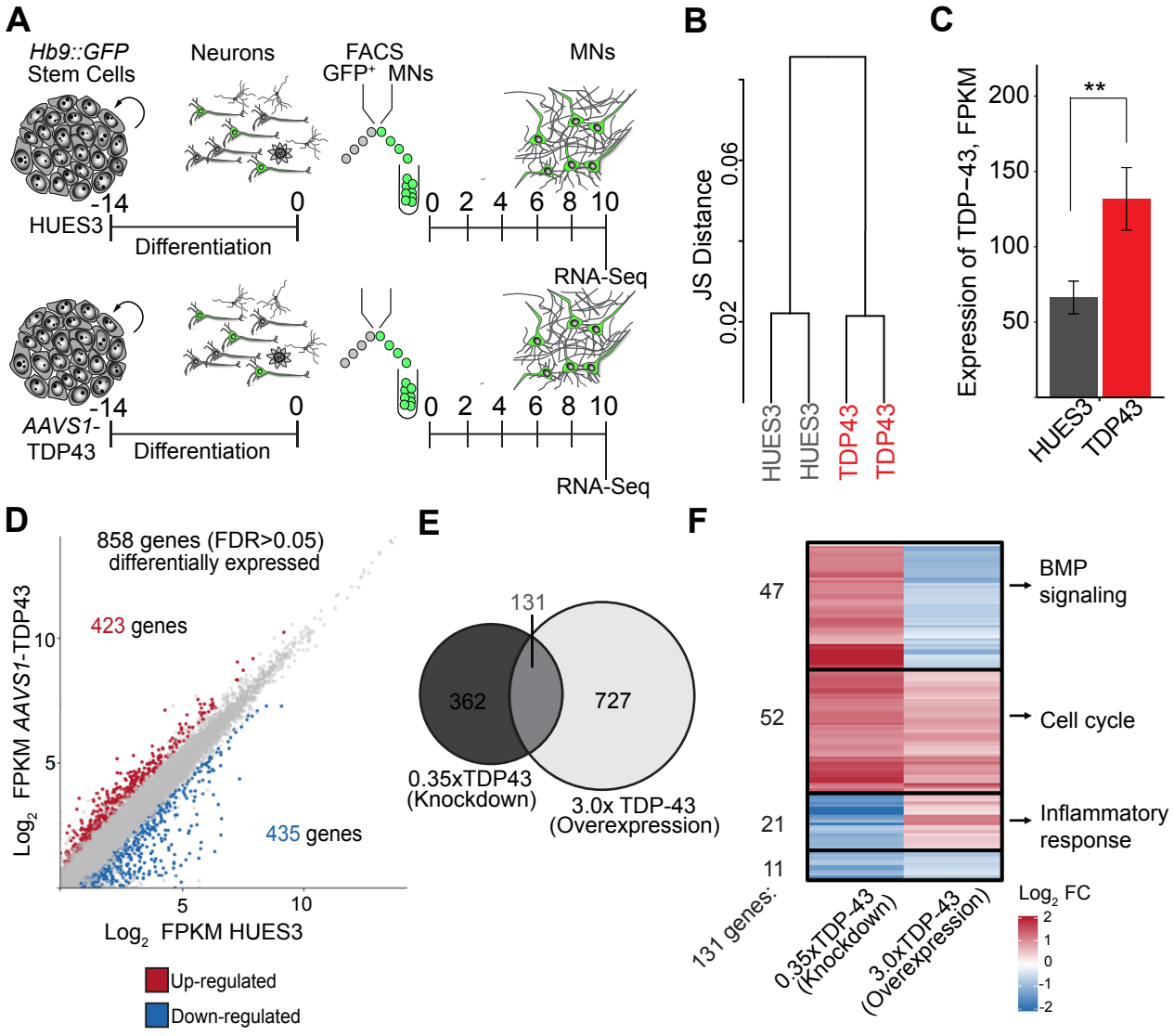

Figure 3.8 RNA-Seq of MNs with increased TDP-43 and overlap with knockdown data

A. Strategy used for the generation of RNA-Seq MN samples expressing increased levels of TDP-43. Similar to the conditions used in the TDP-43 RNAi experiment, cells were cultured for 10 days after FACS. **B.** Dendogram generated after unsupervised hierarchical clustering of the RNA-Seq data demonstrated separation of biological samples according to the levels of expression of TDP-43. A scatter plot comparing the FPKM values (gene expression) in human MNs differentiated from the HUES3 parental line (x-axis) versus those in the *AAVS1*-TDP43 MNs (y-axis). Genes identified as significant (FDR>0.05) after differential expression analysis are highlighted (red and blue), **E.** Venn diagram depicting the number of significant genes for each RNA-Seq experiment (TDP-43 knockdown and TDP-43 overexpression) and the overlap between the two data sets. **F.** Heat map depicting the fold change (Log_2) in total trasncript levels for the 131 genes that overlapped between the two RNA-Seq experiments. Pathways that were significantly enriched in each of the four categories (according to direction of change in gene expression) are indicated.

HUES3 MNs (Figure 3.8C). Examination of statistically significant changes (FDR>0.05) in transcript abundance between the two genotypes identified 423 genes as upregulated and 435 genes as downregulated in response to increased expression of TDP-43 (Figure 3.8D). Finally, when we compared these results with those of the TDP-43 knockdown experiment we found an overlap of 131 genes (Figure 3.8E), which we hypothesize represent robust candidate genes modulated by TDP-43 levels in human differentiated MNs.

By considering the direction of change in transcript levels (upregulation versus downregulation) in each of the two RNA-Seq experiments, we further grouped each of these 131 genes into four categories (Figure 3.8F). Gene ontology analyses revealed that the group of 47 genes downregulated after TDP-43 knockdown and upregulated by TDP-43 overexpression was enriched for several components of the BMP branch of TGF-β signaling, including *BMP4, GDF6, SMAD6, ID1* and *ID2* (Figure 3.8F). In the group of 52 genes upregulated in both experiments, 22 genes were called as functionally associated with cell cycle processes, in particular with cdk1/cyclinB signaling (Figure 3.8F). Other genes found to be associated with dysregulation of TDP-43 levels included components of neuroinflammatory processes (*IFI6, CXCL5, GBP2, MX1*[49-52], and the neural-specific ADCY1-$Ca2^{+}$ dependent, which is involved in brain development and in memory plasticity[53] (Figure 3.8F).

3.2.5 Validation of TDP-43 knockdown RNA-Seq data using qRT-PCR

Of the 493 identified as significantly deregulated in MNs after TDP-43 knockdown, we decided to use three non-exclusive parameters, to select a subset of these genes for further validation. First, we considered genes that overlapped with the TDP-43 overexpression RNA-Seq data. In addition, we selected candidates with enriched neuronal expression (*STMN2*[54, 55], *ELAVL3*[56], *NAT8L*[57]), association with neurodevelopment and neurological disorders

(*RCAN1*[58], *NAT8L*[57]), or genes whose modulation affects neuronal survival and function (*BMP4*[59], *GDF6*[60]). Finally, we also included genes with reasonable expression levels (FPKM ≥ 5) and high fold changes as 'positive controls' (*SELPLG*, *ALOX5P*), as we hypothesized these candidates would be more robust and likely to validate.

We then obtained RNA from independent biological replicas after TDP-43 knockdown and determined by qRT-PCR the relative expression levels for 12 candidate genes, including *TDP-43*. To account for potential off-target effects of the single siTDP43 used in the RNA-Seq experiment, we included in the validation assays a second siRNA targeting a different region of the *TDP-43* transcript (siTDP43_2). Notably, we confirmed differential gene expression for 75% (9/12) of these genes in cells treated with either siTDP-43 relative to those treated with the scrambled controls (Figure 3.9A-B). These results indicate reproducible expression differences among the genes we selected, validating the findings from RNA-Seq analyses.

3.2.6 STMN2 protein levels are downregulated after TDP-43 knockdown

Of the genes identified in RNA-Seq analyses and validated by qRT-PCR, the gene encoding for the microtubule-binding phosphoprotein STMN2[54] exhibited one of the highest levels of transcript abundance in MNs and significant fold changes after partial loss of TDP-43 (Figure 3.10A). We decided to focus our work on the further characterization of this finding, considering the growing evidence for the relevance of cytoskeletal pathways in ALS[61, 62], and the reports of STMN2 protein as a factor associated with neuronal growth and axonal repair after injury[54, 55, 63]. First, we examined if the significant downregulation of the *STMN2* transcripts as result of *TDP-43* knockdown had an effect on the levels of STMN2 protein. In RNAi experiments independent from the ones described above, we obtained total RNA and protein from differentiated MNs after knockdown of *TDP-43* with two distinct *TDP43*-

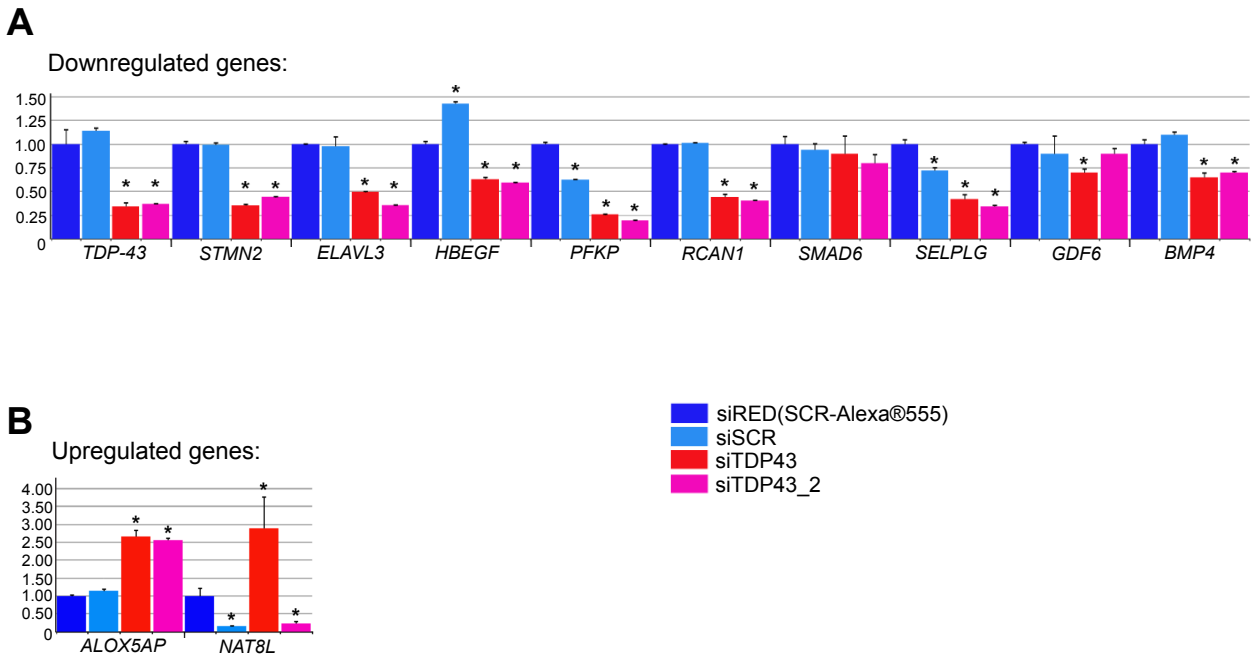

Figure 3.9 qRT-PCR validation of a subset of candidate genes selected after RNA-Seq analyses
A-B. A subset of genes initially identified as 'hits' in the TDP43 knockdown experiment were selected for validation by qRT-PCR in independent experiments (see text for details on the criteria used to include genes in this group). MNs were obtained and RNAi targeting TDP-43 was induced. For these assays, an additional siRNA against the TDP-43 mRNA (siTDP43_2) was included. RNA was obtained from MNs 4 days after siRNA delivery, and qRT-PCR was carried out to determine transcript levels for 12 genes, including *TDP-43*. Genes are separated based on the direction of change initially determined by RNA-Seq in the TDP-43 knockdown experiment. A total of 9 out 12 of these genes (including *TDP-43*) exhibited the predicted response to TDP-43 depletion when their expression was assayed by qRT-PCR.

targeting siRNAs (siTDP43 and siTDP43_2). Using qRT-PCR, this time with two different sets of primer pairs binding the *STMN2* mRNA, we once again detected significant downregulation (~50-60%) of this gene in MNs treated with either siTDP43, but not in cells treated with controls (Figure 3.10B). We then carried out immunoblot assays on the obtained MN protein lysates and determined that STMN2 protein levels were also significantly reduced in cells with partial depletion of TDP-43 (Figure 3.10C). Interestingly, these protein assays also revealed a difference between the levels of TDP-43 knockdown achieved with each siTDP43 (62% with siTDP43 vs. 54% with siTDP43_2), which correlated with the loss of STMN2 levels (68% vs. 50%) (Figure 3.10C).

Finally, it is important to mention that although we did not detect *STMN2* transcriptional levels as significantly altered in the RNA-Seq data from MNs overexpressing TDP-43, in subsequent independent experiments we did observe by qRT-PCR a modest, but significant upregulation of *STMN2* mRNA in response to increased TDP-43 (Figure 3.10D). Perhaps this variability in experiments in the context of upregulated *TDP-43* but not *TDP-43* RNAi, results from the difference in the length of time that cells were exposed to TDP-43 dysregulation. While in both sets of experiments MNs were assayed 10 days after FACS isolation, the cells in the TDP-43 knockdown experiments follow a more acute model (RNAi for 4 days) compared to cells with a stable and more prolonged overexpression of the targeted *CAGs::TDP-43* construct.

3.2.7 Downregulation of two other ALS-linked genes does not alter *STMN2* levels

Next, we investigated whether *STMN2* levels also changed in response to the downregulation of two other ALS-linked genes, *FUS* and *C9ORF72*[64, 65]. The FUS protein, structurally similar to TDP-43, is also involved in RNA metabolism[66], and FUS variants can be

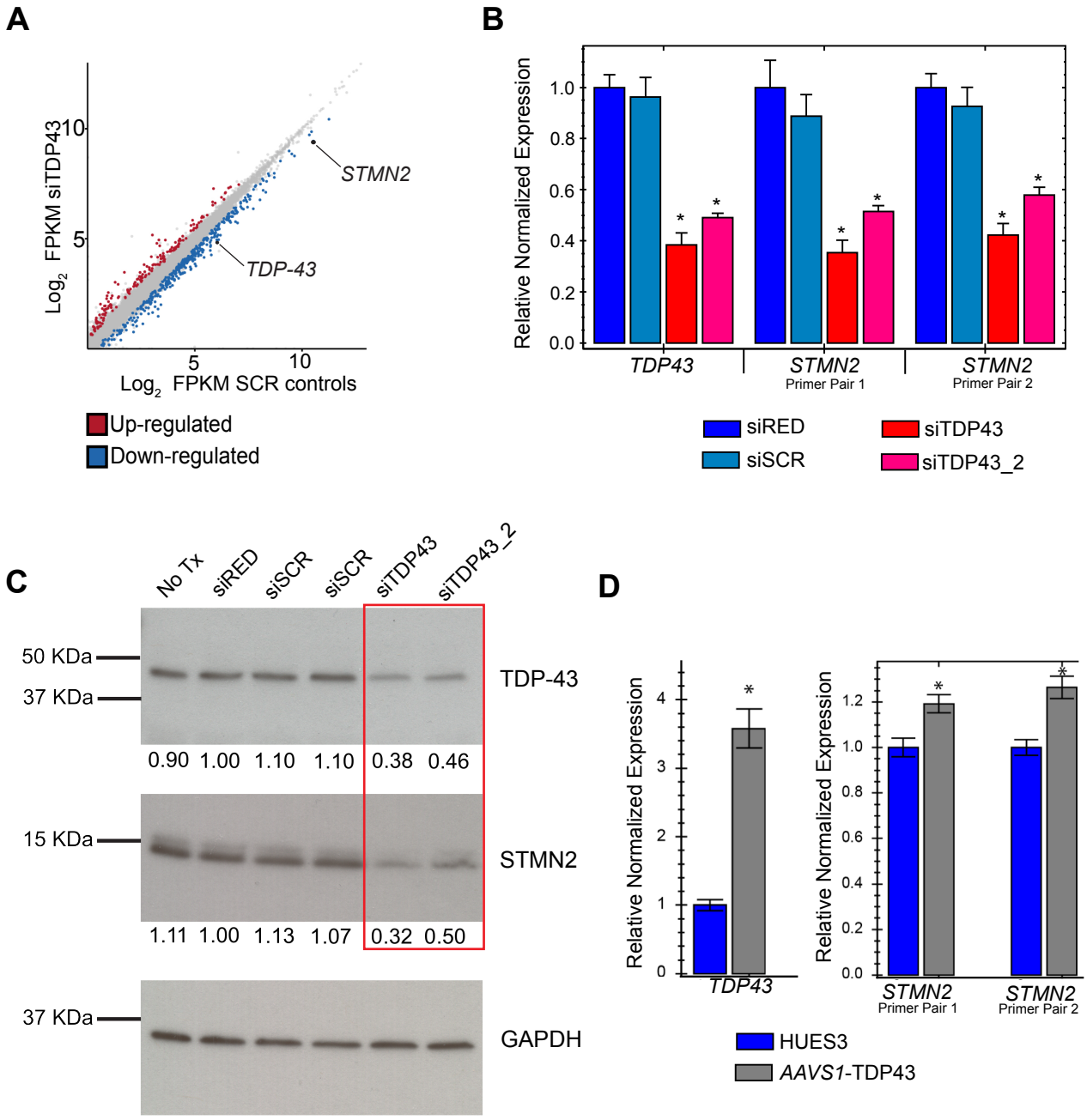

Figure 3.10 Validation of STMN2 protein depletion following RNAi targeting *TDP-43*

A. Scatter plot for gene expression values (in FPKMs) in MNs after induction of RNAi targeting TDP-43 (y-axis) and those in control samples treated with scrambled (SCR) sequence siRNAs (x-axis). Genes identified by RNA-Seq analyses (FDR>0.05) as differentially expressed between the two biological samples are highlighted in red (upregulated) and blue (downregulated). The values for the *TDP-43* and *STMN2* genes are indicated. *STMN2* is one of the most abundant transcripts in MNs and exhibits one of the highest fold changes (downregulation) in response to reduced TDP-43 levels. **B.** *STMN2* mRNA downregulation following TDP-43 depletion was confirmed by qRT-PCR in independent experiments. Two different sets of primer pairs binding the *STMN2* transcript were used. **C.** STMN2 protein levels were reduced following partial depletion of TDP-43. Protein levels were normalized to GAPDH and are expressed relative to the levels in MNs treated with the siRED control. **D.** qRT-PCR analysis of *STMN2* expression in HUES3 and *AAVS1*-TDP43 MNs showed a modest but significant increase in *STMN2* transcript levels cells overexpressing TDP-43.

detected in ~5% of familial ALS cases[67]. While the exact function of the *C9ORF72* gene product is an active area of research, large repeat expansions in the intronic regions of this gene are responsible for ~40-50% of familial and ~7% of sporadic ALS cases[68-70]. These *C9ORF72*-linked ALS cases typically exhibit pathological loss of nuclear TDP-43 in neural tissues, and reduced *C9ORF72* transcript levels[64, 68, 69]. In order to assess the effect of *FUS* or *C9ORF72* knockdown on the *STMN2* gene, we measured *STMN2* relative transcript levels in human differentiated MNs following induction of RNAi targeting *TDP-43*, *FUS* or *C9ORF72*. After confirming the significant downregulation of the respective siRNA-targeted genes by qRT-PCR (Figure 3.11A-C), we determined that knockdown of only *TDP-43*, but not of *FUS* or *C9ORF72*, reduced the levels of *STMN2* (Figure 3.11D). Downregulation of *TDP-43* did not alter the expression levels of *FUS* or *C9ORF72* (Figure 3.11A), and reduced expression of either *FUS* or *C9ORF72* showed no effect on the other ALS-linked genes (Figure 3.11B-C). Importantly, these results demonstrate that *STMN2* downregulation is not a consequence of RNAi induction targeting any functional gene in the human differentiated MNs, but rather a specific molecular phenomenon in response to partial loss of TDP-43 function.

3.2.8 Localization of STMN in human differentiated MNs

STATHMIN-LIKE 2 (STMN2) is one of four proteins (STATHMIN, STMN2, SCLIP/STMN3, and RB3/STMN4) belonging to the STATHMIN family of microtubule-binding proteins with functional roles in neuronal cytoskeletal regulation, and axonal regeneration pathways[54, 55, 63, 71-75]. The founding member of this family was first identified biochemically as a ubiquitous phosphoprotein, and initially proposed to function as an intracellular 'relay' (or '*stathmos*' in greek) for extracellular signals regulating cell proliferation and differentiation[76, 77]. In humans,

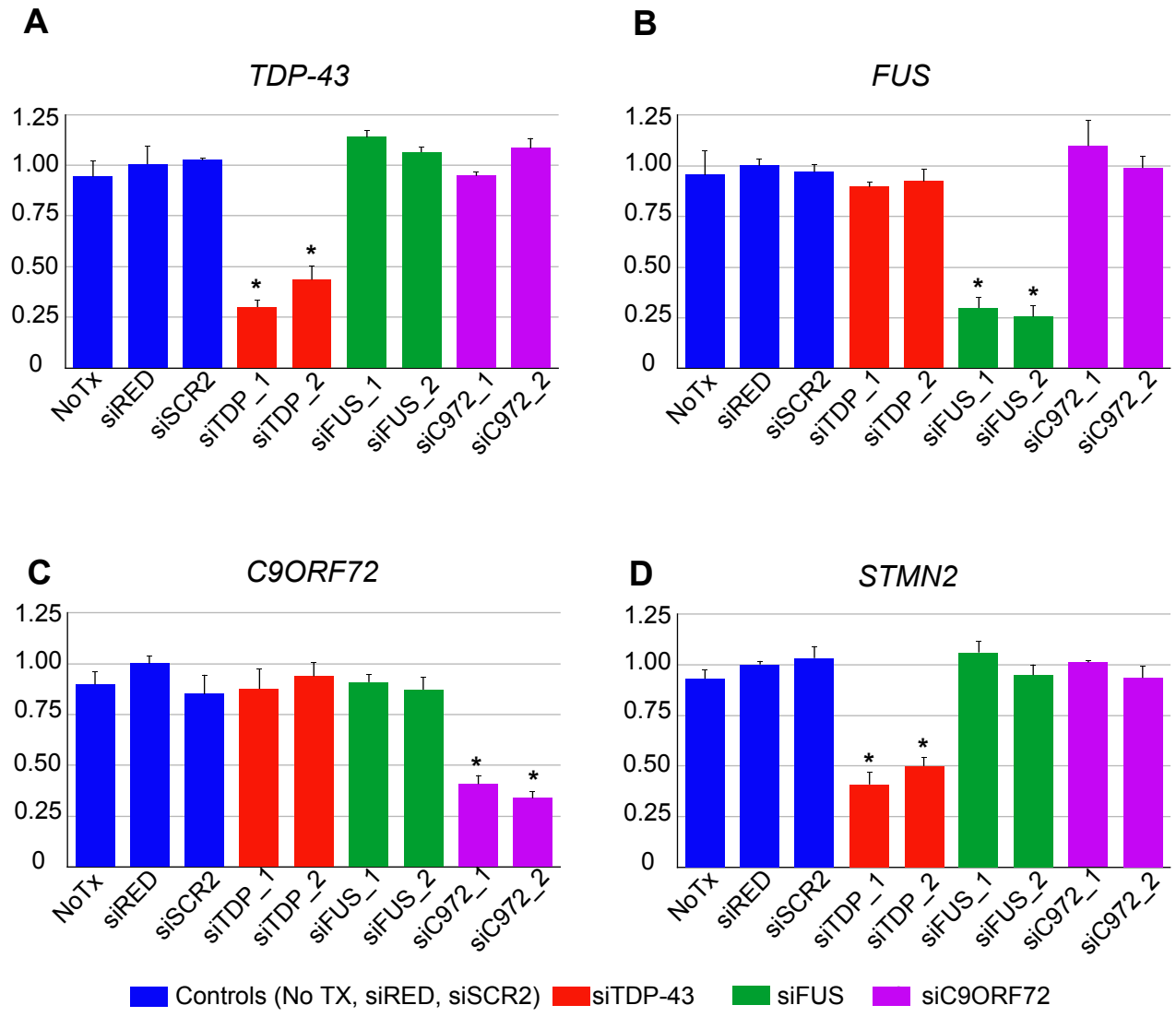

Figure 3.11 ***STMN2*** **levels do not change following downregulation in two other ALS-linked genes**
*Hb9::*GFP^{+} MNs were independently treated with siRNAs targeting each of three ALS-linked genes (*TDP-43, FUS,* and *C9ORF72*). qRT-PCR was used to determine the expression for each of these genes and that of *STMN2*. **A-C.** qRT-PCR validation of RNAi-mediated knockdown for (A)*TDP-43*, (B)*FUS* and (C)*C9ORF72*. **D.** *STMN2* downregulation was specific to RNAi targeting *TDP-43*.

STATHMIN and *SCLIP/STMN3* genes exhibit ubiquitous expression, whereas *STMN2* and *RB3/STMN4* have been reported as preferentially enriched in CNS tissues[78]. To gain further insights into the role of STMN2 in human differentiated MNs we probed the subcellular localization of this protein by immunocytochemistry. STMN2 localized to discrete cytoplasmic puncta, that were present along TUJ1+ neuronal projections and were particular enriched in the perinuclear region (Figure 3.12A). Using a human-specific antibody against the Golgi-associated protein GOLGIN97, we determined this perinuclear region to correspond to the Golgi apparatus (Figure 3.12B-C), which is consistent with the prediction of STMN2 N-terminus as the target of palmitoylation for vesicle trafficking and membrane binding[79]. Supporting previous expression studies of the mammalian *STMN2* gene[75, 78, 80], we found the STMN2 protein to be neuronal-specific, as it was not detected in the supportive monolayer of primary glial cells co-cultured with the differentiated MNs (Figure 3.12B-C)

3.2.9 Preliminary phenotyping of MNs after TDP43 knockdown using outgrowth assays

To determine whether the transcriptional changes we have identified and validated in this study have a functional impact, particularly the reduced levels of the neuronal growth-associated factor STMN2 following depletion of TDP-43 in MNs, we are currently using neurite outgrowth assays to characterize the phenotype of these cells. In a preliminary experiment, we imaged *Hb9::*GFP$^+$ differentiated cells that were initially transfected in suspension with an siRNA targeting *TDP-43*, *STMN2,* or a non-targeting scrambled sequence (siSCR) control, and then cultured as cell aggregates for 6 days after transfection. We treated the cultures with a live-cell fluorescent dye before imaging in order to capture with better resolution the neuronal projections using epifluorescence microscopy (Figure 3.13). Although

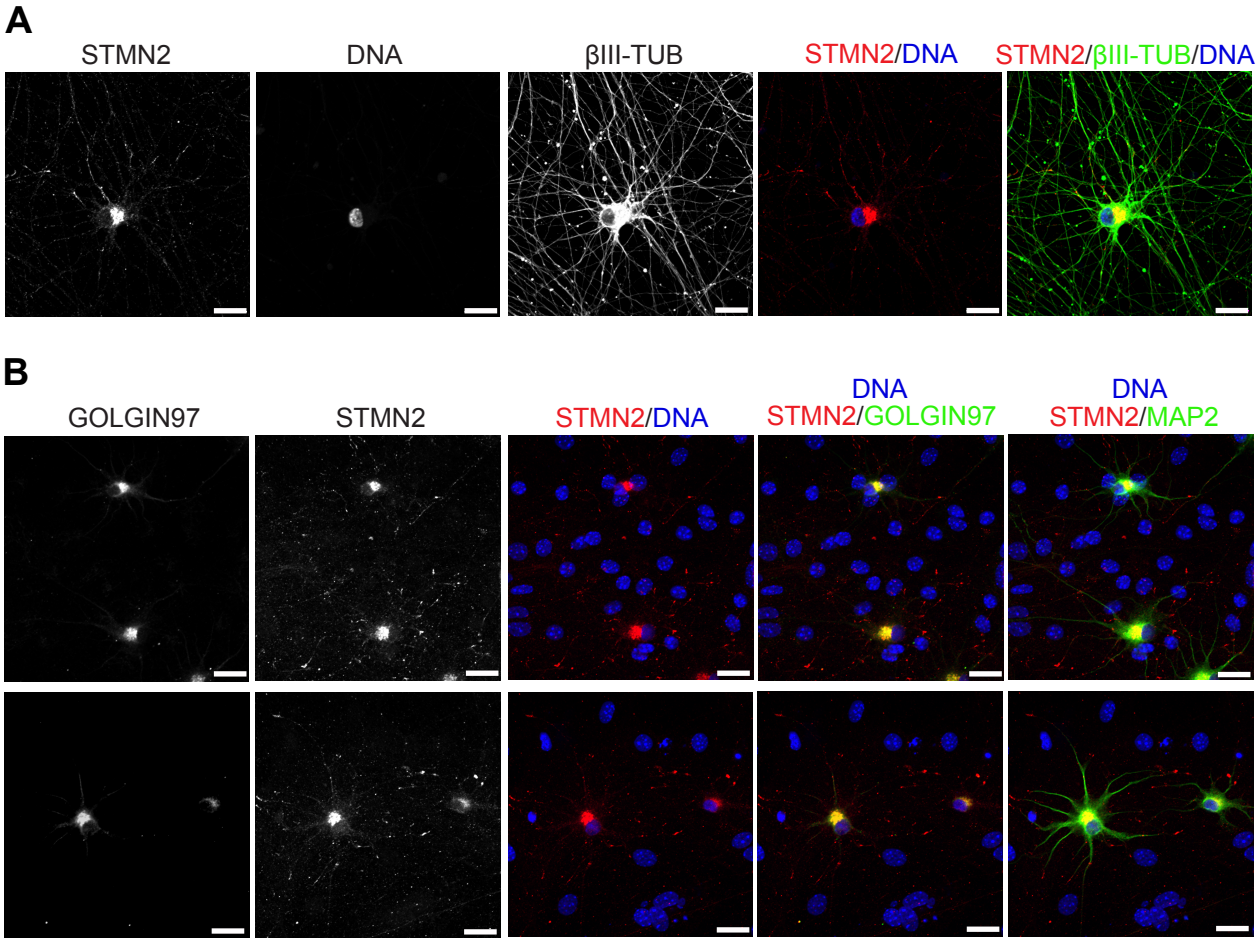

Figure 3.12 STMN2 subcellular localization in cultured differentiated MNs

A. STMN2 protein is enriched in the perinuclear region of human differentiated MNs. STMN2 can also be detected in discrete 'puncti' along the neuronal processes, as determined by co-staining with the cytoskeletal protein β-III TUBULIN. **B.** STMN2 immunoreactivity was not detected in the primary glial cells in the co-culture, indicating neuronal-specific expression (only in $MAP2^{+}$ cells). The perinuclear region immunoreactive to STMN2 corresponds to the Golgi apparatus, as determined by co-localization with the golgi marker GOLGIN97. Image J was used to calculate the correlation (r^2) between mean intensities for images obtained in different channels with $r^2 = 0.948 \pm 0.03$ for STMN2 and GOLGIN97 vs. $r^2 = 0.11 \pm 0.08$ for STMN2 and DAPI. Approximately 50 cells were analyzed. (Scale bar = 20 μm)

only 2 to 3 samples per siRNA treatment were examined in this experiment, we observed gross phenotypic differences in terms of the thickness and length of bundles of neurites emanating from the cell aggregates, particularly in the samples with RNAi targeting *TDP43* (Figure 3.13). We used ImageJ software to quantify the mean fluorescence intensity along 20 concentric circles drawn relative to the clustered cell bodies (Figure 3.14A), and detected statistically significant differences between the cells treated with siTDP43 and those treated with scrambled control, along areas encompassed by circles 7-10 (Figure 3.14B). Although, not statistically significant, a trend in reduced mean fluorescence intensity was also detected in the same area for the samples treated with siSTMN2 (Figure 3.14B). Interestingly, using mean fluorescence intensity as a readout for the presence of neurites, with outermost circles having a mean intensity of zero (indicating absence of neuronal projections), we observed that samples with RNAi targeting *TDP-43* or *STMN2* both reached this '0' value at a smaller concentric circle (circles 11-12) compared to the scrambled control (circles 17-18) (Figure 3.14B). These preliminary results suggest that downregulation of *TDP-43,* and perhaps *STMN2* as well, can have measurable phenotypic effects on the growth of MN neurites.

3.2.10 STMN2 is expressed in human adult primary spinal MNs and is altered in ALS

In order to further explore if STMN2 regulation by TDP-43 levels could be relevant to MN biology and ALS, we used immunohistochemistry to interrogate whether this protein is expressed in human adult spinal cord tissues. Similar to what we observed in the cultures of stem cell-derived MNs (Figure 3.12), we detected strong STMN2 immunoreactivity in the perinuclear region of human adult lumbar spinal MNs, which was not present in the surrounding glial cells (Figure 3.15A).

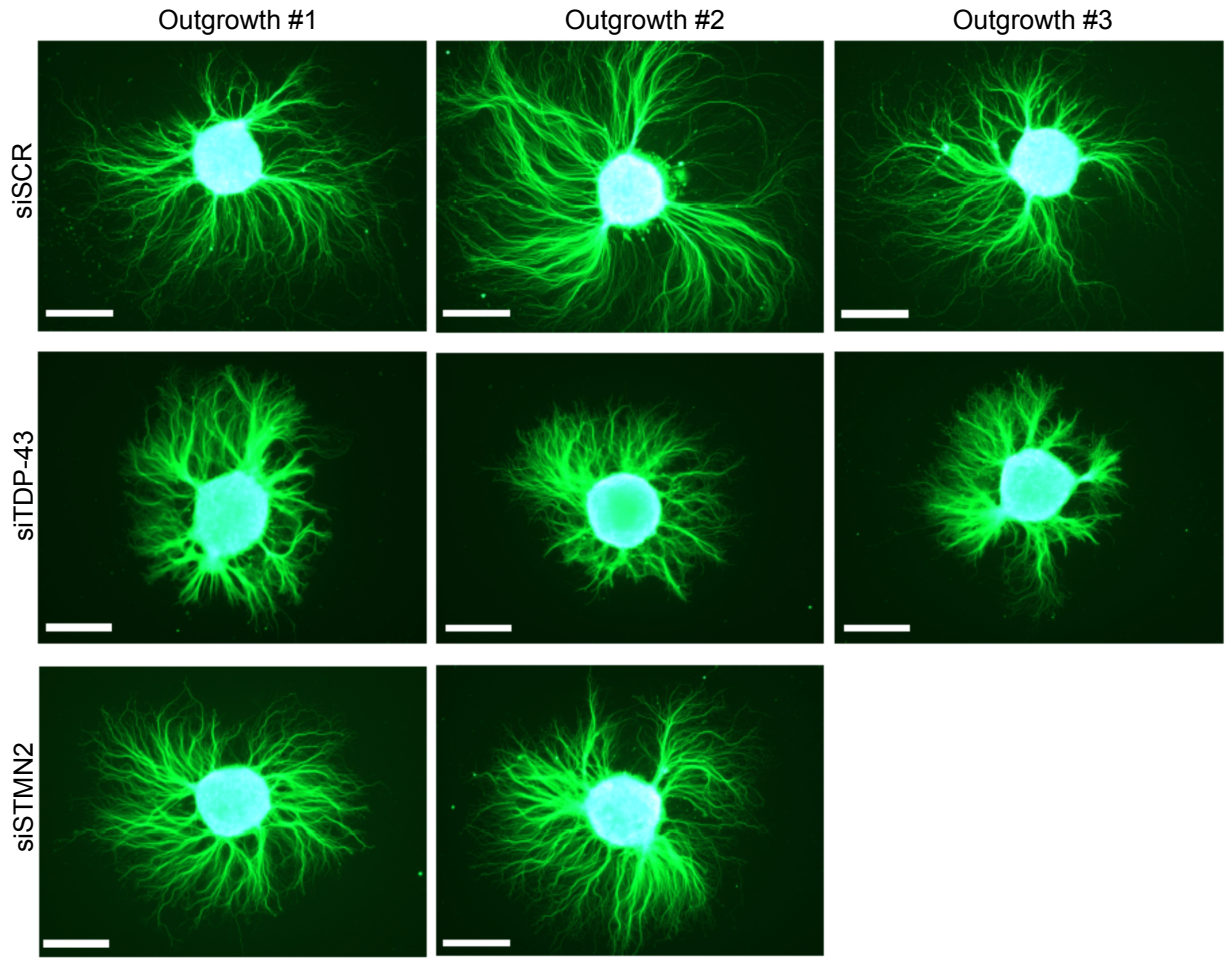

Figure 3.13 Phenotype of differentiated MNs following RNAi targeting *TDP-43* or *STMN2*
*Hb9::*GFP^{+} MNs were treated in suspension with siRNAs targeting TDP-43 or STMN2. Cells were then aggregated and plated (see Methods section for details). A live-cell fluorescent dye (Calcein AM) and epifluorescence microscopy was used to image each aggregate (outgrowth) 6 days after siRNA delivery. All images were taken using the same exposure.

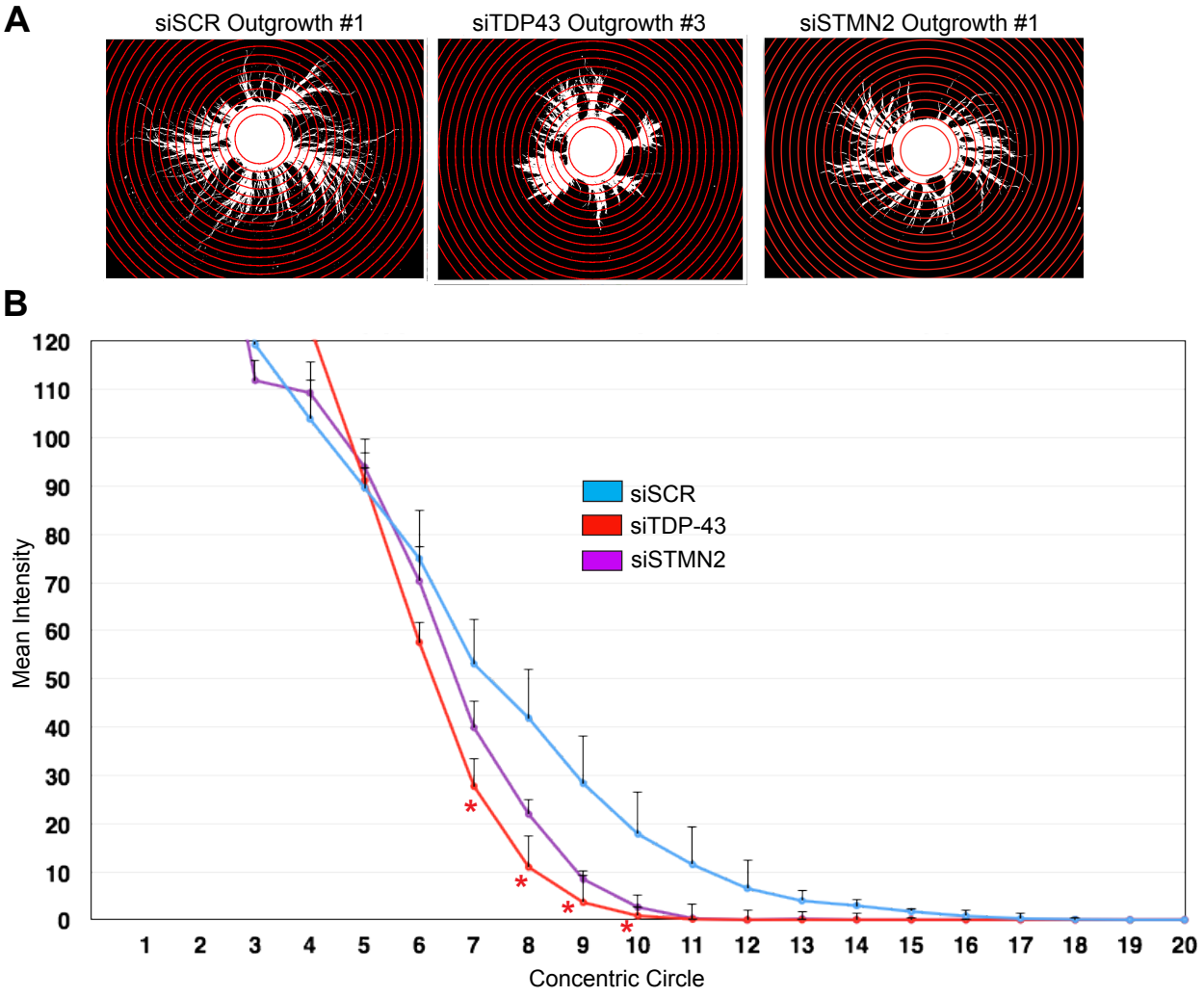

Figure 3.14 Analysis of neurite outgrowth in differentiated MNs following RNAi targeting *TDP-43* or *STMN2*
A. Images collected for each aggregate (outgrowth) 6 days after siRNA delivery were analyzed using the Image J software package. Images obtained for 3 different outgrowths following image processing with the 'concentric circle' and 'mean intensity' commands are shown. For each image, the region of the outgrowth containing the cell bodies was set up as reference to draw concentric circle 1. A 'threshold' function was used to convert fluorescence intensity to two discrete values (0 and 255) **B.** 'Mean Intensity' within the area unique to each concentric circle was calculated. This value was interpreted as readout of the density of neuronal processes within each circle, so that for concentric circle 1 it was always 255 (maximum value) and for more outward circles these values reached 0, indicating absence of neurites. MN aggregates from cells treated with siTDP-43 exhibited reduced neurite growth, as indicated by the significant reduction in 'mean intensity' in circles 7-10 relative to the scrambled siRNA-treated (siSCR control) cells. For cells treated with siSTMN2 there was a trend, although not statistically significant, for reduced growth. Mean intensity values for cells treated with siTDP43 or siSTMN2 reached '0' at smaller circles (11-12) compared to control cells (17-18), suggesting a reduction in the length of neuronal processes.

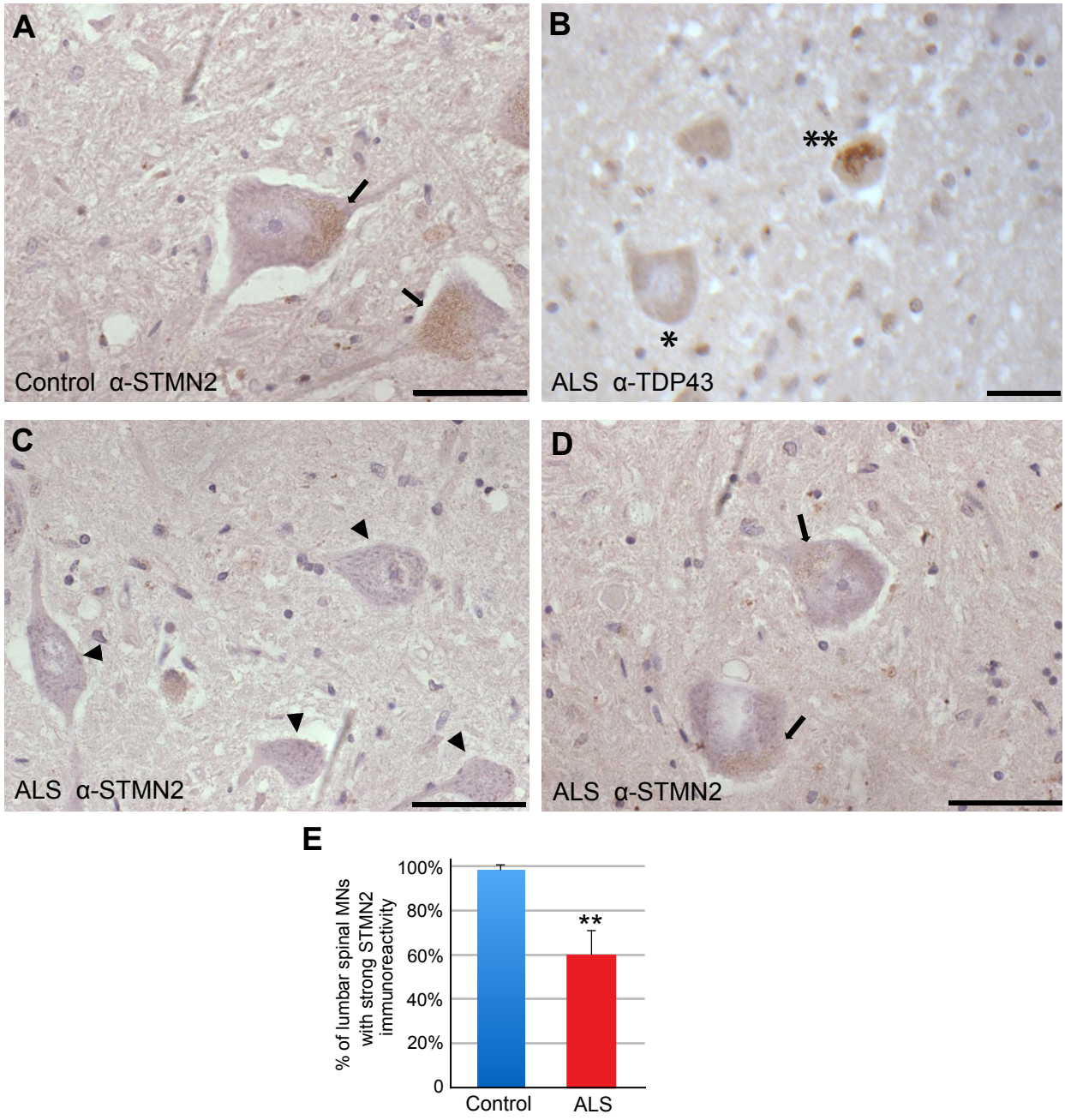

Figure 3.15 STMN2 is expressed in human adult MNs and is altered in ALS tissues
A. Histologic analysis of human adult lumbar spinal cord from post-mortem samples collected from a subject with no evidence of spinal cord disease (control). Immunoreactivity to STMN2 was detected in the perinuclear region (indicated by arrows) of spinal motor neurons but not in the surrounding glial cells. **B.** Histologic analysis of post-mortem spinal cord tissue collected from a sporadic ALS case. TDP-43 neuropathology, detected as reduced TDP-43 immunoreactivity in the nucleaus (indicated by *) and/or cytoplasmic TDP-43 immunoreactive inclusions (indicated by **), was used to confirm the diagnosis for all cases used in this study. **A,C-D.** STMN2 immunoreactivity in lumbar spinal motor neurons from control and ALS cases was scored as 'strong' [as indicated by arrows in A (control) and D (sporadic ALS)] or as 'absent' [as indicated by arrowheads in C (sporadic ALS)]. (Scale bar = 50 μm). **E.** The percentage of lumbar spinal motor neurons with strong STMN2 immunoreactivity was significantly lower in ALS tissue samples, suggesting altered expression of STMN2 protein in ALS (n= 3 controls and 3 ALS cases; approximately 40 MNs were scored for each subject; **p<0.01).

Given our findings regarding the loss of STMN2 in human differentiated MNs after depletion of TDP-43 (Figure 3.10C), we predicted that the levels of STMN2 protein would be altered in post-mortem spinal MNs from sporadic ALS cases, which usually manifest pathological loss of nuclear TDP-43 staining and accumulation of cytoplasmic TDP-43 immunoreactive inclusions[16, 17]. To test this prediction, we used immunohistochemical analysis to determine the percentage of MNs exhibiting strong STMN2 immunoreactivity in lumbar spinal cord tissue sections obtained from 3 control cases (no evidence of spinal cord disease) and from 3 ALS cases with confirmed TDP-43 pathology (Figure 3.15B). Consistent with our hypothesis, we found that the percentage of lumbar MNs with clear immunoreactivity to the STMN2 antibody was significantly reduced in the tissue samples collected from sporadic ALS cases (Figure 3.15A-E).

3.3 Discussion

Since the initial biochemical[16, 17] and genetic[10-12, 81]studies linking the RNA binding protein TDP-43 to ALS, RNA metabolism has emerged as a major candidate pathway underlying the biology of neurodegeneration. *FUS*, *TAF15*, *HNRNPA1*, *HNRNPA2B1*, and *MATR3*, are just some of the more recently added members to the growing list of ALS-associated genes functionally connected to the multiple steps in RNA synthesis and processing[64, 65]. How disturbances in RNA metabolism contribute to the selective death of MNs manifested in ALS remains elusive. In this study, we hypothesized that interrogation of transcriptional changes resulting from dysregulation of TDP-43 in the context of human MN physiology could uncover novel molecular disease mechanisms. We used high throughput sequencing to identify differentially expressed transcripts in human embryonic stem cell-derived spinal MNs after either reduction or upregulation of TDP-43 levels, and further demonstrated that partial loss of

TDP-43 function in these cells can have measurable and reproducible molecular consequences (Figure 3.9-3.10). Of note, the 65% downregulation in levels of TDP-43 achieved in our experiments (Figure 2.5B) exceeds the recently reported ~20-60% reduction in the CNS of RNAi transgenic mice, which was sufficient to drive ALS-like phenotypes in these animals[20].

Additional evidence of compromised TDP-43 function in the human differentiated MNs we investigated here was presented following computational examination of their differentially spliced RNAs. Remarkably, the two significant alterations we detected in the splicing pattern of the gene encoding POLDIP3 (Figure 3.5F) have been extensively associated with loss of TDP-43 function in cultured cells[43, 47], mouse CNS[20], human spinal cord tissues[20], and in laser capture microdissected MNs from sporadic ALS patients with confirmed TDP-43 pathology[47]. POLDIP3 regulates cell growth and efficiency of RNA translation by interacting with the mTOR pathway kinase S6K1[82]. The POLDIP3 protein variant resulting from isoform 2, which lacks *EXON3* and is upregulated in response to reduced TDP-43 levels (Figure 3.5F), has been previously shown to drive higher global translational yields compared to the variant encoded by isoform 1[43]. Taken together, our findings and those of previous sudies[20, 43, 47], suggest a model whereby TDP-43 deficiency in MNs leads to disturbances in anabolic processes and cellular protein homeostasis, perhaps by upregulation of toxic or aggregation-prone proteins. Additional work will be required to determine whether a global increase in protein synthesis indeed occurs in MNs as result of TDP-43 depletion. Recent advances in proteomics[83], combined with our ability to generate large amounts of protein extracts from human differentiated MNs (Joseph Klim and Kevin Eggan, unpublished experiments) will make it possible to test this hypothesis, in addition to further elucidating the identity of any dysregulated proteins.

Two other pathways identified as downstream of TDP-43 activity were BMP signaling and core cell cycle regulators (Figure 3.8F). Interestingly, recent reports link components of the BMP branch of TFGβ signaling to motor neuron survival both *in vitro* and *in vivo*[59, 60]. Particularly, *GDF6* (also known as *BMP13*), has been proposed as a putative risk factor in neuromuscular degeneration, following genetic studies in zebrafish demonstrating that homozygous null mutations in *gdf6* lead to disruption of neuromuscular junction (NMJ) morphology, loss of spinal motor neurons, severe swimming deficits, reduced life-span, and increased susceptibility to the expression of ALS-linked SOD1 variant[60]. BMP signaling has also been found to mediate interactions between motor neurons and muscle in the mammalian NMJ and to promote survival in neuronal cultures and in the adult mouse retina following damage *in vivo*[59, 84]. Our additional findings of transcriptional expression and dysregulation of cell cycle genes in MNs is seemingly at odds with their postmitotic state (Figure 3.2E-F, Figure 3.8F). However, several studies have demonstrated that cell cycle proteins in postmitotic neurons can acquire alternatively functions in non-proliferative pathways including neuronal migration, axonal elongation, and synaptic maturation and plasticity[85]. Experiments with cultured cells and animal models have also shown activation of cell death pathways following overexpression of cell cycle genes in post-mitotic neurons[86]. Furthermore, there is increasing evidence that neuronal types at risk of neurodegeneration in Alzheimer's disease, Parkinson's disease and ALS, exhibit upregulation and altered subcellular localization of various cell cycle proteins[86-89]. Our observations that loss of TDP-43 function results in decreased *GDF6/BMP4* and induction of various cell cycle genes (Figure 3.8F), combined with the aforementioned findings from other groups, argue for further studies into the potential roles of these two pathways in human MN biology and pathophysiology. For instance, it would be interesting to

determine if the survival of differentiated MNs in culture can be modulated either by activation of BMP signaling with recombinant ligands and small molecule agonists, or by inhibition of cell cycle signaling with RNAi or kinase inhibitors.

Our results also demonstrated that partial depletion of TDP-43 in human differentiated MNs alters STMN2 protein levels (Figures 3.10-3.11). To our knowledge, this study is the first to link loss of TDP-43 function with downregulation of this neuronal growth-associated factor. STMN2 is one of four members of the STATHMIN family of tubulin-binding proteins, which regulate axonal growth by promoting the dynamic instability of microtubules[54, 55, 63, 73-75]. Although all four *STATHMIN* genes were detected in human differentiated MNs, *STMN2* displayed the highest transcript abundance, and is the only family member influenced by *TDP-43* knockdown (data not shown). Additional RNAi assays found the regulation of *STMN2* levels to be downstream of *TDP-43* but not *FUS* or *C9ORF72* (Figure 3.11). This observed lack of immediate response to other ALS-linked genes does not undermine the potential significance of dysregulated *STMN2* to different genetic forms of ALS, given that TDP-43 neuropathology can be detected in the majority of ALS cases[16, 17, 90]. Therefore, a plausible model incorporating these results is that defects in other ALS-associated genes *eventually* converge on the loss of TDP-43, which in turn has a more immediate effect on *STMN2*. The RNAi experimental system we have established here will facilitate the interrogation of epistatic interactions among all the players in the rapidly-increasing catalog of ALS-causative genes and risk factors with diverse cellular functions[62, 65, 91].

Using TDP-43 immunoprecipitation assays coupled with next generation sequencing, different groups have generated large-scale interaction maps of TDP-43 protein and its thousands of RNA targets in different cell types, including rat cultured neurons[92], whole mouse

brain[4], SHSY5Y neuroblastoma cells[93], and human cortical tissues[94]. Manual and computational[95] reanalysis of the supplementary data in these reports, indicated that TDP-43 protein associates with the *STMN2* transcript in mammalian cells, and that this interaction can occur through direct binding to *3'-UTR* of the *STMN2* mRNA. Thus, a general direct regulatory mechanism by which STMN2 levels are sustained in MNs could involve TDP-43 functional roles in mRNA stability and axonal transport[9, 94, 96].

Finally, although MNs generated *in vitro* share several molecular and functional properties with *bona fide* MNs[28], the *in vivo* validation of discoveries from stem cell-based models of ALS is a critical test of their relevance to disease mechanisms and therapeutic strategies[37]. Of significance, using human adult spinal cord tissues we provide *in vivo* evidence corroborating the finding that TDP-43 dysregulation alters the expression of the cytoskeletal phosphoprotein STMN2 (Figure 3.10). Recent discoveries linking familial ALS to variants in the actin-binding protein PROFILIN[61] and the microtubule component TUBULIN ALPHA-4A[62], have reinforced the notion that disruption of cytoskeletal integrity plays a major role in ALS pathogenesis[62]. Our *in vitro* and *in vivo* findings concerning STMN2 levels (Figures 3.10-12, and Figure 3.15), together with previous reports demonstrating STMN2 critical role in microtubule dynamics[54,73,75], NMJ stability[97], and survival and regeneration pathways after axonal insults[55,63], suggest a molecular mechanism whereby loss of TDP-43 function in MNs depletes STMN2 levels which may contribute to the development and progression of the ALS phenotype. In the context of our *in vitro* experimental system, this proposed hypothesis predicts that 1) Downregulation of *TDP-43* in human differentiated MNs will cause reduced neurite outgrowth, and 2) This deficit is mediated, at least partially, by downregulation of *STMN2*. In order to test these predictions, we are currently developing neurite outgrowth assays to

characterize the functional impact of RNAi targeting *TDP-43* and *STMN2*. Thus far, preliminary results obtained with a small set of experimental samples are consistent with the first prediction (Figure 3.13-3.14). Future work aimed at validating our proposed model, as well as additional experimental approaches designed to further elucidate the molecular relationship between TDP-43 and STMN2 are discussed further in Chapter 5.

3.4 Materials and Methods

3.4.1 Cell culture and Differentiation of HUES3 *Hb9::GFP* cells into MNs

HUES3 cells were grown with mTeSR1 medium (Stem Cell Technologies) on tissue culture dishes coated with Matrigel™ (BD Biosciences), and maintained in 5% CO2 incubators at 37ºC. ES cells were passaged as single-cell suspensions after accutase™ (Stem Cell Technologies) treatment. 10 μM ROCK inhibitor (Sigma, Y-27632) were added to the cultures for 16-24 hours after dissociation to prevent cell death. MN differentiation was carried out using a modified protocol based on adherent culture conditions in combination with dual inhibition of SMAD signaling, inhibition of NOTCH and FGF signaling, and patterning by retinoic acid and SHH signaling[38, 39]. In brief, ES cells were dissociated to single cells using accutase™ (Stem Cell Technologies) and plated at a density of 80,000 cells/cm^2 on matrigel-coated culture plates with mTeSR1 medium (Stem Cell Technologies) supplemented with ROCK inhibitor (10μM Y-27632, Sigma). When cells reached 100% confluency, medium was changed to KSR medium (KO-DMEM (Life Technologies™) supplemented with 15% Knockout Serum Replacement (Life Technologies™), 1x Gibco® GlutaMAX™ (Life Technologies™) and 100μM non-essential amino-acids (NEAA)). This time point was defined as day 0 (d0) of motor neuron differentiation. Cells were fed every 24 hours, and after 4 days (on d4), increasing amounts of N2 medium (Neurobasal (Life Technologies™) supplemented

with 1x N-2 (Life Technologies™), 1x Gibco® GlutaMAX™ (Life Technologies™) and 100μM NEAA) were used to replace KSR medium, with complete replacement by d10. Cells were then cultured in N2 medium for 4 additional days. Treatment with small molecules was carried out as follows: 10μM SB431542 (Sigma) and 100nM LDN-193189 (Stemgent) on d0-d5; 1μM retinoic acid (Sigma) and 1μM Smoothend agonist (EMD Millipore) on d2-d14; 5μM DAPT (EMD Millipore) and 4μM SU-5402 (BIOVISION) on d2-d14.

3.4.2 Fluorescent Activated Cell Sorting (FACS) of GFP$^+$ MNs

On d14, HUES3-differentiated cultures were dissociated to single cells using accutase™ treatment for 1 hour inside a 5% CO2 / 37ºC incubator. Repeated (10-20 times) but gentle pipetting with a 1000μL Pipetman® was used to achieve a single cell preparation. Cells were spun down, wash 1x with PBS and resuspended in sorting buffer (1x cation-free PBS 15mM HEPES at pH 7 (Gibco®), 1% BSA (Gibco®), 1x penicillin-streptomycin (Gibco®), 1 mM EDTA, and DAPI (1μg/mL). Cells were passed through a 45μm filter immediately before FACS analysis and purification at the Harvard University FAS Bauer Core Facility. The Beckman Coulter Moflo XDP cell sorter was routinely used to purify *Hb9::*GFP$^+$ cells into collection tubes containing MN medium (Neurobasal (Life Technologies™, N2 supplement (Gibco®), B-27 supplement (Gibco®), GlutaMax and NEAA) with 10μM ROCK inhibitor (Sigma, Y-27632) and 10ng/mL of neurotrophic factors GDNF, BDNF and CNTF (R&D). DAPI signal was used to resolve cell viability, and differentiated cells not exposed to MN patterning molecules (RA and SAG) were used as negative controls to gate for green fluorescence. For RNA-Seq experiments, 200,000 GFP$^+$ cells per well were plated in 24-well tissue culture dishes pre-coated with matrigel. MN medium, conditioned for 2-3 days by mouse glial cells and supplemented with 10ng/mL of each GDNF, BDNF and CNTF(R&D), was used to feed and mature

the purified MNs. RNA-Seq experiments and most downstream assays were carried with d10 purified MNs (10 days in culture after FACS).

3.4.3 RNAi

RNAi in cultures of purified GFP^+ MNs was induced with Silencer® Select siRNAs (Life Technologies™) targeting the *TDP-43* mRNA or with a non-targeting siRNA control with scrambled sequence that is not predicted to bind to any human transcripts. Lyophilized siRNAs were resuspended in nuclease-free water and stored at -20C as 20μM stocks until ready to use. For transfection, siRNAs were diluted in Optimem (Gibco®) and mixed with RNAiMAX (Invitrogen) according to manufacturer's instructions. After 30 min incubation, the mix was added drop-wise to the MN cultures, so that the final siRNA concentration in each well was 60nM in 1:1 Optimem:MN medium (Neurobasal (Life Technologies™, N2 supplement (Gibco®), B-27 supplement (Gibco®), GlutaMax and NEAA) and 10ng/mL of each GDNF, BDNF and CNTF (R&D). 12-16 hours post-transfection media was changed. RNA-Seq experiments and validation assays were carried with material collected 4 days after transfection.

3.4.4 Immunocytochemistry

Immunofluorescence was carried out as previously described[30, 98]. Briefly, 8-well chamber culture slides (BD biosciences) were fixed with ice-cold 4% PFA for 15 minutes at 4°C, permeabilized with 0.2% Triton-X in 1x PBS for 45 minutes and blocked with 10% donkey serum in 1x PBS-T (0.1% Tween-20) for 1 hour. Cells were then incubated overnight at 4°C with primary antibody (diluted in blocking solution). At least 4 washes (5 min incubation each) with 1xPBS-T were carried out, before incubating the cells with secondary antibodies for 1 hour at room temperature (diluted in blocking solution). Nuclei were stained with DAPI. The following antibodies were used in this study: Hb9 (1:100, DSHB, MNR2 81.5C10-c), TUJ1

(1:1000, Sigma, T2200), MAP2 (1:10000, Abcam ab5392), Ki67 (1:400, Abcam, ab833), GFP (1:500, Life Technologies™, A10262), Islet1 (1:1000, Abcam ab20670), TDP-43 (1:1000, ProteinTech Group), STMN2 (1:4000, Novus). Secondary antibodies used (488, 555, 594, and 647) were Alexa Alexa®Fluor (1:1000, Life Technologies™) and DyLight (1:500, Jackson ImmunoResearch Laboratories).

3.4.5 Immunoblot Assays

For analysis of TDP-43 and STMN2 protein expression levels, d10 MNs were lysed in RIPA buffer (150mM Sodium Chloride; 1% Triton X-100; 0.5% sodium deoxycholate; 0.1% SDS; 50 mM Tris pH 8.0) containing protease and phosphatase inhibitors (Roche) for 20 min on ice, and centrifuged at high speed. 200µL of RIPA buffer per well of 24-well culture were routinely used, which yielded ~20µg of total protein as determined by BCA (Thermo Scientific). For immunoblot assays 2-3µg of total protein were separated by SDS-PAGE (BioRad), transferred to PDVF membranes (BioRad) and probed with antibodies against TDP-43 (1:1000, ProteinTech Group), GAPDH (1:1000, Millipore) and STMN2 (1:3000, Novus). The same PDVF membrane was immunoassayed 2-3 times using Restore™ PLUS Western Blot Stripping Buffer (Thermo Scientific). GAPDH levels were used to normalized each sample, and Image J software was used to quantify protein band signal.

3.4.6 RNA preparation, qRT-PCR and RNA sequencing

Total RNA was isolated from d10 MNs for RNA-Seq experiments and validation assays using Trizol LS (Invitrogen) according to manufacturer's instructions. 500µL were added per well of the 24-well cultures. A total of 300-1000ng of total RNA was used to synthesize cDNA by reverse transcription according to the iSCRIPT kit (Bio-rad). Quantitative RT-PCR (qRT-

PCR) was then performed using SYBR green (Bio-Rad) and the iCycler system (Bio-rad). Quantitative levels for all genes assayed were normalized using *GAPDH* expression. Normalized expression was displayed relative to the relevant control sample (mostly siRED-treated MNs or cells with 1x TDP-43 levels). All primer sequences are available upon request. For next-generation RNA sequencing (RNA-Seq), at least two technical replicas per siRNA sample or AAVS1-TDP43 genotype were included in the analyses. After RNA extraction, samples with RNA integrity numbers (RIN) above 7.5, determined by a bioAnalyzer, were used for library preparation. In brief, RNA sequencing libraries were generated from ~250ng of total RNA using the illumina TruSeq RNA kit v2, according to the manufacturer's directions. Libraries were sequenced at the Harvard Bauer Core Sequencing facility on a HiSeq 2000 platform. All FASTQ files were analyzed using FastQC software (v0.10.1) to confirm that Phred scores were acceptable at all read positions. The FASTQ files were aligned to the GRCh37/hg19 reference genome using Tophat (v 2.0.7)[40]. Differential expression testing was performed using 'Cufflinks' (v 2.1.1)[40]. The Cuffdiff module of Cufflinks identifies differential expression by first generating, for each transcript, a probabilistic model for read generation that incorporates both uncertainty in mapping of reads to the genome and variability in read counts across biological replicates. After estimating the parameters of this model directly from the data, it then generates a null distribution of thousands of log-fold change values across experimental conditions for each gene (under the assumption of no differential expression) using reads randomly generated from the probabilistic model. The actual log-fold change observed in the experiment is then compared to this null distribution to generate a p-value. All p-values are then corrected for multiple comparisons using the method of Benjamini and Hochberg. The Cufflinks output was visualized with the cummeRbund R package using a false discovery rate

of 0.05. Gene Ontology term enrichment was determined for significantly differentially expressed genes at a false discovery rate cutoff of 0.05 using the Database for Annotation, Visualization and Integrated Discovery (DAVID) v6.7 and Gene Set Enrichment Analysis (GSEA, Broad Institute) with the REACTOME and KEGG Pathway MSigDB collections.

3.4.7 Outgrowth assays

HUES3 *Hb9::*GFP$^+$ differentiated MNs were purified by FACS as described above, but cells were collected in tubes containing MN medium [Neurobasal (Life Technologies™, N2® supplement (Gibco®), B-27® supplement (Gibco®), GlutaMax (Gibco®) and NEAA] without any additional supplements. 100,000 GFP$^+$ were transfected in suspension with 60nM of Silencer® Select siRNAs (Life Technologies™) in 1:1 Optimem:MN medium (without additional supplements) for 2 hours. Cells were then aggregated in the 1:1 Optimem:MN medium containing the siRNAs by centrifugation in 96-well low-adhesion culture plates (Lipidure®-Coat) at low speed (84x g) for 3 min. Cell aggregates were incubated in the 1:1 Optimem:MN medium for 12-16 hours, after which they were transferred to 12-well tissue culture dishes pre-coated with Poly-D-Lysine/Laminin. Each aggregate was placed in one well using a cut 200µL Pipetman® pipette tip. Cell aggregates ('outgrowths') were cultured for 5 additional days and imaged using epifluorescence after a 15-minute incubation step with the live-cell dye Calcein-AM (Life Technologies™). All images were taken using the same exposure and were analyzed with the ImageJ software package using the 'concentric circle' and 'mean intensity' functions.

3.4.8 Electrophysiology recordings

GFP$^+$ MNs were plated at a density of 5,000 cells/cm^2 on poly-D-lysine/laminin-coated coverslips and cultured for 10 days in MN medium, conditioned for 2-3 days by mouse glial

cells and supplemented with 10ng/mL of each GDNF, BDNF and CNTF(R&D). Electrophysiology recordings were carried out as previously reported[30, 35]. Briefly, whole-cell voltage-clamp or current-clamp recordings were made using a Multiclamp 700B(Molecular Devices) at room temperature (21-23C). Data were digitized with a Digidata 1440A A/D interface and recorded using pCLAMP 10_software (Molecular Devices). Data were sampled at 20 kHz and low-pass filtered at 2 kHz. Patch pipettes were pulled from borosilicate glass capillaries on a Sutter Instruments P-97 puller and had resistances of 2-4 MW. The pipette capacitance was reduced by wrapping the shank with Parafilm and compensated for using the amplifier circuitry. Series resistance was typically 5-10 MW, always less than 15 MW, and compensated by at least 80%. Linear leakage currents were digitally subtracted using a P/4 protocol. Voltages were elicited from a holding potential of -80 mV to test potentials ranging from -80 mV to 30 mV in 10 mV increments. The intracellular solution was a potassium-based solution and contained K gluconate, 135; MgCl2, 2; KCl, 6; HEPES, 10; Mg ATP, 5; 0.5 (pH 7.4 with KOH). The extracellular was sodium-based and contained NaCl, 135; KCl, 5; CaCl2, 2; MgCl2, 1; glucose, 10; HEPES, 10, pH 7.4 with NaOH). Kainate and GABA were purchased from Sigma.

3.4.9 TDP-43 and STMN2 immunohistochemical analyses

Post-mortem samples from 3 sporadic ALS cases and 3 controls (no evidence of spinal cord disease) were gathered from the Massachusetts Alzheimer's Disease Research Center (ADRC) in accordance with Partners and Harvard IRB protocols. Histologic analysis of TDP-43 immunoreactivity (rabbit polyclonal, ProteinTech Group) was performed to confirm the diagnosis. For STMN2 analyses, sections of formalin fixed lumbar spinal cord were stained using standard immunohistochemical procedure with the exception that citrate buffer antigen retrieval was performed before blocking. Briefly, samples were rehydrated, rinsed with water,

blocked in 3% hydrogen peroxide then normal serum, incubated with primary STMN2 rabbit-derived antibody (1:100 dilution, Novus), followed by incubation with the appropriate secondary antibody (anti-rabbit IgG conjugated to horseradish peroxidase 1:200), and exposure to ABC Vectastain kit and DAB peroxidase substrate, and briefly counterstained with hematoxylin before mounting. Multiple levels were examined for each sample.

3.4.10 Statistical analysis

Statistical significance for qRT-PCR assays and STMN2 immunohistochemical analyses was assessed using a 2 tail unpaired Student's *t*-test, with a p value of *$p<0.05$ considered as significant. For analysis of outgrowth assays, a two-way ANOVA was used with *post hoc* analysis via pair-wise Student's *t*-test with Bonferroni correction (GraphPad Prism® Software). Type II Error was controlled at the customary level of 0.05. All error bars represent ±s.e.m, unless otherwise stated.

3.5 References

1. Chen-Plotkin, A.S., Lee, V.M. & Trojanowski, J.Q. TAR DNA-binding protein 43 in neurodegenerative disease. *Nat Rev Neurol* **6**, 211-20 (2010).

2. Ou, S.H., Wu, F., Harrich, D., Garcia-Martinez, L.F. & Gaynor, R.B. Cloning and characterization of a novel cellular protein, TDP-43, that binds to human immunodeficiency virus type 1 TAR DNA sequence motifs. *J Virol* **69**, 3584-96 (1995).

3. Buratti, E. et al. Nuclear factor TDP-43 and SR proteins promote in vitro and in vivo CFTR exon 9 skipping. *EMBO J* **20**, 1774-84 (2001).

4. Polymenidou, M. et al. Long pre-mRNA depletion and RNA missplicing contribute to neuronal vulnerability from loss of TDP-43. *Nat Neurosci* **14**, 459-68 (2011).

5. Kawahara, Y. & Mieda-Sato, A. TDP-43 promotes microRNA biogenesis as a component of the Drosha and Dicer complexes. *Proc Natl Acad Sci U S A* **109**, 3347-52 (2012).

6. Parker, S.J. et al. Endogenous TDP-43 localized to stress granules can subsequently form protein aggregates. *Neurochem Int* **60**, 415-24 (2012).

7. Liu-Yesucevitz, L. et al. Tar DNA binding protein-43 (TDP-43) associates with stress granules: analysis of cultured cells and pathological brain tissue. *PLoS One* **5**, e13250 (2010).

8. Volkening, K., Leystra-Lantz, C., Yang, W., Jaffee, H. & Strong, M.J. Tar DNA binding protein of 43 kDa (TDP-43), 14-3-3 proteins and copper/zinc superoxide dismutase (SOD1) interact to modulate NFL mRNA stability. Implications for altered RNA processing in amyotrophic lateral sclerosis (ALS). *Brain Res* **1305**, 168-82 (2009).

9. Alami, N.H. et al. Axonal transport of TDP-43 mRNA granules is impaired by ALS-causing mutations. *Neuron* **81**, 536-43 (2014).

10. Rutherford, N.J. et al. Novel mutations in TARDBP (TDP-43) in patients with familial amyotrophic lateral sclerosis. *PLoS Genet* **4**, e1000193 (2008).

11. Sreedharan, J. et al. TDP-43 mutations in familial and sporadic amyotrophic lateral sclerosis. *Science* **319**, 1668-72 (2008).

12. Van Deerlin, V.M. et al. TARDBP mutations in amyotrophic lateral sclerosis with TDP-43 neuropathology: a genetic and histopathological analysis. *Lancet Neurol* **7**, 409-16 (2008).

13. Yokoseki, A. et al. TDP-43 mutation in familial amyotrophic lateral sclerosis. *Ann Neurol* **63**, 538-42 (2008).

14. Ravits, J. et al. Deciphering amyotrophic lateral sclerosis: what phenotype, neuropathology and genetics are telling us about pathogenesis. *Amyotroph Lateral Scler Frontotemporal Degener* **14 Suppl 1**, 5-18 (2013).

15. Lee, E.B., Lee, V.M. & Trojanowski, J.Q. Gains or losses: molecular mechanisms of TDP43-mediated neurodegeneration. *Nat Rev Neurosci* **13**, 38-50 (2012).

16. Mackenzie, I.R. et al. Pathological TDP-43 distinguishes sporadic amyotrophic lateral sclerosis from amyotrophic lateral sclerosis with SOD1 mutations. *Ann Neurol* **61**, 427-34 (2007).

17. Neumann, M. et al. Ubiquitinated TDP-43 in frontotemporal lobar degeneration and amyotrophic lateral sclerosis. *Science* **314**, 130-3 (2006).

18. Wu, L.S., Cheng, W.C. & Shen, C.K. Targeted depletion of TDP-43 expression in the spinal cord motor neurons leads to the development of amyotrophic lateral sclerosis-like phenotypes in mice. *J Biol Chem* **287**, 27335-44 (2012).

19. Iguchi, Y. et al. Loss of TDP-43 causes age-dependent progressive motor neuron degeneration. *Brain* **136**, 1371-82 (2013).

20. Yang, C. et al. Partial loss of TDP-43 function causes phenotypes of amyotrophic lateral sclerosis. *Proc Natl Acad Sci U S A* **111**, E1121-9 (2014).

21. Sephton, C.F. et al. TDP-43 is a developmentally regulated protein essential for early embryonic development. *J Biol Chem* **285**, 6826-34 (2010).

22. Kraemer, B.C. et al. Loss of murine TDP-43 disrupts motor function and plays an essential role in embryogenesis. *Acta Neuropathol* **119**, 409-19 (2010).

23. Ayala, Y.M. et al. TDP-43 regulates its mRNA levels through a negative feedback loop. *EMBO J* **30**, 277-88 (2010).

24. Avendano-Vazquez, S.E. et al. Autoregulation of TDP-43 mRNA levels involves interplay between transcription, splicing, and alternative polyA site selection. *Genes Dev* **26**, 1679-84 (2012).

25. Igaz, L.M. et al. Dysregulation of the ALS-associated gene TDP-43 leads to neuronal death and degeneration in mice. *J Clin Invest* **121**, 726-38 (2011).

26. Xu, Y.F. et al. Wild-type human TDP-43 expression causes TDP-43 phosphorylation, mitochondrial aggregation, motor deficits, and early mortality in transgenic mice. *J Neurosci* **30**, 10851-9 (2010).

27. Tsao, W. et al. Rodent models of TDP-43: recent advances. *Brain Res* **1462**, 26-39 (2012).

28. Davis-Dusenbery, B.N., Williams, L.A., Klim, J.R. & Eggan, K. How to make spinal motor neurons. *Development* **141**, 491-501 (2014).

29. Han, S.S., Williams, L.A. & Eggan, K.C. Constructing and deconstructing stem cell models of neurological disease. *Neuron* **70**, 626-44 (2011).

30. Kiskinis, E. et al. Pathways disrupted in human ALS motor neurons identified through genetic correction of mutant SOD1. *Cell Stem Cell* **14**, 781-95 (2014).

31. Wainger, B.J. et al. Intrinsic membrane hyperexcitability of amyotrophic lateral sclerosis patient-derived motor neurons. *Cell Rep* **7**, 1-11 (2014).

32. Di Giorgio, F., Boulting, G., Bobrowicz, S. & Eggan, K. Human embryonic stem cell-derived motor neurons are sensitive to the toxic effect of glial cells carrying an ALS-causing mutation. *Cell Stem Cell* **3**, 637-648 (2008).

33. Hester, M. et al. Rapid and efficient generation of functional motor neurons from human pluripotent stem cells using gene delivered transcription factor codes. *Molecular therapy : the journal of the American Society of Gene Therapy* **19**, 1905-1912 (2011).

34. Amoroso, M.W. et al. Accelerated High-Yield Generation of Limb-Innervating Motor Neurons from Human Stem Cells. *J Neurosci* **33**, 574-586 (2013).

35. Son, E.Y. et al. Conversion of mouse and human fibroblasts into functional spinal motor neurons. *Cell Stem Cell* **9**, 205-18 (2011).

36. Lamas, N.J. et al. Neurotrophic requirements of human motor neurons defined using amplified and purified stem cell-derived cultures. *PLoS One* **9**, e110324 (2014).

37. de Boer, A.S. et al. Genetic validation of a therapeutic target in a mouse model of ALS. *Sci Transl Med* **6**, 248ra104 (2014).

38. Chambers, S. et al. Highly efficient neural conversion of human ES and iPS cells by dual inhibition of SMAD signaling. *Nature biotechnology* **27**, 275-280 (2009).

39. Chambers, S. et al. Combined small-molecule inhibition accelerates developmental timing and converts human pluripotent stem cells into nociceptors. *Nature biotechnology* **30**, 715-720 (2012).

40. Trapnell, C. et al. Differential gene and transcript expression analysis of RNA-seq experiments with TopHat and Cufflinks. *Nature protocols* **7**, 562-578 (2012).

41. Trapnell, C. et al. Differential analysis of gene regulation at transcript resolution with RNA-seq. *Nat Biotechnol* **31**, 46-53 (2013).

42. Prudencio, M. et al. Misregulation of human sortilin splicing leads to the generation of a nonfunctional progranulin receptor. *Proc Natl Acad Sci U S A* **109**, 21510-5 (2012).

43. Fiesel, F.C., Weber, S.S., Supper, J., Zell, A. & Kahle, P.J. TDP-43 regulates global translational yield by splicing of exon junction complex component SKAR. *Nucleic Acids Res* **40**, 2668-82 (2011).

44. Arnold, E.S. et al. ALS-linked TDP-43 mutations produce aberrant RNA splicing and adult-onset motor neuron disease without aggregation or loss of nuclear TDP-43. *Proc Natl Acad Sci U S A* **110**, E736-45 (2013).

45. Bryant, D.W., Jr., Priest, H.D. & Mockler, T.C. Detection and quantification of alternative splicing variants using RNA-seq. *Methods Mol Biol* **883**, 97-110 (2012).

46. Bernard, E., Jacob, L., Mairal, J. & Vert, J.P. Efficient RNA isoform identification and quantification from RNA-Seq data with network flows. *Bioinformatics* **30**, 2447-55 (2014).

47. Shiga, A. et al. Alteration of POLDIP3 splicing associated with loss of function of TDP-43 in tissues affected with ALS. *PLoS One* **7**, e43120 (2012).

48. Hockemeyer, D. et al. Efficient targeting of expressed and silent genes in human ESCs and iPSCs using zinc-finger nucleases. *Nature biotechnology* **27**, 851-857 (2009).

49. Zaremba, J., Skrobanski, P. & Losy, J. The level of chemokine CXCL5 in the cerebrospinal fluid is increased during the first 24 hours of ischaemic stroke and correlates with the size of early brain damage. *Folia Morphol (Warsz)* **65**, 1-5 (2006).

50. Neun, R., Richter, M.F., Staeheli, P. & Schwemmle, M. GTPase properties of the interferon-induced human guanylate-binding protein 2. *FEBS Lett* **390**, 69-72 (1996).

51. Thomson, C.A., McColl, A., Cavanagh, J. & Graham, G.J. Peripheral inflammation is associated with remote global gene expression changes in the brain. *J Neuroinflammation* **11**, 73 (2014).

52. Lehnardt, S. Innate immunity and neuroinflammation in the CNS: the role of microglia in Toll-like receptor-mediated neuronal injury. *Glia* **58**, 253-63 (2009).

53. Wang, H., Ferguson, G.D., Pineda, V.V., Cundiff, P.E. & Storm, D.R. Overexpression of type-1 adenylyl cyclase in mouse forebrain enhances recognition memory and LTP. *Nat Neurosci* **7**, 635-42 (2004).

54. Grenningloh, G., Soehrman, S., Bondallaz, P., Ruchti, E. & Cadas, H. Role of the microtubule destabilizing proteins SCG10 and stathmin in neuronal growth. *J Neurobiol* **58**, 60-9 (2004).

55. Shin, J.E., Geisler, S. & DiAntonio, A. Dynamic regulation of SCG10 in regenerating axons after injury. *Exp Neurol* **252**, 1-11 (2013).

56. Kasashima, K., Sakashita, E., Saito, K. & Sakamoto, H. Complex formation of the neuron-specific ELAV-like Hu RNA-binding proteins. *Nucleic Acids Res* **30**, 4519-26 (2002).

57. Ariyannur, P.S. et al. Methamphetamine-induced neuronal protein NAT8L is the NAA biosynthetic enzyme: implications for specialized acetyl coenzyme A metabolism in the CNS. *Brain Res* **1335**, 1-13 (2010).

58. Martin, K.R. et al. Over-expression of RCAN1 causes Down syndrome-like hippocampal deficits that alter learning and memory. *Hum Mol Genet* **21**, 3025-41 (2012).

59. Chou, H.J. et al. BMP4 is a peripherally-derived factor for motor neurons and attenuates glutamate-induced excitotoxicity in vitro. *PLoS One* **8**, e58441 (2013).

60. DuVal, M.G. et al. Growth differentiation factor 6 as a putative risk factor in neuromuscular degeneration. *PLoS One* **9**, e89183 (2014).

61. Wu, C.H. et al. Mutations in the profilin 1 gene cause familial amyotrophic lateral sclerosis. *Nature* **488**, 499-503 (2012).

62. Smith, B.N. et al. Exome-wide rare variant analysis identifies TUBA4A mutations associated with familial ALS. *Neuron* **84**, 324-31 (2014).

63. Shin, J.E. et al. SCG10 is a JNK target in the axonal degeneration pathway. *Proc Natl Acad Sci U S A* **109**, E3696-705 (2012).

64. Ling, S.C., Polymenidou, M. & Cleveland, D.W. Converging Mechanisms in ALS and FTD: Disrupted RNA and Protein Homeostasis. *Neuron* **79**, 416-38 (2013).

65. Guerreiro, R., Bras, J. & Hardy, J. SnapShot: Genetics of ALS and FTD. *Cell* **160**, 798-798 e1 (2015).

66. Lagier-Tourenne, C. et al. Divergent roles of ALS-linked proteins FUS/TLS and TDP-43 intersect in processing long pre-mRNAs. *Nature neuroscience* **15**, 1488-1497 (2012).

67. Lattante, S., Rouleau, G.A. & Kabashi, E. TARDBP and FUS mutations associated with amyotrophic lateral sclerosis: summary and update. *Hum Mutat* **34**, 812-26 (2013).

68. Renton, A.E. et al. A hexanucleotide repeat expansion in C9ORF72 is the cause of chromosome 9p21-linked ALS-FTD. *Neuron* **72**, 257-68 (2011).

69. DeJesus-Hernandez, M. et al. Expanded GGGGCC hexanucleotide repeat in noncoding region of C9ORF72 causes chromosome 9p-linked FTD and ALS. *Neuron* **72**, 245-56 (2011).

70. Renton, A.E., Chio, A. & Traynor, B.J. State of play in amyotrophic lateral sclerosis genetics. *Nat Neurosci* **17**, 17-23 (2014).

71. Mason, M.R., Lieberman, A.R., Grenningloh, G. & Anderson, P.N. Transcriptional upregulation of SCG10 and CAP-23 is correlated with regeneration of the axons of peripheral and central neurons in vivo. *Mol Cell Neurosci* **20**, 595-615 (2002).

72. Sobczak, A. et al. Calmyrin1 binds to SCG10 protein (stathmin2) to modulate neurite outgrowth. *Biochim Biophys Acta* **1813**, 1025-37 (2011).

73. Morii, H., Shiraishi-Yamaguchi, Y. & Mori, N. SCG10, a microtubule destabilizing factor, stimulates the neurite outgrowth by modulating microtubule dynamics in rat hippocampal primary cultured neurons. *J Neurobiol* **66**, 1101-14 (2006).

74. Mori, N. & Morii, H. SCG10-related neuronal growth-associated proteins in neural development, plasticity, degeneration, and aging. *J Neurosci Res* **70**, 264-73 (2002).

75. Stein, R., Mori, N., Matthews, K., Lo, L.C. & Anderson, D.J. The NGF-inducible SCG10 mRNA encodes a novel membrane-bound protein present in growth cones and abundant in developing neurons. *Neuron* **1**, 463-76 (1988).

76. Sobel, A. et al. Intracellular substrates for extracellular signaling. Characterization of a ubiquitous, neuron-enriched phosphoprotein (stathmin). *J Biol Chem* **264**, 3765-72 (1989).

77. Doye, V. et al. A single cDNA encodes two isoforms of stathmin, a developmentally regulated neuron-enriched phosphoprotein. *J Biol Chem* **264**, 12134-7 (1989).

78. Bieche, I. et al. Expression of stathmin family genes in human tissues: non-neural-restricted expression for SCLIP. *Genomics* **81**, 400-10 (2003).

79. Levy, A.D. et al. Subcellular Golgi localization of stathmin family proteins is promoted by a specific set of DHHC palmitoyl transferases. *Mol Biol Cell* **22**, 1930-42 (2011).

80. Sugiura, Y. & Mori, N. SCG10 expresses growth-associated manner in developing rat brain, but shows a different pattern to p19/stathmin or GAP-43. *Brain Res Dev Brain Res* **90**, 73-91 (1995).

81. Kabashi, E. et al. TARDBP mutations in individuals with sporadic and familial amyotrophic lateral sclerosis. *Nat Genet* **40**, 572-4 (2008).

82. Ma, X.M., Yoon, S.O., Richardson, C.J., Julich, K. & Blenis, J. SKAR links pre-mRNA splicing to mTOR/S6K1-mediated enhanced translation efficiency of spliced mRNAs. *Cell* **133**, 303-13 (2008).

83. Phanstiel, D.H. et al. Proteomic and phosphoproteomic comparison of human ES and iPS cells. *Nat Methods* **8**, 821-7 (2011).

84. Ueki, Y. & Reh, T.A. Activation of BMP-Smad1/5/8 signaling promotes survival of retinal ganglion cells after damage in vivo. *PLoS One* **7**, e38690 (2012).

85. Frank, C.L. & Tsai, L.H. Alternative functions of core cell cycle regulators in neuronal migration, neuronal maturation, and synaptic plasticity. *Neuron* **62**, 312-26 (2009).

86. Herrup, K. & Yang, Y. Cell cycle regulation in the postmitotic neuron: oxymoron or new biology? *Nat Rev Neurosci* **8**, 368-78 (2007).

87. Ranganathan, S., Scudiere, S. & Bowser, R. Hyperphosphorylation of the retinoblastoma gene product and altered subcellular distribution of E2F-1 during Alzheimer's disease and amyotrophic lateral sclerosis. *J Alzheimers Dis* **3**, 377-385 (2001).

88. Ranganathan, S. & Bowser, R. Alterations in G(1) to S phase cell-cycle regulators during amyotrophic lateral sclerosis. *Am J Pathol* **162**, 823-35 (2003).

89. Nguyen, M.D. et al. Cell cycle regulators in the neuronal death pathway of amyotrophic lateral sclerosis caused by mutant superoxide dismutase 1. *J Neurosci* **23**, 2131-40 (2003).

90. Mackenzie, I.R., Rademakers, R. & Neumann, M. TDP-43 and FUS in amyotrophic lateral sclerosis and frontotemporal dementia. *Lancet Neurol* **9**, 995-1007 (2010).

91. Cirulli, E.T. et al. Exome sequencing in amyotrophic lateral sclerosis identifies risk genes and pathways. *Science* (2015).

92. Sephton, C.F. et al. Identification of Neuronal RNA Targets of TDP-43-containing Ribonucleoprotein Complexes. *J Biol Chem* **286**, 1204-15 (2011).

93. Xiao, S. et al. RNA targets of TDP-43 identified by UV-CLIP are deregulated in ALS. *Mol Cell Neurosci* **47**, 167-80 (2011).

94. Tollervey, J.R. et al. Characterizing the RNA targets and position-dependent splicing regulation by TDP-43. *Nat Neurosci* **14**, 452-8 (2011).

95. Li, J.H., Liu, S., Zhou, H., Qu, L.H. & Yang, J.H. starBase v2.0: decoding miRNA-ceRNA, miRNA-ncRNA and protein-RNA interaction networks from large-scale CLIP-Seq data. *Nucleic Acids Res* **42**, D92-7 (2014).

96. Lagier-Tourenne, C., Polymenidou, M. & Cleveland, D.W. TDP-43 and FUS/TLS: emerging roles in RNA processing and neurodegeneration. *Hum Mol Genet* **19**, R46-64 (2010).

97. Graf, E.R., Heerssen, H.M., Wright, C.M., Davis, G.W. & DiAntonio, A. Stathmin is required for stability of the Drosophila neuromuscular junction. *J Neurosci* **31**, 15026-34 (2011).

98. Boulting, G.L. et al. A functionally characterized test set of human induced pluripotent stem cells. *Nature biotechnology* **29**, 279-286 (2011).

CHAPTER 4:

Generation and characterization of iPS cell lines

from familial ALS patients with variants in TDP-43

Portions of this chapter have been published as:

• Alami NH*, Smith RB*, Carrasco MA, **Williams LA**, Winborn CS, Han SS, Kiskinis E, Winborn B, Freibaum BD, Kanagaraj A, Clare AJ, Badders NM, Bilican B, Chaum E, Chandran S, Shaw CE, Eggan KC, Maniatis T, Taylor JP. Axonal transport of TDP-43 mRNA granules is impaired by ALS-causing mutations. *Neuron* **81**, 536-43 (2014).

Author contributions to the work presented in this Chapter: L.A.W. derived TDP-43 iPS cell lines and carried out all MN differentiation experiments; S.S.H. assisted with analysis of TDP-43 pathology in human differentiated neurons. N.H.A. performed live-cell imaging experiments of iPS cell-derived MNs with assistance from L.A.W.; Robert H. Brown collected and provided Patient RB20 material; N.H.A., M.A.C. and T.M. carried out independent axonal transport assays with a distinct set of TDP-43 iPS cell-derived MNs; N.H.A. and J.P.T. designed the axonal transport studies and wrote the manuscript published in *Neuron* describing some of the work presented in this Chapter; L.A.W. wrote the sections of the manuscript describing the experiments with the human differentiated MNs; L.A.W. wrote the sections of the work described here that are not part of the *Neuron* manuscripts; K.E. supervised all aspects of the study presented in this Chapter.

4.1 Introduction

Transactive response DNA-binding protein 43 (TDP-43) is a highly conserved, ubiquitously expressed heterogeneous ribonucleoprotein (hnRNP) that is primarily nuclear but shuttles between the cytoplasm and nucleus. TDP-43 was initially identified as a transcription repressor[1] and splicing regulator[2] and later recognized as the major component of pathological protein inclusions characteristic of frontotemporal dementia (FTD) and amyotrophic lateral sclerosis (ALS)[3, 4]. In affected CNS tissues from most ALS and a subset of FTD cases, the normal nuclear TDP-43 staining pattern is absent, and cytoplasmic aggregates immunoreactive to TDP-43 are commonly detected[3-6]. Dominant missense mutations in *TARDBP*, the gene encoding TDP-43, are sufficient to cause familial forms of ALS, underscoring the important role of this protein in pathogenesis[7-13].

The identification of mutations in related RNA processing proteins has focused interest on perturbed RNA metabolism as a potential common defect underlying neurodegenerative diseases[14-16], yet our understanding of the role(s) of TDP-43 in RNA metabolism is far from complete. How disease-causing mutations disrupt TDP-43 function(s), the relative contribution of toxic gain versus loss of function to disease, and the cellular compartment(s) in which this perturbation occurs, remain to be determined.

TDP-43 binds to thousands of mRNAs, many of which are important in brain development and synaptic function[17-19]. Isolation of TDP-43 from a cytoplasmic fraction of human brain revealed binding to the 3'-UTR of numerous target mRNAs, suggesting a role in mRNA stability and/or transport[19]. TDP-43 co-purifies with proteins involved in RNA transport[20], it is trafficked in neurons[21, 22], and can be detected in distal compartments such as the presynaptic membrane of axon terminals in the neuromuscular junction in mice[23]. As such, it has been

suggested that TDP-43 plays a role in the transport of certain target mRNAs into distal neuronal processes, but direct evidence is lacking[6, 24]. The extent to which this hypothetical function might be compromised by disease mutations has not been explored.

TDP-43 participates in an autoregulatory loop, whereby it downregulates its own protein synthesis by promoting the nuclear retention and degradation of the *TDP-43* transcript[17, 25, 26]. Thus, the toxicity associated with higher TDP-43 expression in multiple cellular and animal systems could reflect the importance of maintaining proper levels of this protein for cellular homeostasis[6, 27]. However, this response to TDP-43 overexpression, particularly in the CNS of transgenic animals[17, 28, 29], has made it challenging to discern the contribution of TDP-43 variants to the phenotypes observed[30]. Thus, novel disease models that can address this issue using more physiological settings are needed. Our group and others have recently demonstrated that induced pluripotent stem (iPS) cell technology in combination with directed differentiation methods, can be used to develop informative human cellular models of ALS by allowing the *in vitro* generation of human MNs expressing endogenous levels of ALS-associated proteins[31-37].

In this chapter, we describe the generation of iPS cells derived from familial ALS patients with known mutations in TDP-43. In addition, we show that, at least under basal culture conditions, human differentiated MNs expressing TDP-43 variants do not commonly exhibit the TDP-43 pathology characteristic of most ALS cases. Finally, by studying the axonal transport of the *NELF-L* mRNA in these cells, we validate findings from other *in vitro and in vivo* experimental systems, in which TDP-43 mutations were found to impair the transport of TDP43-bound cytoplasmic RNA granules.

4.2 Results

4.2.1 Generation of iPS cell lines from ALS patients with mutations in TDP-43

After informed consent, we obtained skin biopsies from three familial ALS patients with known mutations in the *TARDBP* gene, resulting in the TDP-43 variants: TDP43Q343R (Patient 36), TDP43G298S (Patient 47) and TDP43A315T (Patient RB20) (FIGURE 4.1A). We derived dermal fibroblasts from these patient samples, which were then transduced with retroviral constructs expressing the pluripotency genes *OCT4, SOX2,* and *KLF4* (FIGURE 4.1B). Initial iPS cell colonies with ES-cell-like morphology were picked and expanded to establish 3-5 iPS cell lines per genotype, and a subset of these cell lines (36a, 47a, 47d, and RB20a) was used in downstream experiments. The pluripotent state of the newly derived iPS cell lines was assessed using immunocytochemistry to determine the expression of pluripotency-associated transcription factors and cell membrane surface antigens (FIGURE 4.1C-D). We obtained gDNA from these cells and following sequencing of *EXON6* of the *TARDBP* gene we corroborated the presence of the different ALS-linked TDP-43 mutations (FIGURE 4.1E-F). iPS cell lines 47d and RB20a were confirmed to carry a normal karyotype (FIGURE 4.1G), and their pluripotency was further validated using a well-established qRT-PCR-based 'scorecard assay'[38](data not shown).

4.2.2 Differentiation of TDP-43 iPS cells into MNs

We then asked if we could use TDP-43 iPS cell lines to generate differentiated cells with spinal motor neuron (MN) properties for ALS-related phenotypic assays. To this end, we directed the differentiation of these iPS cells into MNs using either embryoid body (EB)-based[33, 39, 40] or 2D-monolayer[41, 42] strategies, both relying on neural induction by inhibition of

A

Patient	Sex	Diagnosis	Genotype	Age of onset	Age at Biopsy	Reference
47	Male	FALS	*TARDBP*$^{+/G298S}$	43	43	This study
RB20	Male	FALS	*TARDBP*$^{+/A315T}$	67	69	This study
36	Male	FALS	*TARDBP*$^{+/Q343R}$	51	53	This study
18	Female	Healthy	*TARDBP*$^{+/+}$	N.A.	48	[39]
11	Male	Healthy	*TARDBP*$^{+/+}$	N.A.	37	[39]

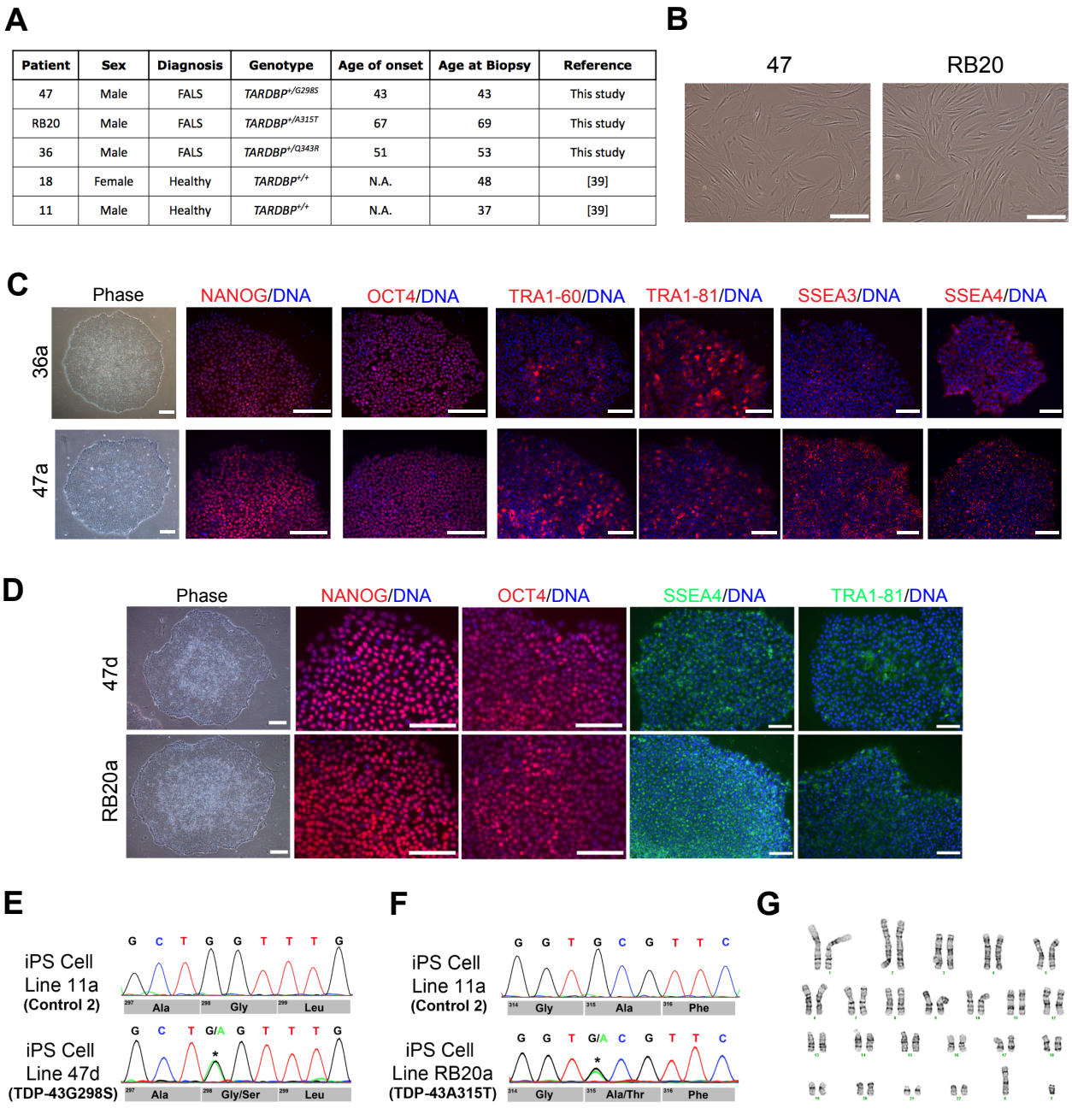

Figure 4.1 Generation of iPS cell lines from familial ALS patients with mutations in TDP-43
A. Summary of information for familial ALS (FALS) patients and healthy controls used in this study. **B.** Patient fibroblasts were transduced with reprogramming genes *OCT4, SOX2* and *KLF4* to generate TDP-43 iPS cells. Phase image of cultured fibroblasts derived from Patient 47 and Patient RB20 are shown. **C-D.** TDP-43 iPS cell lines express transcription factors and cell surface antigens characteristic of the pluripotent state (Scale bar = 100µm). **E-F.** *Exon6* of the *TARDBP* gene was sequenced using genomic DNA from TDP-43 and control iPS cell lines to confirm the presence of mutations encoding the ALS-linked TDP-43 variants. Relevant sections of the sequencing chromatograms for iPS cell lines 47d (TDP-43G298S) and RB20a (TDP-43A315T) are shown. **G.** TDP43 iPS cell lines exhibited a normal karyotype after prolonged culture, as determined by G-banding. Karyotype for TDP-43 iPS cell line 47d after 17 passages is shown.

dual SMAD signaling, and MN patterning by activation of retinoid and SONIC HEDGEHOG signaling pathways (see Methods section for details). Using either of these approaches, we produced differentiated cells that expressed the MN transcription factor ISLET1, the panneuronal cytoskeletal protein β-III TUBULIN, and the marker of neuronal differentiation and maturation MICROTUBULE-ASSOCIATED PROTEIN 2 (FIGURE 4.2A-B). We also confirmed that TDP43-iPS cell-differentiated neurons expressed the TDP-43 protein (FIGURE 4.2C). Additionally, using whole-cell patch clamp recordings, we demonstrated electrical activity in these cells consistent with the expression of functional voltage-gated sodium and potassium channels, and the capacity to fire multiple action potentials (FIGURE 4.2D).

4.3.3 TDP-43 pathology is not evident in TDP-43 iPS cell-derived neurons

Loss of nuclear TDP-43 immunoreactivity and cytoplasmic aggregation is a pathological hallmark of ALS and FTD cases, and can be detected in 95% of ALS cases[4-6]. Therefore, we interrogated if differentiated neurons expressing TDP-43 variants associated with ALS exhibit TDP-43 subcellular mislocalization and aggregation. To this end, three TDP-43 iPS cell lines (36a-TDP43Q343R, 47a-TDP43G298S and 47d-TDP43G298S), and two previously reported control iPS cell lines derived from healthy individuals (18a, 11a)[39], were differentiated toward a MN fate as embryoid bodies (EBs) for 24 days[33, 40]. EBs were then dissociated to single cells and plated onto a monolayer of murine glial cells for further culture and maturation. Cultures were fixed and stained for ISLET1/2, MAP2 and TDP-43 at day 30 after plating. Examination of TDP-43 staining pattern in differentiated neurons from mutant TDP-43 and control cultures indicated that TDP-43 remains predominantly localized to the nucleus (FIGURE 4.3A-B). We did not detect evidence of any $MAP2^+$ neurons or $MAP2^+ISLET^+$ MNs exhibiting TDP-43 nuclear clearance. However, we determined extremely rare occurrences of neurons (1-3%) with a

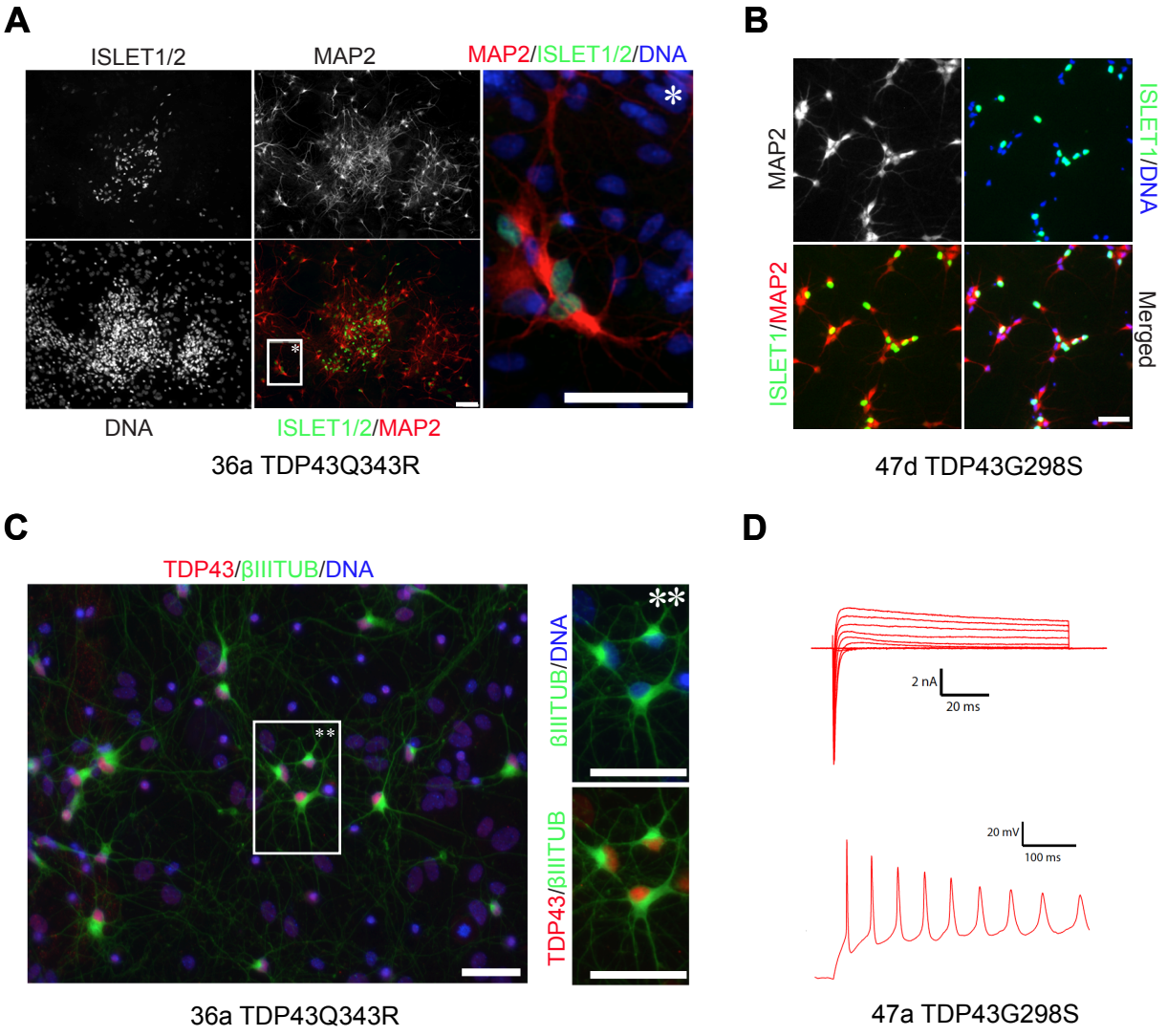

Figure 4.2 TDP-43 iPS cells can be differentiated into MNs

TDP-43 iPS cells were differentiated into MNs following dual inhibition of SMAD signaling for neural induction, and activation of retinoid and SHH signaling for MN patterning (see Methods section for details). **A-B.** Differentiated cells express the MN transcription factor ISLET and the panneuronal cytoskeletal protein MAP2. Differentiated MNs derived from the iPS cell lines 36a (TDP-43Q343R) and 47d (TDP-43G298S), and cultured for 7 days after dissociation are shown (Scale bar = 50μm). **C.** Differentiated neurons express TDP-43. Differentiated cells derived from iPS cell line 36a (TDP-43Q343R) are shown. Cells were cultured on a monolayer of murine glial cells for 2 weeks after dissociation (see Methods section for details). Neurons were stained with the TUJ1 antibody against the cytoskeletal protein β-III TUBULIN (Scale bar = 50μm). **D.** Differentiated neurons are electrophysiologically active after 2 weeks in culture. Whole-cell patch clamp recordings indicated expression of functional voltage-gated sodium and potassium channels (upper panel) and ability to fire multiple action potentials (bottom panel). Representative results are shown for neurons differentiated from iPS cell line 47a(TDP-43G298S).

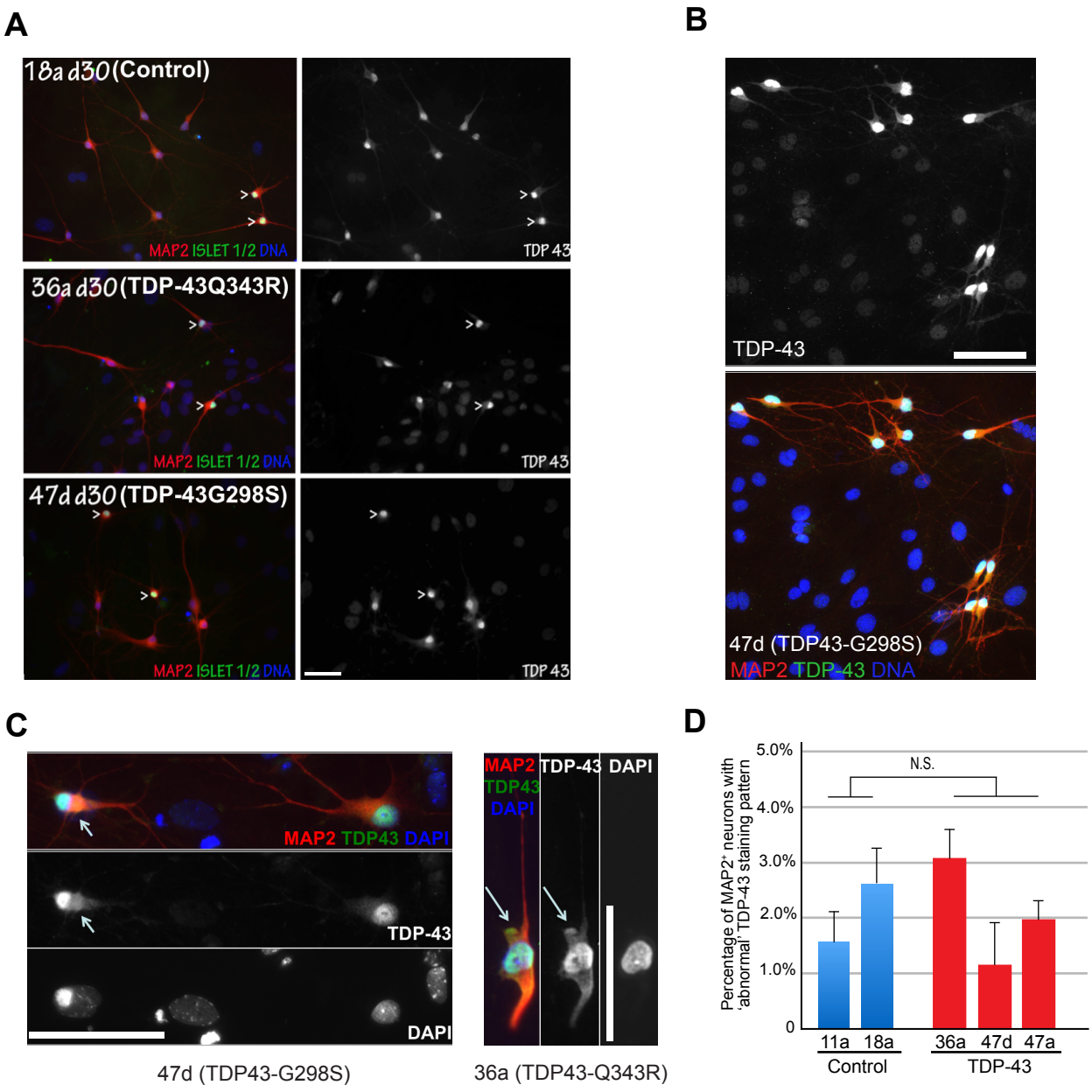

Figure 4.3 Neurons differentiated from TDP-43 iPS cells do not commonly exhibit 'TDP-43 pathology'
MNs were differentiated from two control (11a, 18a) and three TDP-43 (36a, 47a, 47d) iPS cell lines as EBs for 24 days (see Methods section for details). Differentiated EBs were dissociated to single cells and plated onto glial cells for additional culture and maturation. Cells were fixed and stained 30 days after plating (d30). **A.** MNs ($MAP2^+ISLET^+$ cells) differentiated from control and TDP-43 iPS cells exhibit 'normal' (predominantly nuclear) TDP-43 staining pattern. Representative results for one control (18a) and two TDP-43 (36a, 47d) genotypes are shown. $ISLET^+$ cells are indicated (Scale bar = 50µm). **B-C.** TDP-43 immunoreactivity in $MAP2^+$ neurons is predominantly nuclear (97-99% of cells), except in rare instances where there was indication of increased cytoplasmic accumulation (cell with arrow in (C), left panel) or aggregation (cell in (C), right panel) (Scale bar = 50µm). **D.** The percentage of $MAP2^+$ neurons with 'abnormal' TDP-43 staining pattern (cytoplasmic accumulation or aggregation) was not significantly different (n.s.) between control and mutant TDP-43 genotypes. Results shown are from two independent experiments.

TDP-43 staining pattern suggesting increased TDP-43 cytoplasmic accumulation or mislocalization (FIGURE 4.3C), but these events did not correlate with the genotype of the cells (FIGURE 4.3D). These results suggest that, at least under basal culture conditions, TDP-43 neuropathology detected in most ALS cases is not a common phenotype in differentiated neurons expressing ALS-associated TDP-43 variants.

4.3.4 Validation of axonal transport deficit phenotype with iPS cell-derived MNs

One of the powerful promises offered by iPS cell technology is the possibility to both validate previous findings and uncover new disease-relevant phenotypes using human differentiated cells that share properties with the vulnerable cell types, including the expression of endogenous levels of disease-associated proteins[31-37]. Initial studies in J. Paul Taylor's group using *Drosophila* larvae motor neurons and mouse cortical neurons, established the TDP-43 protein as a component of mRNP transport granules[43]. They also identified a new role for TDP-43 in the cytoplasm, supporting anterograde axonal transport of target mRNAs from the soma to distal axonal compartments, a process that was impaired in *Drosophila* and mouse neurons overexpressing ALS-associated variants TDP-43M337V and TDP-43A315T[43]. Since they generated these data by monitoring the trafficking of exogenous, fluorescently-tagged TDP-43, there remained the possibility that overexpression of TDP-43 influences its behavior in these assays. In order to address this issue with a human iPS-cell based approach, we first differentiated iPS cell lines 47d (TDP43G298S), RB20a (TDP43A315T) and 11a(control[39]) into MNs using adherent culture conditions for 14 days. Differentiated cultures were then dissociated to single cells, transfected with an *Hb9::GFP* MN reporter construct[44, 45], and plated onto tissue-culture surfaces precoated with Matrigel™ for further culture. In collaboration with Nael Alami (from J. Paul Taylor's group), we studied in GFP^+ MNs the axonal transport of the

NEFL (*NEUROFILAMENT-L*) mRNA, which is directly bound by the TDP-43 protein[17, 43]. We monitored *NEFL* movement in live cells with a Cy3-tagged oligonucleotide 'molecular beacon' that specifically hybridized to the *NEFL* mRNA (FIGURE 4.4A), and found that differentiated human MNs expressing ALS-associated TDP-43 variants showed defective trafficking of a TDP-43 cognate mRNA (FIGURE 4.4B-E). In particular, compared to control cells (11a-'control line 2'), TDP43G298S and TDP43A315T MNs exhibited significantly reduced anterograde displacement of *NEFL* mRNA granules, a disturbance that was exacerbated over time in culture (FIGURE 4.4B). In addition, the frequency of *NEFL* mRNA granule reversals per hour, and the percentage of these granules moving retrogradely, was significantly higher in neurons expressing mutant TDP-43 (FIGURE 4.4D-E). Notably, an independent research group, using a different set of control and TDP-43 iPS cell lines ('control line 1' and TDP43M337V) also confirmed the axonal transport deficit (FIGURE 4.5C-E)[43], suggesting that this phenotype is associated with different TDP-43 variants, and supporting the notion that these phenotypic differences are not the result of the inherit variability in iPS cell-based experiments[39, 46].

4.3 Discussion

In this study we used reprogramming technology to establish iPS cell lines from ALS patients bearing different genetic mutations in *TDP-43*. Using these cell lines, we demonstrate that hypotheses originating from findings in pathological tissues, and *in vitro* and *in vivo* experimental systems, can be further investigated in human cells bearing properties of relevance to ALS, including the MN phenotype and expression of endogenous levels of disease-associated variants.

Our observation that TDP-43 nuclear clearance, commonly seen in ALS/FTD affected tissues, does not occur in the differentiated neurons expressing TDP-43 variants is intriguing.

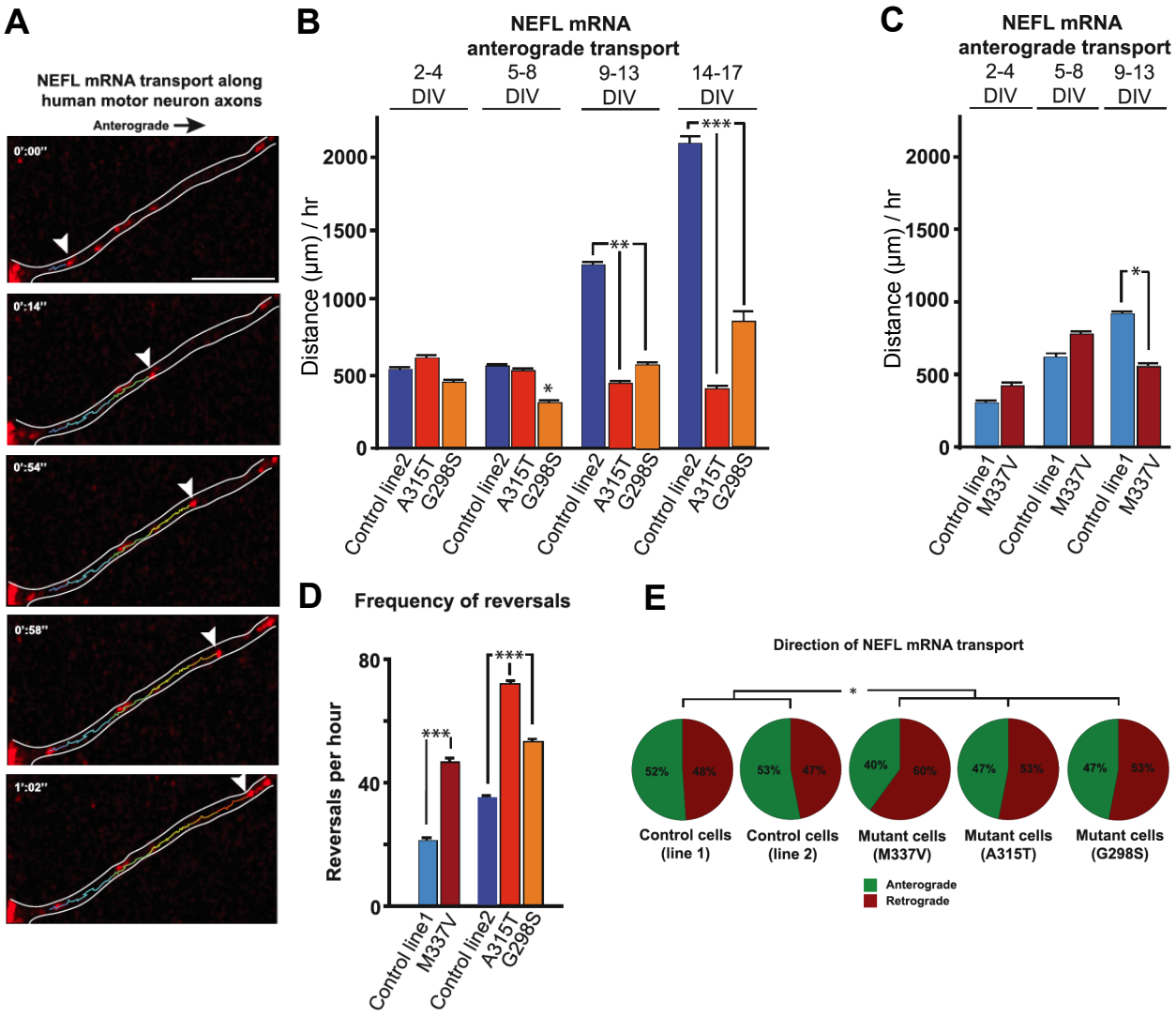

Figure 4.4 MNs expressing mutant TDP-43 exhibit deficits in the axonal transport of *NEFL* mRNA
A. Live imaging of human iPS cell-derived MNs with a 5'-Cy3 'molecular beacon' shows endogenous *NEFL* mRNA transport along axons. (Scale bar = 5 µm). **B** *NEFL* mRNA anterograde displacement was significantly altered in MNs from iPS cells of ALS patient with TDP43G298S mutation after 5 days in culture (DIV: days *in vitro*) as compared to control (11a-'control line 2'). After 9 days in culture, *NEFL* mRNA anterograde transport is significantly altered in MNs from both TDP-43 iPS cell lines (as compared to control). This defect becomes more pronounced over time. **C.** Validation of axonal transport deficit by an independent group using a distinct set of control and TDP-43 cell lines. There is no significant difference in net anterograde displacement of *NEFL* mRNA granules in control versus patient differentiated MNs with TDP-43M337V mutation during the first week of observation. The transport defect was apparent 9 days after plating (9-13 days *in vitro*) when a significant decrease in net anterograde transport of *NEFL* mRNA granules was also documented. **D.** Frequency of *NEFL* mRNA granule reversals per hour is significantly higher in neurons expressing mutant TDP-43 compared to controls (2 weeks after plating) ($p < 0.001$). **E** The percentage of retrogradely moving NEFL mRNA granules is significantly higher in iPS cell-derived MNs expressing mutant TDP-43 relative to controls (after 9 days in culture). All error bars are shown as mean ± SEM.

Most studies using animal models of TDP-43 have also reported the absence of this pathology[30, 47], suggesting that *complete* loss of nuclear TDP-43 may not be necessary to drive the ALS phenotype. Consistent with this hypothesis, a recent study demonstrated that only partial depletion of TDP-43 levels (20-60% reduction) in the CNS of mice was sufficient to cause neurodegeneration and paralysis[48]. Thus, as demonstrated by our axonal transport experiments, even if human differentiated MNs do not recapitulate this aspect of TDP-43 pathology *in vitro*, they can still execute certain molecular and cellular phenotypes associated with ALS-causing mutations.

It is important to note that iPS cell-based studies by other groups have reported phenotypes related to the subcellular localization and aggregation of TDP-43 in differentiated neural progenitors and MNs[49-51]. One study obtained neurons from a large cohort of sporadic ALS cases, and reported small TDP-43 immunoreactive nuclear aggregates in differentiated MNs for 3 out of 16 cases, which were present in up to 30% of the cells[50]. A second study described a two-fold increase in cytosolic TDP-43 immunofluorescent signal in iPS cell-derived neural progenitors expressing TDP43M337V compared to control cells[49]. Although these studies, similar to our findings, did not did not document complete loss of nuclear TDP-43 or its aggregation in large cytoplasmic inclusions, their results are not entirely consistent with what we commonly observed in the differentiated neurons bearing the TDP-43 mutations. This difference is perhaps due to differential susceptibility of cells to distinct TDP-43 variants, with the M337V mutation driving a more drastic phenotype. Another, not necessarily exclusive explanation is the presence of additional genetic modifiers that influence the behavior of TDP-43. One experimental approach that would address these conflicting results is to use gene-targeting tools to either introduce the TDP43M337V mutation in a control iPS cell line, or to

modify the patient iPS cell line bearing the M337V with either wild-type or one of the TDP-43 mutations we have characterized here. As discussed in Chapter 5, CRISPR/Cas9-based technology can facilitate the execution of these experiments.

Studies in J. Paul Taylor's group using Drosophila and mouse neurons first uncovered a role for TDP-43 in the axonal transport of target mRNA/TDP-43 RNP granules, a function that was compromised when these neurons overexpressed the ALS-linked variants TDP43M337V and TDP43A315T[43]. Using familial ALS patient iPS cells, we validated this axonal transport deficit in differentiated MNs expressing endogenous levels of TDP43G298S and TDP43A315T variants. An independent research group also corroborated this phenotype in differentiated MNs bearing the TDP43M337V-encoding mutation[43]. Given this clear and consistent defect in TDP-43 granule transport in multiple experimental systems, we conclude that deficient axonal transport of mRNA targeted by TDP-43 may contribute to pathogenesis of ALS. This particular mechanism could influence specific disease features such as cell-type susceptibility or the pattern of degeneration. ALS has been described as a 'distal axonopathy' because morphological abnormalities of the distal axon, including dismantling of the neuromuscular junction leading to denervation, are among the earliest pathological features[52]. Many of the mRNA targets of TDP-43 encode proteins that function in this compartment[17, 53], suggesting perhaps that a failure of TDP-43 to adequately support spatially appropriate translation of target mRNAs could contribute to this pattern of neurodegeneration.

The mechanism by which disease-causing mutations impair RNA granule transport is unclear but could involve a defect in the ability of mutant TDP-43 granules to engage motor proteins or a physical impediment to their movement based on an abnormality in their size or shape. However, it is worth noting that most ALS-causing TDP-43 mutations, including all the

ones studied here, impact a prion-like domain in the C terminus of TDP-43[6, 27]. Prion-like domains in TDP-43 and related RNA-binding proteins mediate the assembly of RNA granules, and disease mutations in these prion-like domains disturb the dynamics of RNA granule assembly and disassembly[16]. Normally, RNA transport granules in neurons are highly dynamic[54] and this relates to their ability to deliver mRNAs to distal sites for local translation[55]. The correlation between the impairment of RNA granule dynamics and impairment of RNA granule transport by ALS mutations support the model of a significant role of these two processes in ALS pathogenesis. MNs differentiated from patient iPS cells, as demonstrated here, will likely be a great research tool in the additional studies required to further elucidate this hypothesis.

4.4 Materials and Methods

4.4.1 Cell culture

All cell cultures (fibroblasts, iPS cells and neurons) were maintained in 5% CO2 incubators at 37ºC. Human fibroblasts were cultured in KO-DMEM (Life Tecnologies™), supplemented with 20% Earl's salts 199 (GIBCO®), 10% Hyclone (GIBCO®), 1x GlutaMax (GIBCO®), and 100μM 2-mercaptoethanol, and passaged by trypsinization (0.25% trypsin- EDTA, GIBCO®). iPS cell lines were maintained on tissue culture dishes pre-coated with Matrigel™ (BD Biosciences) and fed with mTeSR™ media (STEMCELL Technologies). Media was changed every 24 hours and cell lines were passaged by dispase (GIBCO®, 1mg/mL for 30min at 37ºC).

4.4.2 Generation of TDP-43 iPS cell lines

Following informed consent, dermal biopsies were obtained from three familial ALS patients with mutations in the *TARDBP* locus. From these explants, fibroblasts were generated

and expanded. TDP-43 iPS cells were derived by transduction of 30,000 fibroblasts with retroviruses expressing the reprogramming genes *OCT4*, *SOX2* and *KLF4*, at an MOI of 3-5 per gene, as described previously[39]. Retrovirus preparations were produced at the Harvard Gene Therapy Initiative at Harvard Medical School (Boston, MA). After 3-4 weeks, primary iPS cell colonies were manually picked based on morphology and independently expanded in mTeSR™ medium (STEMCELL Technologies) to generate 3-5 different iPS cell lines per patient. The presence of a mutation linked to ALS in the *TARDBP* locus was confirmed by PCR amplification of a genomic region surrounding *Exon* 6, followed by Sanger DNA sequencing. The pluripotency of the novel iPS cell lines (47d and RB20a) used in the axonal transport assays was validated using the TaqMan® hPSC Scorecard™ Panel (Life Technologies™) as previously described[33, 38].

4.4.3 Motor neuron differentiation for TDP-43 localization studies

Two different MN differentiation strategies were used in this study. For TDP-43 localization studies, iPS cell lines were differentiated as using an embryoid body (EB)-based protocol as previously described[33, 39], with some modifications. Briefly, pluripotent stem cell colonies were dissociated with accutase (STEMCELL Technologies) and single cells were plated in suspension for 24 hours in mTeSR™ media using low-adherence 75cm^2 flasks, at a density of 400,000 cells/mL, and in the presence of 10 μM ROCK inhibitor (Sigma, Y-27632). This time point was considered as day 0 of differentiation. Cell aggregates (EBs) were formed, and media was gradually diluted between days 2-4 (50% on day 3, and 100% on day 4) to KOSR medium [DMEM/F12 (Life Tecnologies™), 10% Knockout Serum Replacement (KOSR) (GIBCO®), 1X GlutaMAX™ (GIBCO®), and 100μM non-essential amino acids (NEAA, GIBCO®)]. On day 5, medium was replaced with a neural induction medium [NIM: DMEM/F12, NEAA, Heparin

(2mg/ml) and N2® supplement (GIBCO®). EBs were kept in NIM from day 5 to day 24, with media changes every other day. Additional treatments of cells with small molecules and recombinant proteins were as followed, days 0-1: 10μM ROCK inhibitor (Sigma, Y-27632); days 1-6: SB431542 (10μM, Sigma Aldrich) and Dorsmorphin (100nM, Stemgent); days 5-24: BRAIN DERIVED NEUROTROPHIC FACTOR (BDNF, 10ng/mL, R&D), ascorbic acid (AA, 0.4μg/mL, Sigma), retinoic acid (RA, 1μM, Sigma) and Smoothened Agonist (SAG1.3, 1μM, EMD Millipore). On day 24, EBs were dissociated to single cells with Papain/DNase (Worthington Bio), and 100,000 cells/well were seeded onto poly-D-lysine/laminin-coated 8 well chamber slides (BD biosciences). For TDP-43 localization studies, a lower density of 20,000 cells per well was used, and the 8-well chamber slides contained a confluent monolayer of primary cortical mouse glia. Primary glial preparations from P0-P2 mouse pups were generated as previously described[39, 45]. Cultures were fed every 2-3 days with MN medium [Neurobasal (Life Technologies™) supplemented with 1x N-2® (GIBCO®), 1x GlutaMAX™ (GIBCO®), 100μM NEAA, 1x B-27® (GIBCO®), and 10 ng/mL of each of the neurotrophic factors BDNF, GDNF, and CNTF (R&D)].

4.4.4 Motor neuron differentiation for *NEFL* transport experiments

For axonal transport assays, iPS cell lines were differentiated using adherent (2D) culture conditions as previously described[41, 42], with some modifications. Briefly, pluripotent stem cell colonies were dissociated with accutase™ (STEMCELL Technologies) and single cells were plated on 6-well tissue culture plates precoated with Matrigel™ (BD Biosciences) at a density of 800,000 cells per well and fed with mTeSR™ media supplemented with 10 μM ROCK inhibitor (Sigma, Y-27632) for the first 16-24 hours. Cultures were fed with mTeSR™ until they reached 90-100% confluency (3-4 days after initial plating), at which point the media was

replaced by KSR medium [KO-DMEM (Life Technologies™) supplemented with 15% KOSR (GIBCO®), 1x GlutaMAX™ (GIBCO®), and 100μM NEAA)]. This time point was defined as day 0 of motor neuron differentiation. Cells were fed every 24 hours, and after 4 days, increasing amounts of N2 medium [Neurobasal (Life Technologies™) supplemented with 1x N-2® (GIBCO®), 1x GlutaMAX™ (GIBCO®) and 100μM NEAA] were used to replace KSR medium, with complete replacement by d10. Cells were cultured in N2 medium for 4 additional days. Treatment with small molecules was carried out as follows: 10μM SB431542 (Sigma) and 100nM LDN-193189 (STEMGENT) on d0-d5; 1μM retinoic acid (Sigma) and 1μM Smoothend agonist (EMD Millipore) on d2-d14; 5μM DAPT (EMD Millipore) and 4μM SU-5402 (BIOVISION) on d2-d14. On d14, differentiated cells were dissociated to single cells using accutase™ (STEMCELL Technologies) and plated onto Matrigel™-coated glass cover-slips (BD BioCoat™) or 8-well chamber slides (BD Biosciences), for live-cell fluorescence imaging or immunocytochemistry, respectively. For live-cell fluorescence imaging, dissociated cells were transfected immediately with a 'molecular beacon' for *NEFL* and an *Hb9(9Kb)::GFP* reporter construct[44, 45], using the Lonza Amaxa Nucleofector. Cultures were fed every 2-3 days with MN medium [Neurobasal (Life Technologies™) supplemented with 1x N-2® (GIBCO®), 1x GlutaMAX™ (GIBCO®), 100μM NEAA, 1x B-27® (GIBCO®), and 10 ng/mL of each of the neurotrophic factors BDNF, GDNF, and CNTF (R&D)], previously 'conditioned' by murine glial cells for 3 days. Primary glial preparations for 'conditioning' of MN medium were carried out from P0-P2 mouse pups as previously described[39, 45].

4.4.5 Immunocytochemistry and TDP-43 localization studies

8-well chamber slides (BD Biosciences) were fixed in ice-cold 4% PFA for 15-20 minutes at 4°C, washed 3 times with 1x PBS, permeabilized with 0.2% Triton-X in 1x PBS for 45 min,

and blocked with 10% donkey serum in 1x PBS-T (0.1% Tween® 20) for 1 hour at room temperature. Cells were then incubated overnight at 4°C with primary antibody (diluted in blocking solution). At least 4 washes (5 min incubation each) with 1xPBS-T were carried out before incubating the cells with secondary antibodies for 1 hour at room temperature (diluted in blocking solution). Cell nuclei (DNA) were visualized by DAPI stain. The following primary antibodies were used to assess pluripotency in iPS cells: NANOG (1:100, R&D, AF1997), OCT3/4 (1:500, Santa Cruz), SSEA4 (1:1000, Santa Cruz) and TRA-1-81 (1:1000, Millipore). To assay for the expression of neuronal and MN markers, the following primary antibodies were used: ISLET1/2 (1:200, DSHB, 40.2D6), ISLET1 (1:2000, abcam®, ab20670), TUJ1 (1:1000, Sigma, T2200), MAP2 (1:10000, abcam®, ab5392). Secondary antibodies used (488, 555, 594, and 647) were Alexa®Fluor (1:1000, Life Technologies) and DyLight (1:500, Jackson ImmunoResearch Laboratories). For TDP-43 localization studies, the rabbit polyclonal antibody 10782-2-AP from Proteintech™ was used (1:1000). For each genotype, several images from different wells (technical replicas) and from independent differentiation experiments (biological replicas) were collected using epifluorescence microscopy with a 40X objective. Approximately 200 $MAP2^+$ neurons per genotype per experiment were scored for the presence of a 'TDP-43 nuclear clearance phenotype' (i.e. TDP-43 immunoreactivity absent from the nucleus) or a 'TDP-43 cytoplasmic accumulation or possible aggregation' phenotype (i.e. TDP-43 cytoplasmic immunofluorescent signal in a cell was clearly higher than in surrounding cells, or if there were inclusions immunoreactive to the TDP-43 antibody). Percentages of MAP2+ neurons displaying a phenotype were determined by dividing by the total number of cells scored in the experiment.

4.4.6 *NEFL* molecular beacon synthesis, design and testing

Beacon loop sequences of 23–25 nt were designed manually to detect the human *NFL*

transcript using three different programs in parallel: (1) OLIGOWALK, (2) mFold, and (3) MicroInspector. Using this approach, beacons were predicted to stably hybridize to single-stranded regions of the transcript in areas not bound by endogenous microRNAs[56]. Beacons were synthesized using a nuclease-resistant 2'-O-methylribonucleotide backbone and were prevented from nuclear localization by conjugation to NeutrAvidin[57, 58]. Beacons were synthesized with a biotin-modified-dT nucleotide in the 30 stem sequence and were labeled with 5'Cy3 and 3' BHQ2 by Sigma Aldrich. The molecular beacon sequence *NEFL* 5'-Cy3 cacaGGTTCAATCTTTCTTCTTAGCTGC(Bio-dT)gtg BHQ2-3'. Underlined sequences form the self-hybridizing stem sequence and uppercase letters hybridize to the transcript. Beacon hybridization to its target sequence was tested *in vitro* using synthetic oligonucleotides in solution.

4.4.7 Live-cell imaging experiments and analyses

Time-lapse movies were obtained with a Nikon Eclipse Ti equipped with an automated stage and In Vivo Scientific incubator and using a Plan Apo 63X/1.4 NA oil-immersion objective with 2-4 s intervals. Movie length ranged from 5 to 15 min. To detect GFP/ and Cy3, 488 and 561 laser lines, both with band pass settings, were used. Time-lapse movies were analyzed using SlideBook Software (Intelligent Imaging Innovations Inc., Denver, CO) or Imaris 7.6 (Bitplane Science Software, South Windsor, CT) with the manual particle-tracking module. Granules that moved at least 3 μm during the length of the movie were analyzed. Statistical analyses were performed with Prism6 (GraphPad Software Inc., La Jolla, CA). Comparing the TDP-43 controls to the mutant TDP-43 datasets yielded all p-values. A Mann-Whitney unpaired test with one-tailed p-value was completed for comparing distances travelled, velocity analysis, and the directional percentages of granules within populations.

KaleidaGraph (Synergy software) was used to make the axonal particle trafficking distance and velocity bar graphs. All error bars are shown as mean ± SEM.

4.5 References

1. Ou, S.H., Wu, F., Harrich, D., Garcia-Martinez, L.F. & Gaynor, R.B. Cloning and characterization of a novel cellular protein, TDP-43, that binds to human immunodeficiency virus type 1 TAR DNA sequence motifs. *J Virol* **69**, 3584-96 (1995).

2. Buratti, E. et al. Nuclear factor TDP-43 and SR proteins promote in vitro and in vivo CFTR exon 9 skipping. *EMBO J* **20**, 1774-84 (2001).

3. Arai, T. et al. TDP-43 is a component of ubiquitin-positive tau-negative inclusions in frontotemporal lobar degeneration and amyotrophic lateral sclerosis. *Biochem Biophys Res Commun* **351**, 602-11 (2006).

4. Neumann, M. et al. Ubiquitinated TDP-43 in frontotemporal lobar degeneration and amyotrophic lateral sclerosis. *Science* **314**, 130-3 (2006).

5. Mackenzie, I.R. et al. Pathological TDP-43 distinguishes sporadic amyotrophic lateral sclerosis from amyotrophic lateral sclerosis with SOD1 mutations. *Ann Neurol* **61**, 427-34 (2007).

6. Ling, S.C., Polymenidou, M. & Cleveland, D.W. Converging mechanisms in ALS and FTD: disrupted RNA and protein homeostasis. *Neuron* **79**, 416-38 (2013).

7. Al-Chalabi, A. et al. The genetics and neuropathology of amyotrophic lateral sclerosis. *Acta Neuropathol* **124**, 339-52 (2012).

8. Gitcho, M.A. et al. TDP-43 A315T mutation in familial motor neuron disease. *Ann Neurol* **63**, 535-8 (2008).

9. Kabashi, E. et al. TARDBP mutations in individuals with sporadic and familial amyotrophic lateral sclerosis. *Nat Genet* **40**, 572-4 (2008).

10. Van Deerlin, V.M. et al. TARDBP mutations in amyotrophic lateral sclerosis with TDP-43 neuropathology: a genetic and histopathological analysis. *Lancet Neurol* **7**, 409-16 (2008).

11. Yokoseki, A. et al. TDP-43 mutation in familial amyotrophic lateral sclerosis. *Ann Neurol* **63**, 538-42 (2008).

12. Rutherford, N.J. et al. Novel mutations in TARDBP (TDP-43) in patients with familial amyotrophic lateral sclerosis. *PLoS Genet* **4**, e1000193 (2008).

13. Sreedharan, J. et al. TDP-43 mutations in familial and sporadic amyotrophic lateral sclerosis. *Science* **319**, 1668-72 (2008).

14. Kwiatkowski, T.J., Jr. et al. Mutations in the FUS/TLS gene on chromosome 16 cause familial amyotrophic lateral sclerosis. *Science* **323**, 1205-8 (2009).

15. Kim, H.J. et al. Mutations in prion-like domains in hnRNPA2B1 and hnRNPA1 cause multisystem proteinopathy and ALS. *Nature* **495**, 467-73.

16. Ramaswami, M., Taylor, J.P. & Parker, R. Altered ribostasis: RNA-protein granules in degenerative disorders. *Cell* **154**, 727-36 (2013).

17. Polymenidou, M. et al. Long pre-mRNA depletion and RNA missplicing contribute to neuronal vulnerability from loss of TDP-43. *Nat Neurosci* **14**, 459-68 (2011).

18. Xiao, S. et al. RNA targets of TDP-43 identified by UV-CLIP are deregulated in ALS. *Mol Cell Neurosci* **47**, 167-80 (2011).

19. Tollervey, J.R. et al. Characterizing the RNA targets and position-dependent splicing regulation by TDP-43. *Nat Neurosci* **14**, 452-8 (2011).

20. Freibaum, B.D., Chitta, R.K., High, A.A. & Taylor, J.P. Global analysis of TDP-43 interacting proteins reveals strong association with RNA splicing and translation machinery. *J Proteome Res* **9**, 1104-20 (2010).

21. Fallini, C., Bassell, G.J. & Rossoll, W. The ALS disease protein TDP-43 is actively transported in motor neuron axons and regulates axon outgrowth. *Hum Mol Genet* **21**, 3703-18 (2012).

22. Wang, I.F., Wu, L.S., Chang, H.Y. & Shen, C.K. TDP-43, the signature protein of FTLD-U, is a neuronal activity-responsive factor. *J Neurochem* **105**, 797-806 (2008).

23. Narayanan, R.K. et al. Identification of RNA bound to the TDP-43 ribonucleoprotein complex in the adult mouse brain. *Amyotroph Lateral Scler Frontotemporal Degener* **14**, 252-60 (2013).

24. Lagier-Tourenne, C., Polymenidou, M. & Cleveland, D.W. TDP-43 and FUS/TLS: emerging roles in RNA processing and neurodegeneration. *Hum Mol Genet* **19**, R46-64 (2010).

25. Avendano-Vazquez, S.E. et al. Autoregulation of TDP-43 mRNA levels involves interplay between transcription, splicing, and alternative polyA site selection. *Genes Dev* **26**, 1679-84 (2012).

26. Ayala, Y.M. et al. TDP-43 regulates its mRNA levels through a negative feedback loop. *EMBO J* **30**, 277-88 (2010).

27. Lee, E.B., Lee, V.M. & Trojanowski, J.Q. Gains or losses: molecular mechanisms of TDP43-mediated neurodegeneration. *Nat Rev Neurosci* **13**, 38-50 (2012).

28. Xu, Y.F. et al. Wild-type human TDP-43 expression causes TDP-43 phosphorylation, mitochondrial aggregation, motor deficits, and early mortality in transgenic mice. *J Neurosci* **30**, 10851-9 (2010).

29. Igaz, L.M. et al. Dysregulation of the ALS-associated gene TDP-43 leads to neuronal death and degeneration in mice. *J Clin Invest* **121**, 726-38 (2011).

30. Da Cruz, S. & Cleveland, D.W. Understanding the role of TDP-43 and FUS/TLS in ALS and beyond. *Curr Opin Neurobiol* **21**, 904-19 (2011).

31. Egawa, N. et al. Drug screening for ALS using patient-specific induced pluripotent stem cells. *Sci Transl Med* **4**, 145ra104 (2012).

32. Bilican, B. et al. Mutant induced pluripotent stem cell lines recapitulate aspects of TDP-43 proteinopathies and reveal cell-specific vulnerability. *Proc Natl Acad Sci U S A* **109**, 5803-8 (2012).

33. Kiskinis, E. et al. Pathways disrupted in human ALS motor neurons identified through genetic correction of mutant SOD1. *Cell Stem Cell* **14**, 781-95 (2014).

34. Wainger, B. et al. Intrinsic Membrane Hyperexcitability of ALS Patient-Derived Motor Neurons. *Cell Reports* (2014).

35. Sareen, D. et al. Targeting RNA foci in iPSC-derived motor neurons from ALS patients with a C9ORF72 repeat expansion. *Sci Transl Med* **5**, 208ra149 (2013).

36. Donnelly, C.J. et al. RNA toxicity from the ALS/FTD C9ORF72 expansion is mitigated by antisense intervention. *Neuron* **80**, 415-28 (2013).

37. Chen, H. et al. Modeling ALS with iPSCs reveals that mutant SOD1 misregulates neurofilament balance in motor neurons. *Cell Stem Cell* **14**, 796-809 (2014).

38. Bock, C. et al. Reference maps of human ES and iPS cell variation enable high-throughput characterization of pluripotent cell lines. *Cell* **144**, 439-452 (2011).

39. Boulting, G.L. et al. A functionally characterized test set of human induced pluripotent stem cells. *Nature biotechnology* (2011).

40. Amoroso, M.W. et al. Accelerated high-yield generation of limb-innervating motor neurons from human stem cells. *J Neurosci* **33**, 574-86 (2013).

41. Chambers, S.M. et al. Highly efficient neural conversion of human ES and iPS cells by dual inhibition of SMAD signaling. *Nat Biotechnol* **27**, 275-80 (2009).

42. Chambers, S.M. et al. Combined small-molecule inhibition accelerates developmental timing and converts human pluripotent stem cells into nociceptors. *Nat Biotechnol* **30**, 715-20 (2012).

43. Alami, N.H. et al. Axonal transport of TDP-43 mRNA granules is impaired by ALS-causing mutations. *Neuron* **81**, 536-43 (2014).

44. Wichterle, H., Lieberam, I., Porter, J.A. & Jessell, T.M. Directed differentiation of embryonic stem cells into motor neurons. *Cell* **110**, 385-97 (2002).

45. Di Giorgio, F.P., Boulting, G.L., Bobrowicz, S. & Eggan, K.C. Human embryonic stem cell-derived motor neurons are sensitive to the toxic effect of glial cells carrying an ALS-causing mutation. *Cell Stem Cell* **3**, 637-48 (2008).

46. Sandoe, J. & Eggan, K. Opportunities and challenges of pluripotent stem cell neurodegenerative disease models. *Nat Neurosci* **16**, 780-9 (2013).

47. Arnold, E.S. et al. ALS-linked TDP-43 mutations produce aberrant RNA splicing and adult-onset motor neuron disease without aggregation or loss of nuclear TDP-43. *Proc Natl Acad Sci U S A* **110**, E736-45 (2013).

48. Yang, C. et al. Partial loss of TDP-43 function causes phenotypes of amyotrophic lateral sclerosis. *Proc Natl Acad Sci U S A* **111**, E1121-9 (2014).

49. Nishimura, A.L. et al. Allele-specific knockdown of ALS-associated mutant TDP-43 in neural stem cells derived from induced pluripotent stem cells. *PLoS One* **9**, e91269 (2014).

50. Burkhardt, M.F. et al. A cellular model for sporadic ALS using patient-derived induced pluripotent stem cells. *Mol Cell Neurosci* **56**, 355-64 (2013).

51. Zhang, Z. et al. Downregulation of microRNA-9 in iPSC-derived neurons of FTD/ALS patients with TDP-43 mutations. *PLoS One* **8**, e76055 (2013).

52. Fischer, L.R. et al. Amyotrophic lateral sclerosis is a distal axonopathy: evidence in mice and man. *Exp Neurol* **185**, 232-40 (2004).

53. Lagier-Tourenne, C. et al. Divergent roles of ALS-linked proteins FUS/TLS and TDP-43 intersect in processing long pre-mRNAs. *Nature neuroscience* **15**, 1488-1497 (2012).

54. Barbee, S.A. et al. Staufen- and FMRP-containing neuronal RNPs are structurally and functionally related to somatic P bodies. *Neuron* **52**, 997-1009 (2006).

55. Krichevsky, A.M. & Kosik, K.S. Neuronal RNA granules: a link between RNA localization and stimulation-dependent translation. *Neuron* **32**, 683-96 (2001).

56. Bratu, D.P., Cha, B.J., Mhlanga, M.M., Kramer, F.R. & Tyagi, S. Visualizing the distribution and transport of mRNAs in living cells. *Proc Natl Acad Sci U S A* **100**, 13308-13 (2003).

57. Chen, A.K., Behlke, M.A. & Tsourkas, A. Sub-cellular trafficking and functionality of 2'-O-methyl and 2'-O-methyl-phosphorothioate molecular beacons. *Nucleic Acids Res* **37**, e149 (2009).

58. Chen, A.K., Davydenko, O., Behlke, M.A. & Tsourkas, A. Ratiometric bimolecular beacons for the sensitive detection of RNA in single living cells. *Nucleic Acids Res* **38**, e148 (2010).

CHAPTER 5

Future Directions

5.1 Research Summary

Overall, the work described in the three previous chapters supports our main premise that human pluripotent stem cell-derived MNs expressing ALS-associated variants represent a great tool for the development of novel models to study this neurological disorder. We show that these differentiated cells share several properties with *bona fide* MNs, and are able to recapitulate some of the molecular and functional phenotypes reported in ALS patients and animal models. The phenotypes we observed included transcriptional and morphological alterations in mitochondria, changes in protein solubility, increased membrane excitability, and defects in cell survival and axonal transport (Chapter 2 and Chapter 4). Utilizing gene-targeting technology we further validated the requirement, and in some cases sufficiency, of the ALS-linked *SOD1A4V* mutation to drive some of these cellular phenotypes (Chapter 2). Additionally, by utilizing unbiased transcriptome profiling of human differentiated MNs following modulation of TDP-43 levels, we uncovered novel molecular targets downstream of the activity of this ALS-associated RNA binding protein (Chapter 3). One of the targets identified is the gene encoding for the tubulin-binding protein STMN2, which has functional roles in cytoskeletal dynamics and axonal regeneration. We propose that depletion of this neuronal growth-associated factor following TDP-43 dysregulation could be a molecular mechanism by which the loss of normal nuclear TDP-43, seen in most ALS cases, contributes to MN degeneration.

5.2 Future directions

While the ability to produce otherwise inaccessible human neurons bearing disease-associated mutations has revolutionized the study of neurological disorders[1-14], the incorporation of recent advances in genome-editing, stem cell differentiation, single-cell

analysis, and tissue engineering methods to future experiments will further advance our understanding of disease mechanisms and facilitate the development of novel therapies. In this chapter, we present a few experimental approaches to exemplify this claim, mainly in the context of ALS studies. Additionally, we propose experiments aimed at addressing some of the intriguing questions resulting from the research described in previous chapters.

5.2.1 Overcoming challenges in human stem cell-based disease models with *CRISPR*/Cas9

One of the major technical challenges when modeling any disease with human ES or iPS cells is their inherit variability, driven in part by their genetic background, which could be the source of experimental noise in phenotypic assays[1, 15]. A few studies have addressed this issue by drawing phenotypic correlations after comparing large cohorts of patient versus control cells[7, 16], which can be extremely laborious. With monogenetic disorders for which the causative genetic defect is known, a more rigorous solution is the use of genome editing strategies to generate cell lines whose genomes vary only at the disease-associated locus. In Chapter 2, we exemplified the use of this approach by creating two isogenic pairs of $SOD1^{+/A4V}$ and $SOD1^{+/+}$ human pluripotent stem cells with zinc-finger nucleases[17] (ZFN) targeting the *SOD1* locus. While this system proved useful, the engineering of ZFNs that can efficiently bind to a specific genomic region can be a costly and laborious process with significant lab expertise required[18-21]. More recently the development of gene-targeting technologies based on the *CRISPR*/Cas9 components of the prokaryotic 'immune system' has generated considerable excitement in various areas of biological research[22-25]. In bacteria, the *CRISPR*-loci associated nuclease Cas9 cleaves foreign DNA that is recognized by RNA molecules complexed to Cas9[26, 27]. This property can be exploited to deliver Cas9 into a variety of cells in conjunction with 'guide' RNA molecules containing sequences recognizing specific locations in the

genome, thus immensely reducing the time, cost and cloning tools required to achieve successful targeting[22-24].

We anticipate that CRISPR/Cas9-based technology, by facilitating the targeted genetic modification of human ES and iPS cells, will vastly improve current stem cell-based models of ALS. For instance, we could more rapidly generate *TDP-43* isogenic versions of the iPS cell lines described in Chapter 4 to further study the requirement or sufficiency of mutant TDP-43 in the axonal transport deficits we observed. Additionally, we could modify several ALS-linked loci into the same genetic background, HUES3 *Hb9::GFP* for example, eliminating the confounding influence of the variability seen in different ES and iPS cell lines. Multi-gene targeting in a single experiment is also possible with CRISPR/Cas9-based methods[28], therefore we could investigate the effect of multiple mutations on the *in vitro* phenotypes of HUES3 GFP^+ MNs. The relevance of this latter experimental approach is supported by recent reports demonstrating that a significant number of ALS subjects can carry risk variants in more than one gene, and that the number of additional variants can influence the age of symptom onset[29-32]. The incorporation in these experiments of RNAi and RNA-Seq methods similar to the ones presented in Chapter 3 could help us address whether mutations in different ALS-linked genes or their reduced function, converge on similar molecular pathways leading to neurodegeneration. Considering the growing list of ALS-causative genes associated with diverse biological processes[33, 34], and the time it will require to develop animal models for each of these genes, the possibility of more immediately addressing this question with human stem cell-derived MNs will be critical to elucidate common disease mechanisms, and in turn, better candidate targets for therapeutic interventions.

Another aspect of stem cell-based models where more rapid and efficient targeting technologies will have a positive impact is in the generation of human ES and iPS cell lines that, upon differentiation, can report on the acquisition of a particular cell identity. In the context of neurological studies this will be significant, considering that even the most efficient neuronal differentiation protocols commonly generate heterogeneous mixtures of neurons and neural progenitors[5], where the undesired cell types can mask or influence phenotypic outcomes. The creation of additional *Hb9::GFP* reporters in a background different from the HUES3 cell line will help us investigate the cell-autonomous contribution and sufficiency of various mutations to different molecular and cellular phenotypes. For instance this approach could address the possibility presented in Chapter 2 that unknown mutations in the HUES3 *Hb9::GFP* cell line influence the survival phenotype of the purified GFP^{+} $SOD1^{+/A4V}$ MNs.

5.2.2 Understanding MN-specific vulnerability by studying 'ALS-resistant' neurons

A pivotal question in the study of neurological disorders is the susceptibility of a particular population of neurons to the disease-associated variants, which are commonly expressed throughout the CNS and other tissues. In ALS, several of the disease-associated genes such as *TDP-43* and *SOD1* are ubiquitously expressed, but cortical and spinal motor neurons are the specific neuronal types that degenerate in this disorder. One possibility is that mutant variants induce in MNs molecular pathways and more downstream responses that do not occur in other cell types. Thus far, the question of MN-specificity of observed ALS-related *in vitro* phenotypes has been primarily addressed by interrogating non-neuronal cells like fibroblasts[11,35] or by comparisons with poorly characterized heterogeneous neurons presumed to be non-MNs[11, 36]. This issue has mainly been driven by the lack of well-established directed differentiation protocols for the production and purification and human neurons of various

types. However, recent studies have demonstrated the efficient generation of differentiated interneurons[37, 38] and sensory neurons[39] from human ES and iPS cells. The incorporation of these 'ALS-resistant' neuronal cell types as additional controls into some of the assays we have described in the previous chapters will more robustly address the question of MN specific susceptibility. For instance, we could generate differentiated interneurons or sensory neurons from the control and patient iPS cell lines described in Chapters 2 and 5, and using similar *in vitro* assays, compare their response to the ALS-associated variants relative to that of cognate differentiated MNs. Additionally, we could reduce the levels of TDP-43 in differentiated sensory neurons and interneurons derived from the HUES3 cell line and determine the sets of both overlapping and non-overlapping transcriptional changes compared to the results presented in Chapter 3. Both lists of genes would be highly informative, with overlapping transcripts indicating likely general neuronal targets, and non-overlapping results highlighting molecular pathways with a potential contribution to the MN selective vulnerability phenotype manifested in ALS.

5.2.3 Characterizing MN subtypes and disease susceptibility at the single-cell level

Most human MN differentiation strategies rely on the high induction of retinoid signaling, which results in a large fraction of cells with a more anterior cervical and lateral motor column identity (LMC)[11, 40-43]. However, the exact distribution of this and other MN subtypes across experiments, and the possibility of different sensitivity to ALS-related stimuli, remain poorly characterized. Furthermore, in addition to MNs, other neuronal types, glial cells and neural progenitors can account for a significant proportion of the resulting stem cell-differentiated cells[5], which can confound downstream phenotypic assays[1, 5]. We anticipate that the rapid evolution and increasingly routine application of methods to analyze the expression of

candidate gene sets[44, 45] and even whole transcriptomes[46] at the single-cell level will help resolve these issues of cellular heterogeneity and provide relevant insights into MN biology and ALS disease mechanisms. For example, by utilizing microfluidic technology followed by qRT-PCR, we could assay the expression for various MN type and subtype genes[47, 48] to better characterize GFP^+ MNs obtained from the HUES3 cell line we described in Chapters 2 and 3. The incorporation of gene markers for other cell types (interneurons, astrocytes and neural progenitors) could also determine more rigorously the composition of differentiated cells in unsorted cultures. This platform can be used to retrospectively identify MNs or other desired cell types in a heterogeneous culture, without the need for stable or lentiviral reporters, which will facilitate the molecular characterization of cells differentiated from multiple genetic backgrounds.

Experiments described in Chapter 3 identified pathways in differentiated MNs downstream of TDP-43 dysregulation. Since RNA-sequencing relies on population averages, it is possible we have underestimated the number and level of significant transcriptional changes in these cells. In this case, the use of single-cell RNA-Seq could reveal additional mechanistic insights. For example, it would be interesting to determine whether the level of TDP-43 dysregulation correlates with different responses, e.g. do MNs with less *TDP-43* express less *STMN2*? Is there a threshold effect in the response of this and other genes?

5.2.4 Building the 'ALS-circuit' in a dish

Thus far, our stem cell-based studies of ALS[2, 4, 10, 11, 35] and those of other groups[6-9] have relied on the characterization of mostly differentiated lower MNs, cultured in isolation or in the presence of glial cell types. While these experiments have yielded convincing phenotypes and some promising therapeutic targets[4, 7-11], the contribution of other ALS-relevant cell types, like

upper cortical MNs and skeletal muscle remains unaddressed. Recent advances in tissue engineering[49, 50], coupled with novel differentiation approaches[51-55], will allow future experiments to address this issue. Several reports have demonstrated that *Hb9::GFP*$^{+}$ MNs differentiated from stem cells can form neuromuscular junctions *in vitro*[41]; therefore, additional similar assays could be carried out in which the molecular or functional effect of ALS-associated variants on this interaction is determined. For instance, we can obtain *SOD1*$^{+/+}$ and *SOD1*$^{+/A4V}$ GFP^{+} MNs and co-culture them with primary skeletal muscle in compartmentalized microfluidic devices[49], such that MN cell bodies are contained within one chamber and extend axons to a distal chamber where the muscle cells are located. Interrogation of molecular pathways at different time points by RNA-Seq of each of the two cell types could help uncover relevant mechanisms underlying MN maturation, functional activity, and vulnerability to mutant SOD1. Once MN-primary muscle experimental conditions are well established, more complex assays could then incorporate human differentiated cortical MNs[51-53] in a separate chamber of the microfluidic device, or the use of human differentiated skeletal muscle[54, 55], so that eventually a biomimetic model of the ALS circuit is created. Investigating the contribution of disease variants to the electrical activity of MNs in these culture settings could also prove informative. For example, it will worthwhile to determine if the changes in membrane excitability that we described in Chapter 2 for *SOD1*$^{+/A4V}$ MNs effect alterations in muscle contraction properties. The incorporation of more recent approaches that enable 'all-optical' ('electrode-free') recordings through genetically delivered light-sensitive voltage activators and indicators[56], will facilitate the electrophysiological study of these cells.

5.2.5 Elucidating the TDP43-STMN2 molecular association and relevance to ALS

One of the targets identified in the RNAi/RNA-Seq screen presented in Chapter 3 was the gene encoding for the neuronal-growth associated and tubulin-binding factor STMN2[57]. In independent experiments we demonstrated that TDP-43 function is important for sustaining the levels of STMN2 transcript and protein in human differentiated MNs. Furthermore, using immunohistochemical analysis of spinal cord tissues with confirmed TDP-43 pathology, we showed that STMN2 expression is altered in ALS. However, additional experiments are required to strengthen our hypothesis of STMN2 downregulation as a potential mechanism of relevance to ALS. For instance, it will be critical to further interrogate STMN2 expression levels in additional ALS autopsy samples using other methods such as *in situ* hybridization, immunoblot assays, and fluorescence immunohistochemistry. This last technique in particular, as exemplified by a recent study[58], will allow the examination of individual MNs within the same post-mortem tissue sample to determine if there is a strong correlation between manifestation of TDP-43 pathology[59, 60] and depletion of STMN2 fluorescent signal. Antibodies against TDP-43 and STMN2 used in Chapter 3 were raised in the same animal species, which precludes their use in the same tissue sample. We are currently validating additional antibodies raised in other species, which will facilitate downstream assays.

Although we have demonstrated reproducible molecular alterations following depletion of TDP-43 in human differentiated MNs, it will be important to investigate if these changes result in measurable cellular phenotypes. Considering the functional roles of STMN2 in cytoskeletal dynamics[61, 62] and axonal growth[57] and regeneration pathways[63, 64], we have initiated phenotypic assays characterizing neurite outgrowth. Preliminary results with a small number of samples suggest that differentiated MNs can exhibit a significant deficit in neurite outgrowth in

response to downregulation of TDP-43. While the phenotypic response to STMN2 downregulation was not statistically significant, the data indicated a trend for compromised neurite growth. We are currently pursuing the validation of these findings with a larger sample size and additional experimental conditions, including physical insults to the neuronal projections.

Studies have demonstrated that the STMN2 protein is the target of c-Jun NH_2-terminal kinases (JNKs) both *in vitro* and *in vivo*[61, 62, 65]. More recently, phosphorylation of STMN2 protein by JNKs was shown to drive its rapid turnover in the axons of cultured mouse sensory neurons, where STMN2 is a labile protein with a very short half-life of 0.8-1.5 hours[64]. Furthermore, maintaining STMN2 levels in cultured neurons by small molecule inhibition of JNK activity (JNKi) delayed axonal degeneration after mechanical injury (axotomy)[64]. Of note, several research groups are actively exploring pharmacological inhibition of JNK as a suitable therapeutic strategy for the prevention of neurodegeneration[66-70], with current efforts focusing in the design of isoform-selective JNK inhibitors with good CNS penetration[67].

Examination of the RNA-Seq FPKM expression values for the three genes (*JNK1*, *JNK2* and *JNK3*) encoding all JNK proteins[71], did not detect significant changes in differentiated MNs in response to dysregulation of TDP-43 levels (data not shown). This suggests that the reduction in STMN2 levels following TDP-43 depletion is not mediated by a transcriptional upregulation of *JNK*s. Additional work is in progress to characterize how modulation of JNK activity in human differentiated MNs influences STMN2 levels. To this end, we have generated protein extracts from cells in which RNAi targeting *TDP-43* or *STMN2* was induced, followed by treatment with DMSO or JNKi[64]. If we find that JNKi increases STMN2 levels, this could easily be incorporated as a strategy to 'rescue' any potential phenotypes observed in the

outgrowth assays proposed above. Genetic delivery into these cells of overexpression constructs encoding wild-type STMN2 or STMN2 variants resistant to phosphorylation by JNK will also help establish correlations with any robust phenotypes. Gene targeting technology could also be incorporated into these experiments to deplete or modify the endogenous *STMN2* gene in a more rigorous manner.

The exact molecular mechanism by which TDP-43 sustains STMN2 levels in MNs is unknown. As discussed in Chapter 3, functional roles of TDP-43 in mRNA stability and axonal transport[2,72,73] could be at play, as reanalysis of TDP43/RNA interaction results[58,73-76] provided data suggesting a direct association of TDP-43 to *STMN2* in rat cultured neurons[76] and in mouse brain tissues[74]. Furthermore, in the latter study, TDP-43 binding could be mapped to the *3'-UTR* of *STMN2*[74]. In order to experimentally validate these findings, we have obtained TDP-43 immunoprecipitate (IP) from cultures of human differentiated MNs and will assay for interaction with the *STMN2* RNA and, if possible, specifically for *STMN2-3'UTR* binding.

We could also gain additional insights into potential mechanisms of TDP-43 regulation of STMN2 by performing live-cell imaging experiments similar to the ones described in Chapter 4. If TDP-43 IP assays provide evidence for a direct interaction with the *STMN2*-3'UTR, we could design a fluorescent 'molecular beacon'[2] that hybridizes to the *STMN2* mRNA to study the transport of this transcript in human differentiated MNs. If successful, we could extend this approach to interrogate the potential functional contribution of ALS-associated TDP-43 variants. Additionally, at the molecular level, we could use cell population based methods (qRT-PCR and immunoblot blot assays) or single-cell analyses to determine if a particular mutation results in altered *STMN2* expression levels. As discussed in a previous section, the use of engineered isogenic cell lines in these experiments will provide the most rigorous controls.

While *Stmn2*$^{-/-}$ animal models have not been reported, mouse embryonic stem cells with a *Stm2* KO first allele (reporter-tagged insertion with conditional potential) are available through the International Mouse Phenotyping Consortium[77]. Interestingly, mice deficient for the ubiquitous *Stathmin* (*Stmn*$^{-/-}$) can develop normally[78], but with age they manifest an axonopathy of the central and peripheral nervous systems, with significant reduction of motor nerve conduction[79]. Therefore, if some of the experiments with human differentiated MNs or ALS tissues further corroborate our hypothesis connecting TDP-43 and STMN2, it would worthwhile to explore both the generation of a mouse model for *Stmn2* depletion, and the use of methods like JNKi to reduce the turnover of this protein in existing animal models of ALS.

Finally, spinal MNs were among the first specific neuronal cell types to be generated by directed differentiation of pluripotent stem cells, and the advances made in the past few years by exploiting these cells to study ALS have been remarkable. This significant progress might have provided inspiration to author Jean-Dominique Bauby, who despite his 'locked-in' syndrome, communicated by blinking more than 200,000 times his entire memoir 'The Diving Bell and the Butterfly', where he wondered: '*Does the cosmos contain keys for opening my diving bell? A subway line with no terminus? A currency strong enough to buy my freedom back? We must keep looking*'[80]. We are optimistic that the findings presented in this thesis, along with continued efforts in the areas of human MN differentiation and *in vitro* disease modeling, will provide the keys to unlock novel therapeutic strategies for devastating neurological conditions, such as ALS.

5.3 References

1. Sandoe, J. & Eggan, K. Opportunities and challenges of pluripotent stem cell neurodegenerative disease models. *Nat Neurosci* **16**, 780-9 (2013).

2. Alami, N.H. et al. Axonal transport of TDP-43 mRNA granules is impaired by ALS-causing mutations. *Neuron* **81**, 536-43 (2014).

3. Dimos, J.T. et al. Induced pluripotent stem cells generated from patients with ALS can be differentiated into motor neurons. *Science* **321**, 1218-21 (2008).

4. de Boer, A.S. et al. Genetic validation of a therapeutic target in a mouse model of ALS. *Sci Transl Med* **6**, 248ra104 (2014).

5. Han, S.S., Williams, L.A. & Eggan, K.C. Constructing and deconstructing stem cell models of neurological disease. *Neuron* **70**, 626-44 (2011).

6. Bilican, B. et al. Mutant induced pluripotent stem cell lines recapitulate aspects of TDP-43 proteinopathies and reveal cell-specific vulnerability. *Proc Natl Acad Sci U S A* **109**, 5803-8 (2012).

7. Egawa, N. et al. Drug screening for ALS using patient-specific induced pluripotent stem cells. *Sci Transl Med* **4**, 145ra104 (2012).

8. Sareen, D. et al. Targeting RNA foci in iPSC-derived motor neurons from ALS patients with a C9ORF72 repeat expansion. *Sci Transl Med* **5**, 208ra149 (2013).

9. Donnelly, C.J. et al. RNA toxicity from the ALS/FTD C9ORF72 expansion is mitigated by antisense intervention. *Neuron* **80**, 415-28 (2013).

10. Wainger, B. et al. Intrinsic Membrane Hyperexcitability of ALS Patient-Derived Motor Neurons. *Cell Reports* (2014).

11. Kiskinis, E. et al. Pathways disrupted in human ALS motor neurons identified through genetic correction of mutant SOD1. *Cell Stem Cell* **14**, 781-95 (2014).

12. Chung, C.Y. et al. Identification and rescue of alpha-synuclein toxicity in Parkinson patient-derived neurons. *Science* **342**, 983-7 (2013).

13. Yang, Y.M. et al. A small molecule screen in stem-cell-derived motor neurons identifies a kinase inhibitor as a candidate therapeutic for ALS. *Cell Stem Cell* **12**, 713-26 (2013).

14. Corti, S. et al. Genetic correction of human induced pluripotent stem cells from patients with spinal muscular atrophy. *Sci Transl Med* **4**, 165ra162 (2012).

15. Boulting, G.L. et al. A functionally characterized test set of human induced pluripotent stem cells. *Nature biotechnology* (2011).

16. Kondo, T. et al. Modeling Alzheimer's disease with iPSCs reveals stress phenotypes associated with intracellular Abeta and differential drug responsiveness. *Cell Stem Cell* **12**, 487-96 (2013).

17. Klug, A. The discovery of zinc fingers and their applications in gene regulation and genome manipulation. *Annu Rev Biochem* **79**, 213-31 (2010).

18. Maeder, M.L. et al. Rapid "open-source" engineering of customized zinc-finger nucleases for highly efficient gene modification. *Mol Cell* **31**, 294-301 (2008).

19. Doyon, Y. et al. Heritable targeted gene disruption in zebrafish using designed zinc-finger nucleases. *Nat Biotechnol* **26**, 702-8 (2008).

20. Isalan, M., Klug, A. & Choo, Y. A rapid, generally applicable method to engineer zinc fingers illustrated by targeting the HIV-1 promoter. *Nat Biotechnol* **19**, 656-60 (2001).

21. Pearson, H. Protein engineering: The fate of fingers. *Nature* **455**, 160-4 (2008).

22. Mali, P. et al. RNA-guided human genome engineering via Cas9. *Science* **339**, 823-6 (2013).

23. Cong, L. et al. Multiplex genome engineering using CRISPR/Cas systems. *Science* **339**, 819-23 (2013).

24. Jiang, W., Bikard, D., Cox, D., Zhang, F. & Marraffini, L.A. RNA-guided editing of bacterial genomes using CRISPR-Cas systems. *Nat Biotechnol* **31**, 233-9 (2013).

25. Gaj, T., Gersbach, C.A. & Barbas, C.F., 3rd. ZFN, TALEN, and CRISPR/Cas-based methods for genome engineering. *Trends Biotechnol* **31**, 397-405 (2013).

26. Barrangou, R. et al. CRISPR provides acquired resistance against viruses in prokaryotes. *Science* **315**, 1709-12 (2007).

27. Deltcheva, E. et al. CRISPR RNA maturation by trans-encoded small RNA and host factor RNase III. *Nature* **471**, 602-7 (2011).

28. Wang, H. et al. One-step generation of mice carrying mutations in multiple genes by CRISPR/Cas-mediated genome engineering. *Cell* **153**, 910-8 (2013).

29. Cady, J. et al. Amyotrophic lateral sclerosis onset is influenced by the burden of rare variants in known amyotrophic lateral sclerosis genes. *Ann Neurol* **77**, 100-13 (2015).

30. van Blitterswijk, M. et al. Evidence for an oligogenic basis of amyotrophic lateral sclerosis. *Hum Mol Genet* **21**, 3776-84 (2012).

31. Renton, A.E., Chio, A. & Traynor, B.J. State of play in amyotrophic lateral sclerosis genetics. *Nat Neurosci* **17**, 17-23 (2014).

32. van Blitterswijk, M. et al. VAPB and C9orf72 mutations in 1 familial amyotrophic lateral sclerosis patient. *Neurobiol Aging* **33**, 2950 e1-4 (2012).

33. Guerreiro, R., Bras, J. & Hardy, J. SnapShot: Genetics of ALS and FTD. *Cell* **160**, 798-798 e1 (2015).

34. Cirulli, E.T. et al. Exome sequencing in amyotrophic lateral sclerosis identifies risk genes and pathways. *Science* (2015).

35. Di Giorgio, F.P., Boulting, G.L., Bobrowicz, S. & Eggan, K.C. Human embryonic stem cell-derived motor neurons are sensitive to the toxic effect of glial cells carrying an ALS-causing mutation. *Cell Stem Cell* **3**, 637-48 (2008).

36. Chen, H. et al. Modeling ALS with iPSCs reveals that mutant SOD1 misregulates neurofilament balance in motor neurons. *Cell Stem Cell* **14**, 796-809 (2014).

37. Maroof, A.M. et al. Directed differentiation and functional maturation of cortical interneurons from human embryonic stem cells. *Cell Stem Cell* **12**, 559-72 (2013).

38. Nicholas, C.R. et al. Functional maturation of hPSC-derived forebrain interneurons requires an extended timeline and mimics human neural development. *Cell Stem Cell* **12**, 573-86 (2013).

39. Chambers, S.M. et al. Combined small-molecule inhibition accelerates developmental timing and converts human pluripotent stem cells into nociceptors. *Nat Biotechnol* **30**, 715-20 (2012).

40. Amoroso, M.W. et al. Accelerated high-yield generation of limb-innervating motor neurons from human stem cells. *J Neurosci* **33**, 574-86 (2013).

41. Davis-Dusenbery, B.N., Williams, L.A., Klim, J.R. & Eggan, K. How to make spinal motor neurons. *Development* **141**, 491-501 (2014).

42. Liu, J.P., Laufer, E. & Jessell, T.M. Assigning the positional identity of spinal motor neurons: rostrocaudal patterning of Hox-c expression by FGFs, Gdf11, and retinoids. *Neuron* **32**, 997-1012 (2001).

43. Novitch, B.G., Wichterle, H., Jessell, T.M. & Sockanathan, S. A requirement for retinoic acid-mediated transcriptional activation in ventral neural patterning and motor neuron specification. *Neuron* **40**, 81-95 (2003).

44. Guo, G. et al. Resolution of cell fate decisions revealed by single-cell gene expression analysis from zygote to blastocyst. *Dev Cell* **18**, 675-85 (2010).

45. Young, G.T. et al. Characterizing human stem cell-derived sensory neurons at the single-cell level reveals their ion channel expression and utility in pain research. *Mol Ther* **22**, 1530-43 (2014).

46. Usoskin, D. et al. Unbiased classification of sensory neuron types by large-scale single-cell RNA sequencing. *Nat Neurosci* **18**, 145-53 (2014).

47. Dasen, J.S. & Jessell, T.M. Hox networks and the origins of motor neuron diversity. *Curr Top Dev Biol* **88**, 169-200 (2009).

48. Alaynick, W.A., Jessell, T.M. & Pfaff, S.L. SnapShot: spinal cord development. *Cell* **146**, 178-178 e1 (2011).

49. Southam, K.A., King, A.E., Blizzard, C.A., McCormack, G.H. & Dickson, T.C. Microfluidic primary culture model of the lower motor neuron-neuromuscular junction circuit. *J Neurosci Methods* **218**, 164-9 (2013).

50. Ito, A. et al. Induction of functional tissue-engineered skeletal muscle constructs by defined electrical stimulation. *Sci Rep* **4**, 4781 (2014).

51. Espuny-Camacho, I. et al. Pyramidal neurons derived from human pluripotent stem cells integrate efficiently into mouse brain circuits in vivo. *Neuron* **77**, 440-56 (2013).

52. Shi, Y., Kirwan, P. & Livesey, F.J. Directed differentiation of human pluripotent stem cells to cerebral cortex neurons and neural networks. *Nat Protoc* **7**, 1836-46 (2012).

53. Shi, Y., Kirwan, P., Smith, J., Robinson, H.P. & Livesey, F.J. Human cerebral cortex development from pluripotent stem cells to functional excitatory synapses. *Nat Neurosci* **15**, 477-86, S1 (2012).

54. Tanaka, A. et al. Efficient and reproducible myogenic differentiation from human iPS cells: prospects for modeling Miyoshi Myopathy in vitro. *PLoS One* **8**, e61540 (2013).

55. Xu, C. et al. A zebrafish embryo culture system defines factors that promote vertebrate myogenesis across species. *Cell* **155**, 909-21 (2013).

56. Hochbaum, D.R. et al. All-optical electrophysiology in mammalian neurons using engineered microbial rhodopsins. *Nat Methods* **11**, 825-33 (2014).

57. Grenningloh, G., Soehrman, S., Bondallaz, P., Ruchti, E. & Cadas, H. Role of the microtubule destabilizing proteins SCG10 and stathmin in neuronal growth. *J Neurobiol* **58**, 60-9 (2004).

58. Lagier-Tourenne, C. et al. Divergent roles of ALS-linked proteins FUS/TLS and TDP-43 intersect in processing long pre-mRNAs. *Nature neuroscience* **15**, 1488-1497 (2012).

59. Mackenzie, I.R. et al. Pathological TDP-43 distinguishes sporadic amyotrophic lateral sclerosis from amyotrophic lateral sclerosis with SOD1 mutations. *Ann Neurol* **61**, 427-34 (2007).

60. Neumann, M. et al. Ubiquitinated TDP-43 in frontotemporal lobar degeneration and amyotrophic lateral sclerosis. *Science* **314**, 130-3 (2006).

61. Antonsson, B. et al. Identification of in vitro phosphorylation sites in the growth cone protein SCG10. Effect Of phosphorylation site mutants on microtubule-destabilizing activity. *J Biol Chem* **273**, 8439-46 (1998).

62. Tararuk, T. et al. JNK1 phosphorylation of SCG10 determines microtubule dynamics and axodendritic length. *J Cell Biol* **173**, 265-77 (2006).

63. Shin, J.E., Geisler, S. & DiAntonio, A. Dynamic regulation of SCG10 in regenerating axons after injury. *Exp Neurol* **252**, 1-11 (2013).

64. Shin, J.E. et al. SCG10 is a JNK target in the axonal degeneration pathway. *Proc Natl Acad Sci U S A* **109**, E3696-705 (2012).

65. Westerlund, N. et al. Phosphorylation of SCG10/stathmin-2 determines multipolar stage exit and neuronal migration rate. *Nat Neurosci* **14**, 305-13 (2011).

66. Waetzig, V. & Herdegen, T. Context-specific inhibition of JNKs: overcoming the dilemma of protection and damage. *Trends Pharmacol Sci* **26**, 455-61 (2005).

67. Graczyk, P.P. JNK inhibitors as anti-inflammatory and neuroprotective agents. *Future Med Chem* **5**, 539-51 (2013).

68. Borsello, T. & Forloni, G. JNK signalling: a possible target to prevent neurodegeneration. *Curr Pharm Des* **13**, 1875-86 (2007).

69. Probst, G.D. et al. Highly selective c-Jun N-terminal kinase (JNK) 2 and 3 inhibitors with in vitro CNS-like pharmacokinetic properties prevent neurodegeneration. *Bioorg Med Chem Lett* **21**, 315-9 (2011).

70. Bowers, S. et al. Design and synthesis of brain penetrant selective JNK inhibitors with improved pharmacokinetic properties for the prevention of neurodegeneration. *Bioorg Med Chem Lett* **21**, 5521-7 (2011).

71. Bode, A.M. & Dong, Z. The functional contrariety of JNK. *Mol Carcinog* **46**, 591-8 (2007).

72. Lagier-Tourenne, C., Polymenidou, M. & Cleveland, D.W. TDP-43 and FUS/TLS: emerging roles in RNA processing and neurodegeneration. *Hum Mol Genet* **19**, R46-64 (2010).

73. Tollervey, J.R. et al. Characterizing the RNA targets and position-dependent splicing regulation by TDP-43. *Nat Neurosci* **14**, 452-8 (2011).

74. Polymenidou, M. et al. Long pre-mRNA depletion and RNA missplicing contribute to neuronal vulnerability from loss of TDP-43. *Nat Neurosci* **14**, 459-68 (2011).

75. Xiao, S. et al. RNA targets of TDP-43 identified by UV-CLIP are deregulated in ALS. *Mol Cell Neurosci* **47**, 167-80 (2011).

76. Sephton, C.F. et al. Identification of neuronal RNA targets of TDP-43-containing ribonucleoprotein complexes. *J Biol Chem* **286**, 1204-15 (2010).

77. https://www.mousephenotype.org/data/genes/MGI:98241#order2.

78. Schubart, U.K. et al. Normal development of mice lacking metablastin (P19), a phosphoprotein implicated in cell cycle regulation. *J Biol Chem* **271**, 14062-6 (1996).

79. Liedtke, W., Leman, E.E., Fyffe, R.E., Raine, C.S. & Schubart, U.K. Stathmin-deficient mice develop an age-dependent axonopathy of the central and peripheral nervous systems. *Am J Pathol* **160**, 469-80 (2002).

80. Bauby, J.-D. The diving bell and the butterfly (A.A. Knopf : Distributed by Random House, New York, 1997).